UNIVERSITÉ DU MAINE

# THÈSE

Présentée pour obtenir le grade de

DOCTEUR DE L'UNIVERSITÉ DU MAINE
Spécialité: Génie Mécanique

Par

M. Khawar FAROOQ

# COMPORTEMENT MÉCANIQUE DES COMPOSITES SANDWICHS EN STATIQUE ET FATIGUE CYCLIQUE

27 Novembre 2003

**JURY**

| | | |
|---|---|---|
| M. Benzeggagh | Professeur, Université de Technologie de Compiègne | Rapporteur |
| P. Davies | Ingénieur de recherche (HDR), IFREMER, Brest | Rapporteur |
| M.-C. Lafarie | Professeur, ENSMA, Poitiers | Examinateur |
| J.-M. Berthelot | Professeur émérite, Université du Maine, Le Mans | Examinateur |
| A. El Mahi | Maître de conférences (HDR), Université du Maine | Directeur |
| S. Sahraoui | Professeur, Université du Maine, Le Mans | Co-Directeur |

Université du Maine

# COMPORTEMENT MÉCANIQUE DES COMPOSITES SANDWICHS EN STATIQUE ET FATIGUE CYCLIQUE

Présentée par: M. Khawar FAROOQ

Directeur A. EL Mahi
Co-Directeur S. Sahraoui

*Institut d'Acoustique et de Mécanique*
*Laboratoire d'Acoustique LAUM*
*Groupe Composites et Structures Mécaniques*
***Université du Maine, Le Mans France***

## Dedication

In the loving memory of my mother

# Acknowledgement

I would like to express my thanks and gratitude to the Almighty God, the Most Beneficent, the Most Merciful Who granted me the ability and willing to start and complete this thesis.

I am very grateful to the Government of Pakistan for financial support. I am highly obliged and indebted to Dr. M. Ashraf Atta for his continuous support throughout the years of my studies and work.

I gratefully acknowledge the generous support of Dr. A. EL Mahi for providing me with invaluable insights, guidance, inspiration and assistance. He always encouraged me and his sound advice, good teaching and friendship helped me throughout the period of my studies.

I would like to express my sincere thanks to Prof. S. Sahraoui for his co-operation, encouragement, friendly attitude and for numerous fruitful discussions. My sincerest thanks are for Professor Jean Pierre Mariot, who provided me support and advice through out the period of my study.

It is also a great honor and privilege for the author to work with Prof. J. M. Berthelot and to share his valuable knowledge and expertise. I am grateful to him for reviewing my thesis and sharing his critical comments and suggestions, which helped me to make further improvements.

I am highly obliged to Professor M. Benzeggagh and a Dr. P. Davies for accepting to be the referees for my thesis. My heartiest thanks are for Professor M.-C. Lafarie for accepting to be a member of jury.

I am grateful to Madam A. M. Brule for help and assistance in different ways during my stay in the university. My appreciation also goes to my colleagues and technicians of IUT, for their support, help and co-operation.

Finally, thanks must go to my family especially to my wife, who always boosted my morale and to my 3 year old daughter, to whom I am indebted a lot, as she missed me during my long stays in the laboratory.

# Abstract

The aim of the present study is to investigate the mechanical behaviour of sandwich composite materials under static and dynamic loadings. Sandwich panels are fabricated in the laboratory with skins of glass fibres/epoxy and core of different foam thicknesses and densities.

In an initial part, an extensive testing programme is implemented so as to derive the mechanical behaviour and the characteristics for the constituents of the sandwich composites. These testing procedures include static and fatigue testing of cores in compression, indentation, shear and three-point bending tests and skins in flexural tests.

Detailed investigations have been carried out with respect to the performance of sandwich specimens of different core thickness and densities at various span lengths in static flexural tests. Phenomena of pure bending and shear are characterised at different span lengths and compared to the results obtained by the sandwich beam theory. A good agreement is found between the experimental and analytical results.

Stiffness degradation approach is used to study the mechanical behaviour of sandwich composites in fatigue. This parameter is chosen for its advantage over other types of parameters such as residual strength. Indeed stiffness can be easily measured during the experiments and can be used as a measure of global damage state in sandwich composites during fatigue.

Mechanical behaviour of sandwich composites is highly affected by the core thickness and the density of the foams and depends on the type of loading, the frequency, as well as the applied loading levels and ratios. Fatigue characterisation of sandwich composites on the basis of these parameters is studied extensively and analysed. This analysis shows that there must be an optimising strategy while choosing core thickness and density for the performance of sandwich structure. Moreover, damage initiation, progression, coalescence and failure are observed in sandwich specimens during the course of fatigue testing and correlated with stiffness degradation. Fatigue life is characterised by Wohler curves using $N_{10}$ criterion for different types of sandwich composites.

Finally, analytical models are developed on the basis of a stiffness degradation approach to predict the fatigue life and damage development in sandwich composite materials. A good agreement is found between experimental and analytical results.

# Publications

1. A. El Mahi, M.-K. Farooq, S. Sahraoui and A. Kondratas. "Static and non-cyclic fatigue tests of sandwich composite materials behaviour in three point bending tests." *Mechanika*, 2002, Nr. 3 (35), pp. 20-25.
2. A. El Mahi, M.-K. Farooq, S. Sahraoui and A. Kondratas. "Cyclic fatigue tests of sandwich composite materials behaviour in three point bending." *Mechanika*, 2002, Nr.4 (36). pp.18-23.
3. M.-K. Farooq, A. El Mahi, S. Sahraoui and W. Ahmed . "Analysis of fatigue behaviour in sandwich composite materials.", *8th Portuguese Conference on Tribology*, , ***Keynote paper***: editors: J Gracio, P Davin, Q H Fan & N. Ali. ISBN NO 972-789-059, pp. 15-21, May 8-11, 2002.
4. M.-K. Farooq, A. El Mahi and S. Sahraoui. "Mechanical behaviour of sandwich composite material under cyclic fatigue. "*New trends in Fatigue and Fracture*, Metz, France, 8-9 April 2002.
5. M.-K. Farooq, A. El Mahi and S. Sahraoui. "Evaluation of fatigue behaviour in sandwich composite materials.", 10th *European Conference on Composite Materials ECCM/10*, Brugge, Belgium June 3-7, 2002.
6. M.-K. Farooq, A. El Mahi, S. Sahraoui and J.-M. Berthelot. "Fatigue behaviour of sandwich composite materials." *Ninth International Conference on composites Engineering, ICCE/9*, July 1-6, 2002 in San Diego. U.S.A.
7. M.-K. Farooq, A. El Mahi, and S. Sahraoui. "Analysis of flexural behaviour of sandwich composites under fatigue." *Matériaux 2002, Tours*, October 2002.
8. M.-K. Farooq, A. El Mahi and S. Sahraoui. "Effect of core thickness on mechanical properties of sandwich composite materials under fatigue.", *JNC13 AMAC, Strasbourg* 2003.
9. A. El Mahi, M.-K. Farooq, S. Sahraoui and J.-M. Berthelot. "Analyse expérimentale du comportement des matériaux sandwichs en flexion 3-points." *Colloque national de la recherche en IUT*, IUT de Tarbes, le 15 et 16 Mai 2003.
10. A. El Mahi, M.-K. Farooq, S. Sahraoui and J.-M. Berthelot. "Analyse du comportement des poutres en matériaux sandwichs en flexion trois points.", *16$^{ème}$ Congrès Français de Mécanique*, Nice, 1-5 Septembre 2003.
11. A. El Mahi, M.-K. Farooq, S. Sahraoui and A. R. Bezazi. "Modelling the flexural behaviour of sandwich composite materials under cyclic fatigue." *Journal of Material Design* (accepted for publication).
12. I. Gimenez, M.-K. Farooq, A. El Mahi, A. Kondratas and M. Assarar. "Experimental analysis of mechanical behaviour and damage development mechanisms of PVC foams in static tests", Submitted, *ISSN 1392-1320, Materials Science. Vol. X, No. X. 2003.*
13. M.-K. Farooq, A. El Mahi, A. Kondratas, M. Assarar, and I. Gimenez. "Experimental investigation of foams behaviour in fatigue tests.", Submitted, *ISSN 1392-1320, Materials Science. Vol. X, No. X. 2003.*
14. A. El Mahi, J.-M. Berthelot, A. Bezazi and M.-K. Farooq. "Reinforcement effect on fatigue behaviour and damage development in cross-ply laminates submitted to flexural loading." Submitted to Journal of *Composite Interfaces.*
15. A. El Mahi, A. Bezazi, J.-M. Berthelot and M.-K. Farooq. "Describing the flexural behaviour of cross-ply laminates under cyclic fatigue." Submitted to *Journal of Composites.*
16. A. El Mahi, M.-K. Farooq, M. Assarar and J.-M. Berthelot, "Comportement en flexion des poutres en matériaux sandwichs" Colloque Composite 2003, Octobre 2003, Paris.

# Table of contents

# Chapter 1
# Introduction

Sandwich composite materials are increasingly being used in a variety of industrial applications such as, marine, aerospace, automobile industry etc. The use of sandwich construction is the result of an increasing demand for light and strong structures, weight saving is a dominant factor in the transport sectors such as high speed trains, high speed boats, cars etc. A lower weight creates an opportunity to save fuel or carry more cargo. The design of a sandwich structure is based on two faces that take up tensile and compressive forces and give structure a stable surface and core material which transfers the shear forces. This sandwich concept has certain advantages over more conventional single skin laminated structures in terms of flexural stiffness at reduced weight. Flexural stiffness and strength are only two of a variety of design criteria to be considered. Other properties of a sandwich panel such as damage tolerance, compressive strength, resistance to water absorption, temperature behaviour and fire resistance, thermal and acoustic insulations are largely obtained by core materials. However, binding of dissimilar materials in a single component inevitably creates interfaces or in-homogeneity which may result in complex stress distribution and failure mechanisms.

Recent advances in materials and construction technique have resulted in further improvement and increased uniformity in sandwich properties. But this resulted in more complexity in mechanical behaviour during static and fatigue testing. With the introduction of new fibrous composite materials, the choice of face materials has become almost infinite in terms of mechanical properties. All material systems have some advantages and some disadvantages implying that choice of materials is given by objectives of specific application and can not be stated in general terms. Therefore, materials are often, in the practical case, already predefined by the service or manufacturing requirements of the structure. However, some material related properties are still to be considered as variables even if the material itself is predefined, e.g. types of skin materials, density and thickness of cores. Anyway, it is convenient to have certain methods, based on suitable parameters selection that can be used to optimise a sandwich panel for certain applications.

The complexity of micro-mechanisms of fatigue damage in sandwich composites necessitate a damage characterization based on a macroscopic set of parameters such as stiffness and residual strength. From a mechanical point of view, stiffness and strength are the properties that can be easily formulated. The gradual deterioration of sandwich composites during fatigue leads to a loss of stiffness in damaged zones which further caused a continuous redistribution of stresses and strains and a reduction of stress concentration inside a structure or component. As a consequence an appraisal of the actual state (when and where final failure is to be expected) requires a complete understanding of the complete path of successive damage states. For a sandwich panel, stiffness can be measured when the deformation is given as a function of applied load. The stiffness properties have been found to change continuously with fatigue cycles and

therefore could provide a basis for non destructive procedures for fatigue damage characterization. The strength on the other hand, depends on failure modes and is destructive in real a sense, which depends on the internal structure of sandwich as well as the applied load.

The contribution of this thesis is to develop tools and methods for the analysis of sandwich structure under static and fatigue loading. In a perspective view, these tools may be transformed into basis of further development in understanding the fatigue phenomenon. Several intermediate objectives had to be met in order to complete objectives. The present work is organised in seven chapters, with main emphasis given in chapters 4, 5, 6 and 7 in which both analytical and experimental work are described.

Chapter 2 is devoted to a detailed literature survey on previous and present status of research in the field of composite and sandwich composite materials with reference to static and fatigue testing. Main emphasis is focussed on the parameters which affect the fatigue lives of the sandwich composites materials. Different modelling approaches based on microscopic and macroscopic levels are presented.

Chapter 3 presents the materials that constitute a sandwich structure. Type of face materials, fibre and epoxy resins, types of core materials, their properties, and their role in sandwich structure are discussed and elaborated. Construction of sandwich composites using vacuum bagging technique is explained. Mechanical properties of the materials and instrumentation employed in experiments are presented.

Chapter 4 is concerned about the static tests performed for sandwich composites and their constituents i.e. skin and core materials. It is necessary to understand the mechanical behaviour of foams and skins separately in order to understand fully their role and influence in sandwich structure. Then it is possible to suggest the methods in which their performances can be improved. Therefore, static tests for foams in compression, indentation, shear and in three point bending were performed. Skins are also tested in flexural. Parameters obtained from static tests are then used for designing fatigue experiments. Fracture topography of foams and sandwich composites are presented.

Chapter 5 presents analytical studies of sandwich composites with reference to sandwich beam theory in three point bending. In engineering design of sandwich structures, deflections and stresses are very important parameters in reliability and serviceability evaluations of structures. Experimental and analytical approaches for deflections of the beams are discussed and implemented in detail. Sandwich beam theory is applied with experimental results obtained in static flexural testing. These experiments were conducted for sandwich specimens of various core thickness and different densities at different span lengths. A reasonable agreement was found between the classical beam theory and experimental results.

Chapter 6 deals with fatigue characterisation of skin, cores and sandwich composites. Fatigue characterisation is directed towards the component (constituents) material behaviour as well as global sandwich beam behaviour. The focus of this chapter is on the fatigue performance and characterisation of sandwich composites hence general fatigue tests methods are employed and fatigue result presentation is given for skins, cores and sandwich composites. Fatigue behaviour of skin and foam are analysed and then compared with overall sandwich composites response. In particular, a wide range of foam materials having different densities and core thickness are covered and effects of variables such as frequency, stress ratio, applied displacement levels are discussed. Fatigue results and hysteresis curves for foams are also presented for fatigue after indentation tests. Then results from fatigue tests on sandwich composite of various core thicknesses and densities are presented. These tests were performed under displacement and load control fatigue. Wöhler curves were plotted using $N_{10}$ criterion permitting to determine the fatigue life of sandwich composite materials. Finally, fractographic studies of the failed sandwich specimens are presented.

In chapter 7, a phenomenological stiffness model has been proposed, which describes fatigue life prediction and damage in terms of stiffness degradation. This model proposes methodologies which describe the gradual deterioration of stiffness in sandwich composites in terms of macroscopically observable properties. Stiffness base model accounts for degradation of elastic properties during fatigue. The proposed model is simple as a single valued stiffness property is predicted. Model results describe well the experimental results and were validated for sandwich specimens of three foam densities under load and displacement control fatigue. In spite of scatter in data, which is quite common in fatigue testing, a reasonable agreement was observed between experimental and theoretical results.

A brief summary of the results is presented in the last chapter 8.

# Chapter 2
# Literature survey

## 2.1 Introduction

The concept of combining two different materials to make a new material with properties greater than those found in either of the individual components is not new. Centuries ago wattle and daub (interlocking twigs and clay) was used as a building material for houses, and papier-mâché (a combination of paper pulp and paste) has long been used as a hard strong moulding material. During the decades, starting with the second world war, the development in the field of construction utilising the principle of sandwich has been tremendous. A main reason for the tremendous development in the field of sandwich construction is the development of new materials and methods using fibre reinforced plastics in sandwich structures. A structural sandwich is a special form of a laminated composite comprising a combination of different materials that are bonded to each other so as to utilise the properties of each separate component to the structural advantage of the whole assembly. Typically a sandwich composite consists of three main parts; two thin, stiff and strong faces separated by a thick, light and weaker core. The faces are adhesively bonded to the core to obtain a load transfer between the components. The combination of a PVC or honeycomb core bonded to skins made of either composites or metals produces a sandwich structure which supports greater loads than either the core or the skins can support on their own.

Modern structural design increasingly incorporates man made composite materials in applications that require components with special materials properties, which are unavailable from conventional metals or alloys. From a structural point of view, composite materials are typically used to improve the stiffness or strength to weight ratio of a structural member. They are often fabricated in the form of plies stacked at desired thickness, called as laminates. Laminated composite materials provide the designer with freedom to tailor the properties and response of the structure for given loads to obtain the maximum weight efficiency. In addition, the variation in lay-up configurations of laminated composite structures allows the designer greater flexibility when incorporating materials into a structure. With the flexibility, however comes added complexity in analysis of composite structures. In particular damage and failure mechanisms under fatigue are very complicated as compared to that of conventional metallic materials. Metal fatigue usually results in cracking of the material, however when composites are fatigued, a more complex form of damage occurs. This is usually in the form of damage that includes matrix cracks, fibre/matrix debonding, fibre fractures and delamination growth. Optimisation of composite structures often involves a large number of design variables. Laminate stacking sequence optimisation using discrete thickness and ply angles is a combinatorial design problem. Laminates optimised using a small number of load cases often are highly tailored to the loading and can perform very poorly in off design conditions. Furthermore, composite laminates exhibit a variety of failure modes that are difficult to model or analyse. Designers in such cases have to rely on data obtained from experiments.

From a structural mechanics viewpoint, sandwich composites are typically used to improve either the stiffness or strength to weight ratio of a structure or a component. Composite properties, e.g. strength and stiffness, are highly dependent upon volume fraction of fibre, and individual properties of fibre, matrix and core materials. Sandwich composite structure may vary their stiffness and strength due to damage accumulation such as matrix cracking, fibre breakage, skin/core debonding, core cracking during the loading history of the sandwich composite members.

## 2.2 Present status of research

A significant prior literature survey has been conducted in order to see the current status of research in the field of laminate composites and sandwich composites materials. It is observed that there is no considerable research work published in the field of sandwich composite materials with reference to fatigue and failure mechanisms. Predictions of fatigue damage and fatigue life are the main areas of research found in the literature. The aim of such research was to establish a process requiring a minimum of experimental data which reliably predicts the condition of the material. Existing fatigue theories can be classified in four categories [1]:

1. Macroscopic failure theories based on static strength criteria modified to account for cyclic loading.
2. Strength degradation fatigue theories, where the damage metric (measure) is the residual strength of composite material after a cyclic program. According to these theories, a failure occurs when the residual strength decreases to the maximum applied cyclic stress.
3. Stiffness change fatigue theories are those assuming stiffness degradation as a fatigue metric. The superiority of these methods, compared to strength degradation based ones, lies in their non-destructive evaluation of fatigue damage growth. Residual strength demonstrates minimal decrease with the number of cycles until a stage close to the end of lifetime when it begins to change rapidly. On the other hand, stiffness exhibits greater changes during loading.
4. Actual damage mechanisms fatigue theories (quite expensive and time consuming).

During the process of reviewing the fatigue related studies significant test parameters were revealed, which defined the individual tests. These test parameters are the type of fibre reinforcement, types of resins, loading frequency, types of load control, specimen geometry, stress ratio, etc. Other parameters of interest are percentage of fibre volume or weight ratio, failure criteria and number of tests representing each data point and failure strain. Too many combinations of these test parameters exist among the fatigue tests to distinguish the effect of an individual parameter on fatigue life and damage. This review looks at the factors that impede adaptation of sandwich composite material to general purpose industrial application.

For the purpose of understanding the overall mechanisms of sandwich composites materials, a detailed review is presented for all the material types which constitute a

sandwich composite such as skins and cores. The present review focuses on the methods to characterise fatigue both on a macroscopic for design purposes and microscopically on the materials level. The skins (laminates) are constructed from glass fibre embedded in epoxy resins. The core materials are closed cell PVC foams. In order to understand the behaviour of sandwich composite as a whole, a thorough understanding of fatigue behaviour in laminates composites as well as in foam cores is necessary. In the subsequent sections, a review of useful test methods for structures is presented and their advantages and shortcomings discussed and highlighted.

## 2.3 Fatigue in composite materials

Fatigue failure is the most common type of failure in service loading of structural materials. Therefore, an important objective of fatigue research is to predict the fatigue performance of composites and sandwich composite materials in order to design damage tolerant structures. Fatigue damage mechanisms in composite materials are considerably more complicated then those of metallic materials. They usually involve various combinations of damage such as matrix cracking, interfacial debonding and fibre breakage. Therefore, it is difficult to develop a theory that can predict the exact type of failure. However, these damage modes have been found to cause changes in materials properties, such as the residual stiffness, strength and life. Thus, it is possible to obtain a measure of damage in composite by measuring and analysing the changes in these properties during fatigue testing.

From a maintenance point of view, it is important to determine non-destructively the extent of fatigue damage that is accumulated after a certain period in a structure or component under service loading conditions. The residual stiffness is a well defined engineering property, which can easily be measured and interpreted. Stiffness changes are directly related to damage development, and may possibly be used to predict the failure. The stiffness is a parameter that can be monitored non-destructively and now becomes a powerful tool in assessing the reliability of a composite structure. The stiffness can be measured directly during damage development. However, a comprehensive data base would be required in fatigue analysis of composite materials, based on stiffness reduction, unless a mathematical relationship can be developed to relate residual stiffness to other material properties such as the residual strength and fatigue life. If such a relationship could be established, extrapolation of data at various stress levels would be possible, thus reducing the amount of test data needed to characterise the material behaviour [2]. However, reliable stiffness degradation models need to be developed before such relations can be established. In the following section, a review of different experimental conditions, which may affect the experimental results, is presented. It is necessary to have knowledge of fatigue parameters such as loading frequency, stress ratios, applied loading level etc, so that correct and meaningful experimental procedures can be adopted.

## 2.4 Effects of experimental parameters

### 2.4.1 Frequency effects

Under cyclic loading, particularly for viscoelastic materials, increasing the frequency increases the rate of mechanical working thus increasing the rate of internal heating. This hysteresis heating effect, which can be detected by an increase in surface temperature of the specimen, is particularly apparent in polymeric materials, resin rich (low volume fraction) laminates or resin dominated (angle ply) lay up because resins are less able to dissipate heat then glass. The temperature increases until either thermal softening occurs, leading to thermal failure caused by severe degradation of materials properties due to internal heating, or the temperature stabilises (heat generated by mechanical working equal to heat dissipation) with mechanical failure occurring. Fatigue failures for many materials at room temperature and at modest frequencies are typically associated with mechanical failures due to gradual embrittlement or damage accumulation due to cyclic nature of the load. Thicker specimens produce a large temperature increase because heat must be transformed through the specimen to surface before it can be dissipated. From a fatigue point of view, the change over from thermal to mechanical behaviour in terms of failure mode is a function of the materials ability to dissipate heat and its softening temperature. Generally, the effect of frequency on fatigue life of the material can be separated into two regimes. In higher frequency region, the fatigue life of the material is reduced because an increase in material temperature can cause the static properties of the material to degrade. Eventually with increasing frequency, the materials fail by thermal mechanisms. In the lower frequency region, the frequency is low enough so that the effect of heat on material properties is negligible and as frequency decreases, the fatigue life decreases as creep-fatigue interaction effects becomes apparent. This has obvious implication for sandwich structures; where due to insulation properties of the core, heat build up is likely and testing frequencies must be kept minimal so that heating effects do not occur [3].

Studies on frequency effect on composite materials have been inconclusive because of variable experimental results. Some fatigue frequency investigations have shown that higher frequencies produced higher cycles-to-failure, other works have shown the inverse. Hohne and Mandell [4,5] studied load frequency (square wave type) effects for cross-ply E-glass/epoxy laminates. They observed that the fatigue life increased with increasing load frequency. Rotem [6], however, observed a 10 times decrease in fatigue life when the frequency increased from 2.8 to 10 Hz for a quasi-isotropic T300/934 graphite/epoxy laminates at R=-1.0. He attributed the decrease in fatigue life to hysterisis heating at the free edges. Demers [7], has evaluated fatigue frequency effect on specimen heating during cycling for E-glass fibre system. Results reported in table 1 indicate a change in temperature up to about 24°C at 3Hz and 60% of ultimate tensile strength [8]. Similar studies by McBagonluri *et al.* [9] did not show this trend for E-glass/vinylester. In fact, they observed that increase in temperature did not exceed 5°C and there was no significant heating between 2 and 10 Hz respectively.

***Table 2.1.*** *Fatigue frequency effect on specimens heating [8].*

| $\sigma_{max}/\sigma_{ult}$ | Stress ratio R | Frequency (Hz) | Max ΔT (C°)[a] |
|---|---|---|---|
| 0.8 | 0.1 | 1 | 8 |
| 0.8 | 0.1 | 3 | 11 |
| 0.8 | 0.1 | 5 | 11 |
| 0.8 | 0.5 | 3.5 | 3 |
| 0.6 | 0.05,0.1 | 1 | 8 |
| 0.6 | 0.1 | 3 | 24 |
| 0.6 | 0.1 | 5 | 21 |
| 0.6 | 0.5 | 3 | 5 |
| 0.6 | 0.5 | 5 | 4 |
| 0.4 | 0.1 | 5 | 12 |
| 0.4 | 0.5 | 5 | 1 |

#### *2.4.1.1 Effect of frequency in laminate composites*

In laminates, the effect of frequency largely depends on the strain rate in the matrix. In glass/epoxy laminates, Ellyin *et al.* [10] observed a noticeable frequency effect for angle-ply laminates which was much less significant for multidirectional ones. This trend was also observed for graphite/epoxy laminates [11]. Thus testing frequency up to 5.0 Hz is possible for resin dominated laminates angle ply laminates but with unidirectional laminates, the matrix strain is significantly reduced and testing frequencies up to 10 Hz are feasible [12]. Above the appropriate testing frequency, the temperature increases in the matrix cause premature fatigue failure. Mandell and Meier [5] observed that for a [0/90] glass/epoxy laminate, the fatigue life decreases with decreasing frequency (1Hz-0.01 Hz) due to increasing influence of creep. However, at low stresses corresponding to a lifetime greater than $10^6$ cycles, the *S-N* curve for each frequency converges.

Ellyin *et al.* [13] examined qualitatively the rate and frequency effects on the stress-strain response of unidirectional tested at 45° fibre orientation, [±45°] angle ply, and multidirectional [±45°,0°] fibre glass/epoxy laminates during tensile and fatigue loadings. Laminates with 0° layers, always exhibited fibre dominated brittle failure mode. This type of failure mode was considered independent of rate/frequency of loading. While matrix dominated failure was rate/frequency dominated due to viscoelastic matrix behaviour. The damage development associated with matrix and matrix-fibre interface cracking involved inelastic resin deformation, which was accompanied by relaxation and creep phenomena. The results from stress-strain behaviour for angle ply [±45°] showed that strain rate became more pronounced with the decreasing tangent modulus of stress strain curve in the higher stress levels. Due to matrix dominated deformation of angle ply laminates; the strain rate effects carry over fatigue performance indicated significant influence of frequency. While for

multidirectional laminates [±45°,0°], the results showed, no significant effect was observed for low and high frequency used in this study for fatigue life. The possible reason was due to constraining action of 0° plies that showed no significant cyclic creep. It was observed from the results that at low stress levels the fatigue life decreased and the cyclic creep rate increased with reduced frequency. While at higher stresses an opposite trend was observed. Therefore, they concluded that frequency effect on fatigue behaviour was a function of cyclic creep and this strongly depended on the stacking sequence of laminates and loading conditions.

Results presented by Cornelia [14], suggested that greater fatigue life was obtained with test frequency 0-2 Hz than with test frequencies 5 Hz and the difference decreases as fatigue life increases. For stress ratios $R$ ($d_{min}/d_{max}$) equal to 0.1 and test frequency of 3 or 5 Hz, the maximum difference between specimen surface temperature and room temperature was recorded as: 12°C for normalised maximum stress of 0.4; 24°C for normalised maximum stress of 0.6; 11°C for normalised maximum stress of 0.8. While for the same value of $R$, but for 1 Hz frequency, the difference of temperature was recorded as 8°C.

#### *2.4.1.2 Effect of frequency in sandwich composites*

Sandwich composites are now widely employed in engineering structures that serve under a wide range of loading conditions and environments. Furthermore, since many structures are subjected to cyclic or variable loading conditions, information about fatigue strength is particularly important. In foam core sandwich structures, the core material is usually more sensitive to temperature than facing. The precise nature of frequency effect of loading rate is little known in sandwich composite materials. Cellular foams, like solid polymers, are known to have excellent insulation properties. Thus, internally generated heat due to mechanical working is not easily dissipated to surroundings. Frequency effects vary with the types of the foams, especially in cases where linear thermoplastic foam are used instead of cross-linked thermoset foams. Thermoplastics by virtue of the fact that they can be reformed upon heating to suitable level, usually have reduced temperature capabilities. In particular, the point at which the mechanical properties can start degrade, for a linear Airex R36.80, can be as low as 60°C. Temperature rise in typical structural foam core material (Divinycel H250) have been measured by Olsson and Lonno [15]. For loading at 45% of the ultimate shear stress value, temperature rise of 6° and 20°C were observed at frequencies of 1 and 5Hz respectively. The deterioration of core shear properties with increasing core temperature for a variety of structural foam is well documented by Challis *et al.* [16]. The results show that a decrease in shear strength approximately 3% and 10% corresponds to temperature of 10° and 20°C respectively.

### 2.4.2 Effect of stress ratio

The applied stress ratio has a considerable influence on the fatigue life of composite and sandwich composite materials. There are various types of loading forms, more

commonly used are tension-tension, compression-compression or tension-compression. It has been established for majority of composite materials that compressive loading is more damaging than tensile loading. Stress ratios with negative values of minimum stress tend to yield shortest fatigue lives. Several authors have investigated the effect of stress ratio on composite laminates [5,13,17]. Mandel and Meier [13] have tested [0/90°] E-glass epoxy specimens for positive values of stress ratios between 0 and 1. Increasing the stress ratio in this range increases the fatigue life until a steady constant load is achieved i.e. $R$ = 1. This indicated that cyclic load is more damaging than a constant uniform load. El Kadi and Ellyin [17] carried out tests on glass/epoxy unidirectional laminates with varying orientations to the applied load axis at three stress ratios, R = 0.5, 0 and -1. They concluded that slopes of the *S-N* curves were greater for small stress ratios and for $R$ = -1, the tensile and compressive parts do not contribute equally to damage. Rotem [6], using new concept called 'fatigue envelope', has formulated a predictive tool enabling the prediction of *S-N* behaviour of any laminate under any load ratio based on two sets of experimental results for the same material under tension-tension loading and compression-compression loading. Amore *et al.* [18] also studied the effect of stress ratio on flexural fatigue behaviour of composites. It was reported that higher the $R$, the higher the number of cycles to failure. Passing from $R$ = 0.1 to $R$ = 0.7 resulted in a two decade increase in fatigue life. Burman and Zenkert [19] studied the influence of stress ratio on crack propagation in sandwich structures. They concluded that at values of $R$ less than zero, fatigue lives were shorter and crack propagate in two directions rather than one direction for stress ratios above zero.

## 2.5 Modelling approaches

### 2.5.1 Introduction

An important objective of fatigue research is to predict the fatigue performance of the materials in order to design-tolerant structures. A best approach to achieve this objective is to first understand the mechanism of damage inception and growth and then with this knowledge to develop models that can form a basis for calculations of fatigue performance and design. Fatigue models can be generally classified into three major categories [1]:

- Fatigue life models, which do not take into account the actual degradation mechanisms but use *S-N* curves (influence of stress amplitude on occurrence of final failure) or Goodman–type diagrams (influence of mean stress level) and introduce some sort of fatigue failure criterion.
- Phenomenological models for residual strength and stiffness degradation, which describe the degradation of initial static strength and stiffness during a test.
- Damage accumulation models that use one or more damage variables related to measurable manifestations of damage (number of transverse matrix cracks, delamination size) or to the residual stiffness. The study of the development of these cracks provides information on fatigue damage.

### 2.5.2 Micro-mechanical modelling

Damage in composite materials occurs through different mechanisms that are complex and usually involve interaction between micro constituents. During the past two decades, a number of models have been developed to simulate damage and failure processes in composites, among which the damage-mechanics approach is particularly attractive in the sense that it provides a viable framework for the description of distributed damage including material stiffness degradation, initiation, growth and coalescence of microcracks and voids. The study of composite materials and structures can be undertaken from two different approaches: micromechanical and macromechanical approaches. In micromechanical approach, the constituent fibre and matrix materials, and their interaction are distinctively considered to predict the overall behaviour of composite structural member. The damage and failure in composites are modelled at fibre and matrix level.

Recently, an extensive comprehensive review on micromechanical modelling of transverse cracking and delamination in cross ply glass fibre and carbon fibre reinforced plastic laminates was presented by Berthelot [20]. The author presented his modelling approaches along with others researchers modelling work. The development of transverse cracking in cross ply laminates has been evaluated by considering either a stress based approach or fracture mechanics approach. In fact these two concepts are related but the development of models differs due to analysis of strength distribution in the cracked laminates. Different models of the development of transverse cracking during monotonic loading have been implemented

Sullivan *et al.* [21] studied periodic hexagonal arrays using the finite element method to investigate the effects of specific fibre-matrix debonding and fibres. They concluded that the fibre-matrix debonding affected the bundle transverse properties significantly, especially for unidirectional composites with high volume fractions, but the wedge opening angle affected the properties very little. Averill and Carman [22] obtained the elasticity solution of micromechanical stresses for fibres in a regular periodic array. The model considers several factors, e.g. fibre-fibre interaction, multiple interfaces and hygro-thermaly dependent material properties. Using this model, they computed the effective material properties of a composite; this model was less numerically sensitive then the finite element method for the case of thick interface. An optimum interphase stiffness was determined from this model to result in smaller stress concentration in the matrix region.

Jones [23] studied the transverse matrix cracking in cross-ply and angle ply composites using a micromechanical analysis. He investigated the effects of matrix failure strain, constraint cracking, thermal strain, and stress due to Poisson's effect and longitudinal splitting on the first transverse matrix cracking. Sorensen *et al*. [24] performed a finite element analysis to investigate the sliding mechanics of a smooth fibre-matrix interface of unidirectional ceramic-matrix composites under mechanical and thermal loading. They considered a representative cylindrical volume element

consisting of a fibre and surrounding matrix, and they assumed the coulomb friction between the fibre and matrix interface. Their analysis showed that the tangential modulus during the sliding loading was lower then that from the rule of mixtures by 10% while tangential modulus during sliding unloading was higher than that from the rule of mixture by 10%. This characteristic agreed with experimental findings. A micromechanical approach using finite element method was performed by King *et al.* [25] to examine the effects of matrix and interfacial bonding strength on the shear strength of composite. Their numerical results were comparable to the experimental data. They concluded the micromechanical approach was valuable tool to predict the constituent and interface effects on the composite shear strength.

However, in order to study the damage evolution for composite structures more simplified form of micromechanical models are necessary. In order to represent the average micro-level state of deformation, stress and micro damage at any point of a composite structure, simplified micromechanical models should computationally efficient while maintaining accuracy. Aboudi [26-28] developed his micromechanical unit cell model to compute effective moduli of composite made of non-linear deformations of constituents, and extended the model to predict the strength and fatigue failure of composites. His model was based on representative unit cell of rectangular shape. The unit cell consisted of four subshells. He assumed a linear variation of displacement within each subshell in terms of local co-ordinate axes. Then, he applied the continuity of displacements and tractions at the interfaces of the subshells in terms of average values. The development of his micromechanical model was very elaborate, but lot of mathematics was involved.

Dvorak [29,30] proposed a vanishing fibre diameter micromechanical model to study the non-linear behaviour of composite. The model consisted of continuum matrix reinforced by cylindrical fibres of vanishing diameters. However, the total fibres occupied a finite volume fraction. Using the model, they studied the yield surfaces of fibrous composites. Kwon and his co-workers [31] derived simplified two dimensional and three dimensional micromechanical models to analyse materially non linear behaviour of composites plates subjected to in-plane or bending loads. Elasto-plastic or elasto-viscoplastic deformation was studies. The micromechanics model considered a representative cell having constant matrix stresses and constant fibre stresses. This micromechanical model was modified later to have stress variation at the matrix surrounding a fibre. The matrix was divided into subcells. The model predicts the effective modulus of fibrous composites, with or without micro damages, very well.

Kwon *et al.*[32] developed a micromechanical model for damage and failure analyses of laminated fibrous composite structures. The micromechanics model provided useful micro-level fibre and matrix stresses. The fibre and matrix stresses were used for failure criteria to investigate failure and damage progress in laminated fibrous composite structures. Progress of damage, as well as final failure loads were computed from present model, which was incorporated into finite element analysis program. The micromechanics model along with the failure criteria could provide the following

important information for study of failure and damage progress, stress redistribution due to local damage and ultimate failure load.

Berthelot *et al.* [33, 34] used a stress based approach to analyse the development of transverse cracking in glass fibre laminates and carbon fibre laminates. First, a deterministic strength criterion was used for propagation of transverse cracking and stress distribution in the cracked laminates was evaluated using Hashin's analysis, 2D progressive shear analysis and finite element analysis. The results obtained were compared with experimental results. In the case of carbon-fibre/epoxy laminates, different analyses lead to similar results at the beginning of the development of transverse cracking. When the crack density increases, results are fairly well described by finite element analysis and 2D progressive shear analysis. However, results obtained by Hashin's analysis are notably different. While, in the case of glass-fibre/laminates, initially results from all analysis are found consistent with carbon-fibre laminates, but at the later stage, progressive saturation process of transverse cracking is observed. Next, considering the previous results, a analytical analysis of initiation and development of damage was implemented by the authors, considering also the delamination processes induced at the tip of the transverse cracks. Hashin's analysis described very well the saturation process, when compared to finite element analysis and 2D analysis.

These micromechanics studies are useful to understand the micromechanical factors affecting the effective composite behaviour. However these studies can not be applied to examine the damage evolution and failure of laminated composite structures subjected to general loads in a practical sense because of totally different dimensions of fibre and structure. The state of stresses varies from point to point at the structural level and fibre direction changes from layer to layer. Consequently, the detailed micromechanical study is practically difficult for a general structure unless the states of stresses and fibre direction remain constant within a composite structure.

### 2.5.3 Macro-mechanical modelling

#### *2.5.3.1 Introduction*

The complexity of micromechanisms of fatigue damage in fibrous composites necessitates a damage characterisation based on macroscopically measurable set of parameters. The two procedures for characterisation the materials on macro level have been based on strength degradation and stiffness degradation approaches. In the macromechanical approach, the properties of constituent fibre and matrix materials are averaged or smeared to produce a set of pseudo-homogeneous properties for composite structural member. The macromechanical approach does not consider the distinctive modelling of the fibre and matrix materials. The damage and failure of composite structures are examined on smeared composite stresses and strains. The macromechanical approach has the advantage of requiring less detailed modelling then micromechanical approach.

### *2.5.3.2 Residual strength degradation models*

In literature residual strength models were also named as phenomenological models by many authors to characterise residual strength and life in terms of macroscopically observable properties, such as strength and stiffness. This approach is mainly based on acquiring the large amounts of experimental inputs for each material, lay-up geometry, loading conditions and in extrapolation to different conditions. Many life prediction methods have been based on residual strength degradation. These have been developed on the basis of one or more of the following assumptions [35]:

- The statistical variability of static strength of the material can be described by two parameter Weibull distributions.
- The residual strength after *N* cycles of fatigue loading can be related to the static strength by deterministic equation.
- When the residual strength decreases to maximum applied stress, fatigue failure occurs.

Hwang and Han [36] suggested four requirements for universal fatigue damage model:

1. It should explain fatigue phenomena at an applied stress level.
2. It should explain fatigue phenomena for an over all applied stress range. During a cycle at high applied stress level the material should be more damaged than that at low applied stress level. If it is true that failure occurs at applied stress level, then the final damage (damage just before failure) at a low applied stress level should be larger than that of a high applied stress level.
3. It should explain multi-stress level fatigue phenomena.
4. It is desirable to establish the fatigue damage model without *S*-*N* curves.

In the residual strength degradation approach, fatigue failure is typically assumed to occur when the residual strength becomes equal to the applied maximum stress amplitude. Such an approach was used by Broutman and Sahu [37], who proposed a cumulative damage theory based on a linear strength degradation approach to explain the fatigue damage of fibre glass reinforced composites. Using this approach, they were able to make predictions for residual strength of laminates, which were subjected to low-high, high-low stress tests. These predictions were compared with the experimentally measured residual strengths.

Reifsnider [38] and his co-workers proposed a mechanistic non-linear residual strength prediction based on critical element model. In this model, a representative volume was selected which was typical of the material in question. This representative volume may contain damage, such as matrix cracks, delamination, fibres fracture, but some part of it still retains the ability to carry load. It is the failure of this part of representative volume, the so-called "critical element", which determines the fracture of the entire representative volume. The remaining strength of the critical element was

calculated by using a non-linear damage evolution equation that accounts for the changing stress amplitude in the critical element. The prediction of the model was compared with laboratory data for polymeric as well as ceramic composite systems. The general approach given by Reifsnider was extended by Subramanian *et al.* [39] to include the effects of an interphace region on the tensile fatigue behaviour of composite laminates. The effect of this interphace region was modelled by the introduction of an "efficiency" parameter, which was taken to be a measure of displacement transfer between fibre and the matrix. The effect of this efficiency parameter on the tensile strength was assessed using micromechanical tensile strength model. Changes in the interphase property were used in conjunction with a maximum strain criterion to determine the fatigue life of the laminate.

According to Rotem [40], the initial static strength is maintained almost up to final failure by fatigue. He then defined an imaginary strength $S_0$ in the first loading cycle, which has higher value than the static strength. If the *S-N* curve for tension-tension fatigue of graphite/epoxy laminates is expressed as:

$$s = 1 + K.\log(N) \tag{2.1}$$

Where $s = S_f / S_0$ with $S_f$ the fatigue strength for constant amplitude and $S_0$ the imaginary strength, then the remaining fatigue life after certain amount of load cycles can be given by a curve similar to *S-N* curve, but with different slope and passing through point $S_0$. Such a curve called a damage line and family of such damage lines is defined by:

$$s = 1 + k.\log(N) \quad k < K \tag{2.2}$$

As long as the degradation of the residual strength is situated in the region between the imaginary strength and the actual strength, there is no apparent degradation of the strength.

Extensive experimental and theoretical research has been done by Schaff *et al.* [41,42]. They presented a strength based wearout model for predicting residual strength and life of composite structures subjected to constant amplitude and spectrum loading. The model was derived based on the fundamental assumption that strength was monotonically function of the number of cycles, and that both the distribution of fatigue due to constant amplitude loading and the residual strength distribution after an arbitrary load history could be represented by two parameter Weibull functions. The following model for residual strength was proposed.

$$R(n) = R_0 - (R_0 - S_p)\left(\frac{n}{N}\right)^{\upsilon} \tag{2.3}$$

Where $R$ is the residual strength, $S_p$ is the peak stress magnitude of the loading and $\upsilon$ is a parameter. Linear strength degradation corresponds to $\upsilon$ =1. Sudden death behaviour obtained for $\upsilon >> 1$, and rapid initial loss in strength is obtained for $\upsilon < 1$.

The model was applied first to two stress amplitude fatigue loading. Because decrease of strength under stress level $S_2$ depends on the number of cycles $n_1$ that the material has previously sustained under the stress level $S_1$, the contribution of ($S_1$, $n_1$) has to be considered. Therefore an effective number of cycles $n_{eff}$ has been defined, such that ($S_1$, $n_1$) causes same decrease of strength as ($S_2$, $n_{eff}$). The model shows good correlation to variety of experimental results.

A residual strength degradation model was proposed to predict the fatigue life of composite materials [18]. An equation, explicitly accounting for stress ratio, is proposed in order to express analytically the strength variation during fatigue. Then the critical number of cycles for catastrophic failure was calculated, equalling the maximum applied stress during fatigue and material residual strength. The hypothesis for their damage law is that decrease in material strength as a function of number of cycles was described by a power law and can be written as:

$$\frac{d\sigma_n}{dn} = -a.n^{-b} \tag{2.4}$$

Where $\sigma_n$ was the residual material strength after $n$ cycles and $a$, $b$ are constants. The constant $b$ is only dependent on the material type and loading conditions, whereas '$a$' linearly increases with stress amplitude. Integrating equation (2.4), and introducing stress ratio $R = \sigma_{\min}/\sigma_{\max}$, following equation was obtained by applying the boundary conditions

$$\sigma_0 - \sigma_n = \alpha.\sigma_{\max}.(1-R)(n^{\beta} - 1) \tag{2.5}$$

The evolution of strength degradation with fatigue can be calculated by using equation (2.5) when constants $\alpha$ and $\beta$ are known. The critical number of cycles for failure, $N$, can be calculated by putting $\sigma_n = \sigma_{\max}$ in equation (2.5). Solving for $N$, we obtain:

$$N = \left[1 + \frac{1}{\alpha.(1-R)}.\left(\frac{\sigma_0}{\sigma_{\max}} - 1\right)\right]^{1/\beta} \tag{2.6}$$

From this equation it is important to observe that, the stress amplitude uniquely governs the strength degradation, the number of cycles to failure is affected by the stress ratio and the maximum applied stress.

In the later papers by the same authors [43,44], to resort to a statistical analysis of fatigue data, a method conceptually similar to that presented in reference [18] was followed. It was assumed that probability of failure of virgin material follows a two parameter Weibull distribution. Moreover, in agreement with strength-life equal rank assumption [45], it was postulated that scatter in fatigue life is correlated with the scatter in monotonic strength, in the sense, that for fixed test conditions, a lower ultimate strength results in lower fatigue life. Of course, in this case $N$ is also statistical

variable, as appears from equation (2.6). The expected number of cycles to failure $N^*$ pertaining to a given probability of failure $F_N(N^*)$ was obtained as:

$$N^* = \sqrt[\beta]{1+\frac{1}{\alpha(1-1/R)}\left\{\frac{\gamma}{\sigma_{\max}}\left|\ln\left[1-F_N(N^*)\right]\right|^{\frac{1}{\delta}}-1\right\}} \tag{2.7}$$

Where $\gamma$ and $\delta$ are the scale parameters (or characteristic strength) and the shape parameter of two-parameter Weibull distribution of the monotonic strength. The ultimate strength can be written:

$$\sigma_0 = \sigma_{0N} = \sigma_{\max}.\left[1+\alpha(1-R)(N^{\beta}-1)\right] \tag{2.8}$$

From a physical point of view, equation (2.8) indicates that the ultimate strength of virgin material can be calculated from the fatigue life $N$. The symbol $\sigma_{0N}$ has been used in equation (2.8) just to distinguish the calculated strength from that $\sigma_0$, directly measured in a static characteristic test. Finally, the distribution of $\sigma_{0N}$ was compared with $\sigma_0$ obtained from monotonic tests, a good agreement was found.

The fatigue behaviour of a composite lamina varies under different states of stress. For instance under high level state of stress, the residual strength as a function of number of cycles is nearly constant and it decreases drastically at the number of cycles to failure. The sudden death model has been used to describe this behaviour. However, at low level state of stress the residual strength of the lamina, as a function of number of cycles, degrades gradually as can be seen in figure 1.

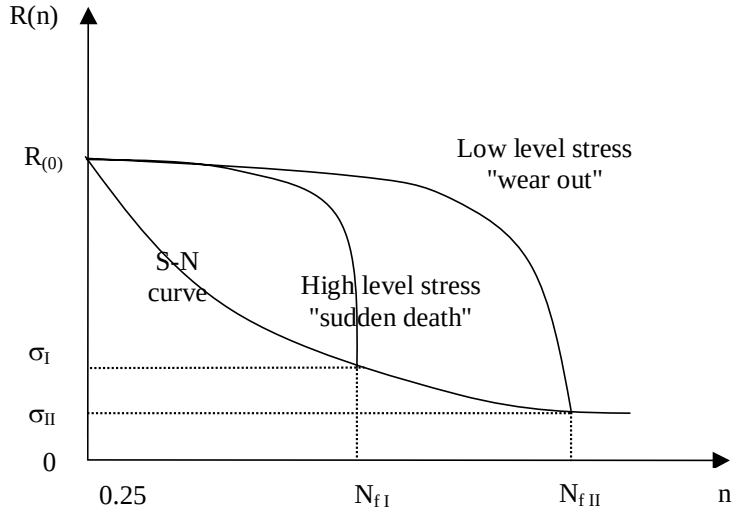


***Figure 1.*** *Strength degradation under different states of stress.*

The wear out model has been used to present this behaviour. These two models represents extremes in the observations of fatigue degradation representing sudden and more gradual behaviour, thus are not implied to be comprehensive list of failure modes.

Shokreih *et al.*[46] developed a residual strength model based on multiaxial fatigue behaviour of unidirectional plies. They had made comparison of different models already presented in the literature and considered only mechanistic characteristics. In the wear out model, which was initially presented by Haplin *et al.* [47], it is assumed that residual strength (*R(n)*) is a monotonically decreasing function of number of cycles (*n*), and the change of residual strength is approximated by a power-law equation:

$$\frac{dR(n)}{dn} = \frac{-A(\sigma)}{m}\left[R(n)\right]^{m-1} \tag{2.9}$$

In which $A(\sigma)$ is function of the maximum cyclic stress (σ), and *m* is constant. Many authors have used this model. By integrating equation (2.9) and using boundary conditions and considering that the number of cycles to failure ($N_f$), the residual strength ($R(n)$) is equal to applied stress (σ), equation (2.9) reduces to:

$$R^m(n) = R^m(0) - \frac{R^m(0) - \sigma^m}{N_f} n \tag{2.10}$$

Equation (2.10) expresses the residual strength ($R(n)$), as a function of static strength ($R(0)$), the number of cycles ($n$), and number of cycles to failure ($N_f$). In addition, *m* is constant which is found experimentally. For different states of stresses *m* has different values. For comparing between different models proposed by different authors, equation (2.10) can be written in the form

$$\frac{R^m(n) - \sigma^m}{R^m(0) - \sigma^m} = 1 - \frac{n}{N_f} \tag{2.11}$$

Equation (2.11) is a normalised form of equation (2.10), which can be used for the purpose of comparing different models.

A summery of the residual strength models obtained from the available literature is presented in the form of a table 2.1. As shown in table 2.1, Hahn and Kim [48], Yang *et al.* [49], Chou and Croman [50,51] and Sendeckyj [52] applied exactly same model proposed by Haplin *et al.* [47]. Broutman and Sahu [37] assumed a linear relationship between the fatigue strength and number of cycles. This assumption is neither inconsistent with experimental evidence of strength degradation at low level state of stress nor at high level state of stress. In a model presented by Daniel *et al.* [53] an undefined function of normalised number of cycles "g" is introduced. There is no effort in their paper to define the function. In algebraic equation, a reduced form of integral equation proposed by Reifsnider and Stinchcomb [54] and Reifsnider [55-57], 'K' is curve fitting parameter which must be found experimentally. Adam *et al.* [58] presented a normalised equation consisting of two curve fitting parameters. They showed that '$\alpha$' and '$\beta$' are stress independent curve fitting parameters which must be found experimentally.

***Table 1.*** *A summery of different strength degradation models.*

| References | Models | Explanation |
|---|---|---|
| Halpin *et al* [47]<br>Hahn and Kim[48]<br>Yang *et al*[49].<br>Chou and Croman[51]<br>Sendeckyj[52] | $\frac{R^m(n)-\sigma^m}{R^m(0)-\sigma^m}=1-\frac{n}{N_f}$ | 'm' is a curve fitting parameter, found experimentally |
| Broutman and Sahu[37] | $\frac{R(n)-\sigma}{R(0)-\sigma}=1-\frac{n}{N_f}$ | Linear strength degradation |
| Daniel *et al*[53]. | $\frac{R(n)-\sigma}{R(0)-\sigma}=g\left(\frac{n}{N_f}\right)$ | $g\left(\frac{n}{N_f}\right)$ is undefined function |
| Reifsnider and Stinchomb[54]<br>Reifsnider[55] | $\frac{R(n)-\sigma}{R(0)-\sigma}=1-\left(\frac{n}{N_f}\right)^k$ | 'k' is a curve fitting parameter, found experimentally |
| Harris *et al*[58] | $\left(\frac{R(n)-\sigma}{R(0)-\sigma}\right)^\alpha=1-\left(\frac{\log(n)-\log(0.5)}{\log(N_f)-\log(0.5)}\right)^\beta$ | 'α' and 'β' are two curve fitting parameters, found experimentally |

Notes: Hahn and Kim[48] use $F = R(n)$, $t = n$
Yang *et al.*[61] uses $m = c$, $s = \sigma$, $N = N_f$
Chou and Croman[50] use $S = \sigma$, $N = N_f$
Sendeckyj[52]uses $\sigma_a = \sigma$, $\sigma_f = R(n)$, $\sigma_e = R(0)$, $1/S = m$, $C = \frac{\left(\frac{R(0)^m}{\sigma}-1\right)}{N_f}$
Broutman and Sahu[37]uses $\sigma_i = R(n)$, $f_i = n/N_f$, $\sigma_{ults}^{i-1} = \sigma_{ults}^0 = R(0)$ for one state of stress
Daniel *et a l.*[53] uses $s = \sigma$, $N = N_f$
Reifsnider and Stinchcomb[54] uses $S_r = R(n)$, $S_u = R(0)$, $S_a = \sigma$, $N=N_f$, $i=k$
Haris *et al.*[58] uses $f_r = R(n)$, , $s = \sigma$, $N = N_f$

They emphasised that stress-independent models, like the model proposed by Fong [59], which is based on the assumption that fatigue process is controlled by a single primary damage mechanism is not realistic. They postulated that their model that their model permitted the incorporation of all modes of damage accumulation, from wear out to sudden death, by adjustment of curve fitting parameters $\alpha$ and $\beta$. In their studies, the equivalent number of fatigue cycles for static loadings is assumed to be 0.5, however by considering that a static loading is a quarter of cycle, the equivalent number of cycles should be changed to 0.25. By using the normalised technique all different curves, for different states of stress, collapse to single curve. Shokrieh *et al.* [46] modified the equation presented by Adam *et al.* [58] as in the following form:

$$(R(n,\sigma,k) = \left[1-\left(\frac{\log(n)-\log(0.25)}{\log(N_f)-\log(0.25)}\right)^{\beta}\right]^{\frac{1}{\alpha}}(R(0)-\sigma)+\sigma \qquad (2.12)$$

By considering that for each combination of stress and stress ratio there is fatigue life for plies, it seems to characterise the residual strength of unidirectional ply under arbitrary state of stress and stress ratio, large number of experiments are needed. To overcome this difficulty, many authors restricted their failures criteria to stress ratio. Using equations 9, Shokreih *et al.* [46] developed a model called generalised residual material property degradation model. By using this model the number of experiments to characterise the material properties of composite lamina can be minimised and the severe restriction of application of failure criteria to certain state of stresses and stress ratio can be avoided.

#### *2.5.3.3 Stiffness degradation models*

A single parameter, usually called the stiffness, has been used to indicate the state of fatigue damage. A complete characterisation of fatigue damage would require measuring changes in all stiffness components and relating these to damage mechanisms. Most of the life prediction methods for composite materials are based on the residual strength degradation. However, theories for fatigue failure based on the reduction of stiffness have one significant advantage over the remaining strength theories, that is remaining life can be assessed by non-destructive techniques. Less testing is needed to be conducted for stiffness degradation-based models.

One such analysis based upon stiffness degradation has been proposed by Poursartip *et al.* [60]. In their analysis, it was assumed that stiffness reduction could be related in a linear manner to the "damage" that was present due to fatigue. By making arguments based upon global stiffness reduction due to cracks in composite materials, they were able to relate the measured stiffness reduction in a linear fashion to the damage (for a low concentration of cracks). The damage parameter could then be integrated from its initial value to some final value (critical) value using the experimentally measured stiffness reduction. Failure was predicted to occur at the point where the damage parameter reached the critical value.

Yang *et al.* [61] also presented a stiffness degradation model for graphite/epoxy laminates that can be used to predict the statistical distribution of the residual stiffness of composite laminates subjected to fatigue loading. Based on such model, the statistical distribution of residual stiffness at any number of load cycles can be predicted. One method is based on linear regression analysis and other on Bayesian approach. According to this model, let *E(n)* be the residual stiffness at the *n*th load cycle. The stiffness degradation rate is assumed to be power function of the number of load cycles and can be written as:

$$\frac{dE(n)}{dn} = -E(0)Q\nu n^{\nu-1} \tag{2.13}$$

Where $Q$ and $\nu$ are two parameters which are correlated by a linear equation. Integrating equation (2.13) from 0 to *n* cycles:

$$E(n) = E(0)\,[1-(d+a_2 BS)(n)^{a_3+BS}] \tag{2.14}$$

It is well known that stiffness degradation of composite laminates varies considerably from specimen to specimen. Such a statistically variability is introduced by random variables *E(*0**)** and *B* in the stiffness degradation model. They suggested that the distribution of both *E(0)* and *B* can be represented reasonably well by the log normal distribution in the experimental data. Later, they modified their approach for matrix dominated composites for which stress strain curve is non-linear. It was observed that fatigue modulus concept is more suitable for matrix dominated behaviour. Modified form of the modulus is as follow:

$$E(n) = g(s)E(0)\,[1-(d+a_2 BS)(n)^{a_3+BS}] \tag{2.15}$$

New term *g(S)* is a function of stress level. This modified approach can easily accommodate differences in the stiffness degradation profile due to flexibility given by the non-linear stress profile term.

Wen-Fang Wu *et al.* [62] presented a stiffness degradation model based on the models presented by Yang *et al.* [61]. Their experimental results indicated that residual stiffness of a composite laminates decreases monotonically and non linearly with respect to loading cycles. Equation 2.13 can be written:

$$E_c(n) = E(0)Qn^{\nu} \tag{2.16}$$

Here $E_c(n)$ indicate the degraded stiffness after the application of n loading cycles. Based on appropriated failure criterion, when $E_c(n)$ reaches a critical value, failure will then occur [60]. In view of dispersion of experimental results, in the probabilistic fatigue analysis, $E_c(0)$, $Q$ and ν in equation (2.16) can be considered as random

variables in which $E_c(0)$ indicates statistical uncertainty of initial stiffness, and $Q$ and v characterise the uncertainty of the material constants. All of them can be obtained in advance through statistical analysis of some easily obtained analysis. The failure probability or reliability of composite component can then be predicted based on statistical data in conjunction with above equation (2.16). A probabilistic modelling proposed by Yang *et al.* was used for stiffness degradation model, and log normal distribution is selected for both $E_c(0)$ and $Q$. These models can be used to predict the probability distribution of the degraded stiffness at specified loading cycle. They found good agreement between their experimental and predicted model results.

In another paper they [64] extended their studies further to investigate the fatigue damage behaviour of composite laminates subjected to service loading conditions. Previous stiffness degradation models were used for composite laminates subjected to spectrum loadings. Baseline stiffness reduction data under spectrum loadings were used to determine the model parameters then stiffness degradation model can be used to predict the statistical distribution of residual stiffness and fatigue life for laminates composites subjected to different levels of spectrum loadings. Typically, the fatigue damage accumulation process can be divided into three distinctive regions in the stiffness versus number of blocks (spectrum loading blocks). In the primary region, a sharp stiffness reduction is developed in first block, followed by a secondary region of little stiffness change. The third region is characterised by a sharp stiffness reduction leading to fracture. A stiffness degradation model under block-type spectrum loadings has been suggested and methodologies for predicting the statistical distribution of the residual stiffness and fatigue life have been presented. Based on the measured stiffness reduction data in service along with this model, the residual stiffness for an individual component in service can also be predicted by employing linear regression analysis and Bayesian approach. Furthermore, an empirical fatigue failure strain criterion has been proposed and the statistical distributions of failure stiffness and fatigue life for composite laminates subjected to service loading spectra can be theoretically derived. It was shown that the theoretical predictions and experimental results correlate reasonable well.

Recently, Whitworth [65] proposed a new residual stiffness model, which follows the degradation law:

$$\frac{dE^*(n)}{dn} = \frac{-a}{(n+1)\left[E^*(n)\right]^{m-1}} \tag{2.17}$$

Where $E^*(n)=E(n)/E(N)$ is the ratio of residual stiffness to failure stiffness $E(N)$, $n$ is the number of loading cycles and $a$ and $m$ are the parameters that depend on the applied stress, loading frequency etc. By introducing the strain failure criterion, the residual stiffness $E(n)$ can be expressed in terms of static tensile strength $S_u$ and statistical distribution of residual stiffness can be obtained, assuming the static ultimate strength can be represented by a two parameters Weibull distribution.

### 2.5.4 Cumulative damage models

A major problem in fatigue of the composite material is the fatigue life prediction under variable amplitude cyclic loading, also called the cumulative damage or multiple stress level. In order to deal with this problem two major analytical approaches named as phenomenological and crack propagation approaches were adopted. The phenomenological approached is concerned with fatigue life prediction in terms of life time test data, mostly the *S-N* data for constant amplitude loading, without enquiring into micro-structural nature of fatigue life. This type of approach is reviewed in the following sections. In general any cumulative fatigue model must quantitatively answer the following questions [66]:

- How much damage is caused in a structure by one single loading cycle?
- How does the damage accumulate for more than one cycle?
- What is the critical damage value indicating the failure?

Multi-stress level fatigue life prediction can be performed using either cumulative damage techniques or fracture mechanics. The application of fracture mechanics to composite is questionable because single cracks of the type observed in metals rarely occur in composites. Instead, complex damage zones are developed in composites usually observed which involve large number of cracks in many directions. The complicated damage regions produced in composites means that fatigue damage is not a simple problem. There are number of variables that could be used for its definition such as crack density, number of debonded fibres, delamination, stiffness degradation, strength degradation or variation in strain.

Due to the difficulties involved in detecting and quantifying physical damage in composites, research mainly been directed towards strength and stiffness (or modulus) degradation methods. The main difference between two methods being the failure criterion used. For strength degradation approaches, failure occurs when the residual static strength deteriorates to the value of the maximum stress amplitude of the last cycle before failure. While for stiffness degradation, a critical value of stiffness decrease is assumed as a failure criteria.

#### *2.5.4.1 Cumulative damage models based on residual strength*

Hashin and Rotem [67] proposed a cumulative damage theory in which damage during cyclic loading may be represented by the residual lifetime under subsequent constant amplitude cycling. The theory was based on the concept of damage curve families, which are defined in terms of residual life times for two stages loading. In the first case, the damage in two components due to two different loading histories was considered equivalent if it gave the same remaining life under subsequent loading at the same stress level. They considered procedures of lifetime prediction for piecewise constant cycle amplitude variation (multi-stage loading) as well as for the case of continuous variation of cycle amplitude with number of cycles. For the second case, the

solution of initial value problems for first order non-linear differential equations was required. The authors compared their analytical results to that of Miner's rule for multi-stage loading programs and found considerable difference.

In another paper, Hashin [68] presented comprehensive analytical studies on cumulative damage concept based on residual strength and residual life theory. Cumulative damage based on residual life can be explained by defining a single non-valued non-dimensional damage function $D$ ($n$, $N$.) which is at least function of the number of elapsed cycles $n$ and of the constant amplitude life time $N(\sigma)$. The function $D$ has the following properties: $D$ (0, $N$) = 0 means no damage, $D$ (0, $N$) = 1 means failure.

The fundamental property of $D$ is that, for two stage loading

$$D(n_1, N_1) = D(n_2, N_2) \tag{2.18}$$

This two-stage loading can be further extended to three and four stage landings in similar manner. Therefore, this concept may be generalised to multi-stage loading as

$$\sum \Delta n_i / N_i = 1 \tag{2.19}$$

This equation has certain limitation as it ignores the sequence of loadings. Since fatigue damage varies more nearly logarithmically than linearly with number of cycles, the damage equation can be written as

$$D = D\left[(\log(n/N_c)/\log(N/N_c)\right] \tag{2.20}$$

Then the residual lifetime in two-stage loading was written as

$$\left(\frac{n_1}{N_1}\right)^{(\log(N_2/N_c)/\log(N_1/N_c)} + \left(\frac{n_{2r}}{N_2}\right) = 1 \tag{2.21}$$

The other form proposed by the same author, defines the damage as a function of applied stress, the residual strength and ultimate stress. The proposed model was written as:

$$D = \frac{\sigma_u - \sigma_r}{\sigma_u - \sigma_a} = \frac{1 - s_r}{1 - s} \tag{2.22}$$

where $\sigma_u$ is the ultimate stress, $\sigma_r$ is the residual strength, and $\sigma_a$ is the applied stress. The ratio of residual stress to ultimate stress is $s_r$ and $s$ is the ratio of applied stress to ultimate stress. However, this kind of model is restrictive in nature as large number of fatigue tests are required to determine static and fatigue strength distributions.

Yao *et al.* [69] also utilised the residual strength as a parameter which connects the macroscopic properties during the fatigue loading with the microscopic damage types to develop a new cumulative damage model. They assumed that strength loss can be used as a metric to model fatigue in FRP globally and phenomenological. They define the damage by the following equation

$$\Delta Di = A\left[R(i-1) - R(i)\right] \tag{2.23}$$

Where $\Delta D_i$ is the damage caused by the *ith* loading cycle, *R(i)* the residual strength at the *ith* loading cycle and *A* is a proportionality coefficient. Because damage develops unevenly during the cyclic loading, another equation was introduced which accounts for cumulative damage mode

$$D_i = \sum_{j=1}^{i} \Delta Dj \Big|_{Dj-1} \tag{2.24}$$

Damage caused by the *jth* cycle is given by

$$D_j = \frac{1}{R(0) - S_j}\left[R(j_{eff}) - R(j_{eff}+1)\right] \tag{2.25}$$

Therefore, fatigue damage can be calculated cycle by cycle by using above equation. The residual strength of FRP under tensions commonly passes through three stages during the fatigue. During the early stage of fatigue life, residual strength decreases rather quickly, which was mainly related to small cracks in the matrix. While in the middle of life, residual strength decreases gradually and evenly which was mainly related to the random fibre breakage and delamination. Finally near to failure, residual strength decreases rapidly due to failure of the specimen. This behaviour can be described by using the following expression:

$$R(i) = R(0) - \left[R(0) - S\right]\frac{\sin(\beta x)\cos(\beta - \alpha)}{\sin\beta\cos(\beta x - \alpha)} \tag{2.26}$$

where $\alpha$ and $\beta$ were the parameters from the experimental results. Authors used experimental data from the literature to validate his model. In addition, for the tests conducted under compression, it was assumed that residual strength was a power function with an exponent less than 1 and they proposed following equation:

$$R(i) = R(0) - \left[R(0) - S\right]\left(\frac{i}{N_f}\right)^{\upsilon} \tag{2.27}$$

where $\upsilon$ was a strength degradation parameter depending on the stress ratio and peak stress. By comparison, with experimental data for glass fibre reinforced plastic and

carbon fibre reinforced plastics, a reasonably good predictive capability of this model has been demonstrated.

Fatigue damage of composite materials depends on many factors such as applied stress level, number of fatigue cycles, mean displacement levels, frequency, temperature, etc. Kam *et al.* [70] also presented a cumulative model and without loss of generality, he considered only the effect of applied stress level and number of fatigue cycles on fatigue damage. The damage in general can be written as

$$D = F(n, r) \tag{2.28}$$

For a constant amplitude stress, the damage is bound by boundary conditions:

$$\begin{aligned} D &= 0 \text{ when } n = 0 \\ D &= 1 \text{ when } n = N \end{aligned} \tag{2.29}$$

The functional form in equation (2.28) can be classified into two categories, namely, linear and non-linear damage models. The linear model of Palmgren-Miner's and several non-linear models were adopted in the fatigue reliability of composites. Brief description of the models are given as

(a) Palmgren-Miner's rule: Palmgren-Miner's rule is linear damage rule which defines damage as a ratio of the number of applied stress cycles $n$ and number of cycles to failure $N$, i.e.

$$D = \left( \frac{n}{N} \right) \tag{2.30}$$

(b) Modified Palmgren-Miner's: The damage is defined

$$D = \left( \frac{n}{N} \right)^{c} \tag{2.31}$$

(c) Hwang-Han's Model I : Fatigue damage is defined as the ratio of the resultant strain at the *nth* cycle ε(n) and failure strain $\varepsilon_f$:

$$D = \frac{\varepsilon(n)}{\varepsilon_f} \tag{2.32}$$

it can be shown that the above equation can be written as:

$$D = \frac{(B - N^c)}{(B - n^c)} \tag{2.33}$$

Where $B$ and $c$ are constants.

(d) Hwang-Han's model II. Herein fatigue damage is defined as

$$D = \frac{(\varepsilon_n - \varepsilon_0)}{(\varepsilon_f - \varepsilon_0)} \tag{2.34}$$

Therefore, fatigue damage can be written as:

$$D = \left(\frac{n}{N}\right)^{c}\left[\frac{B - N^{c}}{B - n^{c}}\right] \tag{2.35}$$

When a specimen is subjected to a spectrum stress which is comprised of a number of stress levels of different amplitudes the total damage is obtained as

$$D = \sum_{i=1}^{m} \Delta D_i \tag{2.36}$$

Where $m$ is number of stress levels, $\Delta D_i$ is the damage accumulated during stress level $r_i$. Failure occurs when the total damages reaches or exceeds 1, i.e. $D \geq 1$. The determination of $\Delta D_i$ is based on equivalent damage.

### *2.5.4.2 Cumulative damage model based on stiffness degradation*

Hwang and Han [71] have proposed four different damage functions based on fatigue modulus and material strains. These models were made mainly for the purpose of predictions of multi-stress level fatigue life. Seven different *S-N* curve characterisation models have been applied to these functions, to produce 23 cumulative models. They have applied all these models to two stages loading for the low cycle fatigue of short glass and carbon fibre reinforced thermoplastic. These models are also discussed in the chapter of analytical modelling.

Whitworth [72] proposed a cumulative damage model which was based on residual stiffness model. Where damage function has been defined as:

$$D = \left[\frac{H(1-\bar{S})^{a}}{1-\bar{S}^{a}}\right].\frac{n}{N} \tag{2.37}$$

Where $\bar{S} = \dfrac{S}{R(0)}$ is the normalised applied stress range and $a$ and $H$ are the parameters. When $D=0$, no cycles have been applied and $E=E(0)$. When $D=1$, then residual modulus equals the failure stiffness $E_f$. This model has been extended to predict the remaining life of composite specimens subjected to variable amplitude loading. To determine the fatigue failure criterion in case of variable amplitude loading, they used the ‘equivalence cycle approach’. In this approach, the number of cycles at a particular stress condition in a variable amplitude loading group is transformed into an equivalent number of cycles at some reference stress condition such that the original and transformed groups produce the same damage. When the sum of damage values at each stress level reaches one, failure occurs. Such an approach holds the assumption that behaviour of the composite specimen is history dependent. The model was tested on experimental data for two stress level fatigue.

## 2.6 Mechanical behaviour of sandwich composites under flexural loading

Many sandwich structures are subjected to fluctuating load stresses, taking place at relatively low or high frequencies and under these conditions failures are found to occur at stress values lower than they would apply for static loading conditions. Compared to single skin structures, sandwich constructions have gained reputation for being very good concept in avoiding fatigue failures. Zenkert [73] states that one reason may be the faces may fail in local instabilities at loads lower than their fatigue limit and the core is often designed with high margin of safety due to lack of knowledge about its fatigue properties. A further point may be that in sandwich, the loading situation for faces is clear, but for the core which exhibits rather complex loadings, fatigue data is found rare. However numerous experiments concerning these properties, mainly cross linked PVC foams have been carried out at university of Naples, Italy, at the University of Southampton, UK, at the department of lightweight structures, Royal Institute of Technology Sweden, Technical University, at Det Norske Veritas Research AS, Norway, Michigan Technical University, USA and in France. The findings based on these most valuable investigations establish a basis for additional work.

### 2.6.1 Failure modes in sandwich beams

A sandwich panel can fail in several ways, each mode giving one constraint on the load bearing capacity of sandwich. Depending on the geometry of sandwich and loading, different failure modes become critical and set the limits for the performance of the structure. The most common failure modes are schematically illustrated in the figure 2.2. In flexural mode, the face may either yield or wrinkle; delamination of bond between face and core may occur; and the core may fail in tension, compression, shear, or by local crushing. A common failure mode of sandwich composite is the yielding of the face material due to high normal stress generated by bending. When these normal stresses exceed the yield stress of face material, it yields and eventually ruptures.

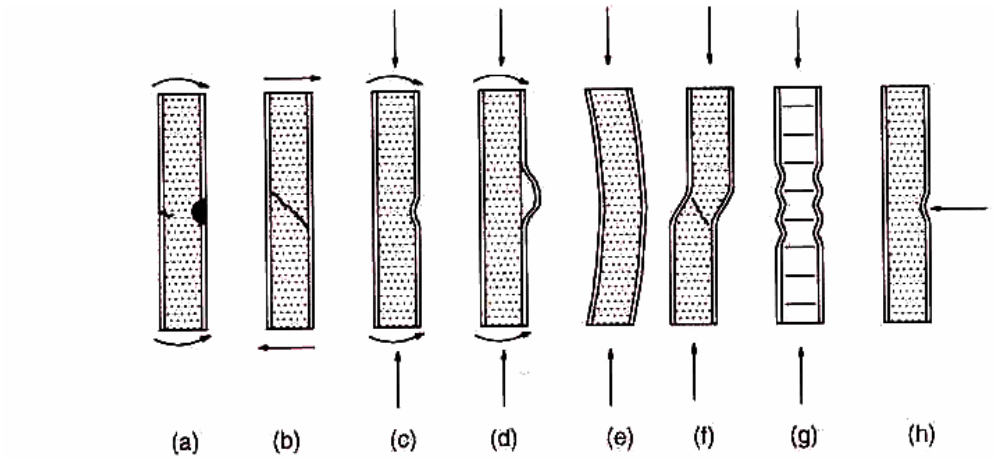


***Figure 2.2.*** *Failure modes: (a) Face yielding/fracture, (b) core shear failure, (c and d) face wrinkling, (e) general buckling, (f) shear crimping, (g) face dimpling and (h) local indentation [73].*

A failure mode of considerable importance is the so called bond decohesion or simply debonding or delamination. Debonding means that adhesive joint bonding of the face to the core fails. This can occur due to loading and unloading. The adhesive joint may also fail due to fatigue, impact, ageing or numerous other causes. The main problem with debonding failures is that they are sub surface, making them difficult to detect and can therefore grow to a critical size before being detected.

Fatigue testing of sandwich specimens is usually undertaken in flexural. The most common bending arrangement is three or four point bending. In the following section, some of the important aspects concerning flexural behaviour are presented.

### 2.6.2 Flexural behaviour of sandwich composites in static tests

Zenkert and Vikstrom [74] presented comprehensive studies on the shear cracks in the foam core sandwich panels in static tests. They used infrared (IR) techniques and fracture mechanics approach for detection and analysis of beams containing simulated shear cracks. By using fundamental material data, such as fracture toughness, the strength of the panels in the presence of cracks are predicted. Zenkert [75] has also shown in his previous paper that debonding in the mid plane of the core drastically reduces the strength of foam core sandwich beams. Shear cracks in the core of sandwich panels may be found as a result of overloading, impact or fatigue. The objective of their studies was to simulate fatigue cracks, to calculate the shear strength in presence of these cracks using finite element method and finally to verify the calculated strengths with experimental data. Generally, in sandwich structures, overloading will result in three types of cracks named as face-to-mid, interface cracks and face-to-face cracks. Normally, cracks would initiate in the mid plane of the core where the shear stress is maximum, or from a material discontinuity, such as large voids, and then grew typically at 45° towards the faces and continue to grow along the face to core interface [76]. They artificially made these types of cracks by fabricating panels by inserting Teflon films. A panel without cracks was used for reference. Four point bending tests were performed under displacement control until fracture. The stiffness of each beam was measured. Experimental result showed that reference beam with no cracks failed by local indentation of the face into the core, which was assumed as core shear fracture. The beam with face to mid crack exhibited unstable crack propagation, and it was therefore difficult to determine which crack front initiated in global failure. For the face to face cracked beam, the onset of crack propagation was also unstable and initiated at peak load. The cracks extended within the core, along the interface, leaving a thin layer of core material on the faces. For the interface crack types beam, all the beams showed pure interfacial crack propagation, that is, the cracks propagated in an unstable manner in the interface leaving the crack surfaces on the faces clean from the core material. The measured failure loads and predicted loads in three types of crack simulated beams were found within the 20% of scatter, which was considered as an acceptable criterion for engineering purposes.

Nordstrand *et al.* [77] used shear and three point bending tests to evaluate the transverse shear stiffness of structural core sandwich (corrugated board) plates. The three point bending tests provide a combination of bending and shear deformation. The sandwich beam is subjected to bending by the lateral force *W* and shear force of magnitude *W/2* will cause transfer shear deformation that contributes to the overall beam deflection. For this situation, the vertical deflection $\Delta$ , under the central load is given by relation:

$$\Delta = \frac{WL^3}{48bD_i} + \frac{WL}{4AG_{c,iz}} \tag{2.38}$$

Where $L$ is the beam span length, $D_i$ is the flexural rigidity per unit width of the beam and $AG_{c,iz}$ is the shear stiffness of the sandwich. Above equation provides a basis for experimental determination of bending and shear rigidities. They observed that shear modulus obtained by three point bending tests were significantly lower than those obtained from block shear tests. The difference was probably caused by the local indentation of the board at the supports and contribution from bending deformation of the facing in three point bending tests.

Danial *et al.* [78] presented a study on the flexural behaviour of sandwich composite beams and compare the results with predictions of theoretical models. Strains in the face sheets and core were measured with strain gauges and moiré gratings. The experimentally obtained stress/strain relationships of the face sheet material in tension and compression and that of core were used to obtain moment/strain relationship. Under three point bending, all beams failed prematurely due to shear crimping of the core. The failure load, being twice the shear force, remained nearly constant for varying span lengths. This implies that as the span length decreases, the applied maximum moment, and thereby the maximum face sheet strains at failure decreases. Results also indicated that even in case of increased loading of core, the bending moment was carried entirely by the face sheets. In this study, two models were implemented, one by assuming linear variation of strain through the face sheet thickness and the other by assuming a constant strain through the face sheet thickness. In both models, core contribution was neglected and face sheets were assumed to behave like membrane. Therefore, the moment/strain relations for face sheets display the same type of non linear behaviour as composite material itself, i.e., a stiffening non-linearity in tension and softening non-linearity in compression. Experimental results were in good agreement with prediction of the simple model.

### 2.6.3 Flexural behaviour of sandwich composites in fatigue tests

Shenoi *et al.* [79] performed fatigue tests on sandwich beams under flexural mode with various loading conditions. Three different core materials (AIREX, R63.80, C70.130, R90.200) of 80, 130, 200 kg/m$^3$ density were tested. Deflection and stiffness were used to identify the type of failures in sandwich beams. Experimental results indicated that deflection is linear up to shear force of 75-85% of the ultimate failure,

beyond this limit deflections increase dramatically with very little increase in shear force. Stiffness remained constant to a certain value and after which there is sharp reduction in the stiffness values. Deflection curve show two distinct linear and non linear regions. Although deflection increases due to the effect of creep and degradation as cycle number increases, the beam is considered safe in the linear region. The deflection becomes very large quickly resulting from the loss of strength and stiffness in the non-linear region. This indicates the failure of the beam. An empirical relation was developed relating to two regions. It is assumed that deflection is a function of cycle number and applied load. It was shown that upper and lower bounds of the linear region for all tested beams and empirically derived curve satisfy the equation developed. All beams tested indicated failures in the core due to excessive shear stresses. They proposed that fatigue is not serious problem for loads up 30% of ultimate failure loads even after six months of loadings. For the loads between 30-55% of the ultimate load, they observed a large scatter in the results. They attributed this to the varied cored density of foam materials. Failure characteristics were cracking and large plastic deformation in the cores. While at higher loading levels, the beams failed between 600 cycles and $1\times10^4$ cycles. Plastic deformation and very faint cracking were the main type of failures. They also conducted experiments on the fatigued specimens to study the strength and stiffness after fatigue. Three beams were subjected to fatigue at a relatively low cyclic load. For each beam the fatigue test was stopped before failure. The beams were then immediately tested under static load. They observed marginal reduction in strength after fatigue that was due to consequential effects of fatigue damage.

Shenoi *et al.* [80] presented an experimental investigation of static and fatigue behaviour of sandwich composite beams. The effects of frequency, temperature, core density and stress ratio was considered. An overall *S-N* characterisation was outlined, combining the various effects in a set of master curves. A typical eight point bending set-up was designed to perform static and fatigue tests at various frequencies. Static strength of the materials was calculated using four point bending tests. Fatigue tests performed in the sandwich specimens with linear PVC foam showed two major failure modes. First failure mode was shear cracking and other was shear yielding. Excessive shear deformation with plastic deformation of the core was observed at high stress levels. Three types of core were used in their studies. In first type of sandwich beam consist of linear co-polymer foam, a crack was initiated at 400,000 cycles and propagated slowly from the interface towards the centre of the core. While in second type of foam sandwich, failure was by tension in the upper face of the skin. In the third type of cross-linked PVC foam, failure was also caused by tensile failure in upper face. In sandwich structures, the relatively low density core was generally found temperature sensitive. They found very little difference (2 %) in the slope of *S-N* curves, which were obtained at lower frequencies. While at frequency 5 Hz, a 10 % decrease in shear properties was observed. They also studied the effect of core density on core shear failures and found a linear correspondence with increasing core density. They reported that for any given shear stress level *R*, the lower the stress ratio the shorter the beams fatigue life. For comparing fatigue results based on the tests conducted at different frequencies, a modified Rotem's approach was modified by normalising the data to a

'reference' stress ratio. The effect of loading conditions and waveform type had no considerable influence on the form of *S-N* curves, if tested at same mean stress ratio and mean stress.

Burman and Zenkert [81] presented the studies concerning the fatigue characteristic of foam core sandwich beams. Three sandwich configurations are investigated, two with cellular foams and one with honeycomb core material. The materials investigated were Divinycell H100 and WF51 and were defined as cross-linked rigid cellular foams with closed cell structure. These corresponds to typical materials and dimensions used in the marine and aeronautical industry. A modified four-point bending rig, which enables reversed loading, is successfully used for constant amplitude fatigue tests of all material configurations. This four point bending set up was an appropriate test configuration for extracting relevant shear fatigue for sandwich core materials. They reported that fracture initiation and fatigue failure occurs in a large zone of the core with well distributed micro cracks rather than a single propagating crack. The fatigue test results were plotted in stress life diagrams including a Weibull type function which provides a good accuracy curve fit to the results. The fatigue life of the core materials is found to be reduced with a increased load ratio, *R*. It was also reported that stiffness is not a good monitoring measure for the ‘health’ of specimen specifically in their findings.

In another paper by the same authors [82], a model for the prediction of fatigue life of damaged beams was proposed. Even though the failure modes were different for the undamaged and damaged beams, the proposed model shows good correlation with the experimental results. The influence on the strength and fatigue performance on sandwich beams with two types of core damages, an interfacial disbond and a flawed butt-joint, were experimentally investigated. The fatigue failure initiated at the stress intensity locations which were present due to the predamage. The specimens with flawed butt-joints displayed fatigue crack propagation in the interface between the core and face of the sandwich while the crack propagated through the thickness of the beams where an initial interface flaw was present. A fatigue failure prediction model is suggested which utilises the fatigue performance of undamaged beams and the strength reduction due to the damages. The approach is correlated with results from fatigue testing and satisfactory correlation is found. A uni-axial fatigue tests method was developed which simplifies the rig and specimens compared to the four point bend method. A comparison between the results from uni-axial tension/compression fatigue tests and shear fatigue tests showed good correlation, although the *R*-dependency differs in some cases. The fatigue crack propagation rates were investigated for two configurations: cracks propagating in pure foam core material and cracks propagating in the core material near and along a sandwich face/core interface. They reported that the rate at which a crack propagates was extracted for both Mode I and Mode II loading. The agreement between the Mode I crack propagation rate in the pure foam and in the core/face sandwich interface layer supported the theory that the crack actually propagated in the sandwich core beneath a stiffened resin rich layer present in the face/core interface. The stress intensity thresholds and the limits at which the crack growth becomes unstable were further established. The results indicated that the

proposed simple approach can be used to predict the reduction in fatigue life due to inflicted damages.

Dransfeld *et al.* [83] investigated the fatigue behaviour of sandwich core materials under four point bending. In their study, specimens were fabricated in such a way, that failure could occur only due to core shear failure. Faces of the sandwich specimens were made of aluminium. The results from static tests showed that all cross-linked PVC foams specimens failed in core shear. They assumed that this was due to the low compressive strength to shear strength ratio of this material. However, the shear stress in the core at the moment of failure was almost equal to ultimate shear strength of the material. In fatigue, all the tests were stopped at $10^7$ cycles. The *S-N* data obtained from four types of core materials showed that maximum shear stress is between 25 and 30% of ultimate shear strength of the material. However, for cross-linked PVC foam cores, this should not be interpreted as a fatigue threshold, beneath which no fatigue failure occurs. The deformation and the effective stiffness for one of specimen were monitored in fatigue test at 50% of shear strength. That specimen showed some creep deformation. The effective shear stiffness did not change during the test; although some shear cracks occurred during the test prior to final catastrophic propagation of one crack. While other two specimens failed in different manner. One specimen failed in shear in a direction 45° to the sample axis near the supporting points. Prior to failure, number of small cracks appears and propagated along the direction of specimen, one crack finally propagated through the sample thickness and then along the interface between the foam and skin, being responsible for the failure of the specimen. In the second specimen, crack initially followed the interface between areas and later propagated in a direction of 45° to the sample axis through the thickness of the sample and caused the final failure. The numerical simulation work was also carried out to better understand the non-uniform stress distribution in foam core and to relate it to crack initiations area. Their results showed that next to the analytical sandwich beam theory, contact analysis with linear material behaviour showed good correlation with actual tests for the respective load levels.

## 2.7 Interlaminar fracture in sandwich composites

Papanicolaou and Bakos [84] investigated interlaminar fracture behaviour of sandwich structure. By using double cantilever beam (DCB) specimens, they found that the interlaminar toughens ($G_{ic}$) values were strongly affected by the applied strain rate and experimentally found values are expected to be strongly rate dependent. The precise evaluation of fracture toughness in composite system is quite complicated, as it is highly dependent on experimental parameters such as strain rate, temperature and the shape of the specimen. Several different analytical approaches have been utilised in determining values of strain energy release rate ($G$), and the critical energy release rate ($G_C$) was used as a measure the interlaminar fracture toughness. A simple model was proposed by these authors based on an improved data reduction method for calculation of $G_i$. This model can be applied to all types of behaviour, such as linear elastic, non-linear elastic and non-linear inelastic. After reviewing the various approaches such as

simple beam theory, corrected beam theory and experimental compliance method, they proposed following simple approach. They used a simple beam and according to geometry of specimen

$$\delta = \frac{8Pa^3}{EBh^3} \tag{2.39}$$

and

$$C = \frac{\delta}{P} = \frac{8a^3}{Ebh^3} \tag{2.40}$$

where $\delta$ is the displacement, $P$ the load, a the crack length, $E$ the bending modulus, $B$ specimen width, h the thickness and $C$ the compliance.

From above we obtain

$$a = \left(\frac{EBC}{8}\right)^{1/3} h \tag{2.41}$$

while from the definition of $G_{ic}$ it follows that:

$$G_{ic} = \left(\frac{P^2}{2B}\frac{dC}{da}\right) = \frac{12P^2a^2}{EB^2h^3} \tag{2.42}$$

by introducing expression above, following expression is obtained

$$G_{ic} = \frac{3P^2}{A}\left(\frac{C^2}{EB}\right)^{1/3} \tag{2.43}$$

where $A = Bh$ is the cross-sectional area of the bending beam.

According to above equation, the parameters needed for revaluation of $G_{ic}$ are $P$, $A$, $C$, $E$ and $B$ which are all completely defined by the experimental procedure applied and specimen's geometry. In the case of sandwich structure where large non-linearity's and plasticity regions are present and where the classical methods can not be applied, the proposed approach was found quite satisfactory. In all tests, three basic regions appeared in load-displacement curves, corresponding to linear elastic, non-linear elastic and non-linear inelastic behaviour representing various types of failure mechanisms. But it was found that in all cases, the linear parts of the curves coincide for all specimens. More precisely, independently of displacements rate applied, the linear elastic region is followed by a large non-linear elastic region and this in turn by an elastic response.

## 2.8 Effect of core density and thickness

Kim *et al.* [85] presented a comprehensive study on the design of sandwich structure for concentrated loading. Series of three point bending tests of sandwich beams with carbon/epoxy faces and polyurethane foam cores were carried out, with variable core

density, dimensions and thicknesses. The stresses and deformation in specimens in three point bending tests were analysed using a number of analysis techniques, which are termed as classical theory, first order shear deformation theory, elasticity theory, high order theory and finite element analysis. Stiffness and failure loads were measured, along with strain gauges readings. Comparison of experimental results with theses analytical method showed that stiffness and strain gauge readings correlated well with the elasticity and finite element analysis, while classical and shear deformation theory were incapable of giving correct results. Stiffness and failure load results from three core densities showed that stiffness and failure load increases with increasing the core density and core thickness. But their rate of increase of stiffness depends upon the porosity of the core material. As the core with higher porosity (especially low-density core) permitted adhesive to be penetrated more, leading to a thick adhesive layer which increased the stiffness of those specimens. While higher density cores showed a much lower adhesive bonds thickness and correspondingly lower stiffness increase of the order of 3 to 5 % were observed. Comparison of predictions of failure loads with those measured for sandwich specimens were found consistent and reproducible. The linear theory employed appeared to be able to predict the failure loads in certain ranges of geometries and materials studied. In particular, using calculated shear stresses in the core appeared to correlate well with shear failure in the core and failure of the faces. While elasticity theory predicts that the loaded face has strain distribution that can be approximated as a combination of uniform compressive strain and linearly varying strain. The potential failure in the core is shear and the other failure mode for the core was taken to be failure in tension. Compression tests of the foam showed that failure in compression was ductile for all three densities, and could generally be taken to be elastic perfectly plastic. For given core density, the predicted failure load for core shear failure, increases with increasing core thickness because the calculated core shear stress decreases. At lower core thickness and lowest density, the predicted failure mode is failure of the core in shear without visible damage to the face. While for higher thickness specimen displayed visible indentation of the core prior to face failure. This face failure showed delamination and fibre failure. They also reported that face failures could not be accurately predicted by linear analysis. The specimen response becomes highly non linear, because of the non-linear core response in compression and the large local deformations. The results showed that failure modes and load levels can be predicted for sandwich structures under concentrated loadings, but accurate predictions required detailed information about the concentrated loadings.

## 2.9 Core failures

Caprino *et al.* [86] presented a study on the long term behaviour of PVC foam cores under fatigue and creep behaviour for structural sandwich constructions. Fatigue tests were carried out on sandwich beams, purposely designed to undergo core shear failure in four point bending. Three PVC foam cores of different densities were utilised. The *S-N* curves for the core materials up to about $10^6$ cycles were obtained. It was shown that the fatigue curves, when normalised to static strength, converges to a single master curve, provided the chemical nature of foam material remains the same. A simple

methodology, involving pure compression of cylindrical samples, was used for creep tests at different temperatures. Preliminary results from creep tests in pure compression seem to demonstrate the applicability of the time dependent superposition principal to PVC foam core materials. According to this principal, the compliance curves obtained at different temperatures becomes superimposed by a simple shift along the time axes, resulting in single curve. This allows for extension of experimental results obtained at high temperature to long term characterisation of core material at room temperature. Simply, the results of tests at high temperature and short times can be extended to lower temperature and longer times. Results from *S-N* curve showed that for a given number of cycles *N*, strength is higher for higher density core material. They assumed that the shear fatigue curve of a PVC foam core is represented by:

$$\frac{\tau_r}{\tau_{r0}} = 1 - \frac{k}{\tau_{r0}}.\log N \tag{2.44}$$

From a physical point of view, *k* is the rate of strength decrease with increasing number of cycles. This equation yields the non –dimensional shear strength $\tau_r/\tau_{r0}$ as a function of *N*. They concluded from the results that *k* is a function of core density: a heavy core is more sensitive to fatigue than a light one, suffering a high loss of strength for a fixed number of cycles.

Caprino *et al.* [87] used three point bending tests to study the shear characterisation of sandwich core materials. Experimental tests were carried out on PVC foams foam having 55 kg/m$^3$ density. They developed equations for measurements of shear modulus and shear strength component using basic formulas for displacement and stress. Core shear modulus $G_c^*$ was given by equation:

$$G_c^* = \frac{F\Delta L}{2b\Delta d} \tag{2.45}$$

Where *F* was applied force, $\Delta L$ was gauge length and *b* was beam width. For comparison, shear characterisation tests were also performed according to ISO 1922 (standard). It was reported that using three point bending together with approximate formula reduction, a shear modulus about 7.5% lower then the ISO value was obtained. The results obtained demonstrated that, when core shear modulus was considered, three point bending and ISO 1922 could provide coincident results. However, three point bending testing, yielded a shear strength about 20 % higher then the ISO standard. They concluded that core shear behaviour was better represented by three point bending when compared to ISO standards after observing failure modes.

Judawisastra *et al.* [88] used three point bending tests and block shear tests to determine the core shear properties of three dimensional woven sandwich composites. They used a new type of sandwich material, which was composed of woven sandwich fabric preforms. The empty core can be foamed up by liquid foam injection to improve shear resistance of the panel. They observed a considerable difference in shear

properties while using two different panels named as unfoamed and foamed panels with different length of pile (threads for woven cloth). The unfoamed panel showed 99% of the deflection caused by core shear means that the sandwich effect due to separation of skins is almost lost on shorter span lengths and there is large risk of core failure at lower loads. While foamed panel showed almost pure bending. Therefore injection of foam into the core was found beneficial. The results obtained from three point bend tests and block shear tests were almost the same. It was proposed that by introducing thicker and stiffer skins, mixed mode failure can be avoided and core shear failure can be generated.

## 2.10 Localised bending effects in sandwich panels

Structural sandwich panels are notoriously sensitive to the application of external loads, localised support conditions and discontinuous changes of geometry and material properties. In such areas, strongly localised bending phenomena are induced, where the face sheets tend to bend about neutral plane of the face sheets rather than about the neutral plane of the complete sandwich assembly. These localised bending effects cause the inducement of severe stress concentrations, which may be the cause of premature structural failure. Sandwich panels with transversely flexible cores such as polymeric foams are highly susceptible to failure due to local stress concentrations. Under these conditions sandwich panels usually fail due to delamination, shear rupture of the core or direct bending of skins.

Fundamental analyses of sandwich beams are presented by Allen [89], assuming that the core is incompressible in the out of plane direction. These models assume that the skins have only bending rigidity while core has only shear rigidity. This approach is good for sandwich structures with incompressible cores. However, to model the effects the local effects at the load points, the compressibility of the core in the vicinity of the applied loads must be included.

The localised bending problem in sandwich panels has been dealt with using two principally different approaches: the elastic foundation concept; and high order sandwich panel theory. In the case of compressible type of sandwich panel the most well known approach is the elastic foundation one, with one (winkler type) and two parameters (Pasternak or Vlasov type), [90,91]. Which consist in describing the behaviour of the core material by continuously distributed tension compression springs. The use of a flexible core in modern sandwich structures along with partially distributed loads, point loads and point supports yields localised deformation along, in the forms of indent, which are associated with non identical displacements at the upper and lower faces. It requires computational models that will be available to deal with localised effects and with unequal vertical displacements at the upper and lower faces. The elastic foundation model replaces the rigidity of the core with uncoupled springs, vertical and shear type, and determines the localised effects at the loaded faces only while assuming that there is no interaction between the loaded and unloaded face sheets [90,91]. The major draw backs of such models are due to: the unclear locations of localised effects within the panel length; the neglect of collaboration between the face sheets in the zones with localised effects; and the assumption that core is not elastic medium. The elasticity

of the core causes an interaction between the shear and vertical normal stresses within the core due to equilibrium requirements. These foundation models also neglects interactions between the top and bottom skins. Frostig and Baruch [90] overcome this difficulty by treating the beam as an ordinary incompressible sandwich beam connected to elastic foundation element.

Frostig and Baruch [92] and Frostig *et al.* [93] developed a higher-order sandwich panel theory capable of describing the general response of the sandwich panels with a soft core. The beam consists of different skins, upper and lower, metallic or composite-laminated, and soft core. The analysis includes the effects of the flexibility of the core, in the vertical direction, on the bending behaviour of the skins, as well as on the overall behaviour. They examined analytically the effect of four types of localised load distribution; a point load, uniform or sinusoidal loading or concentrated loading. These represent very flexible, intermediate and very stiff indentors, respectively. The behaviour of the beam is a superposition of two substructures; the first one is a beam in which the height of the core remains unchanged while shear effects are included. The second beam analysis allows the core height to be changed due to the transverse normal stresses, while keeping the core free from shear stresses. The second analysis highlighted the effects of localised loads. The results obtained by superposing the two analysis show that how these localised effects on the overall bending behaviour become significant when the ratio of length to depth of the beam is reduce. Johnson [94, p.143] investigated thin plates in contact with rigid indentor and concludes that the contact stress distribution changes from having a maximum in the centre to one in which pressure is concentrated at the edges, as the thickness of the plate increases.

Frostig and Frostig *et al.* [95-100] have developed an extensive analysis to consider the influence of the flexibility of the core on the flexural behaviour of sandwich beams. They used variational approach for the development of a high order sandwich panel theory, which includes the transverse flexibility of the core material. The high order theory is rigorous, systematic theory for the analysis of sandwich panels that incorporate as an inherent part of localised effects. The results obtained from this analysis were compared [101] to the results derived by an experimental investigation in a three point bending test using photoelastic evaluation of the local stresses. The investigation includes two specimens differing only by the thickness of their skins. Two different photoelastic models were considered. The experimental isochromatic fringe patterns were compared with theoretical results obtained using high order theory of sandwich panels. The comparison between the analytical and experimental results is presented in the form of contour line maps through the entire length and the depth of the core material, and at the upper and lower glass fibre skins. The comparative study has shown that the high-order theory of sandwich panels provides very accurate results as this predicts the presence of highly stressed zones as well as the level of stresses involved near the vicinity of concentrated loads and support points. In addition, this theory provides accurate stress predictions in the more lightly stressed areas away from load application and support points.

In another paper, Frostig and Baruch [102] extended the previous analytical investigation of sandwich beams to the flexural behaviour of sandwich plates. The analysis developed by the authors in the case of beams or plates considers the skins as two beams or plates respectively, the behaviour of which is described by the beam theory or classical theory of thin plates (first order theory without transverse shear effects). These plates were connected through displacement continuity by a flexible core which is considered as a two dimensional (in the case of sandwich beam) and three dimensional (in the case of sandwich plates) elastic medium. Next, the continuity conditions and stress strain relations for the core allow the displacement field through the thickness of the core to be determined: the variation of the transverse displacement is parabolic and the variations of thin plate displacement are cubic. These non linear variations through the core thickness, referred to as high order effects are especially pronounced in the vicinity of localised loading. The use of the variational principle combined with the linear kinematic relations for the skins and core combined with compatibility conditions for perfectly bonded core and skins yield a set of five differential equations with constant coefficients, seven boundary conditions (at each edge), and fourteen continuity relations. Finally, the governing equations of the sandwich beams or plates are formulated in terms of unknown functions: the in plane displacements in the middle plane of the skins, the transverse displacements of skins and transverse shear stresses the core. The solution of the set of these equations can be obtained analytically in the particular case of simply supported beams or plates or numerically for general types of boundary conditions. The numerical results of the principal stresses in the vicinity of the load show sensitivity to core rigidity and beam length. The analytical results were used to define the values, locations and the directions of possible failure patterns.

## 2.11 Characterisation of *S*-*N* curves

The conventional representation of the fatigue life of materials has been in the form of *S*-*N* curves derived from single stress level fatigue. However, variability of testing material, material characteristics and specimen preparation results in large degree of scatter in the basic fatigue data. It is therefore crucial that the method chosen to characterise the *S*-*N* curve of the material is one that will give good fit to experimental data.

Hwang and Han [103,104] proposed number of equations to characterise the *S*-*N* curve of composite. These equations are derived using concept of fatigue modulus and a strain failure criterion. One such model is of the form:

$$N = [(B(1-s)]^{1/c} \tag{2.46}$$

Where $N$ is the number of cycles to failure, $s$ the ratio of applied stress to ultimate strength, and $B$ and $c$ are material constants. Several other empirical relations have been established for predicting fatigue life such as Basquin relations, the conventional straight line in *S*-*N* curve and Coffin and Manson's relations. Some success has been

made with the Basquin's relations and the straight line *S-N* curve for composite materials. Basquin's relation is a power law of the form:

$$\sigma_a = \sigma_f (2N)^b \tag{2.47}$$

Where $\sigma_a$ is the applied stress, *2N* is the reversals to failure (1 cycle =2 reversals), $\sigma_f$ is the fatigue strength of coefficient, and *b* is the Basquin's exponent and conventional *S-N* curve is :

$$s = k \log N + d \tag{2.48}$$

Where *k* is the slope of *S-N* curve and d is y intercept. Hahn and Kim [44] used a power used a power law of the form

$$sN^d = c \tag{2.49}$$

Where *d* and *c* are material constants. The proposed equation is comparable with Basquin's relation and it will be seen that it produces a similar fit to *S-N* data.

Read and Shenoi [105] collected the data from the others authors work and fitted those data using Basquin's relation, the straight line model, Hahn and Kim's model and one of the models of Hwang and Hahn. The best overall fit was obtained with linear log straight line theory. However the fit at the extreme ends of the data, for low and high cycle fatigue was poor. The power laws of Basquin and Hahn *et al.* [48] both give the same fit to the data. For low cycle fatigue data, pertaining to the glass fibre cloth/epoxy resin laminate loaded in-plain, the best fit was made using the theory proposed by Hwang and Hahn. However the straight line *S-N* curve still gave a good approximation to the data. For high cycle fatigue *S-N* curve for a glass CSM/polyester resin laminate loaded in-plane, the best fit was made using straight line *S-N* curve. Hwang and Han theory was also observed to correlate fairly closely to the data and could possibly give a best fit for the complete *S-N* data. Therefore the general shapes of *S-N* curves should first be assessed and then the curve fit chosen appropriately.

## 2.12 Relaxation and creep in composites

Polymeric based composite materials are viscoelastic; this makes the time dependent behaviour of such materials one of most important factors for use in the analysis and design of FRP structural systems. It is well known that the time dependent behaviour of FRP composites can be significantly influenced by various environmental conditions such as temperature, moister, mechanical loads, etc. Creep tests measure the time-dependent deformation of a material under a constant load. Stress relaxation tests, on the other hand, measure the continuous decrease in stress when a constant deformation is imposed on the material. Important parameters obtained from these tests include steady-state creep rate, strain to failure, and time to failure. Such parameters are very important to characterise viscoelastic materials. Temperature and humidity are the most important environmental factors that influence creep and stress relaxation. Creep often

results in permanent deformation, and may cause a part to fail at stresses much lower than its ultimate strength. Stress relaxation may cause a tightened part to become loose, and thus lead to loss of structure integrity.

Zhang and Zhao [106,107] investigated the viscoelastic response of glass fabric/epoxy specimens subjected to three point bending. Creep tests for determining the creep strains and deflections in the beams were performed along with stress relaxation tests. The test duration for each experiment was 100 minutes at a temperature of 50°C. The specimens with [45°/-45°] ply angles exhibited the most pronounced creep behaviour of the specimens tested, with 0° specimens displaying the least. The authors submitted that the inclusion of in-plane shear deformations explains the advanced creep rate of [45°/-45°] specimens. The experimental results were used to determine the coefficients in a generalised creep equation using the assumptions of small deformations and uniform material behaviour in tension and compression. The theoretical analysis of beam deflection taking into account the effects of transverse shear was performed. Good agreement between the theoretical prediction of beam deflection and experimental results was obtained.

Ericksen [108] studied the long term behaviour of glass/epoxy laminate as well as performance of individual components. The specimens were tested at varying load levels for total duration of 1000 hours. The authors found that there was a relationship between the creep behaviour of laminate itself and creep behaviour of the matrix and the reinforcement. The initial creep of the composite can be correlated with the behaviour of matrix. The creep of laminates over long periods of time was related to creep behaviour of the fibres.

## 2.13 Creep-fatigue interaction

Many loading conditions found in modern engineering construction are not confined to one specific type; the load is often a combination of two or more distinct loading regimes. As such, it is imperative to investigate the possible effects that different loading conditions may have on one another. The interaction between creep and fatigue behaviour is one such example of a possible overlap in loading types.

Sun and Chim [109] investigated the phenomena of fatigue retardation due to creep and higher frequencies in a [45°/-45°] graphite/epoxy laminate. Specimens were subjected to number of fatigue cycles at different frequencies. The cycles were performed at intermittent intervals separated by periods during which specimen was held statically under the peak load, which was given as 66.6% of the ultimate static stress. These specimens were tested with different combinations of cyclic loads and sustained static loads. The results showed that higher frequencies decreased the fatigue life and caused higher temperature. However, as the static load time increased, the fatigue life was found to increase. This phenomenon was attributed to the fact that when cycling is followed by static load, the static load causes a permanent strain at crack tips

which reduces any stress concentration at that point. This phenomenon allows the rate of crack growth to decrease; hence the fatigue life would increase.

Crowther *et al.* [110] chose to investigate creep-fatigue interaction of glass fibre laminates under complex loading in aggressive environments, such as those encountered in cooling water systems of coastal power stations. The experimental investigations was separated into three parts; Phase I, involving low frequency sinusoidal cyclic loads; Phase II, which involved wider frequency range of trapezoidal waveform loading and unloading; and phase III, which employed a sinusoidal cyclic load at a higher frequency than Phase I. All experiments were performed in tension. For Phase I, sinusoidal load of frequency 0.0083 Hz were superimposed over constant mean loads for periods up to $10^8$ seconds. Periodic unloading was performed to represent a typical maintenance cycle of one month. The amplitude of cyclic load was taken as 20% of the mean load. Results from this set of experiments proved consistent with rapid failure by creep at high loads being delayed by the load reduction. At the lower loads, the classical fatigue mechanism intervened to accelerate failure. In Phase II of this investigation, the effect of frequency of periodic unloading was investigated. Specimen were subjected to a constant mean load and then unloaded at frequencies from 0.0005 to 0.25 Hz. The results identified two criteria of failure; at the higher range of tested frequencies, failure occurred after specific number of cycles, regardless of the time under load, while at the lower range of frequencies the system was held at maximum load for a substantially longer time per cycle, so the time at load criterion was satisfied before the required number of cycles for failure reached. Phase III used sinusoidal loading similar to that in phase I, with the main difference being that the cyclic load superimposed over the constant load occurred at a higher frequency (1 Hz as compared to 0.0083 Hz). Results indicated that creep fatigue interaction was apparent for tests at 1 Hz while creep controlled failure occurred. From the experimental results, the authors tentatively identified a critical range for adverse fatigue creep interaction for this set of conditions as 0.01 to 1.0 Hz.

Bowman and Barker [111] investigated the creep/fatigue interaction behaviour of thermoplastic polyethylene. They postulated a method describing the interaction by assuming that during cyclic loadings, the creep component is proportional to the time at maximum load. Thus, the overall creep component at failure can be estimated using Miner's approach, where the time at maximum load is expressed in terms of creep rupture time. The two components are added to yield the total damage equation at failure.

$$D = \frac{N_f}{N_f^0} + \frac{T_F}{T_{CR}} \tag{2.50}$$

Where $N_f^0$ is the number of cycles to failure under conditions of pure fatigue, $T_{CR}$ is the creep rupture time under constant stress, $N_f$ is the number of cycles to failure under mixed loadings and $T_F$ is the total time to failure at maximum load. They demonstrated that for polyethylene, non linear damage was apparent with D values at failure less than

unity. The main limitation of the model is that the creep and fatigue damage components in themselves describe linear damage trends, thus overall model is linear.

## 2.14 Shortcomings of the published literature

Sandwich composite materials are finding increased used in structural application, in particular for aerospace and automotive purposes. However, due to complex mechanical behaviour of sandwich constituents, failure mechanisms are more complicated to predict. Mechanical fatigue and impact are by far most common type of failure of sandwich structure in service loading conditions. Nevertheless, design criteria do not correspond to this relationship. They are generally based on static considerations with concomitant safety factors, mainly because of the complexity of the fatigue damage mechanisms, consequent modelling difficulties, the cost of fatigue testing and larger scatter in fatigue life.

There are two main technical reasons why fatigue damage modelling in general is so expensive and difficult. The first reason is several scales where damage mechanisms are present: from atomic level, to the component and structural levels. The second reason is the impossibility of producing ‘identical’ specimens with well-characterised features. Some pitfalls of fatigue modelling:

- Confusion over scale: information from measurements on different scales levels is combined improperly and leads to erroneous results.
- False generalisation, oversimplification is also a source for fatigue uncertainties.

In the context of fatigue modelling, the main drawback of the fatigue life models is their dependency on large amount of experimental input for each material, lay up and loading conditions. Moreover, these models are difficult to extend towards more general loading conditions, where multiaxial stress conditions are imposed.

There are several parameters which affect the fatigue behaviour in sandwich composites. We noted that most of published literature regarding the type of loading did not make any difference in the type of loadings. In this study, this aspect is also investigated. The type of loading such as load control fatigue and displacement control fatigue are found to be different from each other. Most of studies covered the static testing of sandwich composites. Little relevant literature is found on the fatigue behaviour of sandwich composites. Current research activities mainly focus on non-traditional methods of static testing: energy release mechanisms in composite local fracture, computational simulation of fatigue in composite and sandwich structures. It is highly desirable in sandwich composite technology for evaluating damage tolerance, durability, fatigue life, for representing complex material behaviour, and for designing and implementing in-service monitoring devices, as well as reduce testing time to a bare minimum if not eliminating it entirely. The other major shortcoming is that during fatigue testing in sandwich composite is that some times failure is never achieved at low stress level, no matter how many cycles are applied.

## 2.15 Recommended research

In our view, research in sandwich composite material has come a long way just within the last few decades. To further advance the usage of sandwich composite materials, the following improvements are recommended:

- Develop experimental procedures that would characterise the behaviour of sandwich composite materials and structures because of different states of damage defined by fractures at the macroscopic level. Here the effect of load paths on the damage evolution must be investigated.
- Quantify the degradation in material properties with results obtained from existing non-destructive inspection techniques. Note that non destructive investigations results can also be used as a base for the damage evolution model.
- Conduct studies concerning the effect of different combined loading and the shift of load paths on the long term durability of composite structures. This will need to include the design of experimental apparatus.
- The gradual deterioration of composites materials with a loss of stiffness in damaged zones leads to continuous redistribution of stress and reduction of stress concentration inside a structural component. Consequently, an appraisal of actual state or prediction of the final state of the composite requires simulation of the composite path of successive damage state.

## 2.16 Approach adopted for present studies

In the previous sections, a review of current status of research in the field of composites and sandwich composites has been presented with reference to static and dynamic fatigue. An attempt has been made to establish a database for fatigue studies of composite and sandwich materials from the existing available literature. This understanding has been used to further develop our approach to design the project for this thesis. The specific objectives of the work undertaken includes fatigue characterisation of sandwich composites as well as its constituents with certain aspects, concerning the mechanical behaviour of the skin and core materials, identification of various failure mechanisms leading to final failure of the specimens and predictions of failure modes under various loading conditions. The following areas of studies are highlighted in this research:

- Investigation of influence of variation in span length during static tests;
- Application of sandwich beam theory to analyse the performance of sandwich composites;
- Behaviour of the skin in static and fatigue tests;
- Investigation of the influence of core thickness in static and fatigue tests;
- Investigation of the influence of core density in static and fatigue tests;
- Investigation of the behaviour of core in indentation, compression, flexural and shear in static tests and fatigue tests;
- To investigate the effect of frequency;

- Investigation of residual stiffness and residual strength degradation after fatigue;
- Non-cyclic fatigue (creep and relaxation studies);
- Analysis of the mechanical behaviour of sandwich composites during fatigue;
- Investigation of the variation of stress ratio and applied loading level;
- Evaluation of damage mechanisms;
- Development of analytical models for fatigue life and damage;
- Application of models.

# Chapter 3
# Materials and experimental procedures

## 3.1 Introduction

One problem with using sandwich composites is that high quality fabrication standards are required; otherwise processing defects may highly influence the sandwich structure performance. A good working knowledge of the materials and processes is therefore essential. In addition to the consideration normally made when designing with conventional engineering materials, the designer using sandwich composite materials has also to consider the selection of constituents, that is proportion, types, distribution and orientation, depending on the properties required and selection processes, depending on the shape and production requirement. Mechanical properties of the constituents of sandwich composites also play an important role in the performance of sandwich structure or components. In the following section, a brief introduction to the materials commonly used in the fabrication of sandwich panels is given.

## 3.2 Resins (Matrices)

The resins used in composite materials have the role of transferring the mechanical loadings to the fibres and to maintain the structural integrity by bonding the reinforcement together. Resins also provide a good environmental protection for fibres. The matrix is made up of the base resin and other compounding ingredients that may include plasticizers, stabilisers, surfactants, dyes and pigments, fire retardants and fillers. The choice of matrix material depends on the mechanical, thermal and chemical properties required as well as the processing methods available and permitted cost. There are mainly three types of resins which are commonly are used and they are polyester, vinylester and epoxy.

- Polyester resins are the most widely used resin systems, particularly in the marine industry. By far the majority of dinghies, yachts and work-boats built with composites make use of this resin system. Polyester resins are of the ‘unsaturated’ type. Unsaturated polyester resin is a thermoset, capable of being cured from a liquid or solid state when subject to the right conditions.

- Vinylester resins are similar in their molecular structure to polyesters, but differ primarily in the location of their reactive sites, these being positioned only at the ends of the molecular chains. As the whole length of the molecular chain is available to absorb shock loadings this makes vinylester resins tougher and more resilient than polyesters. The vinylester molecule also features fewer ester groups. These ester groups are susceptible to water degradation by hydrolysis which means that vinylester exhibit better resistance to water and many other chemicals than their polyester counter parts and are frequently found in applications such as pipelines and chemical storage tanks.

- Epoxy resins represent some of the highest performance resins of those available at this time but these are expensive. Epoxies generally out perform most other resin types in terms of mechanical properties and resistance to environmental degradation.

As a laminating resin their increased adhesive properties and resistance to water degradation make these resins ideal for use in many industrial applications. The term ‘epoxy’ refers to a chemical group consisting of an oxygen atom bonded to two carbon atoms that are already bonded in some way. Usually identifiable by their characteristic amber or brown colouring, epoxy resins have a number of useful properties. Both the liquid resin and the curing agents form low viscosity easily processed systems. Epoxy resins are easily and quickly cured at any temperature from 5°C to 150°C, depending on the choice of curing agent. One of the most advantageous properties of epoxies is their low shrinkage during cure which minimises internal stresses. Epoxies have higher strength and adhesion to fibres than polyesters. Epoxies differ from polyester resins in that they are cured by a ‘hardener’ rather than a catalyst. The hardener, often an amine, is used to cure the epoxy by an ‘addition reaction’ where both materials take part in the chemical reaction.. If amine and epoxy are not mixed in the correct ratios, unreacted resin or hardener will remain within the matrix which will affect the final properties after cure.

The choice of a resin system for use in any component depends on a number of its characteristics, with the following probably being the most important for most sandwich composite structures:

- Adhesive properties;
- Micro-cracking resistance;
- Fatigue resistance;
- Mechanical properties.

## 3.3 Reinforcements (Fibres)

Reinforcement gives to composite materials high mechanical characteristics such as stiffness, strength, hardness, etc. All of the different fibres used in composites have different properties and so affect the properties of the composite in different ways. Generally, the characteristics sought for reinforcements are low density, good compatibility with resins, ease of manufacturing, low cost etc. The properties and characteristics of common fibres are given below. However, individual fibres or fibre bundles can only be used on their own in a few processes such as filament winding. For most other applications, the fibres need to be arranged into some form of sheet, known as a fabric, to make handling possible. The most common type of fibre materials are:

- Glass fibre is a mixture of oxides with varying amounts of calcium, aluminium, sodium boron etc. By blending quarry products (sand, kaolin, limestone) at 1600°C, liquid glass is formed. The liquid is passed through micro-fine bushings and simultaneously cooled to produce glass fibre filaments. The filaments are drawn together into a strand (closely associated) or roving (loosely associated), and coated with a "size" to provide filament cohesion and protect the glass from abrasion. By variation of the "recipe", different types of glass can be produced.

- Aramid fibres are a family of man-made organic polymers (aromatic polyamides) produced by spinning a solid fibre from a liquid chemical blend. Kevlar has a crystalline structure with strong covalent bonding in the fibre direction and relatively weaker hydrogen bonding in the fibre transverse direction. The anisotropic

nature of the fibre causes Kevlar to have poor compressive properties. Under compressive loads the fibre develops kinks bands which eventually lead to ductile failure. The bright golden yellow filaments produced can have a range of properties, but all have high strength and low density giving very high specific strength. All grades have good resistance to impact, and lower modulus grades are used extensively in ballistic applications. However, the fibre can degrade rapidly when exposed to ultraviolet light.

- Carbon fibre is produced by the controlled oxidation, carbonisation and graphitisation of carbon-rich organic pre-cursors which are already in fibre form. The most common precursor is polyacrylonitrile (PAN), because it gives the best carbon fibre properties, but fibres can also be made from pitch or cellulose. Variation of the graphitisation process produces either high strength fibres or high modulus fibres. Carbon fibre has the highest specific stiffness of any commercially available fibre, very high strength in both tension and compression and a high resistance to corrosion, creep and fatigue. Their impact strength of fibre, however, is lower than either glass or aramid. However, its cost is high compared to glass fibres.

## 3.4 Core materials

### 3.4.1 Introduction

The purpose of a core in a sandwich composite is therefore to increase the laminate's stiffness by effectively 'thickening' it with a low-density core material. This can provide a dramatic increase in stiffness with very little additional weight. Cellular foams are increasingly being used as core materials in conjunction with high strength skins, to produce strong, stiff and light weight sandwich structures for aerospace, marine and transport industry. They achieve a greater load-bearing capacity per unit weight, as well as greater energy storage and energy dissipation capacities.

Engineering theory shows that the flexural stiffness of any panel is proportional to the cube of its thickness. This can provide a dramatic increase in stiffness for very little additional weight. Figure 3.1, shows the difference in stiffness, strength and weight when core materials of varying thickness is placed between the plies of skin laminate.

The flexural stiffness of a structure is dependent on two factors: the material stiffness or modulus and the cross sectional geometry or moment of inertia. The material properties are often difficult to change (and some time expensive), so a change in geometry can be done to increase stiffness while not compromising on the strength or other properties of skin laminates. The increase in strength and stiffness allows builders to use less skin materials, resulting in lower weight structures. Decreased weight helps to increase the top speed and acceleration, increase cargo capacity and of course reduce fuel consumption.

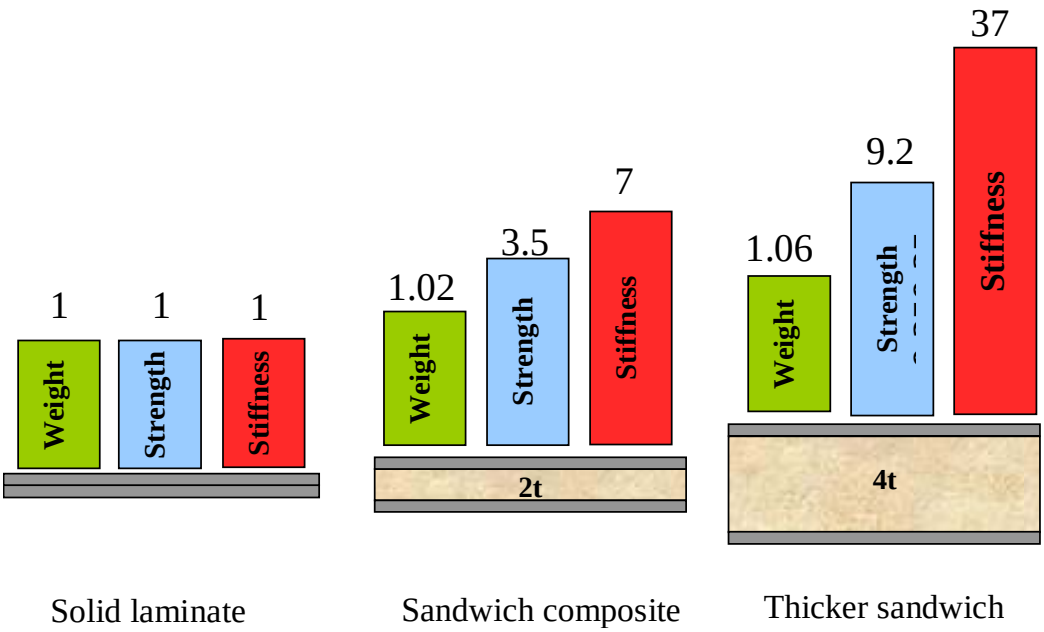


***Figure 3.1**. Sandwich concept*

### 3.4.2 Foams

A plastic foam material consists of a gas phase dispersed in a solid plastic phase and derives its properties from both. The solid plastic component forms the matrix. Foaming of plastics can be achieved in several ways. One possibility is to create gases inside the mass of the polymer. The gas phase is contained in voids or cells and is often referred to as the blowing or foaming agent. It should be noted, however, that the blowing agent used in the production of foams is not always gaseous and chemically identical with the gas component. Some blowing agents are solids, some are liquids. Once the polymer has been expanded, the cellular structure must be stabilized rapidly. If the polymer is thermoplastic, the expansion is carried out above the melting point, and the foam is then immediately cooled below the melting point (such a process is referred to as physical stabilisation). Otherwise chemical stabilisation can be performed. Air can be whipped into a solution of the plastic, low boiling liquid, or incorporated in the plastic mix and then volatilised by heat. Gases can also be generated within the plastic mass by thermal decomposition of a chemical blowing agent.

Foamed plastics can be classified according to the nature of the cells into closed-cell and open-cell types. In closed-cell foams each cell (more or less spherical in shape) is completely enclosed by a thin wall or membrane of plastic, whereas in open-cell foams the individual cells are interconnected. Free expansion during cell formation usually produces open-cell foams. Closed-cell foams are produced in processes where some pressure is maintained during the cell formation stage. Close cell foams can absorb more energy than open cell foams because of entrapped gas within the cell, which act as a medium of energy absorption. Foamed plastics are produced in a wide range of densities. Plastic foams may be flexible, semi-flexible (or semi-rigid) and rigid, depending on chemical composition and the rigidity of the resin used as a matrix. Flexible foams have a glass transition below room temperature, whereas rigid foams have one above room temperature. An excellent discussion of typical behaviour of

cellular materials can be found, e.g., in Gibson [117]. Most common types of cores are discussed in the following section.

Foams are one of the most common forms of core material. They can be manufactured from a variety of synthetic polymers including polyvinyl chloride (PVC), polystyrene (PS), polyurethane (PU), polymethyl methacrylamide (acrylic), polyetherimide (PEI) and styreneacrylonitrile (SAN). They can be supplied in densities ranging from less than 30 kg/m$^3$ to more than 300kg/m$^3$, although the most used densities for composite structures range from 40 to 200 kg/m$^3$.

Closed-cell polyvinyl chloride (PVC) foams are one of the most commonly used core materials for the construction of high performance sandwich structures. Although strictly they are a chemical hybrid of PVC and polyurethane, they tend to be referred to simply as 'PVC foams'. PVC foams offer a balanced combination of static and dynamic properties and good resistance to water absorption. They also have a large operating temperature range of typically –240°C to +80°, and are resistant to many chemicals. There are two main types of PVC foam: cross linked and uncross linked with the uncross linked foams sometimes being referred to as 'linear'. The uncross linked foams are tougher and more flexible, and are easier to heat-form around curves. However, they have some lower mechanical properties than an equivalent density of cross-linked PVC, and a lower resistance to elevated temperatures. Their cross-linked counterparts are harder but more brittle and will produce a stiffer panel, less susceptible to softening or creep in hot climates.

### 3.4.3 Honeycombs

Honeycomb cores are available in a variety of materials for sandwich structures. These range from paper and card for low strength and stiffness, low load applications to high strength and stiffness, extremely lightweight components for aircraft structures. Honeycombs can be processed into both flat and curved composite structures, and can be made to conform to compound curves without excessive mechanical force or heating. Thermoplastic honeycombs are usually produced by extrusion, followed by slicing to thickness. Other honeycombs (such as those made of paper and aluminium) are made by a multi-stage process. In these cases large thin sheets of the are printed with alternating, parallel, thin stripes of adhesive and the sheets are then stacked in a heated press while the adhesive cures. In the case of aluminium honeycomb the stack of sheets is then sliced through its thickness. The slices (known as 'block form') are later gently stretched and expanded to form the sheet of continuous hexagonal cell shapes. The cells of the honeycomb structure can also be filled with a rigid foam. This provides a greater bond area for the skins, increases the mechanical properties of the core by stabilizing the cell walls and increases thermal and acoustic insulation properties. Properties of honeycomb materials depend on the size of the cells and the thickness and strength of the web material. Honeycomb cores can give stiff and very light laminates but due to their very small bonding area they are almost exclusively used with high-performance resin systems such as epoxies so that the necessary adhesion to the laminate skins can be achieved. Types of honeycombs are:

- Aluminium honeycomb produces one of the highest strength/weight ratios of any structural material. There are various configurations of the adhesive-bonding of the

aluminium foil which can lead to a variety of geometric cell shapes (usually hexagonal). Properties can also be controlled by varying the foil thickness and cell size. On impact of a cored laminate, the honeycomb will deform irreversibly whereas the FRP skins, being resilient, will move back to their original position. This can result in an area with an unbonded skin with much reduced mechanical properties.

- Nomex honeycomb is made from Nomex paper - a form of paper based on Kevlar, rather than cellulose fibres. The initial paper honeycomb is usually dipped in a phenolic resin to produce a honeycomb core with high strength and very good fire resistance. It is widely used for lightweight interior panels for aircraft in conjunction with phenolic resins in the skins. Nomex honeycomb is becoming increasingly used in high-performance non aerospace components due to its high mechanical properties, low density and good long-term stability.

### 3.4.4 Other core materials

There are also other natural types of core materials such as wood and their different types:

- Wood can be described as 'nature's honeycomb', as it has a structure that, on a microscopic scale, is similar to the cellular hexagonal structure of synthetic honeycomb. When used in a sandwich structure with the grain running perpendicular to the plane of the skins, the resulting component shows properties similar to those made with man-made honeycombs. However, despite various chemical treatments being available, all wood cores are susceptible to moisture attack and will rot if not well surrounded by laminate or resin.

- Balsa-The most commonly used wood core is end-grain balsa. Balsa wood cores first appeared in the 1940's in aeroplanes, boat hulls, which were aluminium skinned and balsa-cored to withstand the repeated impact of landing on water. This performance led the marine industry to begin using end-grain balsa as a core material in FRP construction. Apart from its high compressive properties, its advantages include being a good thermal insulator offering good acoustic absorption. One of the disadvantages of balsa is its high minimum density, with 100 $kg/m^3$ being a typical minimum.

- Cedar-Another wood that is used sometimes as a core material is cedar. In marine construction it is often the material used as the 'core' in strip-plank construction, with a composite skin on each side and the grain of the cedar running parallel to the laminate faces.

## 3.5 Fabrication of sandwich panels in the present work

### 3.5.1 Introduction

The cores used in our study are PVC foams [135]. The composite skins are composed of continuous glass fibres (density $300g/m^2$) arranged in $[0/90]_s$ sequence

and epoxy resins of type SR1500/SD2505. The details of preparation of sandwich specimen are described in the following section.

Sandwich panels were constructed using a mixed preg/hand lay-up in one stage i.e. the polymerisation of the resin containing fibres constituting the skins and adhesion foam/core are done at the same time using a special technique called vacuum bagging technique.

### 3.5.2 Vacuum bagging technique

Vacuum bagging is an effective, cost-efficient technique by which atmospheric pressure is utilised to provide uniform pressure. The best vacuum bag systems will produce just under 300 mbar. Note that this pressure is applied with little or no stress to the specimens since the pressure on the specimens is the same on all surfaces. Vacuum bagging is a technique employed to create mechanical pressure on a sandwich panel during its cure cycle. Pressurising a core and skin serves several functions. First, it removes trapped air between layers. Second, it compacts the fibre layers for efficient force transmission among fibre bundles and prevents shifting of fibre orientation during cure. Third, it reduces humidity. Finally, and most important, the vacuum bagging technique optimises the fibre-to-resin ratio in the sandwich composite part.

Total bonding of core to facings is the basis of sandwich construction. All predictions of strength and stiffness presuppose that the facings and core are working together as a unified structure. Any area of the sandwich, which is not bonded, will be a location for potential failure or at the very least will be structure, which is not performing to its full potential. Next, a structure which has been vacuum bagged and is completely bonded and void free will maximise the economic value of the material.

### 3.5.3 Materials requirements and equipment

Vacuum bagging requires some basic materials in order to successfully pull vacuum and apply even pressure.

- **Peel Ply** — Against the surface of the last laminate, a peel ply or “RIP RAG” can be applied. Peel ply serves two functions. First, it eliminates the need for sanding or grinding prior to secondary bonding operations. Second, peel ply may be left on the laminate. This will keep it clean until the next step in construction.

- **Bleeder Ply** — Bleeder ply is a lightweight blotter to absorb excess resins or core bonding putties, which “BLEEDS” through the peel ply. Bleeder ply is used only once and is removed with the peel ply.

- **Bubble Pack or Breather** — Breather ply is a material, which will not compress under pressure to the extent that air cannot be drawn through it. Often, an otherwise perfectly sealed bag will not develop full vacuum pressure because the bag under the hose fitting is pinched off preventing evacuation of air from the rest of the part. A commonly used breather ply is bubble pack, which is typically seen as a protection for packaged goods. Bubble pack is inexpensive and can be reused if not loaded too heavily with cured putty.

- **Sealant Tapes** — Sealant tapes are used to seal the bagging film to the tool or part. They are very pliable and similar in texture to “chewing gum”. Most sealant tapes are butyl-based material which will stick to most bagging films (except silicone which is self-sealing) and to most Fibre glass, aluminium, and plate glass tools.

- **Vacuum Pumps** — Vacuum pumps are available in a variety of configurations and capacities. Most pumps use an electric motor to drive the evacuation equipment. Others use compressed air and venturies to create vacuum. These vacuum pumps are very small and quiet but are not as efficient as the motor driven models. Vacuum pumps must fulfil two capacities. First, they must be capable of a high vacuum. Second, they must be able to evacuate a large volume of air quickly.

### 3.5.4 Fabrication procedures

Glass fibre sheets are cut from the roll of fibre bundle in a dimension of 1 meter long and 30 cm wide. In our sandwich specimens, total 8 layers of fibres are used for the top and bottom skins. The orientation of the fibres layers are $[0/90]_s$. PVC cores of various thickness and densities were used for fabrication of sandwich panels. The ratio of mixing of epoxy and hardener is three and one.

Firstly, a sheet of bleeder/breather is laid down on a formica plank whose surface is polished by high quality vacuum grease. This layer serves two purposes. First it absorbs excess resin from the laminate. Second, it is this layer which ensures the vacuum is distributed evenly. On the top of bleeder layer, a perforated release film layer is laid. Perforated release film will also allow excess resin to pass through it which is absorbed by the bleed material. To obtain the best results there must be an avenue to supply an even vacuum to the whole part. This will also necessitate the use of release barrier between the breather and the part. The most convenient material for this is a treated nylon called peel ply. So a layer of this peel-ply is laid. This fabric provides an easy release and a textured surface for secondary bonding. Both air and resin will transfer through every pore, ensuring a void-free laminate. Then, Glass fibre sheets are laid one by one according to desired orientations with rich resin layers. After four layers of glass fibres, a thick PVC plank is bonded with thick and uniformly distributed layer of resin. On the other side of PVC core, four layers of glass fibres of same orientation as mentioned above are laid down one by one. It is followed by laying down of layers of peel-ply, perforated release film and bleeder cloth layer. Finally, formica plank is placed on the top. The whole assembly is carefully wrapped inside a typical plastic covering. This plastic sheet is made of built-in air bubbles usually used for wrapping the fragile material or components and it provides a uniformly distributed pressure under vacuum. This typical wet assembly (sandwich panel) is placed inside a plastic bag . A plastic pipe with large number of holes is inserted inside the plastic bag. The holes in the pipes ensure distributed vacuuming of whole assembly. The pipe and this plastic bag is sealed with sealant tape. A vacuum pump is attached with this pipe. Then the whole assembly is put under vacuum at a pressure 300 mbar for 10 hours. No pressure is applied to the mould during the vacuum bagging. After ten hours, pump is switched off, the plastic

bag is stripped off, the bubble pack ripped away, and the peel ply and bleeder fabric containing the excess resin are discarded. We are left with the finished product, a sandwich panel. After two weeks of polymerisation, the specimens were cut from the sandwich panel according to the desired dimensions using diamond cutting saw.

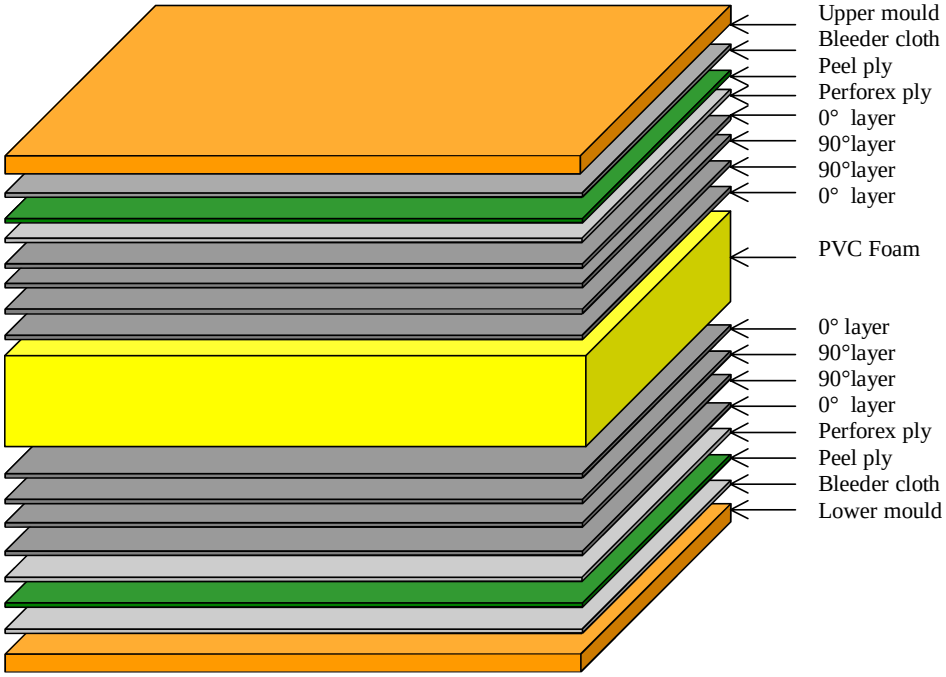


***Figure 3.2.*** *Schematic diagram of a sandwich composite assembly.*

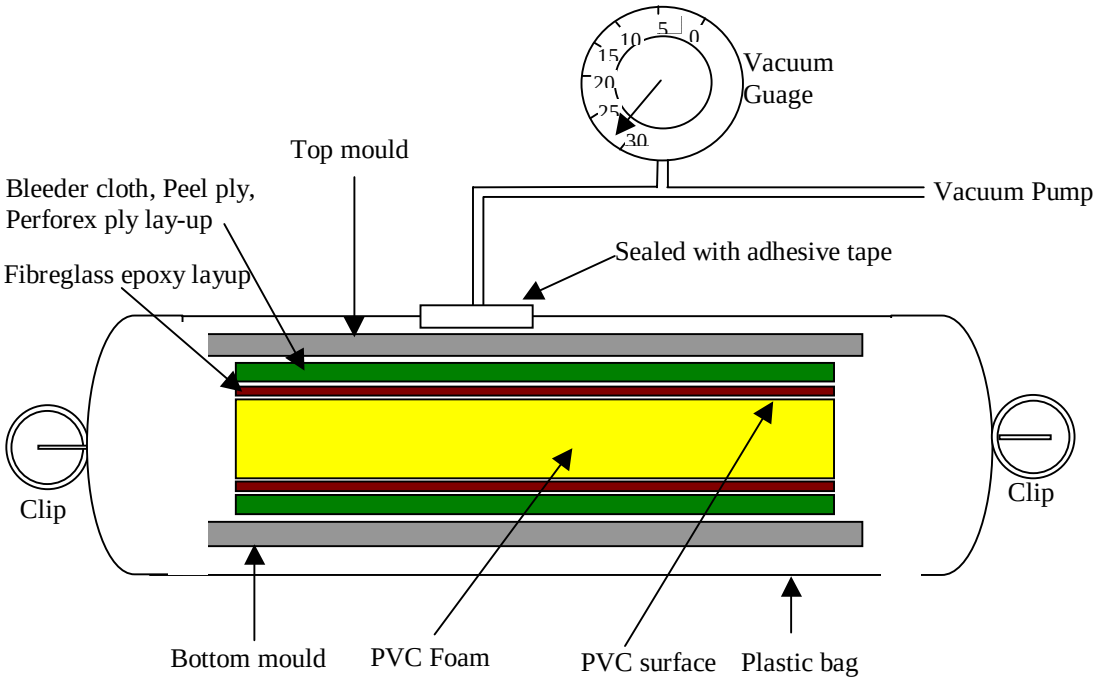


***Figure 3.3.*** *Schematic diagram of a typical vacuum bagging technique set-up.*

## 3.6 Description of the testing machine

The Instron model 8516 is a servohydraulic testing system designed to apply dynamic test forces to specimens of a wide range of materials. The system applies loads using a hydraulic actuator, to a specimen of the material under test. These loads can be applied in a cyclic or ramp loading. Testing of properties such as tensile strength, compressive strength, fatigue resistance, flexural, etc, can be performed. During the progress of a material test, measurements are made of conditions that the test specimen is experiencing. These measurements are of load upon the specimen, the strain or deflection of the specimen in response to the applied load and the position of the hydraulic actuator in response to applied load. Load cells of two different capacities 5 kN and 100 kN can be mounted to measure the applied loads.

The actuator provides the loading force required by the system through servohydraulic unit. The actuator incorporates a built in linear voltage displacement transducer (LVDT) for the measurement and control of actuator piston during a test. External LVDT can also be mounted and can be interfaced with PC for data acquisition. Machine can be operated at frequency range up to 100 Hz at different type load-wave forms: sine, square, triangle or ramp. Machine is interfaced with dedicated computer through a tower control for controlling and data acquisition. Tower control consists of various electronic devices which control the running of the machine and provides a link between machine and computer. Servohydraulic system supplies the oil pressures to run the machine at desired setting. The whole hydraulic assembly is cooled down by air-conditioning unit in order to avoid overheating of oil and the compressor systems of the hydraulic unit. Complete machine set-up is shown in figure 3.4.

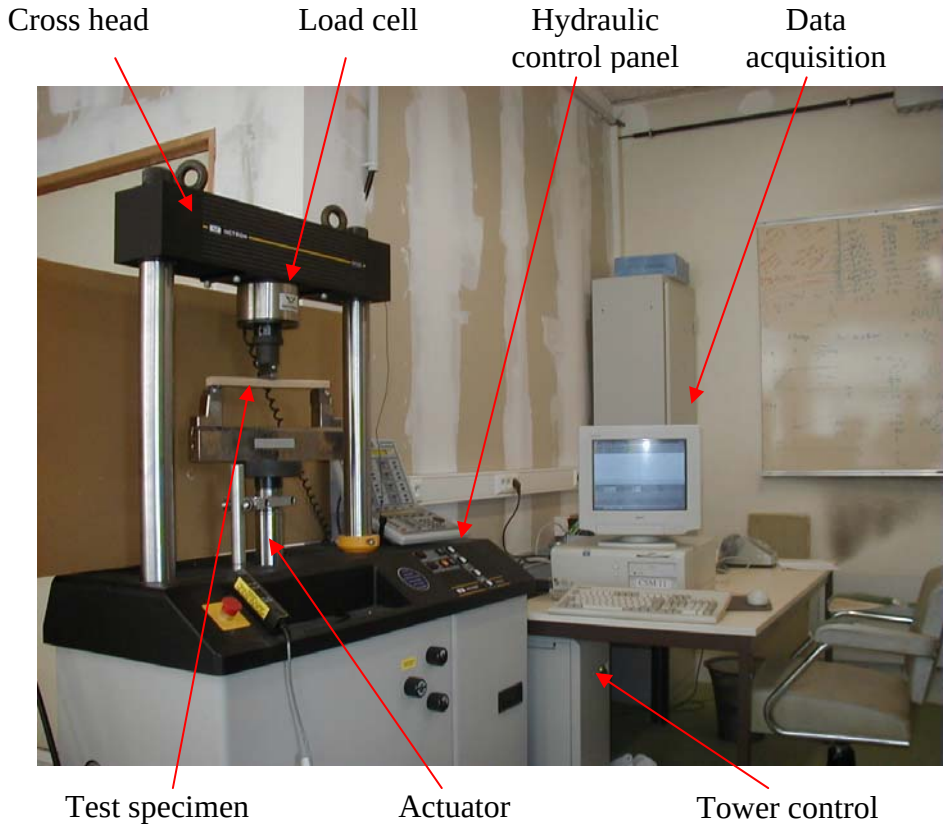


***Figure 3.4.*** *Instron machine.*

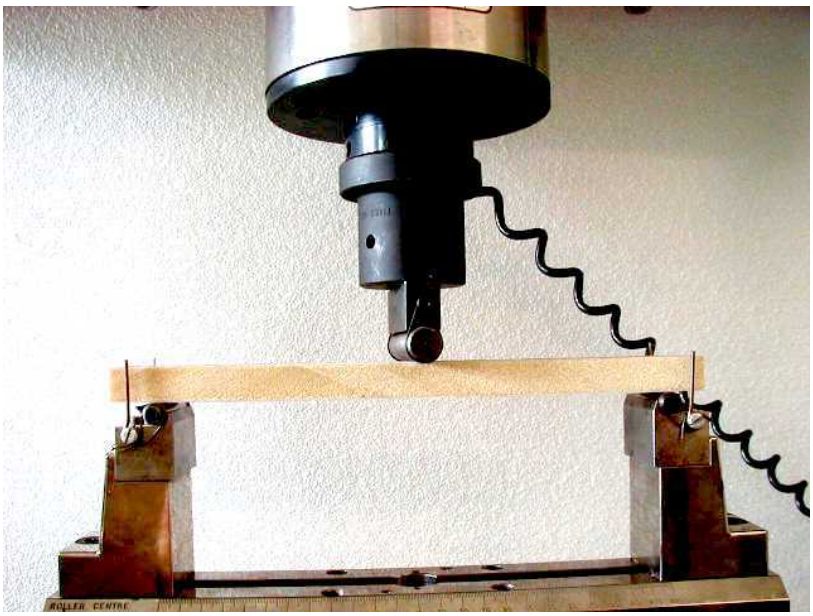

***Figure. 3.5.*** *Three point bending set-up with sandwich specimen.*

## 3.7 Fatigue parameters

Fatigue testing is usually performed using sinusoidal loading. Thus the state of fatigue loading can be described by parameters as shown in figure 3.6. By specifying maximum, minimum stress the other parameters can be easily determined such as mean stress, the range of stress, stress amplitude and the stress ratio.

$$\textit{Mean stress} \quad \sigma_m = \frac{(\sigma_{\max} + \sigma_{\min})}{2}$$

$$\textit{Range of stress} \quad \Delta_a = (\sigma_{\max} - \sigma_{\min})$$

$$\textit{Stress amplitude} \quad \sigma_a = \frac{(\sigma_{\max} - \sigma_{\min})}{2}$$

$$\textit{Stress ratio} \quad R = \frac{\sigma_{\min}}{\sigma_{\max}}$$

$$\textit{Stress level} \quad r = \frac{\sigma_{\max}}{\sigma_{rup}}$$

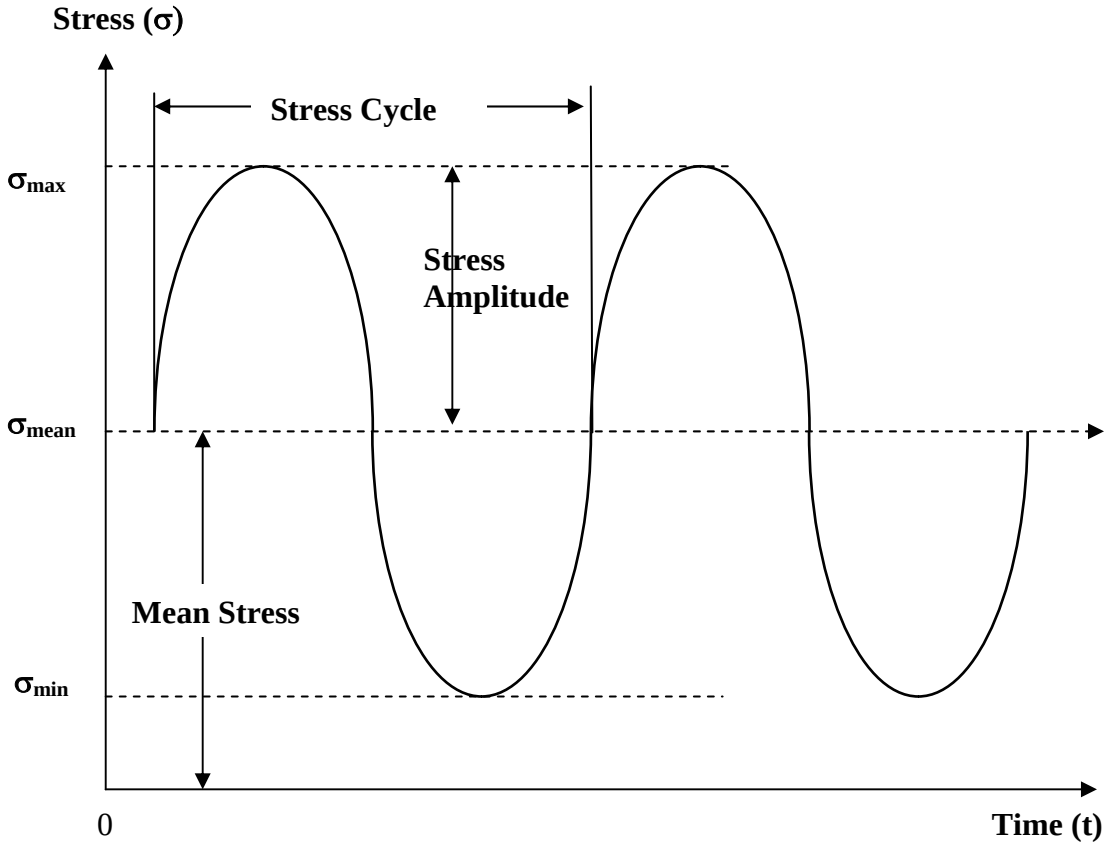


***Figure 3.6.*** *Sinusoidal loading for fatigue testing.*

The *R* value is an indication of the type of fatigue loading. Schematically, it is shown in figure 3.7. Table 3.4, summarised the important loading modes. In general, three different fluctuating stress-time modes are possible. First one, in which the amplitude is symmetrical about mean zero stress level, refereed as reverse stress cycle. Other type is termed as repeated cycle, in which maxima and minima are symmetrical relative to zero stress level. The third one is that in which stress level may vary randomly in amplitude and frequency.

***Table 3.4****. Fatigue loading modes as indicated by R values.*

| Fatigue stress ratio | Fatigue loading type |
|---|---|
| R = 1 | Static loading |
| R = 0 | Tension-unload |
| 0 < R <1 | Tension-tension |
| R = -1 | Tension-compression fully reversed |
| -1 < R <0 | Tension-compression |
| R > 1 | Compression-compression |

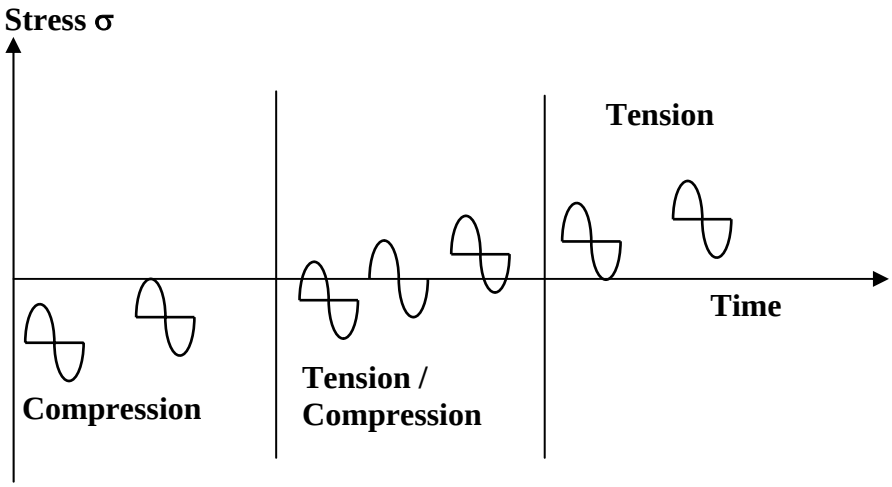


***Figure 3.7.*** *Types of fatigue loading.*

Fatigue loading can be done in number of ways as it is normally observed in real service loading conditions. Common types of applied stress loading are shown in figure 3.8 and can be named as tension, compression, flexural loading, torsion and shear. Types of the loading waveforms are sinusoidal, triangular, square and random.

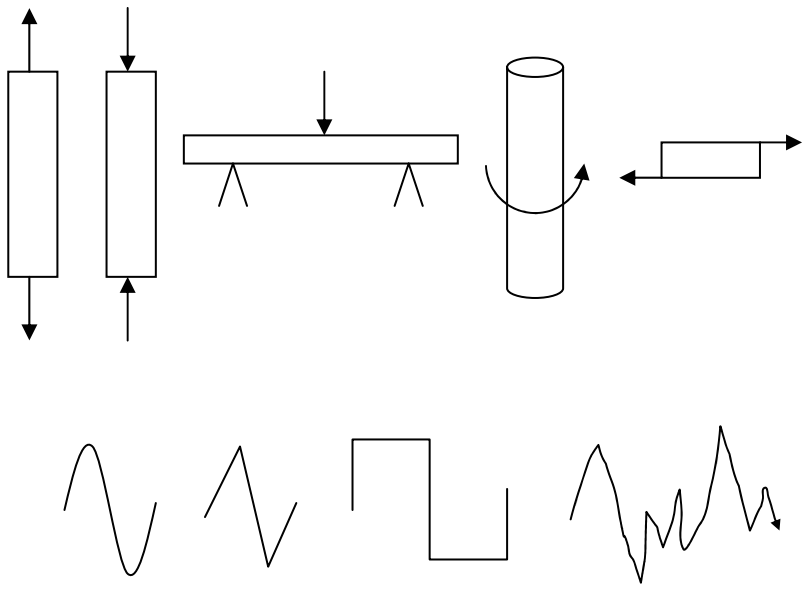

***Figure 3.8****. Types of loading and various type of load cycles wave forms.*

There are generally two kinds of loading controls in fatigue testing. First type is load (stress) type control and other is strain control. In stress control experiments, stress is kept constant and increase in strain is noted with time. On the other hand in strain control, strain is kept constant and reduction in stress with time is noted. Both types of loading control are commonly used in laboratory depending on the type of fatigue experiments. Stress control used to generate baseline data are the same as service loading conditions. Schematic representation of stress and strain control is shown in figure 3.9

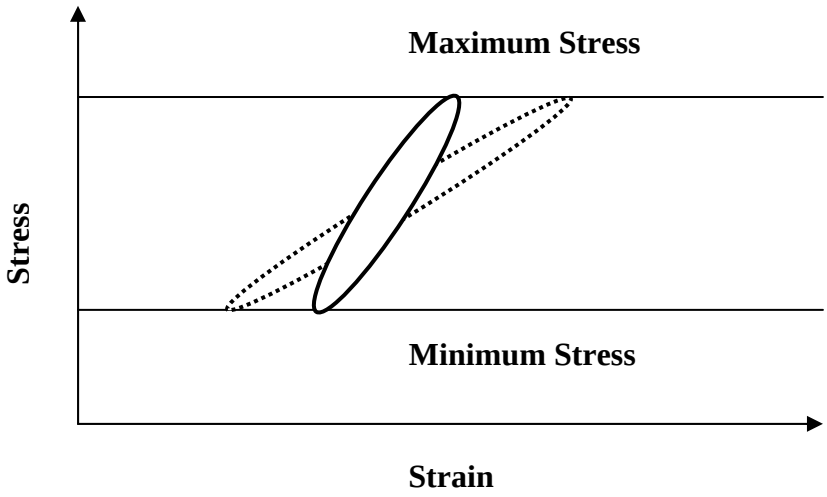


**a) Stress control**

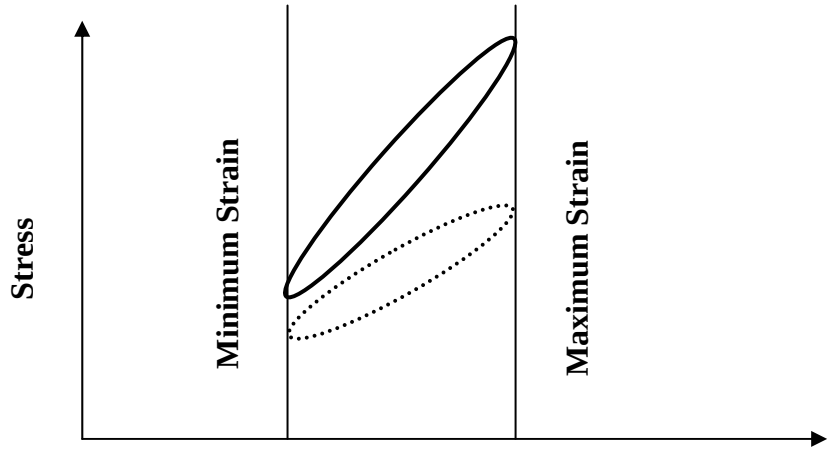


**b) Strain control**

***Figure 3.9.*** *Comparison of stress and strain control modes of fatigue testing on stress and strain behaviour.*

# Chapter 4
# Experimental analysis in static tests

## 4.1 Introduction

Laminate and core materials are non homogeneous and anisotropic, therefore properties will vary throughout the entire structure. Mechanical properties of sandwich composite depend on the properties of constituent materials; laminate and core material. Composites face sheets fail as a result of an interaction among matrix cracks, fibre fracture, delamination etc. In laminates, mechanical properties strongly depend upon the quantity, orientation of fibre and type of the matrix. In the core, it depends upon the thickness, density and cell structure of core. Therefore it is necessary to understand the behaviour of constituents of sandwich in details. In the following sections, experimental studies of skin and core behaviour under different loading conditions are presented.

## 4.2 Mechanical behaviour of skins under flexural loading

### 4.2.1 Introduction

These experiments are jointly performed within the Composites and Mechanical Structural Group of Maine University as a part of common studies for the skin material [112]. Generally, when cross ply laminates are subjected to mechanical loading, different failure mechanisms are induced: transverse matrix cracking in 90° plies, delamination between 0° and 90° plies, longitudinal matrix cracking which develops along fibre direction of 0° plies and fibre fracture in 0° plies [113]. Requirement for flexural static testing of structural elements with various modes of damages and different modes of loading should be defined in the beginning of testing procedure to provide necessary information for fatigue testing.

### 4.2.2 Materials and experiments

The laminates are made of 16 plies of glass fibre reinforced plastics with stacking sequence $[0_4/90_4]_s$. The main characteristic of the glass fibres and resins are given in the tables 3.1 and 3.2 of chapter 3. Specimens were cut from laminate sheets of 300 × 300 mm dimension according to the ASTM standard D 790-84a using diamond saw. Dimensions of the specimen were 90×15×4.2 $mm^3$ respectively. Distance between span supports is kept at 70 mm.

### 4.2.3 Results

Static tests were performed in 3-point bending under displacement control, in which laminates were loaded until failure, at a constant rate of 2 mm/min. Values for $F_u$ (ultimate failure load), $d_u$ (ultimate failure displacement), and stiffness for each laminate specimen were obtained from these tests. An average value of stiffness and fracture characteristics of five specimens were selected.

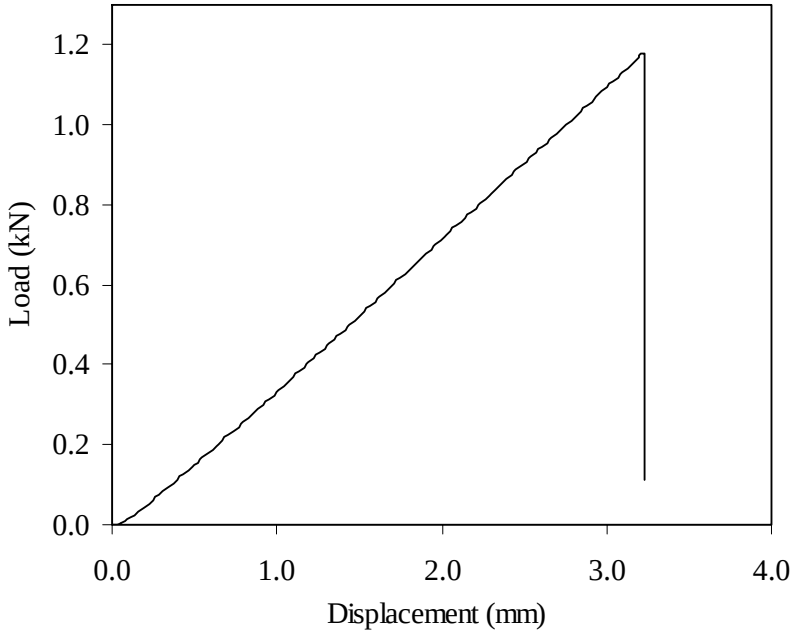


***Figure 4.1.*** *Load-displacement curve of GFRP laminate in three point bending in static test.*

Figure 4.1 represents a typical load-displacement curve obtained for glass fibre laminate $[0_4/90_4]_s$. The behaviour of glass fibre laminate is linear until the failure, which is of brittle type. The values of the stiffness, the load and the deflection at failure for the laminates are 350 N/mm, 1180 N and 3.32 mm respectively.

### 4.2.4 Fracture topography

The fracture topographies of failure of laminates have been observed by optical and scanning electronic microscopes and is shown in figure 4.2 for damaged glass fibre laminates. The analysis of the results shows that the mode of damage and failure strongly depends upon the glass fibre orientation.

The first damage that occurs in the laminates is the transverse cracking, which induce local stress concentration at crack tips and consist in formation of interlaminar cracks running parallel to the fibres in 90° layers due to fibre matrix debonding and matrix cracking [113,114]. Transverse cracking is a progressive damage mechanism which develops with the increase in applied loading. Therefore, there are very small changes observed in the load-displacement response shown in figure 4.1, which can be related to the development of transverse cracks. The total failure was due to delamination and by the failure of the compressed face in the vicinity of the point of application of the load. This mode of rupture in compression is rarely seen in bending of the unidirectional composite glass/epoxy during tests. The presence of the upper roller induces strong local constraints at the point of contact, which are to be superposed to the global stress state generated by the bending of the specimen. Uemura [115] and Binienda *et al.* [116] have studied these problems due to the diameter of the supports and central roller. They

also found a pronounced stress concentration at the vicinity of the central roller in 3-point bending.

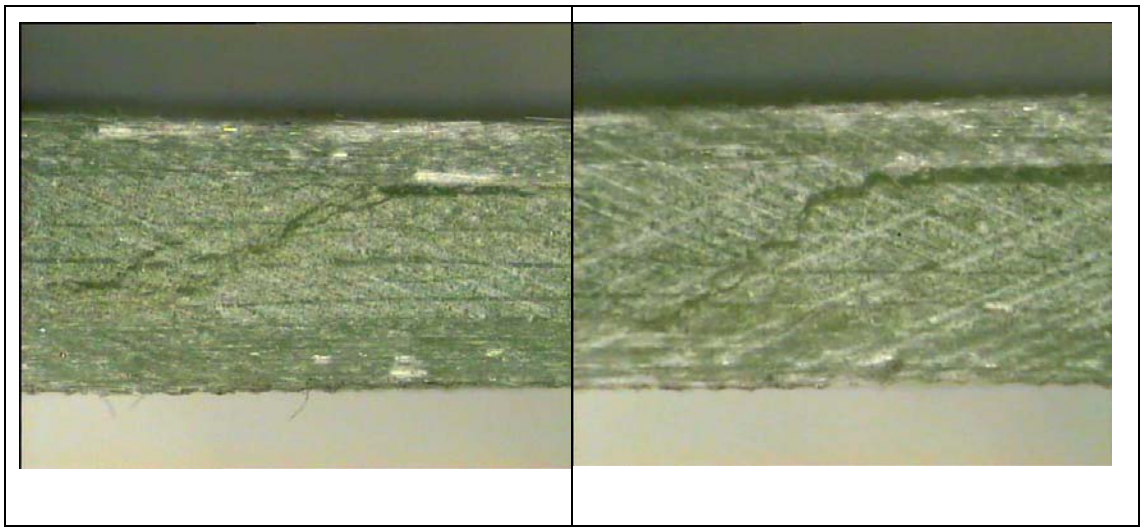

***Figure 4.2.*** *Observations of fracture surfaces in static tests for glass fibre laminate.*

## 4.3 Mechanical behaviour of foams

### 4.3.1 Introduction

For the characterisation of foams and the evaluation of their potential applications, determination of their mechanical behaviour is important. The mechanical response of foams in static tests must be well characterised in order to analyse the extent of damage in sandwich structures. The application of external loads induces significant local deflections of the loaded skin into the core material, thus leading to different kind of damage mechanisms in the core materials. Series of static tests were carried out on foams of different densities to study the mechanical behaviour under compression, indentation, shear and in 3-point bending.

### 4.3.2 Compression tests

Four foams of different densities were considered for the static tests. For each material, the specimens, having nominal dimensions of 50×50×15 $mm^3$ were cut from foam panels of densities ranging from 60, 80, 100 and 200 $kg/m^3$ according to ASTM C 365-57 standard. Each test was repeated five times under the same nominal condition to determine the significance of response variability. These specimens were compressed at a constant rate of 2 mm/min between two steel plates. The tests were performed on a Instron machine using 100 kN load cell. Stress and strains were recorded.

Figure 4.3 shows typical stress-strain curves for rigid closed cell PVC foams for four densities: 60, 80, 100 and 200 kg/m$^3$, obtained by compressing a specimen quasi-statically along one direction. Three distinct regions can be identified from the stress strain curves. Each core density displayed an initial elastic region up to initial damage, followed by stress plateau, then a region of densification. Each of the three phases correlates to specific failure mechanisms that the foam undergoes during compression. At small strains, usually less then 5%, the behaviour is linear elastic, with a slope equal to Young modulus of the foam. For closed cell PVC foams, the linear region is controlled by bending of the cell edges and stretching of cell faces with the application of load. As the load increases, the compression of the air or gas trapped into the cell walls increases resulting in rupture of cell walls, the foam cells also begin to collapse by plastic collapse, plastic yielding or brittle crushing, depending on the mechanical properties of the cell walls. Collapse progresses at roughly constant load, giving a stress plateau, until the opposing walls in the cell meet and touch each other, when densification causes the stress to increase steeply, giving the final region of rapidly increasing strain [117]. It is observed from the figure 4.3 that with increasing the density of foams, the value of stress for starting the plateau region, is increased from 1 MPa to 5 MPa for lower density (60 kg/m$^3$) to higher density (200 kg/m$^3$). More stress is needed for the start of plateau region for high density foams. Therefore an increase in the foam density, allows us to improve mechanical characteristic: stiffness, plateau height, strength value and decrease in the length of yielding domain [117]. Values of mechanical constants obtained from results are presented in table 4.1. All the parameters are found to increase with the increase in density of the foams.

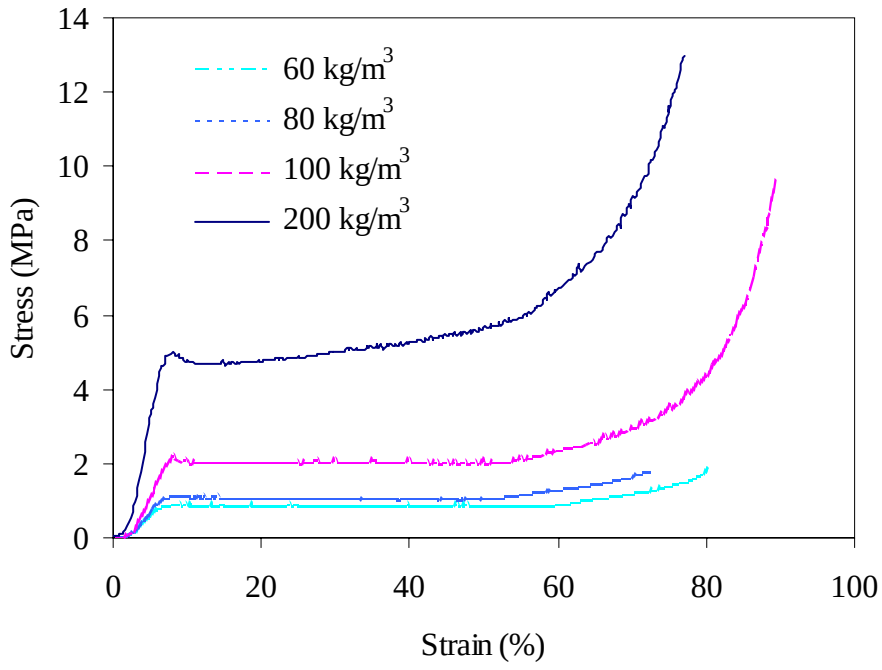


***Figure 4.3.*** *Stress-strain curves obtained for four core densities in monotonic compression tests.*

***Table 4.1.*** *Static characteristic of PVC foams in compression tests.*

| Density (kg/m$^3$) | 60 | 80 | 100 | 200 |
|---|---|---|---|---|
| Young Modulus *E* (MPa) | 25 | 39 | 50 | 110 |
| Poisson ratio | 0. 42 | 0.42 | 0.42 | 0.42 |
| Characteristics at the start of plateau | | | | |
| Stress $\sigma_1$ (MPa) | 0.85 | 1.30 | 2.10 | 4.95 |
| Strain $\varepsilon_1$(%) | 4.8 | 4.9 | 8.9 | 8.5 |
| Characteristics at the end of plateau | | | | |
| Stress $\sigma_2$ (MPa) | 0.90 | 1.20 | 2.16 | 5.92 |
| Strain $\varepsilon_2$ (%) | 45 | 49 | 57 | 56 |

The work done per unit volume in deforming the foam to a given strain or displacement is the area under the stress-strain curve. Very little energy is absorbed in the linear elastic region; it is the long plateau of the stress-strain curve that allows the energy absorption at nearly little increase in the load. It is apparent that with the increase in core density, the energy absorbing rate increased. With increasing the core density, cell size decreased, which offer more resistance in the deformation of the foam thus more energy is needed in compression. Increasing the density of the foams increases the slope of the linear elastic part, raises the plateau and reduces the strain at which densification starts. Also as the density of PVC foam increased, the rapid densification occurs at smaller strains which lead to shortening of stress plateau that can be observed for the foam of 200 kg/m$^3$ density in figure 4.3.

The lower the density of the foams, the wider the plateau, suited for energy absorption for many industrial applications. It is also observed that unlike dense solids, which are incompressible when deformed plastically, foams change their volume when compressed. So when the Poisson's ratio of the studied foam is about 0.42 in the linear domain, it is observed that compression along a given direction does not produce lateral spreading at the plastic yielding, leading to effective Poisson's ratio. Similar findings were also observed by Berthelot *et al.* [118].

### 4.3.3 Indentation tests

Sandwich beams can fail in several different ways. Indentation is one of the failure modes which strongly affect the behaviour of sandwich composites. Indentation of the core generally occurs due to concentrated loadings that can occur at fitting, at the corners, or at joints. Indentation can also be caused by accidental drops of loads on the cores. So it is also necessary to take into account the effect of core indentation in the overall behaviour of sandwich composites. Some tests exhibiting failures by core indentation have been performed by Berthelot *et al.* [118]. Since the main interest in this study is the mechanical behaviour in foams, we will consider, among the possible failure modes, which are governed by deformation of the foam core, that is, the failure by core indentation.

Experimental procedure for indentation tests was same as used in compression tests. In these tests, indentation is performed by a roller of diameter 35 mm. The speed of tests was 2 mm/min. The length, width and thickness of the specimens were 100, 40 and 15 mm respectively.

During the indentation tests, which were carried out on foams of different densities, it is observed that foam is compressed strongly in the proximity of the point of application of the load (indentor), that leads to extensive foam deformation in the area of contact with the indentor. With the further increase in the indentation load, foam densification is observed in the area under indentor, causing an effect similar to that observed during compression tests carried out on foam specimens as explained in the previous section 4.3.2. Load-displacement curves obtained in static indentation tests are shown in the figure 4.4. The load increases with the displacement approximately linearly until a displacement of 1 mm. After this foams continuously behave in a non-linear manner. Three distinctive regions can be identified in figure 4.4. However, evolutions of load versus displacement curves are slightly different in shape due to localised indentation as compared to the compression tests. The penetration of the indentor in the foam induces a high compression zone under the indentor which is propagated partially and progressively through the thickness of the foam specimen when the indentation is increased. In these curves, after very small initial region, there is plateau, which raises gradually in height with the increase in load and density of foams.

The indentation response of the foams is also related to its relative density. For this reason as the density of the PVC foams increases, an increase in failure load is observed. Also as density of PVC foam increased, the rapid densification occurs at smaller strains due to the decrease in cell sizes, which leads to a shortening of plateau, this phenomena can be seen in the figure 4.4 for the foam of 200 $kg/m^3$ density. Indentation is the mechanism which also depends on the roller diameter. There will be a more spread mechanisms of failure with small roller diameters [118,119].

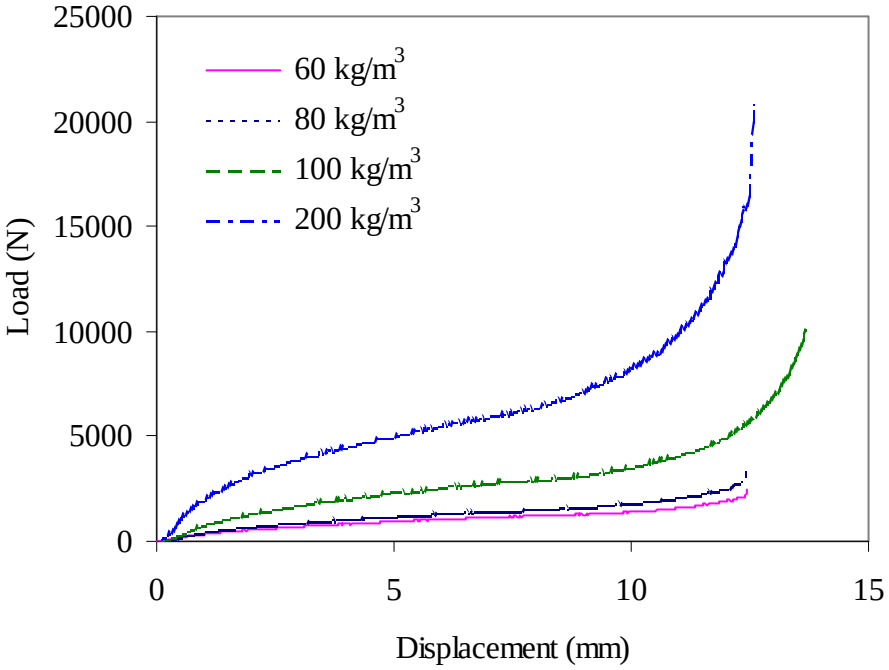


***Figure 4.4.*** *Evolution of load versus displacement for foams of four densities in static indentation tests.*

### 4.3.4 Shear tests

In order to study the shear behaviour of foams, shear tests were performed according to NF T 54-605, for foam specimens of two densities. For a structure made of sandwich material, shear stress plays an important role as the compressive stresses are transmitted between two skins by transverse shear of the core. The shear properties of the foams were determined in shear tests parallel to the planes of foam panels. The specimens used in these tests are cut from panels of PVC foams of thickness 200×50×15 $mm^3$ for two densities of 60 and 80 $kg/m^3$ and bonded to two metallic plates using epoxy resins. These tests were carried out using Instron Machine with load cell of 100 kN and shear test set-up is shown in figure 4.5. The load was applied at a constant rate of 1 mm/min, and the relative displacement between the loading plates was measured with a linear voltage displacement transducer (LVDT). Figure 4.6 shows stress-strain curves for foams of two different densities. In the beginning, load increase linearly with increasing the strain, then, the curve shows a non linear behaviour similar as observed in compression tests and at the end of plateau, foam fracture by the development of several cracks at an angle of 45°. For the foam of 60 $kg/m^3$ density, it is observed that at a strain of about 4.1 %, the first cracks (slips) appears in the corners of the core material, due to stress concentration where the corners of the core material is glued to the loading plates. The mean shear stress is about 0.75 MPa at this first crack. After these cracks (slips) the curves reaches a maximum stress of about 0.8 MPa and numerous cracks occurs causing total fracture of the spacemen at a strain of 15%. A reliable value of shear modulus is assumed to be average slope in the stress interval 0.1 and 0.5 MPa which is 22 and 30 MPa respectively for 60 and 80 $kg/m^3$ foams. Similar trend was observed for other foam

of 80 kg/m$^3$. The static characteristic increases with the increase in density as seen in the table 4.2.

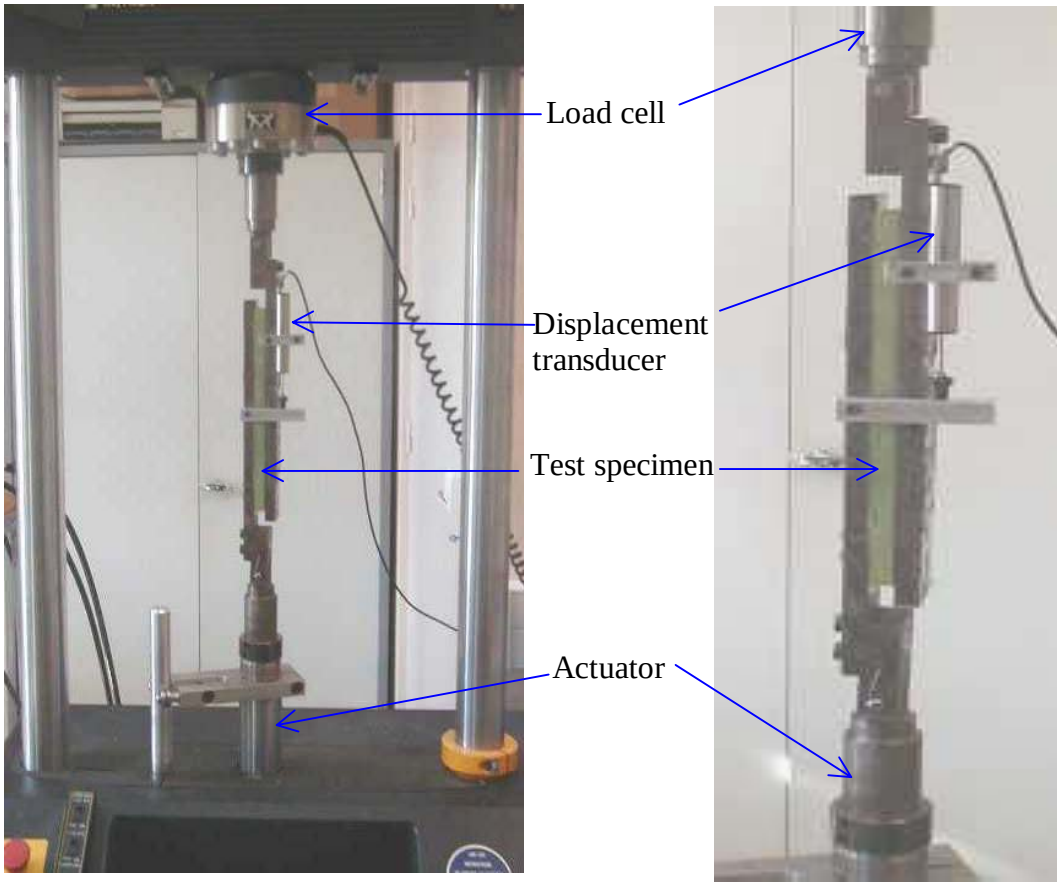


***Figure. 4.5*** *Shear tests set-up.*

***Table. 4.2.*** *Shear characteristics.*

| Proprieties | 60 kg/m$^3$ | 80 kg/m$^3$ |
|---|---|---|
| Shear modulus *G* (MPa) | 22 | 30 |
| Elastic limit | | |
| Stress $\tau_e$ (MPa) | 0.66 | 0.90 |
| Strain $\gamma_e$ % | 3.4 | 3.4 |
| Characteristic at failure | | |
| Stress $\tau_f$ (MPa) | 0.80 | 0.96 |
| Strain $\gamma_f$ % | 11 | 12 |

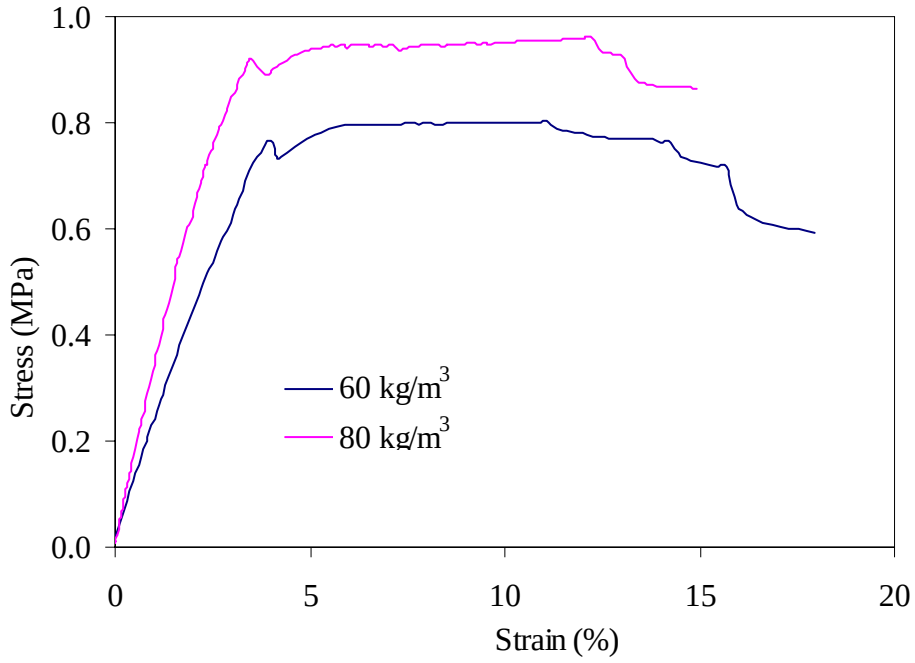


***Figure 4.6.*** *Stress-strain curves for foam of 60 and 80 kg/m$^3$ densities obtained in static shear tests.*

### 4.3.5 Flexural tests

Flexural tests were performed for the PVC foams specimens of four densities. Foam specimens of dimensions 200×40×15 mm$^3$ were cut from the foam panels using saw fitted with a diamond coated steel blade. The specimens were tested in three point bending according to ASTM D790-86 standard, at a span length of 160 mm with central roller of diameter 20 mm. Tests were conducted at a speed of 5 mm/min using Instron machine with 5 kN load cell.

Static tests were performed to obtain strength and stiffness data, which were later used for fatigue tests. Figure 4.7 shows load-displacement curves in static tests for PVC foams of four densities. After an initially linear response region, all curves reveal a substantial non linear response. The non linear response is attributed to plastic deformation of the cell walls under extensional and bending loads [117]. The failure process and load-displacement responses were indicative of ductile material behaviour. The properties of the core material, the density in particular are also found to control the static strength of the foams. The higher the core density the higher the static strength. All the foams show that after maximum load, there is no increase in load, while displacement increases until failure. The failure was characterised by almost vertical crack that initiated on the tension side of the beam and rapidly propagated on compression side. The failure process and the load deformation response are indicative of ductile failure. These cracks are shown in figure 4.8. It is observed that that cracks are of similar shape for four densities, thus assuming a similar kind of failure mechanisms for all foams.

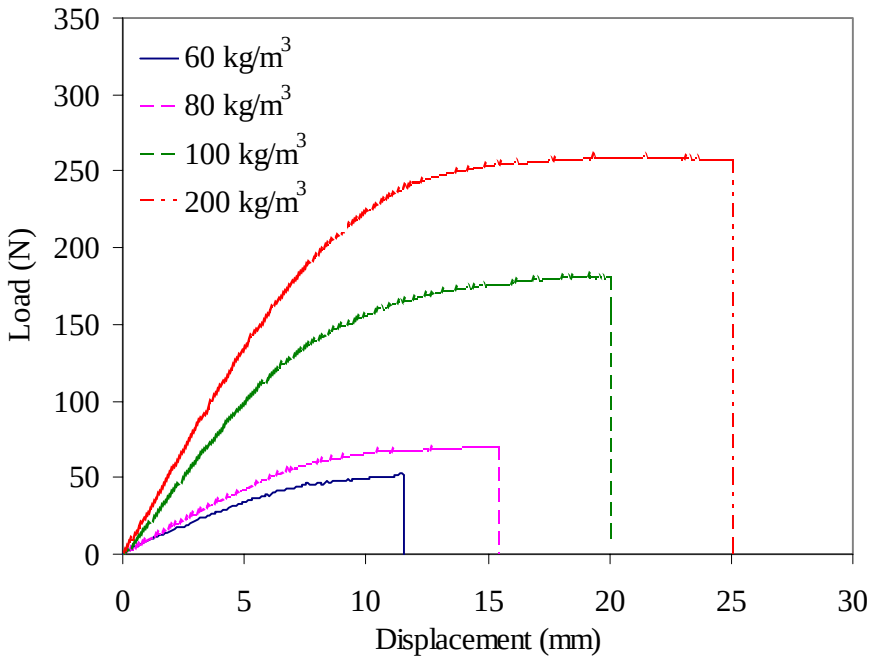


***Figure 4.7.*** *Load displacement curves for cores of four densities in three point bending static tests.*

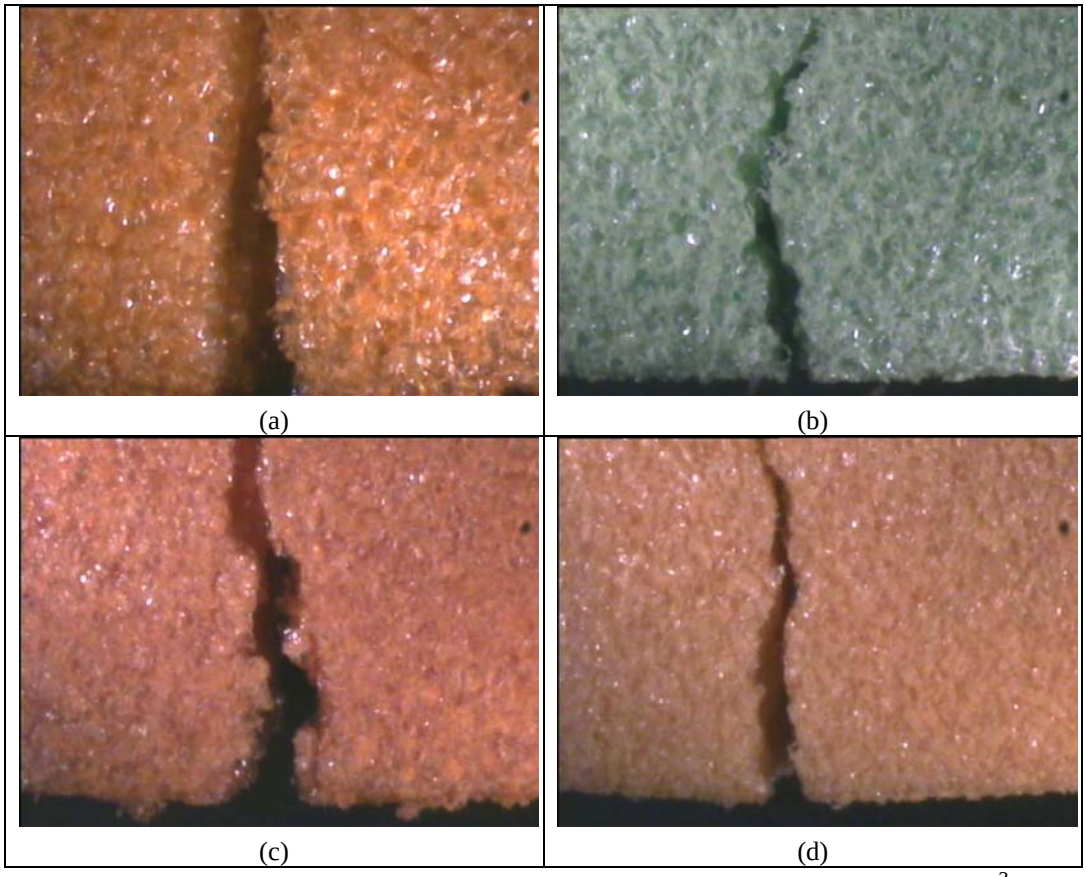


***Figure 4.8.*** *Crack propagation in flexural tests of foams of densities (a) 60 kg/m$^3$,(b) 80 kg/m$^3$ , (c) 100 kg/m$^3$ and (d) 200 kg/m$^3$.*

Values of failure loads, failure displacements and stiffness are presented in table 4.3. All the parameters are found to increase with increasing the density.

***Table 4.3.*** *Static characteristics of PVC foams for different densities in flexural.*

| Density of foams kg/m$^3$ | Failure load (N) | Failure displacement (mm) | Stiffness N/mm |
|---|---|---|---|
| 60 | 52 | 12 | 7 |
| 80 | 70 | 15 | 9 |
| 100 | 181 | 20 | 21 |
| 200 | 258 | 25 | 28 |

### 4.3.6 Failure analysis

The cell is the basic unit of the foam; its morphology and the chemical composition of the struts, both define the final properties of the foam. A cell is connected to the other cell through a series of struts and windows. The deformation of the foams is dependent on mechanical properties of the material of which the cells are made and on dimensions and arrangements of the struts and plates of which cells are composed.

Small sections of the foams from the selected failed specimens of the four densities (60, 80, 100 and 200 kg/m$^3$) were cut transversely to the beam axes 5 mm away from the failed centre region. Also virgin specimens were cut from the foam panels. Figures 4.9 to 4.12 shows representative SEM (scanning electron microscope) micrographs taken at suitable magnification for virgin and failed specimens for four foam densities. It can be clearly seen from the SEM pictures of damaged specimens that for low-density foams that some of the cells deformed by buckling while in the others, cells walls are touching each other. In lower density foams, after deformation, cells shape become irregular due to buckling and bending and stretching of the cell walls. Faces of the closed cells can be seen opened as due to compression of the adjacent cells, air inside the cells compressed, resulting in the rupture of the faces thus opening the cells faces as can be seen in figure 4.9 (a) and (b). Cell of PVC foams is unique among rigid plastic foams since it can be compressed up to 50 percent of its thickness without rupture or crumbling of the cell walls. That can be seen in the damaged specimens of all the densities and this property is well suited for certain industrial applications.

In closed celled PVC foams under compressive loading, the struts and plates oriented in loading directions are under pure compression. While the oblique struts and plates, that is the struts and plates in any other direction, will have bending stresses induced in them. Since most of the members in the foams are oblique struts and plates, bending is believed to the most important deformation mechanisms in foams. Because of the usually large slenderness ratio of struts for low-density foams, a strut in the loading direction will rather fail by elastic buckling than by compressive load. The buckling of the struts will be resisted by cell walls. Actually any bending or buckling of a strut will produce tension and compression in the attached cell walls, and it has also been reported that strut always will move to a state where one wall is tension and other

in compression. When the strut is in tension all the attached cells are stretched in tensile direction. The walls are in addition to stretching in the tensile direction subjected to tensile strains due to bending of oblique struts. For this reason the strains in the walls are larger than those in the struts and the cell walls are likely to rupture first. Cell arrangements of foams under compressive loading changes continuously and thus changes were observed in load displacement curves continuously. Micrographs of the damaged foam specimens reveal that severity of the damage in the foams decreases with increase in core density. Main damages in the cells are: shearing of cell walls, cell wall elongation due to bending, stretching and shearing of cell walls and complete cell wall buckling.

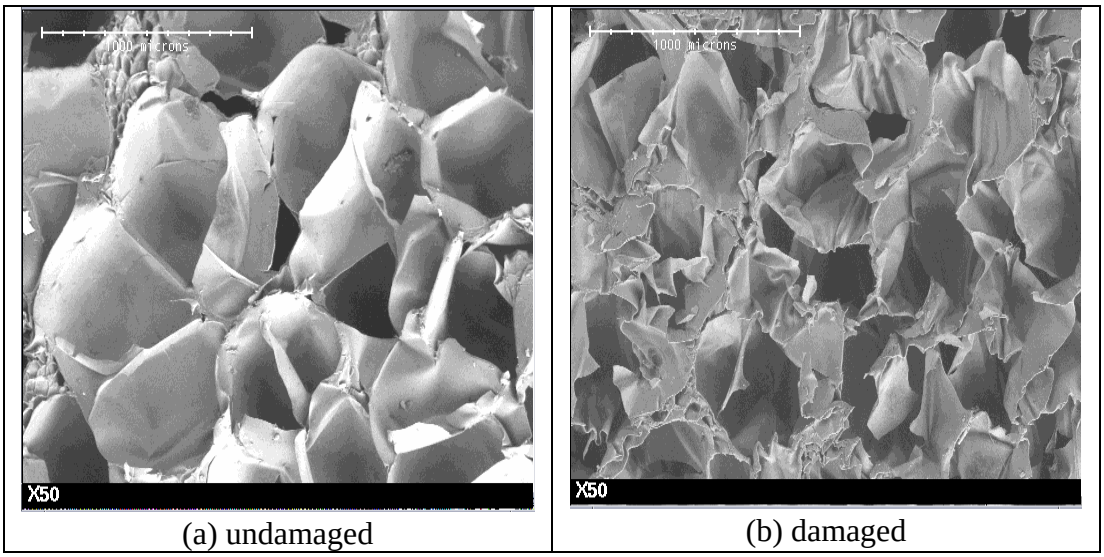


(a) undamaged (b) damaged

***Figure 4.9.*** *SEM photos of 60 kg/m$^3$ density foam for undamaged and damaged specimens in indentation tests.*

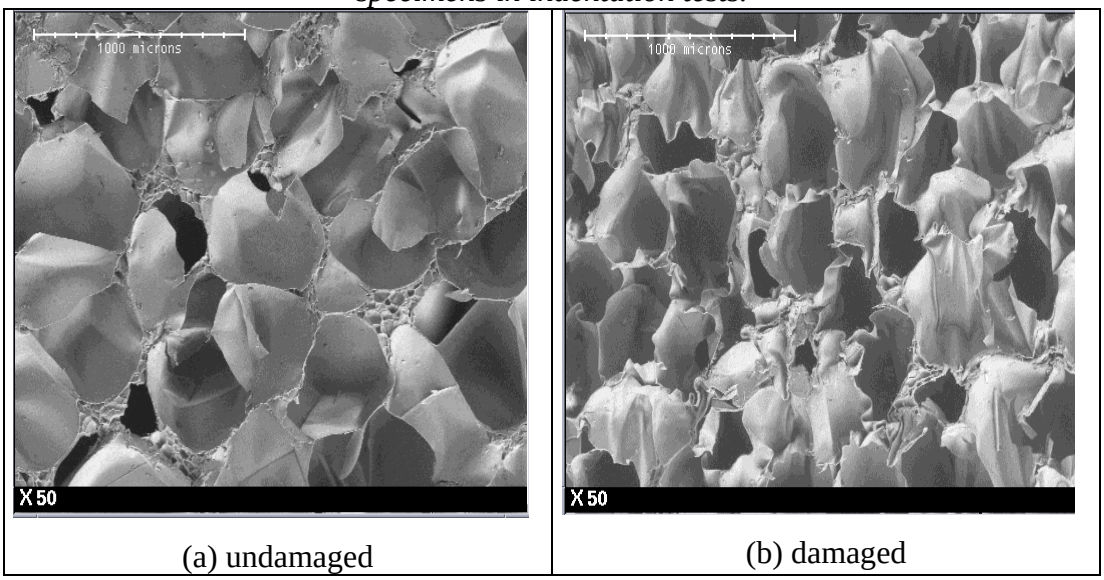


(a) undamaged (b) damaged

***Figure 4.10.*** *SEM photos of 80 kg/m$^3$ density foam for undamaged and damaged specimens in indentation tests.*

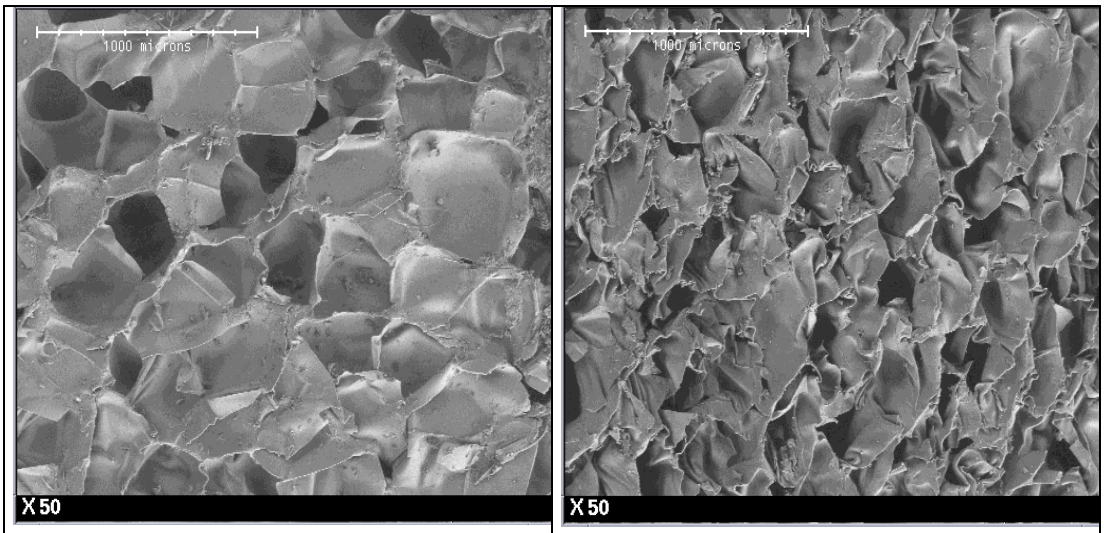


(a) undamaged (b) damaged

***Figure 4.11.*** *SEM photos of 100 kg/m$^3$ density foam for undamaged and damaged specimens in indentation tests.*

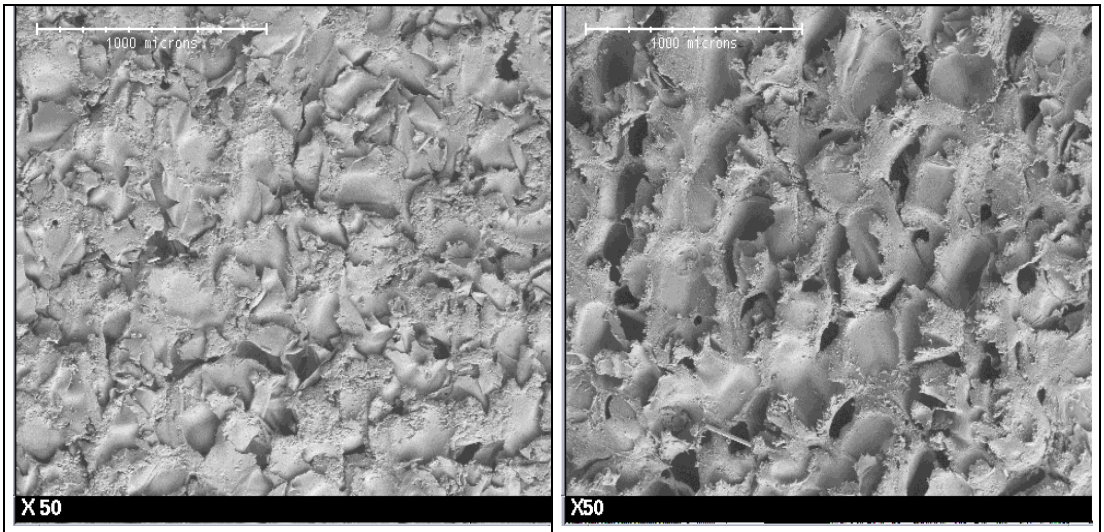


(a) undamaged (b) damaged

***Figure 4.12.*** *SEM photos of 200 kg/m$^3$ density foam for undamaged and damaged specimens in indentation tests.*

## 4.4 Mechanical behaviour of sandwich composites

### 4.4.1 Sandwich concept

In order to study the sandwich composite as a whole unit, static tests were performed with skin, core and then with sandwich as a complete unit. Figure 4.13 shows the three results obtained from static tests performed on skin, core and sandwich separately. These static tests were performed at span length of 50 mm. Thickness of the skin, core and sandwich was 1, 15 and 17 mm respectively. Failure load and displacement for skin at rupture is 227 N and 10.3 mm, while for foam it is 202 N but failure displacement is 3.4 mm. This results show that both element of sandwich have poor performance in static tests when tested separately. But when these two elements are combined in one single element by using epoxy resin, the failure load dramatically increased to 1400 N. This results provides excellent evidence of advantage for using sandwich construction in almost all the industrial applications, where weight saving is a crucial factor and where higher flexural rigidity is a basic need.

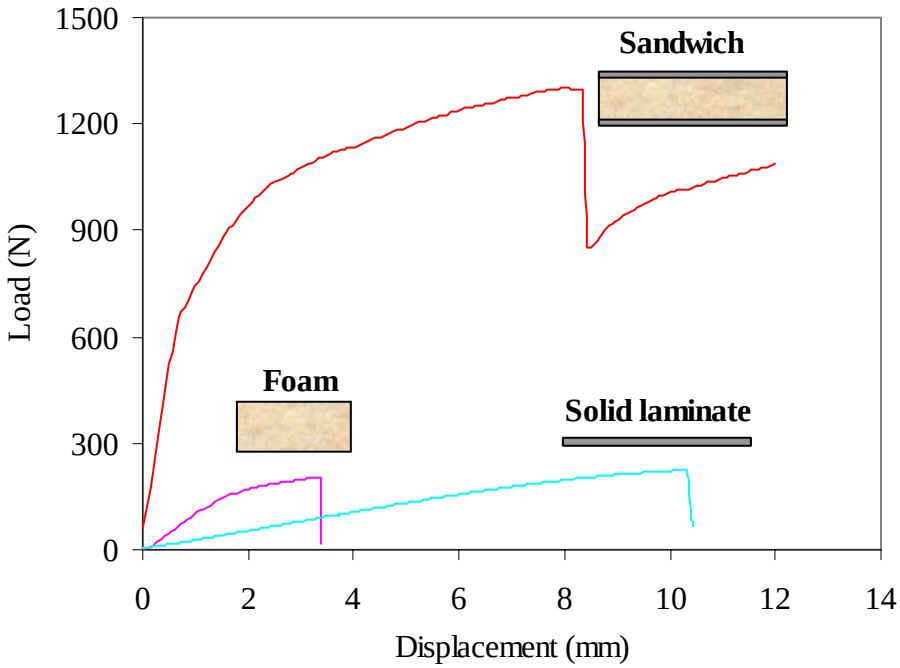


***Figure 4.13.*** *Sandwich Concept.*

***Table 4.3.*** *Static characteristics of foam, skin and sandwich.*

| Characteristics | Foam (15 mm) | Skin (1 mm) | Sandwich (17 mm) |
|---|---|---|---|
| Ultimate failure load (*N*) | 202 | 227 | 1400 |
| Ultimate failure displacement (*mm*) | 3.4 | 10 | 9 |
| Stiffness (*N/mm*) | 104 | 26 | 870 |

### 4.4.2 Experimental procedures

After performing the static tests for individual constituents of sandwich composites, number of static tests were performed to study the mechanical behaviour of sandwich composites as a whole. Sandwich beams were loaded under three point bending until failure at a span length of 250 mm with central roller of diameter 20 mm. Tests were performed at a constant cross head speed of 5 mm/min. The load- displacement curves were used to calculate the values for ultimate failure load ($F_u$), ultimate failure displacement ($d_u$), and stiffness for sandwich composite specimen of various core thickness and densities. Results from the static tests were later used to design the fatigue experiments.

### 4.4.3 Results

Figure 4.14 represents the evolution of the load with displacement for sandwich specimens with foam of 60 kg/m$^3$ and skins made of glass fibre reinforced plastics, at a span length of 250 mm. In this curve, the nearly linear elastic behaviour is evident until the load approaches 500 N. After that, behaviour becomes non-linear until the maximum load. Then the load decreases gradually with increasing displacement and a sudden drop in load is observed and after that it continued decreasing until the complete failure of specimen.

This curve apparently shows three distinct regions. The first region is primary region of compressive behaviour of skin laminates. This region initially corresponds to reversible linear behaviour and initiation, progression and development of transverse cracking in 90° plies of the skin, as observed in flexural testing of skins. The second region exhibits the compressive behaviour of core due to bending of the top skin and leads to non-linear behaviour of load-displacement curve that is mostly dependent on the properties of core. In the third region, with the further increase in load, there is initiation and development of delamination between skin and core which leads to the fracture of the skin. The fracture of skin corresponds to sudden drop of approximately 40% of the maximum load in the load-displacement curve. After the fracture of skin, load is transferred to the core material leading to crushing under concentrated loading.

The PVC foam in the central region of the specimen experiences the compressive stresses, which is reflected in the form a long plateau region in the curve. At the end of this plateau, all failure mechanisms combine and resulted in the complete failure of the specimen. Average values of stiffness, failure load and displacement for sandwich specimen tested in static tests were found to be 140 N/mm, 610 N and 6 mm, respectively. A typical example of above mentioned damage mechanisms can be seen in the figure 4.15. This figure is representing fracture topography of a failed sandwich specimen using optical microscope. It can be seen from figure 4.15(b) that failure is initiated on the lower side of the top skin adjacent with core which is under concentrated loading that leads to cracking of the top skin.

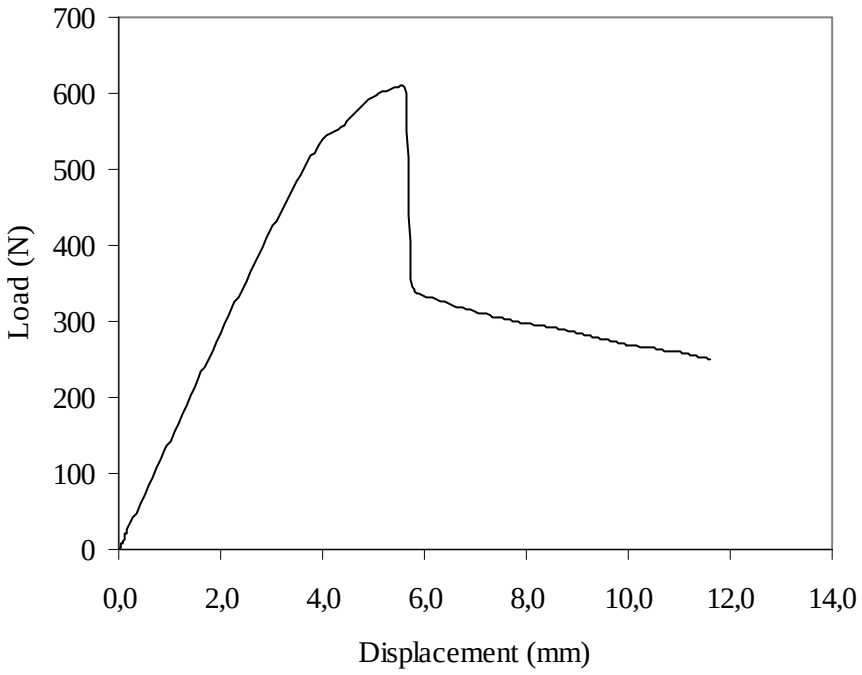


***Figure 4.14.*** *Load-displacement curves for sandwich specimens with glass fibre skin and core of 60 kg/m$^3$ density and thickness of 15 mm at a span length 250 mm in static tests.*

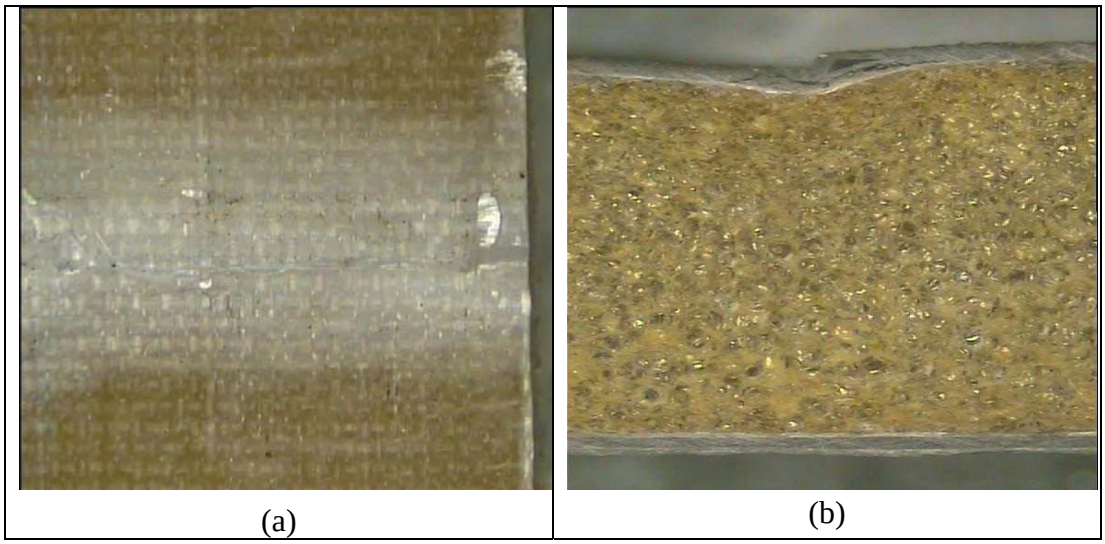


***Figure 4.15.*** *Typical damage modes in top skin during static test.*

### 4.4.4 On-line photography

We used on-line photography to observe the macroscopic damage evolution in sandwich specimens of two foam densities of 80 and 200 kg/m$^3$. Figures 4.16 and 4.17 show the evolution of load versus displacement related with photographs taken for sandwich specimen during static tests. Photographs were taken at a rate of 3 photos per seconds.

First picture was taken just after the start of the test. It is shown as point (**a)** in the load-displacement curve in figure 4.16. Second picture was taken at the point (**b)** of this curve, when due to loading, deflection of the beam started. Third picture is taken when load reaches at point (**c)** of the load-displacement curve and shows an increase in deflection that increased with loading. Finally last picture is taken at point (**d)**, when the deflection is quite high with considerable damage in the skin but before final failure. It was observed that concentrated loading caused a bending of the skin (buckling) to greater extent and core is bearing high compression stresses. The core is taking a lot of bending stresses of the skin without being fracture. This bending (buckling) of skin kept on increasing to a limit when bending stresses of skin reaches to ultimate flexural strength resulting in failure of the top skin leading to failure of the sandwich specimen. At this stage, the skin crushes the panel indicating poor compressive strength of the core. The direction of buckling (crushing vs. separation) depends on the curvature of the panel, its stability and applied load. That was not shown in the figure as duration of the tests becomes large when the specimen broken, however, the post fracture observation showed that failure is similar to that shown in figure 4.15 in the case of sandwich specimen of 60 kg/m$^3$ density.

Figure 4.17 also shows four pictures for a sandwich specimen of high density 200 kg/m$^3$, taken at different stages of the static test. First picture is taken at the start of test representing as point (**a)** in the load-displacement curve. At the beginning the deflection increases linearly with load. Second picture representing by point (**b)** in the load-displacement curve was taken when a cracking noise was heard due to the breaking of the top skin and curve become slightly non-linear and then there was start of an initiation of interfacial debonding between the top skin and core. This mechanism rapidly propagated under the top skin and the core and is represented by point (**c)** in load-displacement curve and by picture (c). In the fourth picture (d), with the further increase in loading, interfacial debonding is seen propagating along the transverse direction and causing the top skin failure resulting in rapid decrease in load and these events are represented by point (**d)** on the load-displacement curve. Failure of sandwich specimens strongly depends upon the density of the foams. It is observed that sandwich specimens with high density foams exhibit a brittle fracture while low density foams exhibited ductile type failure.

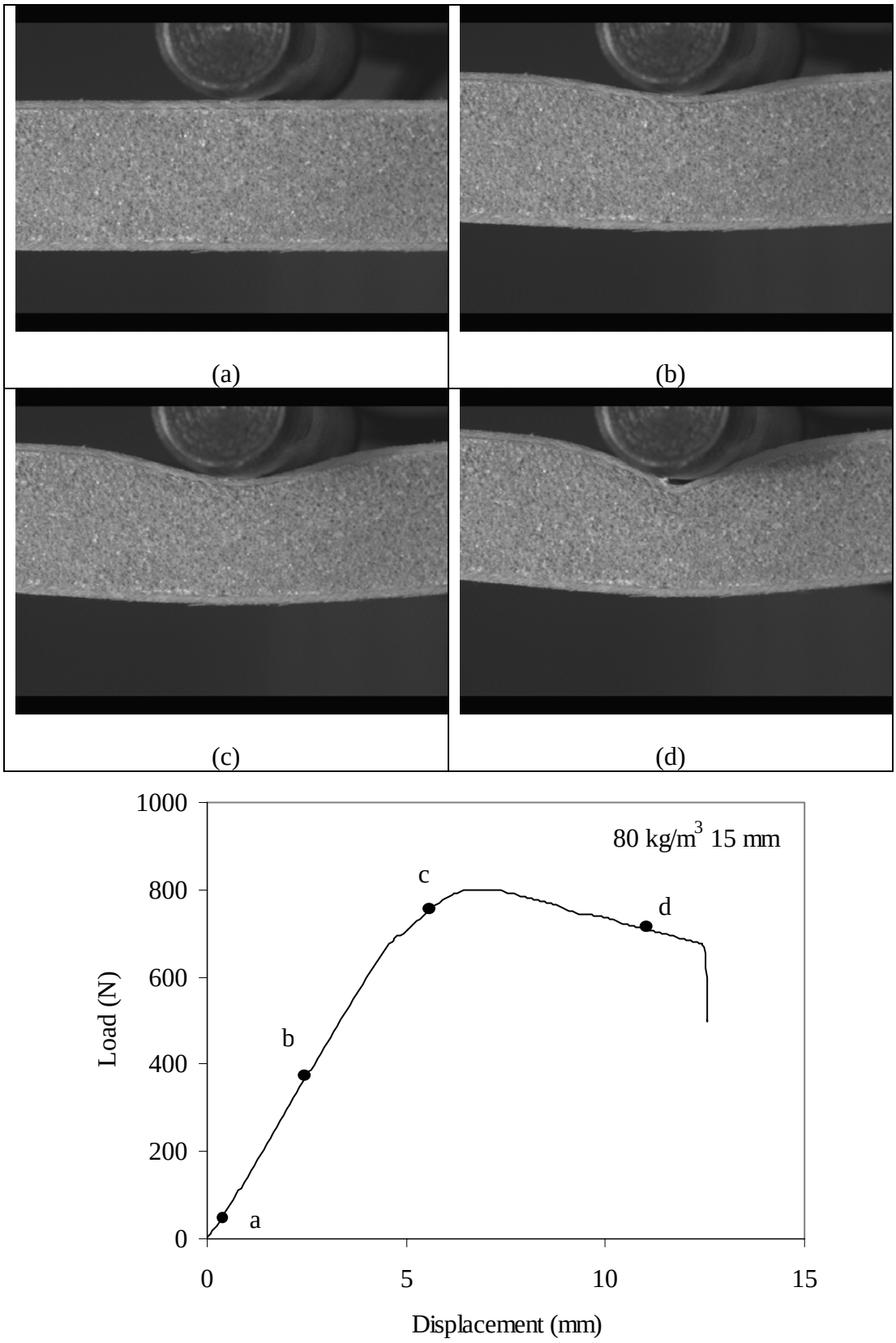


***Figure 4.16.*** *Load-displacement evolution with on-line photography for sandwich specimen of 80 kg/m$^3$ foam density.*

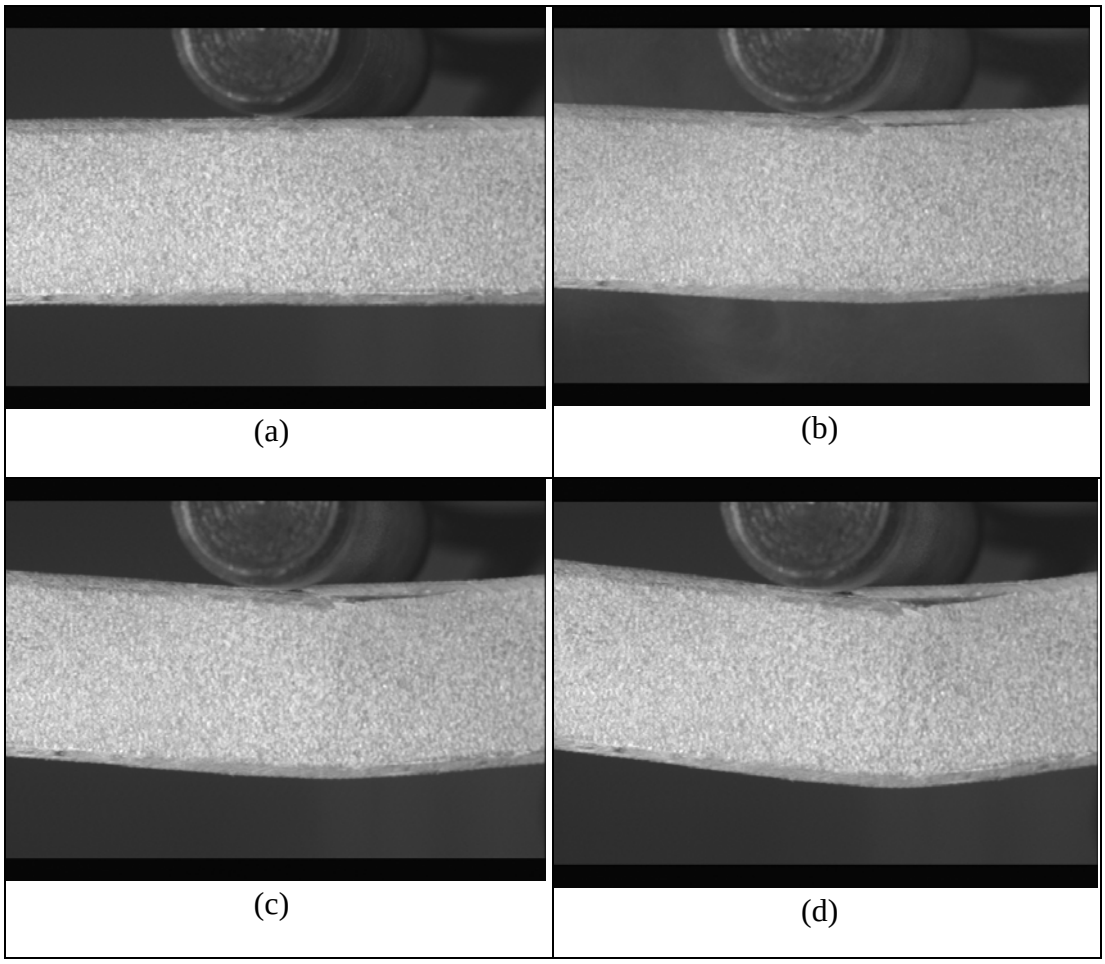


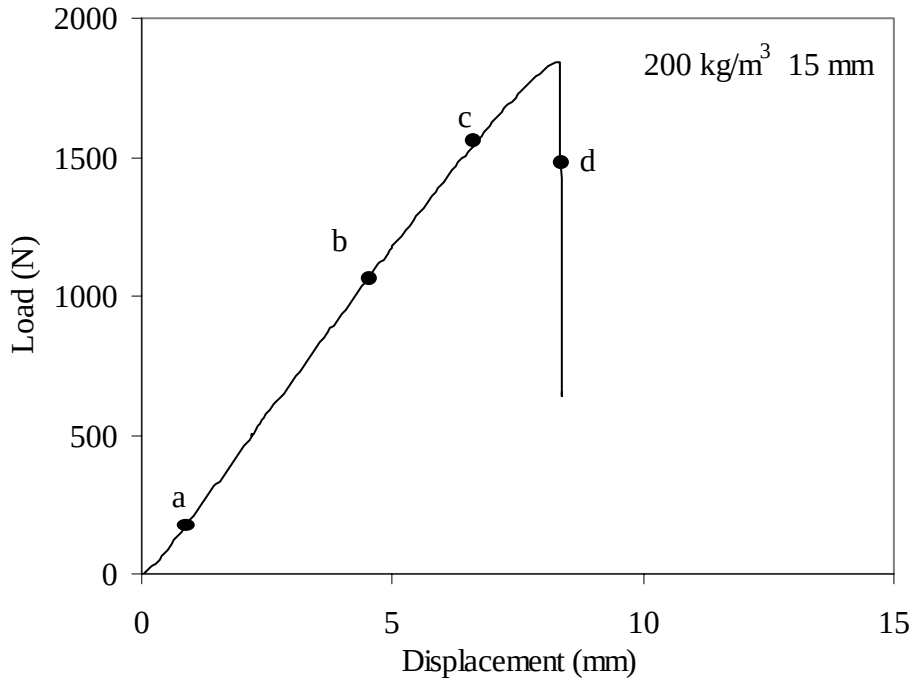


***Figure 4.17.*** *Load-displacement evolution with on-line photography for sandwich specimen of 200 kg/m$^3$ foam density.*

### 4.4.5 Influence of core thickness

In order to study the influence of core thickness on the behaviour of sandwich panels in static tests, PVC cores of 60, 80, 100 kg/m$^3$ density with different core thickness (15, 20 and 25 mm) were used. Thickness of the skin is 1 mm for all the sandwich specimens used in this study. Span length for sandwich specimens was kept constant at 250 mm. Generally increasing the core thickness resulted in greater flexural failure stresses and strains. Because these properties are highly dependent on the quadratic moment of the specimen about the mid plane. Since the quadratic moment is proportional to the cube of thickness, so with increasing the core thickness the bending moment increases with high proportions resulting in an increase in flexural rigidity

Figures 4.18 to 4.20 report the evolution of load-displacement curves for sandwich specimens of various core thickness and different densities. For the sandwich specimen of smaller core thickness of 15 mm, we observe a linear behaviour until failure which was brittle in nature. After post analysis of the failed specimens it was observed that only skin is found to be broken under the point of loading. While for larger core thickness of 25 mm, load-displacement curve initially reveals a linear behaviour and then a non-linear behaviour until maximum loading is achieved. Load then decreases gradually with the increase in deflection. As previously mentioned that failure of the specimens was due to skin failure underneath the central support. Although in the case of higher thickness, sandwich specimens are subjected to transverse loading, but no failure was found by shear. These results showed that after the skin failure of the specimens, a local crushing of the core was observed at the point of application of the concentrated loading. It occurs without any significant local dent or deformation at loading point itself. From the load versus displacement graphs it was clearly observed that by increasing the core thickness failure loads increased. Static strength of larger thickness core sandwich specimens was higher then the shorter thickness core specimens.

From these experimental results, it is observed that with an increase in thickness, the start of plastic deformation can be delayed, resulting in an increase of ultimate failure strength. Table 4.4 shows the various parameters obtained from static tests. It can be seen that with increasing the core thickness bending stiffness and ultimate failure loads increased.

***Table 4.4.*** *Characteristic obtained from static tests for sandwich specimens of various core thickness and densities at same span length of 250 mm.*

| Density kg/m$^3$ | Core thickness (mm) | Stiffness (N/mm) | Failure load (N) | Failure displacement (mm) |
|---|---|---|---|---|
| 60 | 15 | 175 | 762 | 5.5 |
| | 20 | 215 | 941 | 6.3 |
| | 25 | 302 | 1081 | 10 |
| 80 | 15 | 177 | 800 | 6.8 |
| | 25 | 366 | 1516 | 7.5 |
| 100 | 15 | 222 | 1166 | 6.5 |
| | 25 | 487 | 1920 | 6.2 |

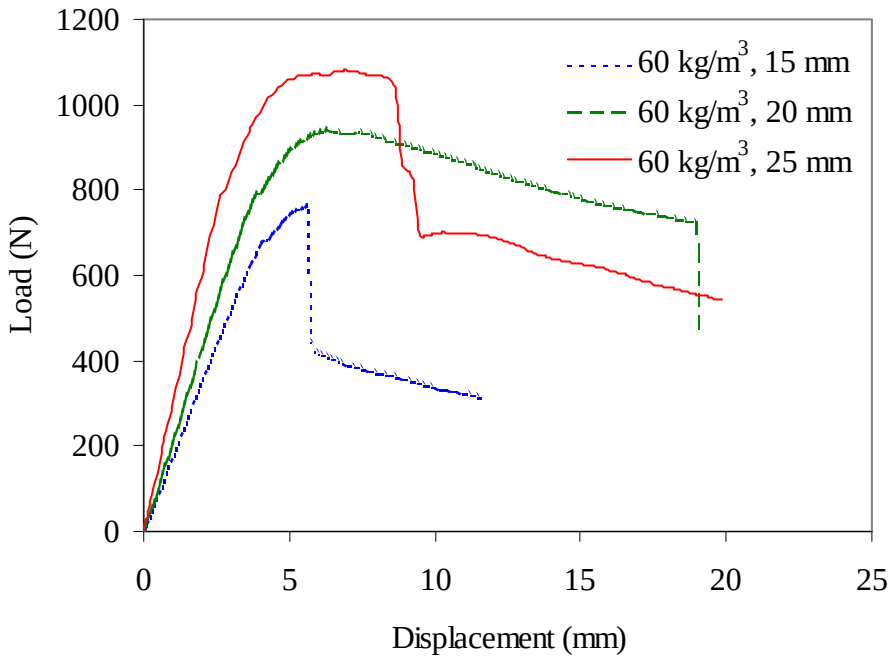


***Figure 4.18.*** *Load-displacement curves obtained in 3-point bending tests at a span length of 250 mm for sandwich specimens with foam cores of different thicknesses of 60 kg/m$^3$ density.*

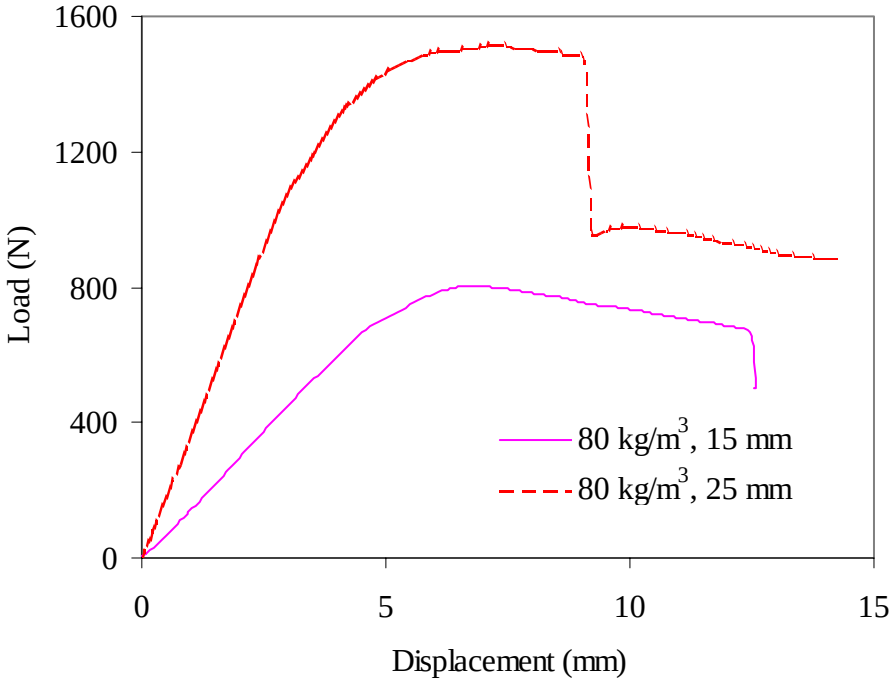


***Figure 4.19.*** *Load-displacement curves obtained in 3-point bending tests at a span length of 250 mm for sandwich specimens with foam cores of different thicknesses of 80 kg/m$^3$ density.*

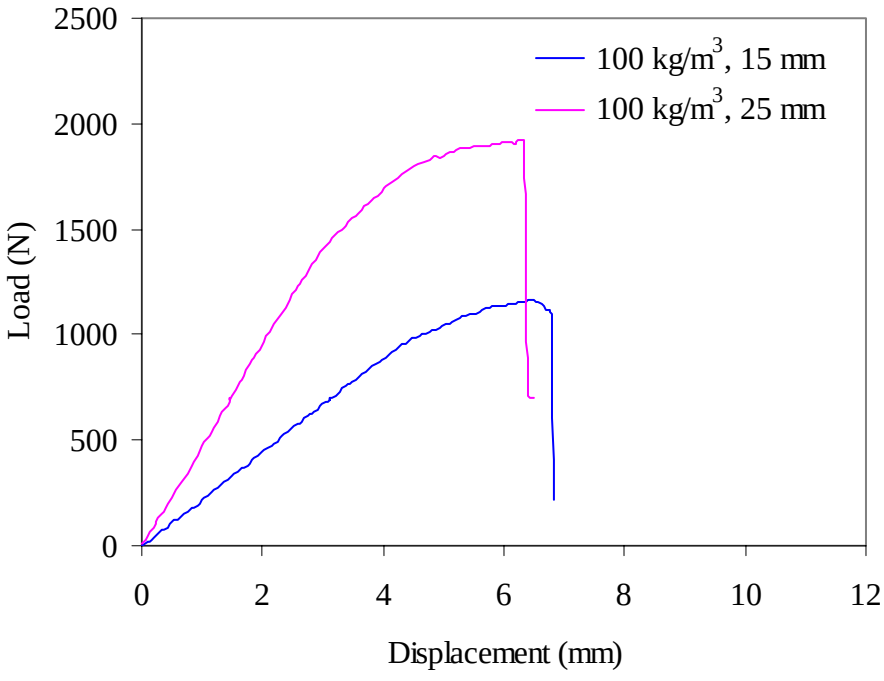


***Figure 4.20.*** *Load-displacement curves obtained in 3-point bending tests at a span length of 250 mm for sandwich specimens with foam cores of different thicknesses of 100 kg/m$^3$ density.*

### 4.4.6 Influence of core density

Sandwich specimens of PVC core of four densities were used for static tests. Figures 4.21 to 4.23 show the evolution of load with displacement for specimens of different densities at three span lengths (100, 250, 400 mm) and for the same core thickness of 15 mm. It is evident from these figures that evolution of load versus displacement strongly depends on the core density of the sandwich specimens. With increasing the core density, the failure load and stiffness increases. These results can be attributed to the cell size of PVC cores. As with increasing the core density, the cell size decreases and therefore these cells offer more resistance to the applied load resulting in increased failure loads.

For sandwich specimens of low foam densities, initially there is linear behaviour, and then behaviour become non-linear until the higher load, after that there is rapid drop in load followed by complete failure of the specimen. While, for sandwich specimens of higher foam densities, there is complete linear behaviour until failure which is brittle in nature. It is also observed that with increasing the span length, failure loads decreases but failure displacement increases due to shifting of shear dominated failures to pure bending failures.

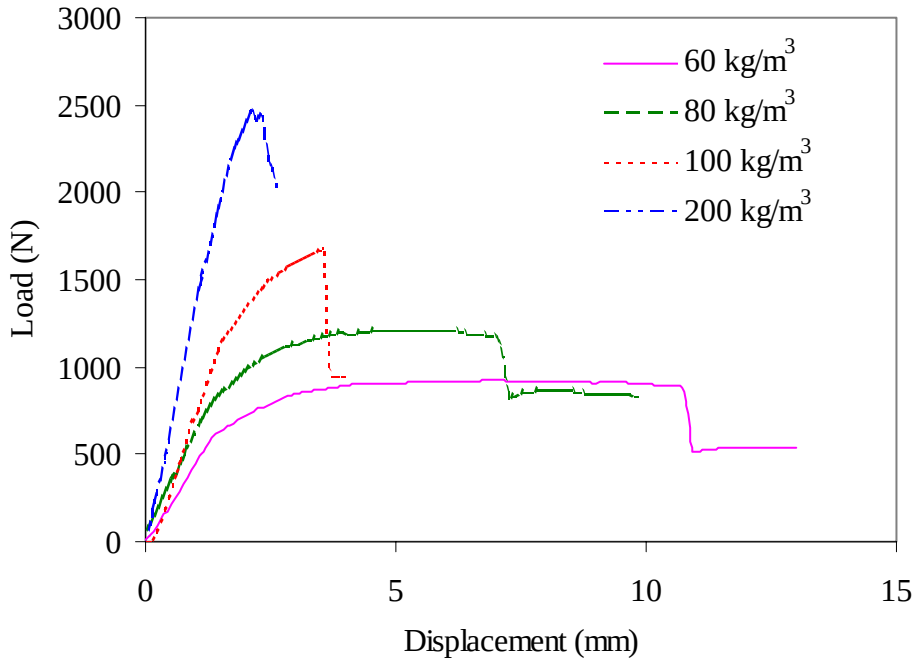


***Figure 4.21.*** *Load-displacement curves obtained for sandwich specimens in 3-point bending tests at a span length of 100 mm with foam cores of 15 mm thickness and different densities.*

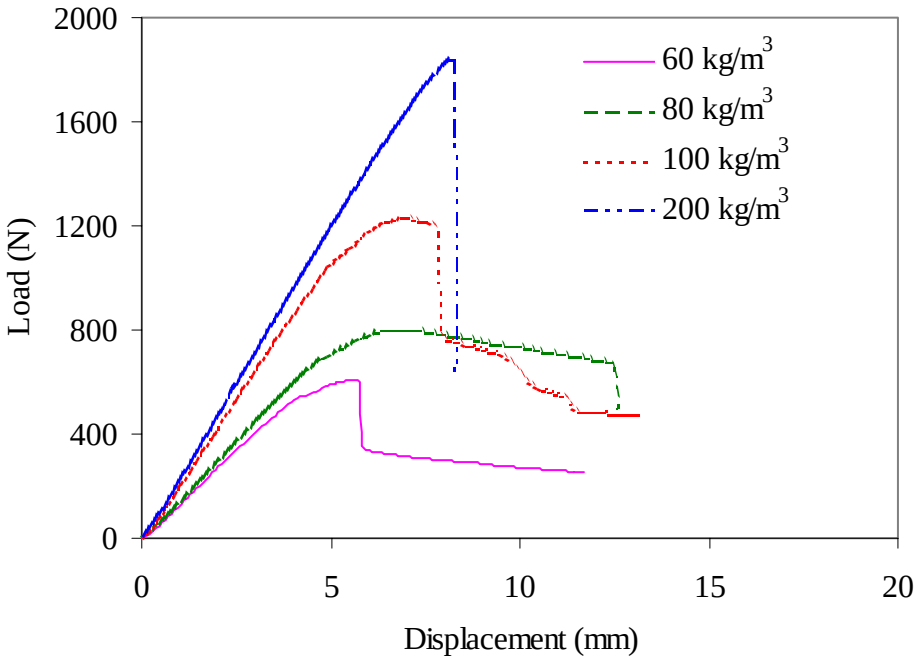


***Figure 4.22.*** *Load-displacement curves obtained for sandwich specimens in 3-point bending tests at a span length of 250 mm with foam cores of 15 mm thickness and different densities.*

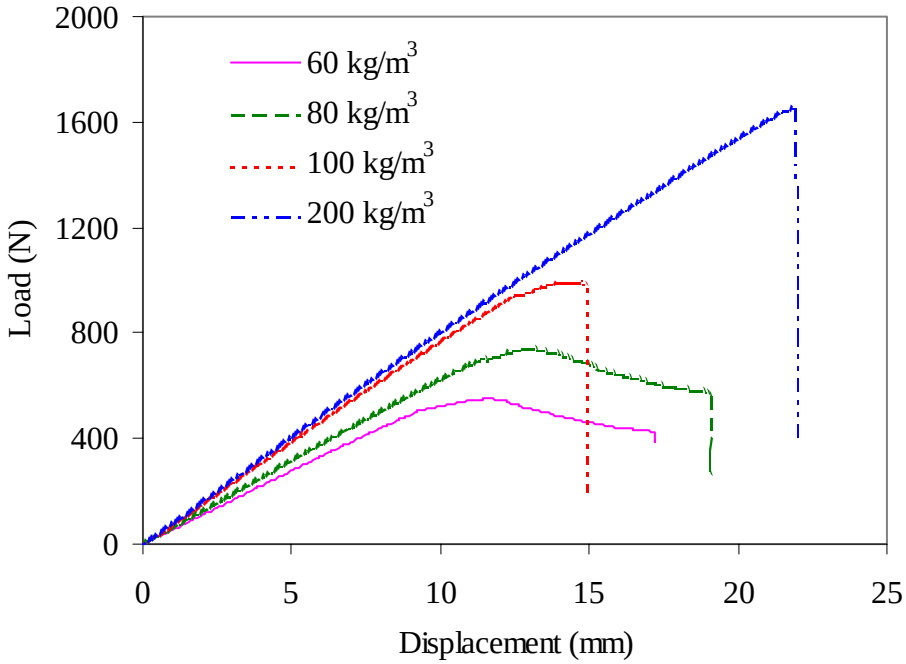


***Figure 4.23.*** *Load-displacement curves obtained for sandwich specimens in 3-point bending tests at a span length of 400 mm with foam cores of 15 mm thickness and different densities.*

### 4.4.7 Bending and shear stresses with span length

In order to study the effect of span length on core shear and face bending stresses, the relations suggested in ASTM C393 standards were used. Face bending stress was calculated by using the following formula:

$$\sigma = \frac{PL}{2t(d+c)b} \tag{4.1}$$

where

$\sigma$ = face bending stress
$P$ = maximum load (N)
$d$ = sandwich thickness (mm)
$c$ = core thickness (mm)
$b$ = sandwich width

Figure 4.24 shows the evolution of face bending stress with the span length for four core densities. It can be seen from this figure, that face bending stress increases with the increase in the span length. Variations of face bending stress for three low core densities are similar. This variation increases with the increase in core density.

The core shear stress $\tau$ can be calculated using the following formula:

$$\tau = \frac{P}{(d+c)b} \tag{4.2}$$

Figure 4.25 shows the evolution of core shear stress versus span length for four core densities. Shear stress decreases with increasing the span length and increase with increasing the core density. For the higher core density of 200 kg/m$^3$, there is slightly rapid decrease in shear stress until 220 mm span length and there after that there is gradual decrease. At higher span lengths, shear stress is found to be almost constant as skins are taking loads in bending. Span to depth ratio plays an important role for shear stress. At smaller span length core shear stress is dominated and at higher span length bending stresses are important. Generally, the failure of sandwich under flexural loading is obtained by the fracture of top skin in the contact with central support. For small span lengths, we rarely observed failure by shear of core during static tests. It is observed that types of the failure of the specimens strongly depend on the span length.

Figures 4.26 and 4.27 shows the face bending stresses and core shear stresses at one span length of 250 mm for sandwich specimens of four densities. Marked increase in face bending and shear stresses is observed for low and high density sandwich foams specimens.

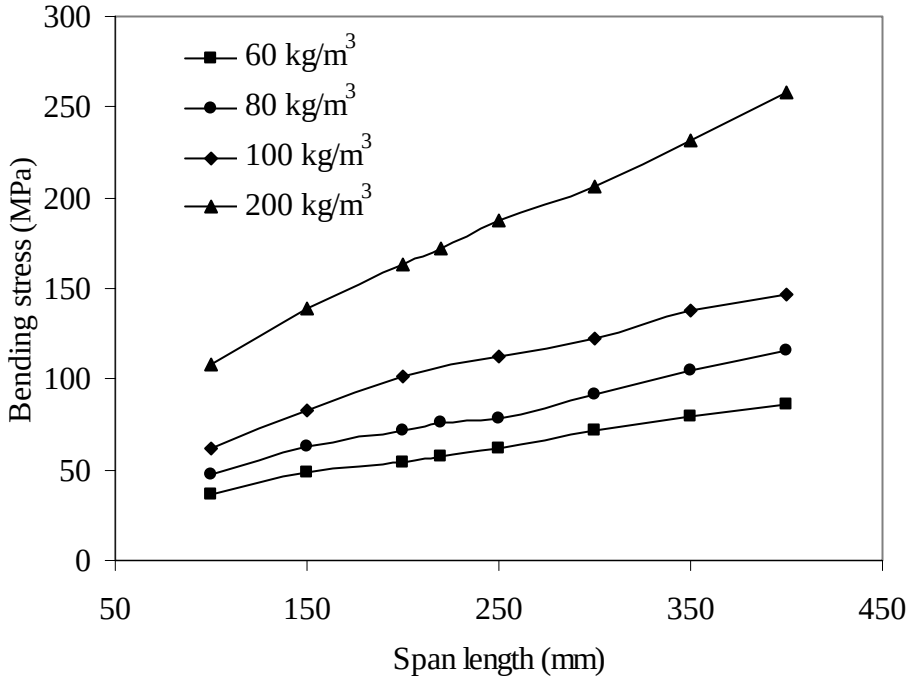


***Figure 4.24.*** *Evolution of bending stress versus span lengths for sandwich specimens* of four densities.

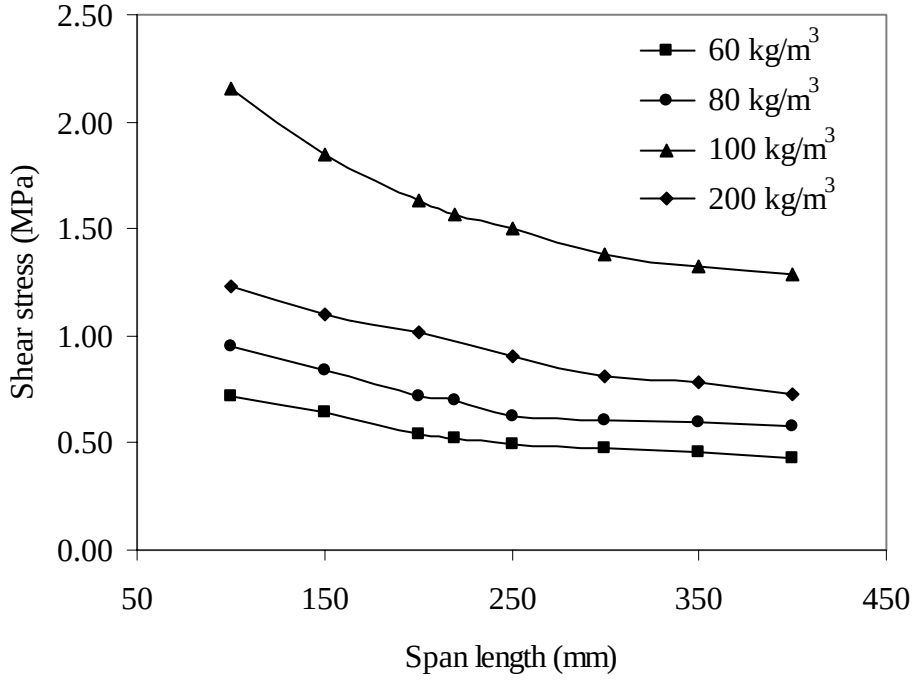


***Figure 4.25.*** *Evolution of shear stress versus span lengths for sandwich specimens of four densities.*

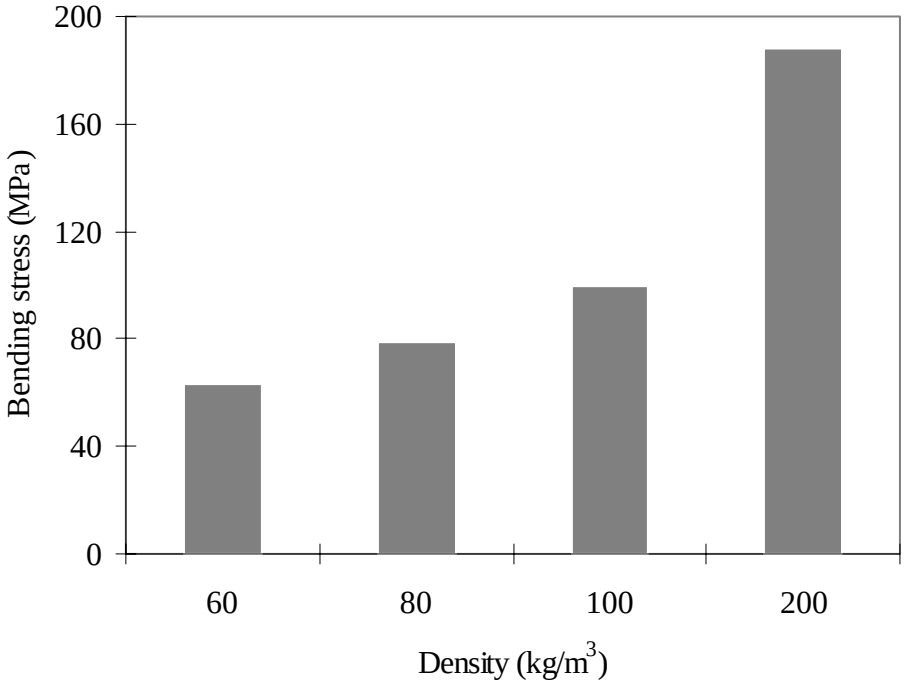


***Figure 4.26.*** *Bending stress for sandwich specimens of four densities at span length of 250 mm.*

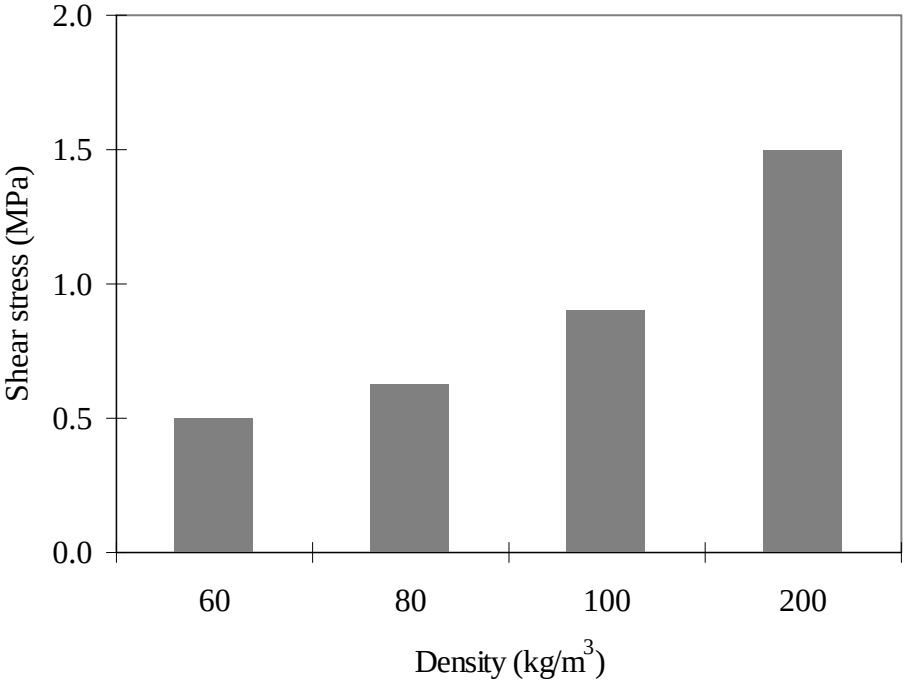


***Figure 4.27.*** *Shear stress for sandwich specimens of four densities at span length of 250 mm.*

# Chapter 5
# Analysis of mechanical behaviour of sandwich composite beams using classical beam theory

## 5.1 Bending of sandwich beams

The mechanical behaviour of a structure made up of sandwich composite materials is generally analysed by the theory of the sandwich plates. This theory is derived from the theory of the laminates taking into account the transverse shearing which is based on an evaluation of the displacement fields. The theory of the sandwich plates considers that only the core of the sandwich material is subjected to a transverse shearing strain. The theory of the laminates with transverse shearing and the theory of the sandwich plates are the tools which can be usually used to analyse the elastic behaviour of sandwich structures by an analytical approach. The importance of developing a method of analysing beam is related on the one hand with the use of beams as basic element of structures, and on the other hand with the mechanical characterisation of laminate or sandwich by bending tests on the specimens in the form of beams. The formulation presented in this section is taken from the theory of sandwich plates presented in the annexe [120]. The theory of beams considers that length $L$ of a beam is much greater then its width. In the case of pure bending, moments equation can be written as following and the axes of the beam can be represented by ($x$, $y$, $z$).

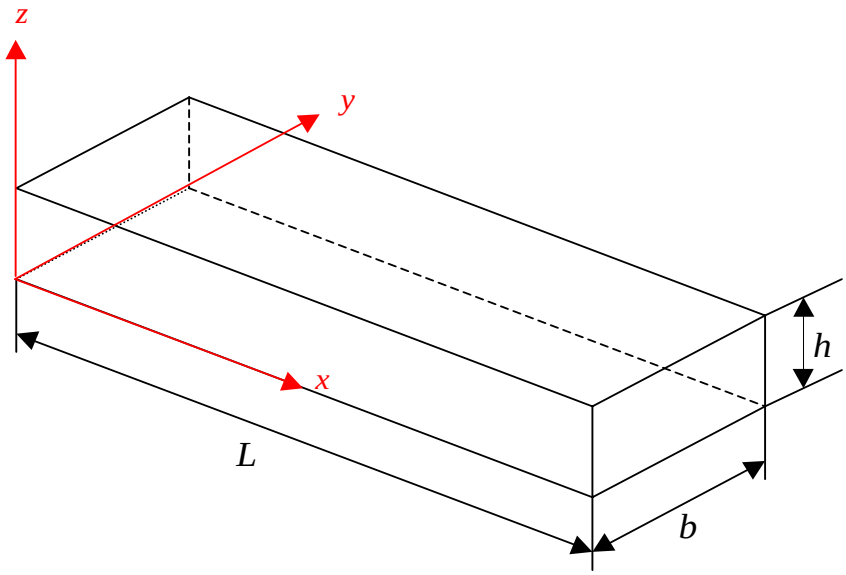


***Figure 5.1*** *Beam element*

$$\begin{bmatrix} M_x \\ M_y \\ M_{xy} \end{bmatrix} = \begin{bmatrix} D_{11} & D_{12} & 0 \\ D_{21} & D_{22} & 0 \\ 0 & 0 & D_{66} \end{bmatrix} \begin{bmatrix} k_x \\ k_y \\ k_{xy} \end{bmatrix} \tag{5.1}$$

$$\begin{bmatrix} Q_y \\ Q_x \end{bmatrix} = \begin{bmatrix} F_{44} & 0 \\ 0 & F_{55} \end{bmatrix} \begin{bmatrix} \gamma_{yz}^a \\ \gamma_{xz}^a \end{bmatrix} \tag{5.2}$$

Where $[F_{ij}]$ is the transverse shear stiffness matrix and $\gamma_{ij}^{a}$ is transverse shearing strains in core. Coefficients of shear by experiment are:

$$F_{ij} = hC_{ij}^{'a} \tag{5.3}$$

where $C_{ij}^{'a}$ is the coefficients of transverse shear in the core.

Equation (5.1) and (5.2) can be written in inverted from:

$$\begin{bmatrix} k_x \\ k_y \\ k_{xy} \end{bmatrix} = \begin{bmatrix} D_{11}^{*} & D_{12}^{*} & 0 \\ D_{21}^{*} & D_{22}^{*} & 0 \\ 0 & 0 & D_{66}^{*} \end{bmatrix} \begin{bmatrix} M_x \\ M_y \\ M_{xy} \end{bmatrix} \tag{5.4}$$

and

$$\begin{bmatrix} \gamma_{yz} \\ \gamma_{xz} \end{bmatrix} = \begin{bmatrix} F_{44}^{*} & 0 \\ 0 & F_{55}^{*} \end{bmatrix} \begin{bmatrix} Q_y \\ Q_x \end{bmatrix} \tag{5.5}$$

with

$$D_{11}^{*} = \frac{D_{22}}{D_{11}D_{12} - D_{12}^{2}} \qquad D_{12}^{*} = \frac{D_{12}}{D_{11}D_{12} - D_{12}^{2}} \qquad D_{22}^{*} = \frac{D_{11}}{D_{11}D_{12} - D_{12}^{2}}$$
$$D_{66}^{*} = \frac{1}{D_{66}} \qquad F_{44}^{*} = \frac{1}{F_{44}} \qquad F_{55}^{*} = \frac{1}{F_{55}} \tag{5.6}$$

In the case of bending along x-axis shown in figure 5.1, one can neglect the variation of the deflection in the width of the beam. The function $\varphi_x$ and $w_0$ are independent of the variable *y*:

$$\varphi_x = \varphi_x(x) \qquad \text{and} \qquad w_0 = w_0(x) \tag{5.7}$$

The deformations $\varepsilon_{xx}^{a}$ and $\gamma_{xz}^{a}$, in the core are given by the expression using equation (A.8) annexe:

$$\varepsilon_{xx}^{a} = z\frac{d\varphi_x}{dx} \tag{5.8}$$

similarly, $\gamma_{xz}^{a}$ is explained as:

$$\gamma_{xz}^{a} = \varphi_x + \frac{dw_0}{dx} \tag{5.9}$$

In addition, the relations for the plates (appendix equation A-23) are reduced to:

$$\frac{\partial Q_x}{\partial x} + \frac{\partial Q_y}{\partial y} + q = 0 \tag{5.10}$$

$$\frac{M_x}{\partial x} + \frac{\partial M_{xy}}{\partial y} - Q_x = 0 \tag{5.11}$$

$$\frac{M_y}{\partial y} + \frac{\partial M_{xy}}{\partial x} - Q_y = 0 \tag{5.12}$$

The beam theory makes the assumption that in the case of bending along *x*-axis, the bending moment $M_y$ and the twisting moment $M_{xy}$ are zero:

$$M_y = M_{xy} = 0 \tag{5.13}$$

Replacing equation (5.13) in equation (5.12), we can verify that shear resultant $Q_y$ is zero:

$$Q_y = 0 \tag{5.14}$$

The relations (5.4), (5.5), (5.13) and (5.14) thus lead to:

$$k_x = \frac{d\varphi_x}{dx} = D_{11}^* M_x \tag{5.15}$$

$$\gamma_{xz}^a = \frac{dw_0}{dx} + \varphi_x = F_{55}^* Q_x \tag{5.16}$$

Equation of equilibrium (5.11) can be written by taking account of equations (5.15) and (5.16) respectively:

$$\frac{d^2\varphi_x}{dx^2} - \frac{D_{11}^*}{F_{55}^*}\left(\varphi_x + \frac{dw_0}{dx}\right) = 0 \tag{5.17}$$

This equation can be rewritten introducing the moduli of elasticity and of shearing of the beam:

$$\frac{d^2\varphi_x}{dx^2} - \frac{bh}{I}\frac{G_{xz}}{E_x}\left(\varphi_x + \frac{dw_0}{dx}\right) = 0 \tag{5.18}$$

The shear modulus $G_{xz}$ and the effective bending modulus $E_x$ are written as:

$$G_{xz} = \frac{1}{hF_{55}^*} \quad \text{and} \quad E_x = \frac{b}{D_{11}^*} \quad \text{with} \quad M = bM_x \quad \text{and} \quad I = \frac{bh_t^3}{12} \tag{5.19}$$

Similarly replacing equation (5.6) in equation (5.10), we obtain:

$$\frac{d^2w_0}{dx^2} + \frac{d\varphi_x}{dx} + F_{55}^* q = 0 \tag{5.20}$$

that is:

$$\frac{d^2w_0}{dx^2} + \frac{d\varphi_x}{dx} + \frac{1}{hG_{xz}} p = 0 \quad \text{with} \quad p = bq \tag{5.21}$$

In the case when the variation of the bending moment is known, the relation (5.15) can thus be put in the form:

$$\frac{d\varphi_x}{dx} = D_{11}^{*} M_x = \frac{M}{E_x I} \tag{5.22}$$

Second equation can be obtained by replacing the relation (5.22), in the expressions (5.17) or (5.18):

$$\frac{dM_x}{dx} = \frac{1}{F_{55}^{*}}(\varphi_x + \frac{dw_0}{dx}) \tag{5.23}$$

$$\frac{dM}{dx} = bhG_{xz}(\varphi_x + \frac{dw_0}{dx}) \tag{5.24}$$

The differential equations (5.18), (5.20) and (5.21) are known as the fundamental relations of the beams in flexural loading. These equations make it possible to determine the deformation in the sandwich as well as the deflection $w_0$ in the centre of the specimen submitted to three point bending tests.

## 5.2 Three-point bending

In the case of three point bending, the bending moment $M_x$ obtained from deflection equations (5.4) and (5.7) becomes:

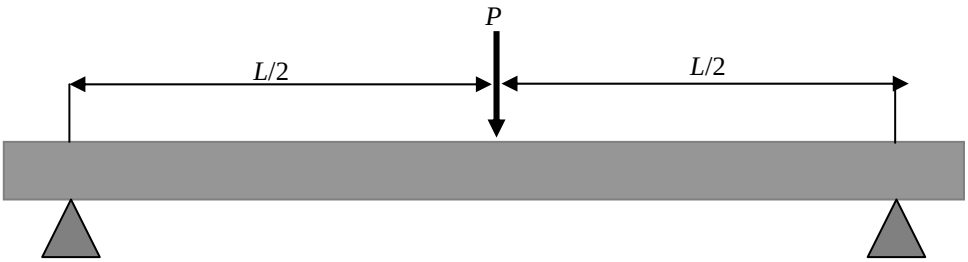


***Figure 5.2.*** *Three-point bending*

Expressing the bending moment *M* in a point of the beam:

$$M = -P\frac{x}{2} \qquad \text{if} \quad 0 \le x \le \frac{L}{2} \tag{5.25}$$

Integrating the equation (5.22) following expression can be obtained:

$$\varphi_x = -\frac{P}{4E_x I}x^2 + c_1 \qquad \text{with}: \quad 0 \le x \le \frac{L}{2} \tag{5.26}$$

The symmetry of loading implies that $\varphi_x(\frac{L}{2}) = 0$. Then equation (5.26) can be written as:

$$\varphi_x = \frac{PL^2}{16E_x I}\left[1-4\left(\frac{x^2}{L}\right)^2\right] \tag{5.27}$$

or

$$\varphi_x = \frac{PL^2}{16b} D_{11}^*(1-4\frac{x^2}{L^2}) \tag{5.28}$$

By substituting equation (5.24) for the moment *M*, we deduce the following expression for the deflection $w_0$ as a function of $\varphi_x$:

$$\frac{dw_0}{dx} = -(\varphi_x + \frac{P}{2bhG_{xz}}) \qquad \text{with}: \quad 0 \le x \le \frac{L}{2} \tag{5.29}$$

It is interesting to note that, by this result, the slope of the deformation does not vanish at the centre of the beam. In fact, since $\varphi_x(\frac{L}{2}) = 0$ it has the value:

$$\frac{dw_0}{dx}\left(\frac{L}{2}\right) = -\frac{P}{2bhG_{xz}} \tag{5.30}$$

After substitution of $\varphi_x$, integration of equation (5.30), allows us to write the deflection equation as:

$$w_0 = \frac{PL^2}{4E_x bh^3} x\left[4\left(\frac{x}{L}\right)^2 - 3 - 2S\right] \tag{5.31}$$

This can be further simplified:

$$w_0 = \frac{PL^2}{48} D_{11}^* x\left[4\left(\frac{x}{L}\right)^2 - 3 - 2S\right] \tag{5.32}$$

on introducing the shear coefficient *S* defined by:

$$S = \frac{E_x}{G_{xz}}\left(\frac{h}{L}\right)^2 = 12\frac{F_{55}^*}{h^2 D_{11}^*}\left(\frac{h}{L}\right)^2 \tag{5.33}$$

The effect of transverse shear deformation thus depends upon the span-to-thickness ratio *L/h* of the beam and the ratio $E_x/G_{xz}$. The deflection at the centre is derived from the equation (5.33) and its absolute value is given by:

$$w_c = \frac{PL^3}{4E_x bh^3}(1+S) \tag{5.34}$$

or:

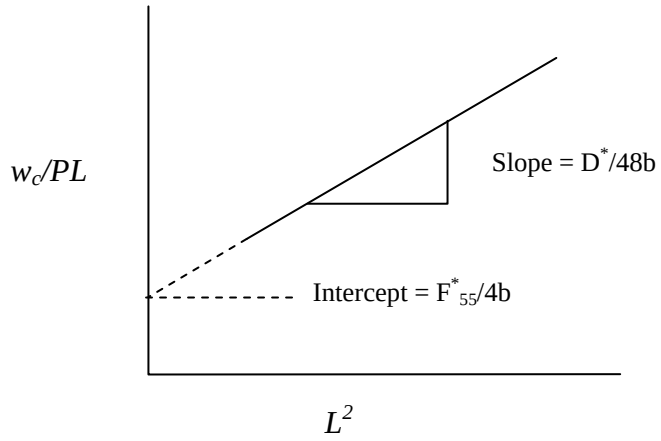


***Figure 5.3.*** *Bending and shear stiffness from three point bending tests* [89].

$$w_c = \frac{PL^3}{48b} D_{11}^* (1 + 12 \frac{F_{55}^*}{D_{11}^*} \frac{1}{L^2}) \tag{5.35}$$

This expression (5.35) shows that it is possible to determine the coefficients $D_{11}^*$ and $F_{55}^*$ from the sizes of $\frac{w_c}{PL}$ for two different values of the span length $L$ between the span supports [77,89,120-122]. Graphically, the values of slope and intercept are shown in figure 5.3.

Equations (5.34) and (5.35) show that the deflection can be written in one of the two forms:

$$w_c(S) = (1 + S) w_c(0) \tag{5.36}$$

$$w_c(S) = \left[ 1 + \frac{E_x}{G_{xz}} \left( \frac{h}{L} \right)^2 \right] w_c(0) \tag{5.37}$$

with

$$\frac{E_x}{G_{xz}} = \frac{12}{h^2} \frac{F_{55}^*}{D_{11}^*} \tag{5.38}$$

Where $w_c(S)$ is the deflection with shear deformation effects included, whereas $w_c(0)$ is the deflection without the effect of shear deformation.

The coefficients $D_{ij}^*$ and $F_{ij}^*$ are clarified according to functions $D_{ij}$ and $F_{ij}$ given in equation (5.6), the transverse coefficient of shear can be written as:

$$F_{55} = hG_a \tag{5.39}$$

Where $G_a$ and its transverse modulus of rigidity of core is $G_{13}^a = G_{xz}^a$. That is with the already introduced notations (figure 5.4), this coefficient can be written by introducing the flexural modulus $E_{Lp}^f$ of the sandwich material in the form:

$$D_{11}^* = \frac{2}{(h+h_1)hh_1}\frac{1}{E_{Lp}^f} \tag{5.40}$$

with:

$$E_{Lp}^f = E_{Lp0}^f\left(1-\frac{D_{12}^2}{D_{11}^2}\right) \tag{5.41}$$

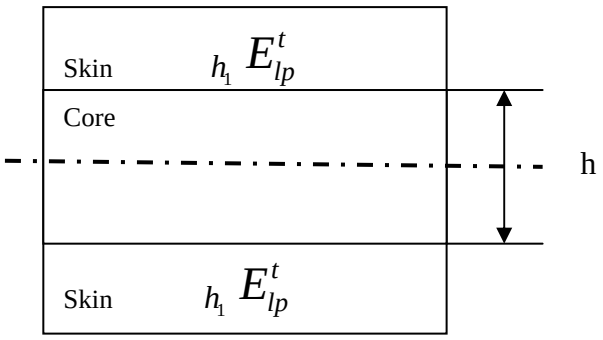


***Figure 5.4.*** *Sandwich with two skins and core.*

Generally:

$$\frac{D_{12}^2}{D_{11}^2} << 1 \qquad \text{that is} \qquad E_{Lp}^f \cong E_{Lp0}^f \tag{5.42}$$

The comparison of the preceding expression shows that the value of the modulus of deflection $E_{Lp}^f$ is close to that of the tensile modulus $E_{Lp}^t$. These values are much closer if the skin thickness is much lower to the core thickness.

In addition, the relation (5.36) leads to an expression of deflection in the centre of specimen, given by the theory of the sandwich plates:

$$w_c = \frac{PL^3}{24b(h+h_1)hh_1E_{Lp}^f}\left[1+6\frac{E_{Lp}^f}{G_a}\frac{(h+h_1)h_1}{L^2}\right] \tag{5.43}$$

In the same way, an approximate expression can be established, by considering that the sandwich materials are made up (figure 5.4) of one only layer of thickness $h_1$, having a modulus $E_{Lp}^t$ determined in a tensile test. Bending expression is identical to that obtained in the preceding equation (5.43). The modulus of deflection $E_{Lp}^f$ is replaced by $E_{Lp}^t$:

$$w_c = \frac{PL^3}{24b(h+h_1)hh_1E_{Lp}^t}\left[1+6\frac{E_{Lp}^t}{G_a}\frac{(h+h_1)h_1}{L^2}\right] \tag{5.44}$$

The equations (5.43) and (5.44) can be written in the form given below:

$$\frac{w_c}{PL} = \frac{A}{E_{Lp}^i}L^2 + \frac{B}{G_a} \tag{5.45}$$

with $i = f, t$ (deflection, tension)

$$A = \frac{1}{24b(h+h_1)hh_1} \qquad \textit{and} \qquad B = \frac{1}{4bh} \tag{5.46}$$

By plotting $\frac{w_c}{PL}$ as a function of $L^2$, allowed obtaining experimental value of $E_{Lp}^i$ *and* $G_a$. The slope and intercept of the equation (5.46) gives the values of $\frac{A}{E_{Lp}^i}$ and $\frac{B}{G_a}$.

## 5.3 Evaluation of performance of sandwich beams

### 5.3.1 Static tests at various span lengths

Static tests for sandwich composite beams in three point bending were performed at different span lengths ranging from 100 to 440 mm at a constant rate of 5 mm/min. In these tests, sandwich specimens of different core densities and thickness were used. Load versus displacements (with reference to upper skin) curves were plotted for each span length and are shown in the figures 5.5 to 5.12. Purpose of these experiments was to apply classical beam theory which is presented in the sections 5.2 and 5.3 and in annexe A. The theory of sandwich beam is limited to the case in which the behaviour of constituents of the sandwich is linear. This theory allows us to calculate the value of bending stiffness and shear stiffness for sandwich structure in linear domain. This also permits the limitation of its operation to be evaluated: limit of the linear behaviour induced by the non linear behaviour of the core, failure of the skin and failure of the skin-core interface in the case where failure is obtained before elastic limit of the core. This theory is applied in the following section to evaluate the performance of sandwich composite in three point bending.

It can be seen that all graphs shows almost similar trends in static tests for different core thicknesses and densities. As after an initially linear response, the curves reveal substantial non-linear response. Failures occurred in a ductile manner for low density foams. While for high density sandwich specimens, the evolution of load versus displacement is linear until failure. Failures generally occurred in a brittle manner with no plastic deformation.

As can be seen from figures 5.5 to 5.12, shorter span length generated higher failure loads and longer span lengths resulted in lower ultimate failure loads. Slope increases with decreasing the span length. For large distance between the span supports, beam behaviour is nearly linear until fracture which is of brittle type for high densities sandwich beams. While, for low densities sandwich beams the behaviour was ductile type in nature. It was observed, after bending tests, that fracture processes are only induced in the layers of skin in contact with central support. Although the sandwich beams were subjected to transverse shear effects in the case of short span lengths, no transverse shear fracture in foams or extensive delamination at the interface between core and skin were observed. These results also show that after the initiation and development of initial fracture processes, local indentation of the sandwich beam is induced due to concentrated loading of the central support.

It is also observed that after sudden drop in load, there is a gradual decrease in load of the sandwich specimens for small span length. This is due to slow progression of micro cracks and crushing in the core after breaking of the top skin and then with further increase in load resulting in the complete failure of the sandwich specimens.

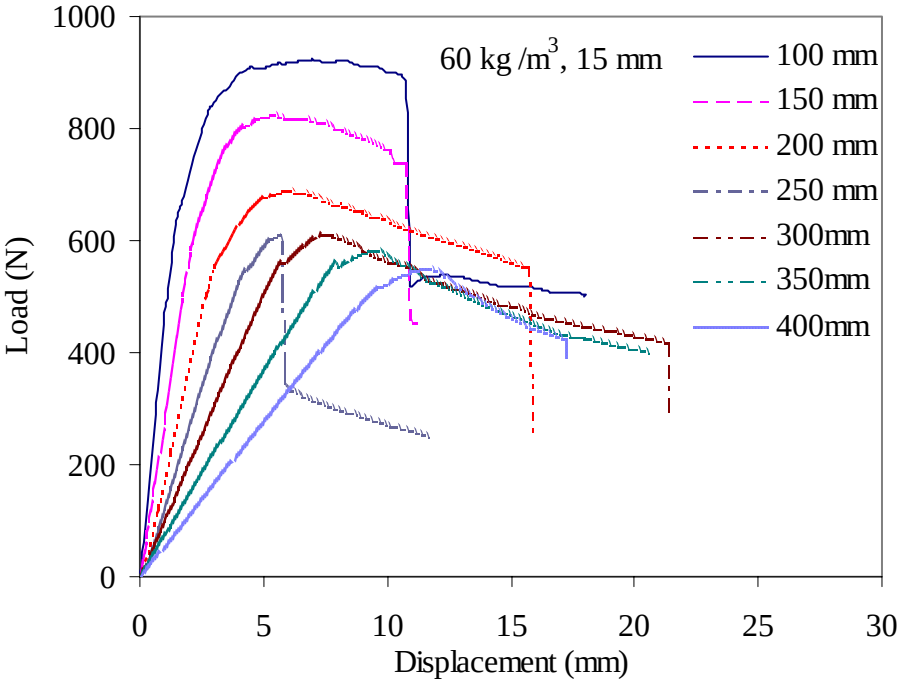


***Figure 5.5.*** *Load-displacement curves derived from 3-point bending tests for sandwich specimens with foam of 60 kg/m$^3$ density and 15 mm thickness at different span lengths.*

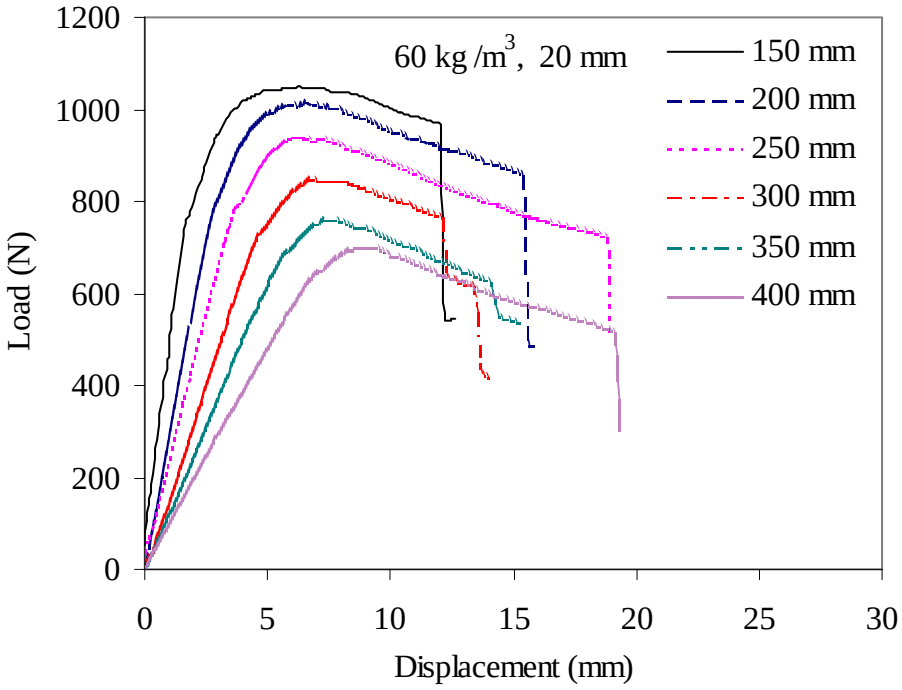


***Figure 5.6.*** *Load-displacement curves derived from 3-point bending tests for sandwich specimens with foam of 60 kg/m$^3$ density and 20 mm thickness at different span lengths.*

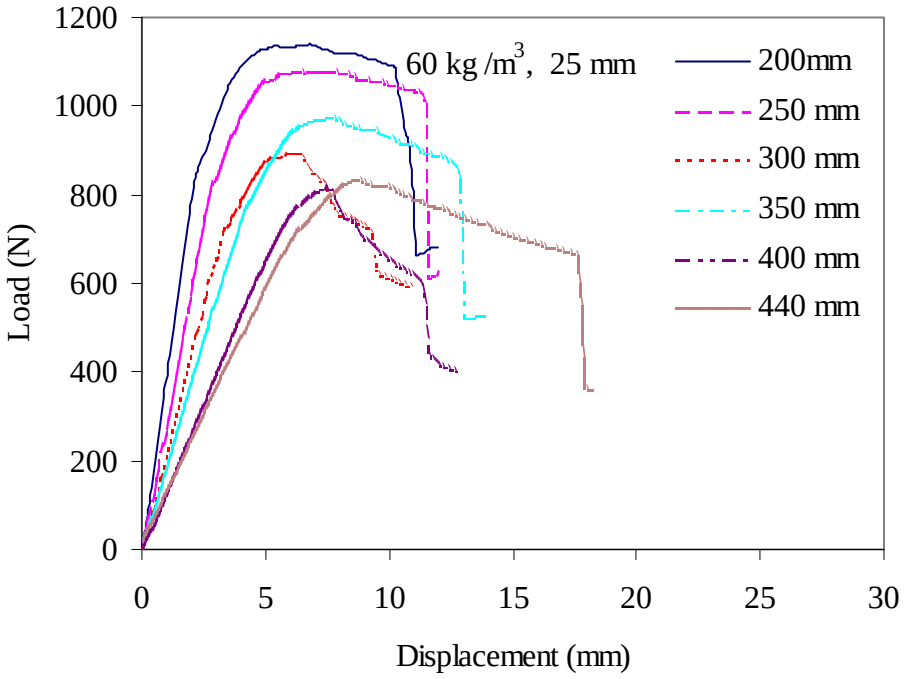


***Figure 5.7.*** *Load-displacement curves for derived from 3-point bending tests sandwich specimens with foam of 60 kg/m$^3$ density and 25 mm thickness at different span lengths.*

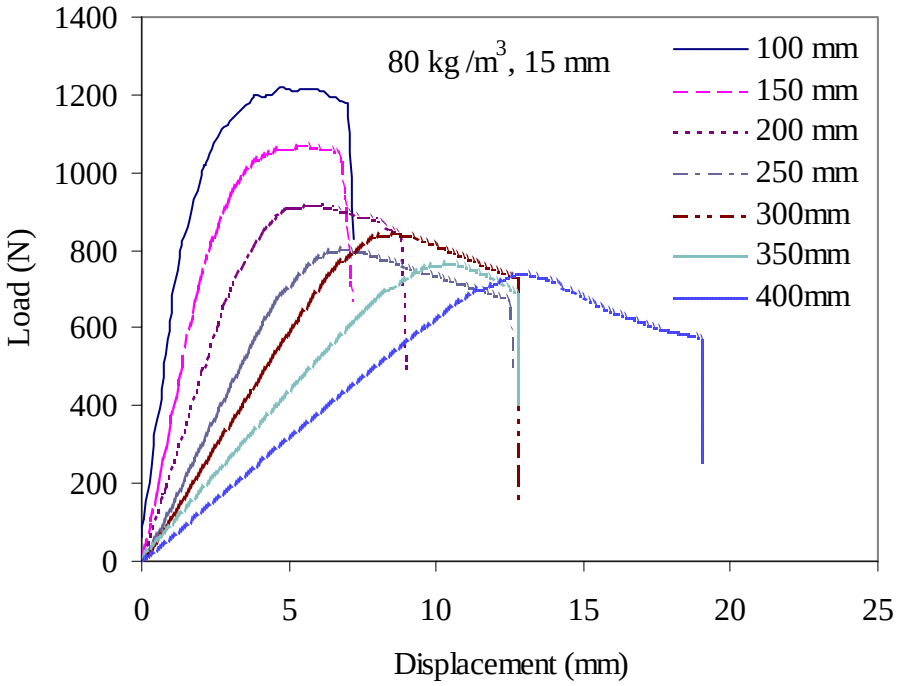


***Figure 5.8.*** *Load-displacement curves derived from 3-point bending tests for sandwich specimens with foam of 80 kg/m$^3$ density and 15 mm thickness at different span lengths.*

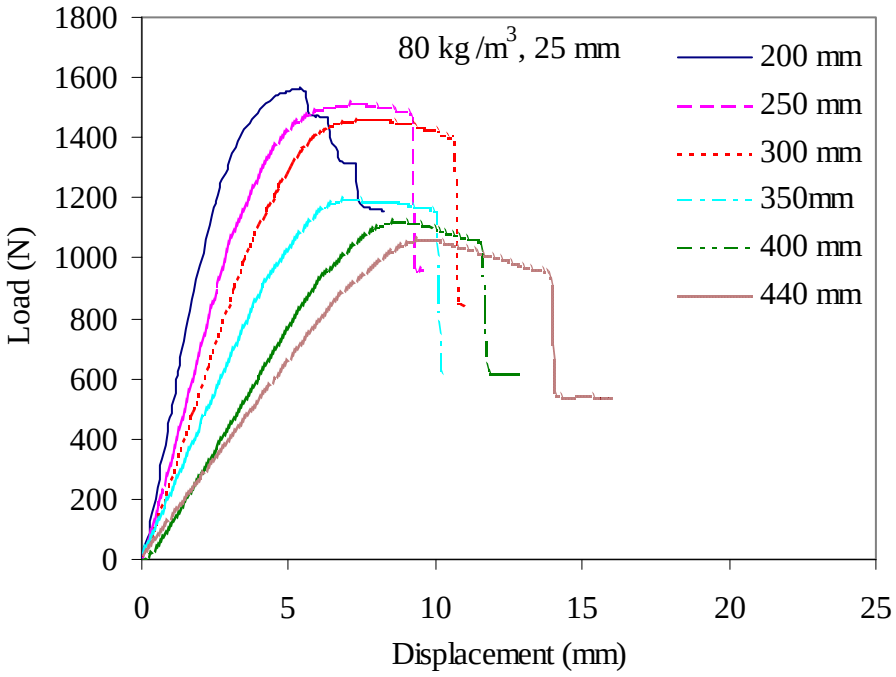


***Figure 5.9.*** *Load-displacement curves f derived from 3-point bending tests or sandwich specimens with foam of 80 kg/m$^3$ density and 25 mm thickness at different span lengths.*

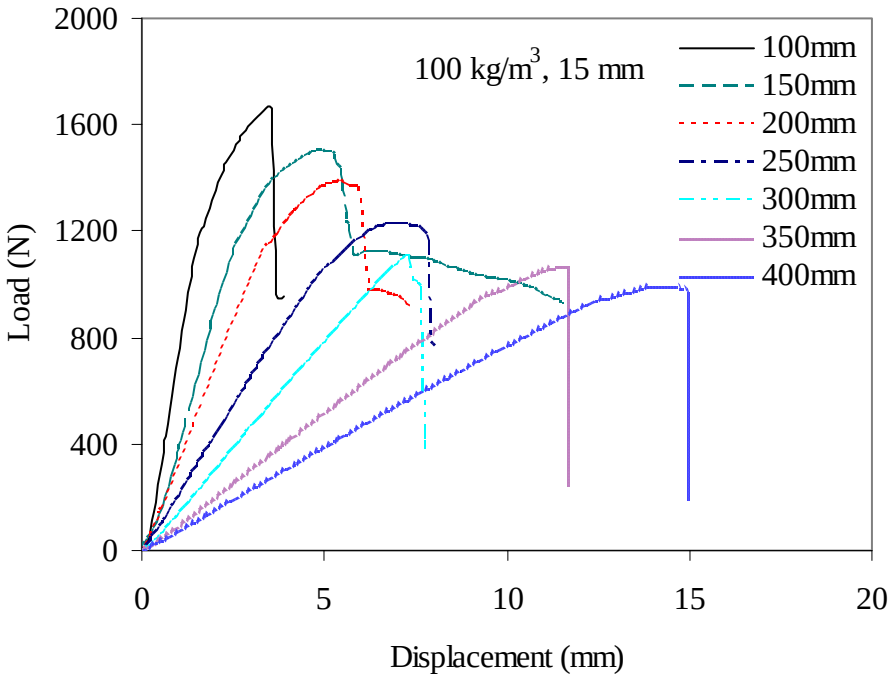


***Figure 5.10.*** *Load-displacement curves derived from 3-point bending tests for sandwich specimens with foam of 100 kg/m$^3$ density and 15 mm thickness at different span lengths.*

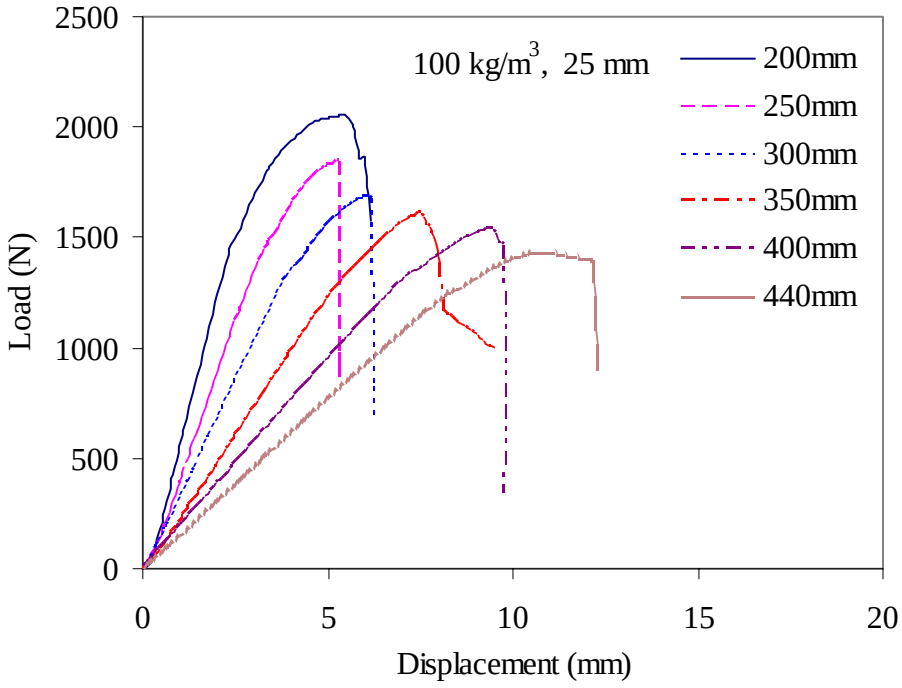


***Figure 5.11.*** *Load-displacement curves derived from 3-point bending tests for sandwich specimens with foam of 100 kg/m$^3$ density and 25 mm thickness at different span lengths.*

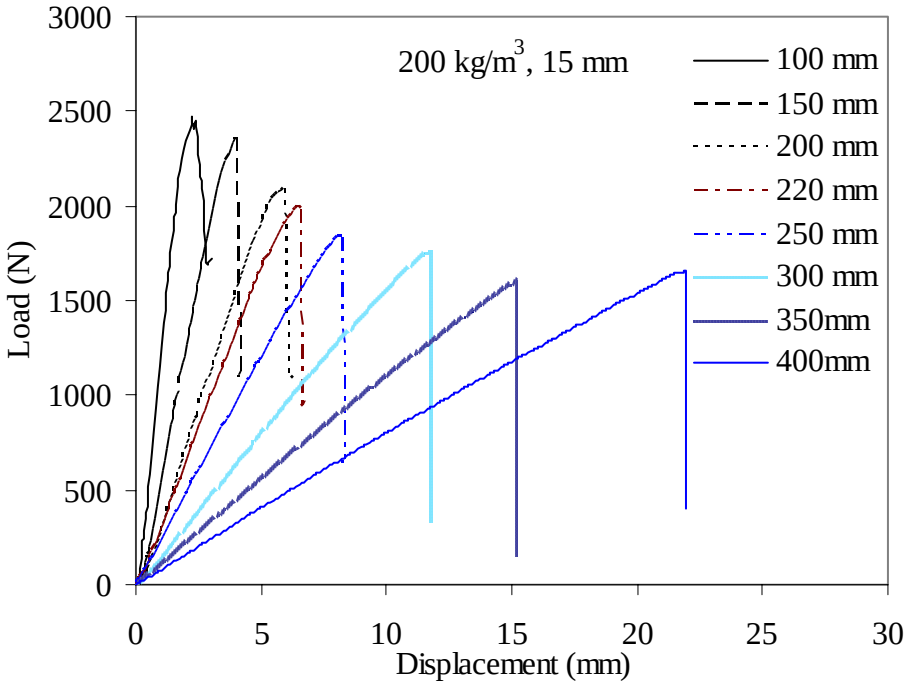


***Figure 5.12.*** *Load-displacement curves derived from 3-point bending tests for sandwich specimens with foam of 200 kg/m$^3$ density and 15 mm thickness at different span lengths.*

### 5.3.2 Coefficients of bending and shear stiffness (experimentally and analytically)

Coefficients of bending and shear stiffness were calculated using the results from figures 5.5 to 5.12. These curves were used to determine the ratio ($w_c/P$) divided by span length $L$. Where $w_c$ is the deflection and $P$ is the load acting, in the centre of the beam. Then these values were plotted versus square of span length ($L^2$) which are presented in series of figures 5.13 to 5.16 for sandwich specimens of different core thickness and four densities. These values are needed for determining the coefficients of bending stiffness $D_{11}^*$ and shear stiffness $F_{55}^*$ in accordance with equation 5.36 presented in section 5.3. Equation (5.36) provides a basis for experimental determination of bending and shear stiffness. The coefficients of $D_{11}^*$ and $F_{55}^*$ were then determined by using the slope and intercept of these graphs (5.13 to 5.16). The experimental values of the coefficients of bending and shear stiffness are given in table 5.1 along with analytical results obtained from beam theory (appendix A).

***Table 5.1.*** *Experimental and analytical results from static flexural tests for sandwich composite of various core thicknesses and densities.*

| Materials (Density) | Thick -ness (mm) | Coefficient of bending stiffness $(D_{11}^*)^{-1}$ ( N m ) | | Coefficient of shear stiffness $(F_{55}^*)^{-1}$ (kN/m) | | Bending modulus of beam $E_x$ ( GPa) | |
|---|---|---|---|---|---|---|---|
| | | Expt. | Analy. | Expt. | Supplied by Manufact -urer | Expt. | Supplied by Manufact -urer |
| 60 kg/m$^3$ | 15 mm | 3305 | 2870 | 332 | 330 | 8.00 | 10.20 |
| | 20 mm | 5943 | 5042 | 357 | 440 | 6.70 | 7.56 |
| | 25 mm | 8300 | 7821 | 476 | 550 | 5.30 | 6.01 |
| 80 kg/m$^3$ | 15 mm | 3619 | 2870 | 406 | 450 | 8.80 | 10.20 |
| | 25 mm | 8663 | 7821 | 694 | 750 | 5.10 | 6.01 |
| 100 kg/m$^3$ | 15 mm | 3700 | 2870 | 665 | 570 | 9.20 | 10.20 |
| | 25 mm | 8573 | 7821 | 962 | 950 | 6.13 | 6.01 |
| 200 kg/m$^3$ | 15 mm | 4079 | 2870 | 1096 | 1215 | 8.82 | 10.20 |

Sandwich composites beams were symmetric and are identified by the core thicknesses and densities. The values of bending stiffness and bending shear stiffness strongly depend on the thickness and density of the core material [117]. It also depends on the skin thickness but in our studies, we used same skin thickness for all the sandwich specimens. It can be seen from the table 5.1 that with increasing the core thickness and density, the values of bending stiffness and shear stiffness increase.

The value of the coefficients of bending stiffness varies between 3305 Nm and 8300 Nm for three core thicknesses for sandwich specimen having 60 kg/m$^3$ core density. Values of coefficients of bending stiffness increase to 45% for 20 mm core thickness and 60% for 25 mm core thickness sandwich specimens. The values of shear stiffness increase to 30% for core thickness of 15 to 25 mm for sandwich specimen with core of 60 kg/m$^3$ density. It is worth noting that increase in core thickness, increases the bending stiffness much higher than the increase in density of the core. Similar trends were also observed for sandwich specimens of other core densities with varying thickness such as sandwich specimens with cores of 80 kg/m$^3$ and 100 kg/m$^3$ densities and this ratio is found as approximately 58%.

While coefficients of bending and shear increases with the increase in density in the ratio as 19% for 80 kg/m$^3$, 50% for 100 kg/m$^3$ and 70% for 200 kg/m$^3$ densities in comparison with the sandwich specimens with core of 60 kg/m$^3$ density. Therefore, densities of the core materials also play a very important role in enhancing the coefficients of bending shear.

Values obtained from analytical results are found to be slightly less then experimental results but show similar trends for bending and shear stiffness for the sandwich specimens with foams of different core thickness and densities. The values of bending modulus $E_x$ as shown in table 5.1, decreases with the increase in core densities and thickness of the sandwich specimens. However, this effect is more pronounced with core thickness as compared to density of the foams.

There is a little difference between the experimental and analytical results and that is attributed to different factors. Values obtained from experimental data points were obtained by the best fit as generally scattering (dispersion) of data points were observed due to various experimental parameters, geometrical variation of the specimens, fabrication processes and analytically this difference is attributed to the assumptions (appendix A1), made in the sandwich beam theory.

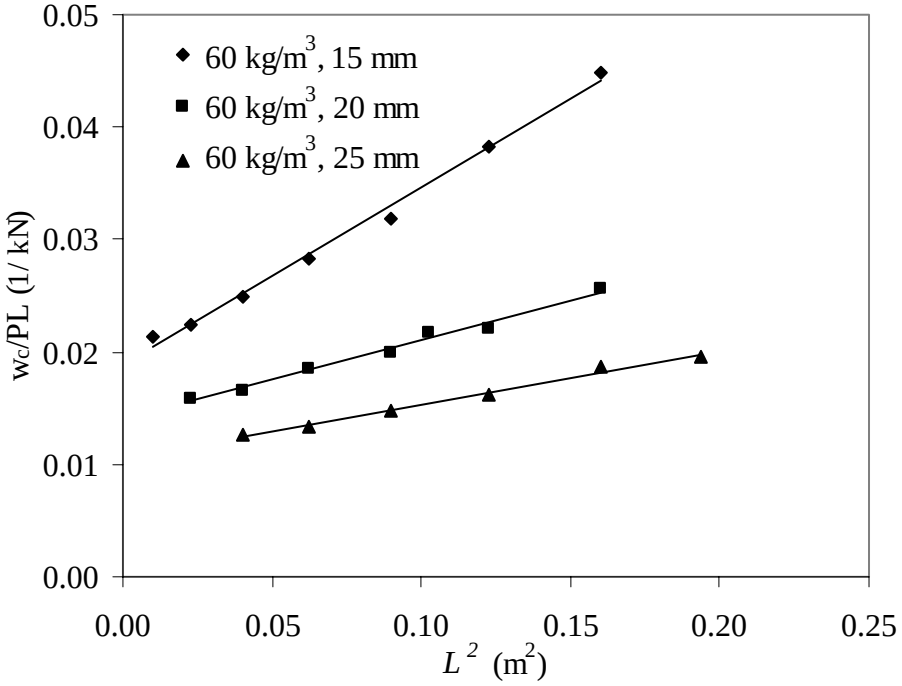


***Figure 5.13**. Deflection versus square of distance ($L^2$) between span supports in three point bending for sandwich specimens with foams of 60 kg/m$^3$ density and 15, 20 and 25 mm thicknesses.*

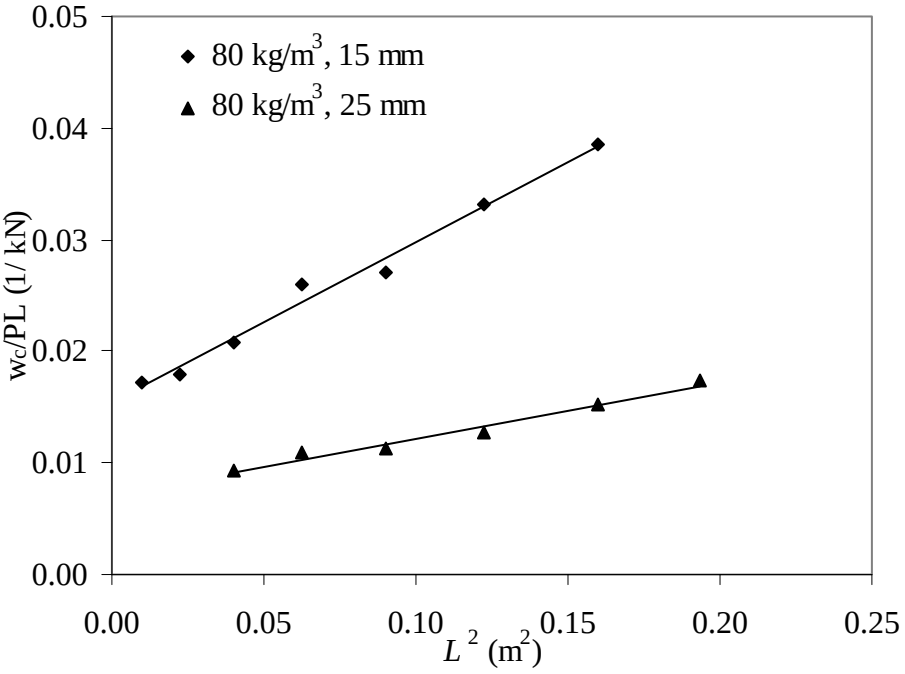


***Figure 5.14.** Deflection versus square of distance ($L^2$) between span supports in three point bending for sandwich specimens with foams of 80 kg/m$^3$ density and 15 and 25 mm thicknesses.*

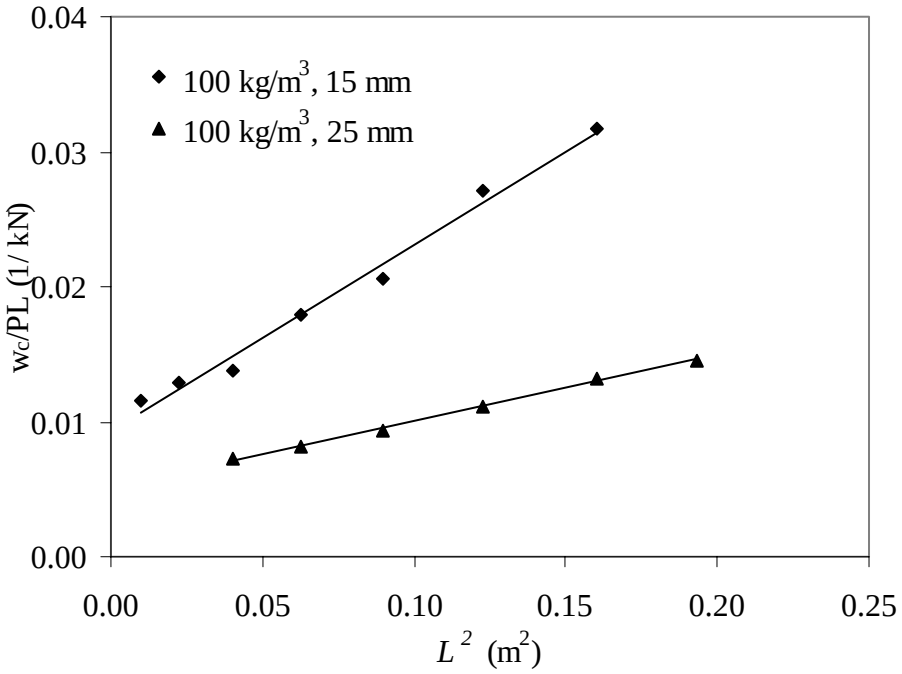


***Figure 5.15.*** *Deflection versus square of distance ($L^2$) between span supports in three point bending for sandwich specimens with foams of 100 kg/m$^3$ density and 15 and 25 mm thicknesses.*

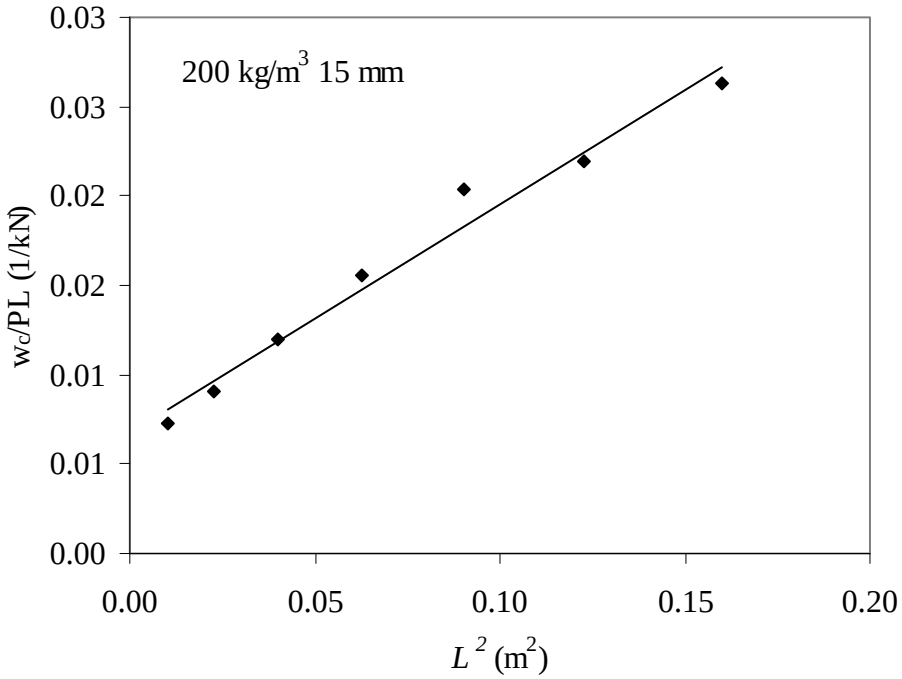


***Figure 5.16.*** *Deflection versus square of distance ($L^2$) between span supports in three point bending for sandwich specimens with foam of 200 kg/m$^3$ density and 15 mm thickness.*

Equation (5.34) introduces the transverse shear coefficient which depends on span to thickness ratio *l/h* of the beam and on the ratio $E_x/G_{xz}$ of bending and shear modulus. For higher values of span lengths such as:

$$\frac{E_x}{G_{xz}}\left(\frac{h}{L}\right)^2 \quad << 1 \tag{5.47}$$

The beam is subjected to simple bending and centre deflection depends mainly on the bending modulus of the beam. The centre deflection can be approximated as:

$$w_c = \frac{P}{4E_x b}\left(\frac{L}{h}\right)^3 \tag{5.48}$$

For small values of span distances such as:

$$\frac{E_X}{G_{Xz}}\left(\frac{h}{L}\right)^2 >> 1 \tag{5.49}$$

The beam is subjected to transverse shear and the centre deflection depends on the shear modulus of the beam, which can be approximated as:

$$w_c = \frac{P}{4G_{xz}b}\frac{L}{h} \tag{5.50}$$

For intermediate span lengths, the beam is subjected to bending and shear.

Before studying the effect of ratio of flexural modulus to shear modulus, we constructed graphs of deflection versus span to thickness ratio for different values of $E_x/G_{xz}$ using equations (5.33) and (5.35). Figures 5.17 and 5.18 shows the variation of deflection as a function of span to thickness ratio for sandwich specimens of three core thickness and four core densities. It can be seen from figure 5.17, that for the sandwich specimens of three different core thicknesses, the result of sandwich specimens with 15 mm thick core is higher then the sandwich specimens of 20 and 25 mm thick cores, thus representing that less thick core leads to pure bending rapidly as compare to thicker cores. For shorter span to thickness ratios, there is shear deformation but for longer span to thickness ratios, deflection is without shear deformation leading to pure deflection. Similarly, for sandwich specimens of different core densities shown in figure 5.18, the sandwich panel with small density core leads to pure bending more rapidly as compared to high density core materials. Small density core exhibits more shear deformation as compared to high density core sandwich. It is observed that for higher span to thickness ratio greater then 24, all densities behave similarly in pure bending. While for small values of span to thickness ratio less then 12, the phenomena of shear is dominant but shear is more pronounced in low density foam materials. Core thickness and density plays an important role for shear deformation for small values of span to thickness ratios.

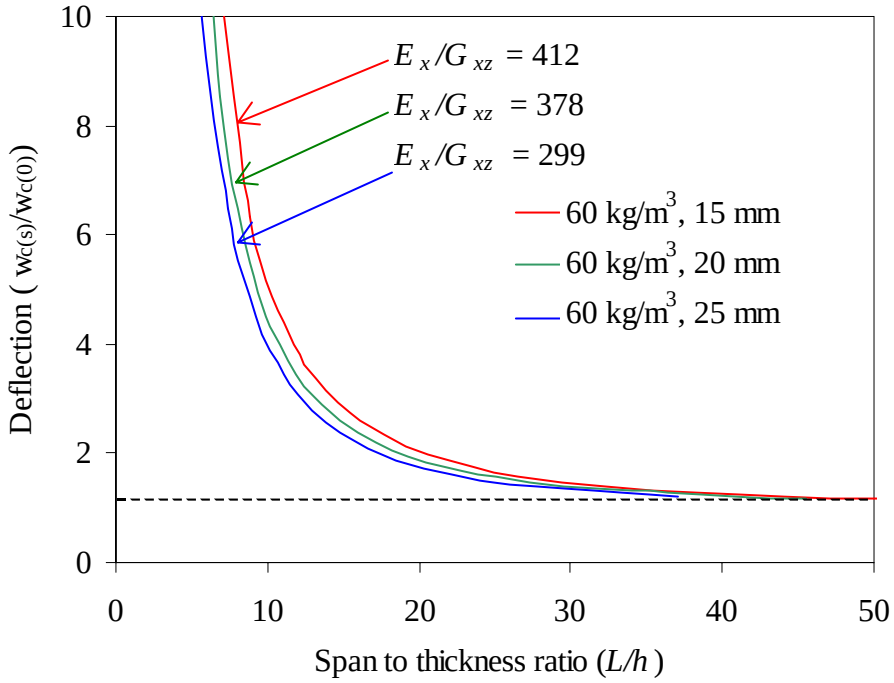


***Figure 5.17.*** *Variation of deflection in three point bending as a function of span to thickness ratio for sandwich specimens having same foam density of three thicknesses.*

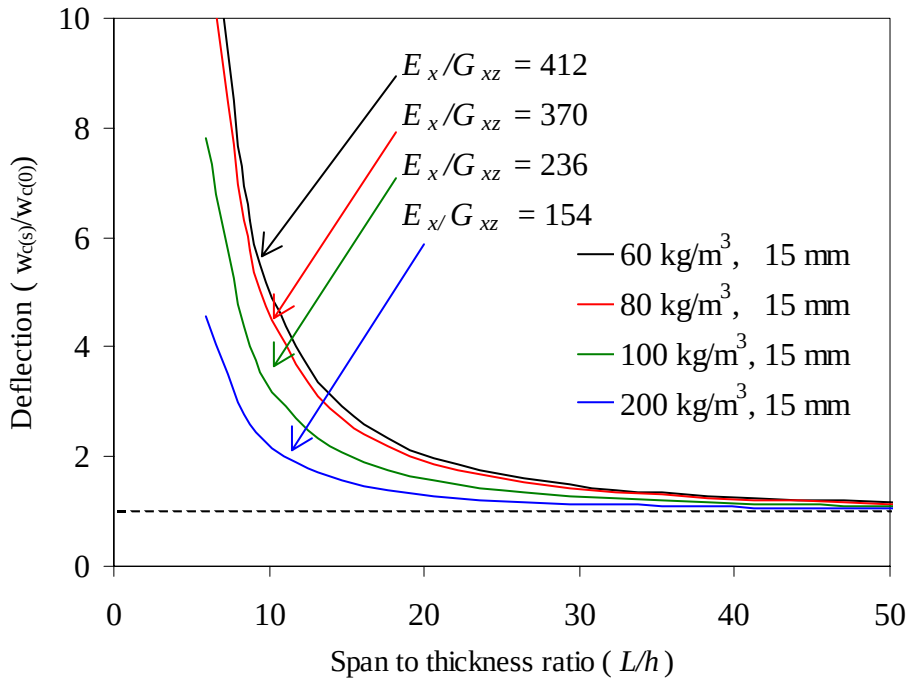


***Figure 5.18.*** *Variation of deflection in three point bending as a function of span to thickness ratio for sandwich specimens having four foam densities and one core thickness.*

But for higher values of span to thickness ratios, there is pure bending irrespective of core thickness and densities. From these results, it is obvious that neglecting the shear deflection leads to underestimating the deflection. The ratio of flexural modulus to the shear modulus allowed to calculate the influence of shear in transverse direction. The effect of transverse shear deformation thus depends upon the span to thickness ratio of the beam and the ratio of flexural modulus to shear modulus. The values of the coefficients of stiffness then make it possible to evaluate the ratio of deflection using equation (5.38). The effective bending modulus and shear modulus were obtained using the values of $D_{11}^{*}$ and $F_{55}^{*}$ in the following equations.

$$E_x = \frac{12}{h^3 D_{11}^{*}} \tag{5.51}$$

$$G_{xz} = \frac{1}{h F_{11}^{*}} \tag{5.52}$$

The values of $E_x$ and $G_{xz}$ obtained experimentally and analytically results are give in tables 5.1 and 5.2 respectively. It is observed that experimental values are found to be slightly less then the analytical values. The values of bending modulus $E_x$ and shear modulus $G_{xz}$ decreases with increasing the core thickness and increases with increasing the core density. A reasonable agreement was found between the experimental and analytical values of bending and shear modulus. Ratio of $E_x/G_{xz}$ decreases with increasing the core thickness and density.

These experimentally results were further validated by using classical beam theory concept. A programme based on classical beam theory was written in Matlab using equations from the classical beam theory that are presented in the annexe A. This programme calculates the values of $D_{11}^{*}$ and $F_{55}^{*}$ on analytical basis. In this programme, characteristic of skins and cores are entered and the programme calculate the values coefficients of bending stiffness $D_{11}^{*}$ and shear stiffness $F_{55}^{*}$ in each layers of skin taking into account the contribution of core thickness and density. Experimental and analytical results were plotted for various core thickness and densities and were presented in series of graphs shown in figures 5.19 to 5.26. A good agreement between experimental and analytical results are observed. The little difference is attributed to the difference found in the experimental and analytical values of bending and shear coefficients given in table 5.1.

Three point bending tests were thus chosen in such a way as to induce the various phenomena. Central region of the these curves are normally chosen for having the reasonable span length that provide a good compromise for sandwich panel optimisation for its performance in bending and shear simultaneously.

***Table 5.2.*** *Experimental and analytical results from static flexural tests for sandwich composite of various core thicknesses and densities.*

| Materials (Density) | Thickness (mm) | Shear modulus of foam $G_{xz}$ (MPa) | | Bending modulus of skin $E_p$ ( GPa ) | | $E_x/G_{xz}$ | |
|---|---|---|---|---|---|---|---|
| | | Expt. | Analy. | Expt. | Analy. | Expt. | Analy. |
| 60 kg/m$^3$ | 15 mm | 19 | 14 | 28 | 23 | 412 | 520 |
| | 20 mm | 16 | 14 | 28 | 24 | 378 | 370 |
| | 25 mm | 18 | 14 | 27 | 23 | 299 | 295 |
| 80 kg/m$^3$ | 15 mm | 23 | 22 | 30 | 24 | 370 | 385 |
| | 25 mm | 25 | 22 | 27 | 24 | 196 | 216 |
| 100 kg/m$^3$ | 15 mm | 39 | 38 | 28 | 24 | 236 | 304 |
| | 25 mm | 37 | 38 | 33 | 24 | 158 | 170 |
| 200 kg/m$^3$ | 15 mm | 64 | 81 | 27 | 24 | 154 | 142 |

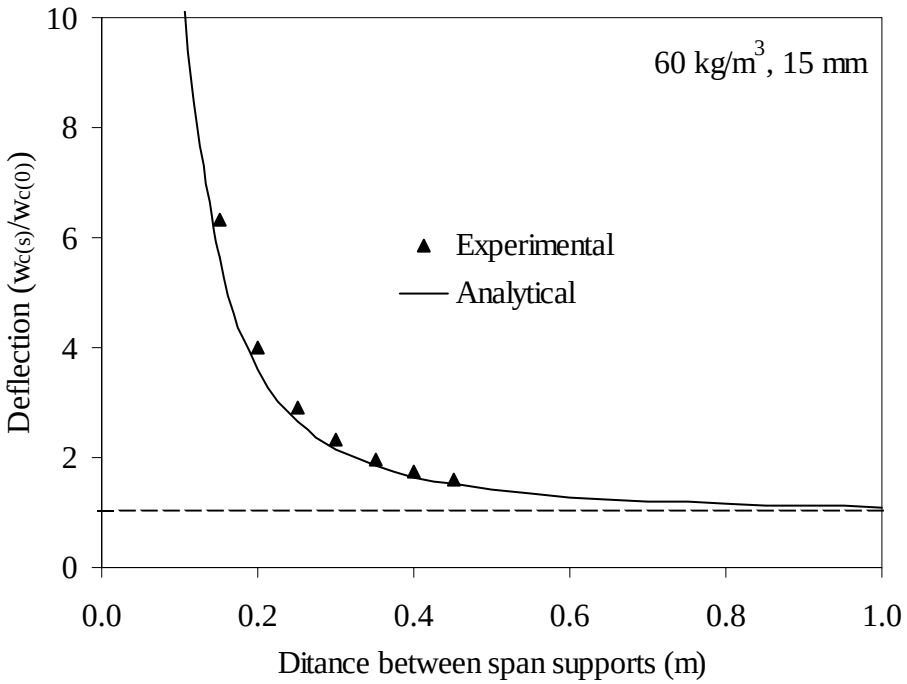


***Figure 5.19.*** *Experimental and analytical results for variation of deflection in three point bending as a function span length for sandwich specimens with foam of 60 kg/m$^3$ density and 15 mm thickness.*

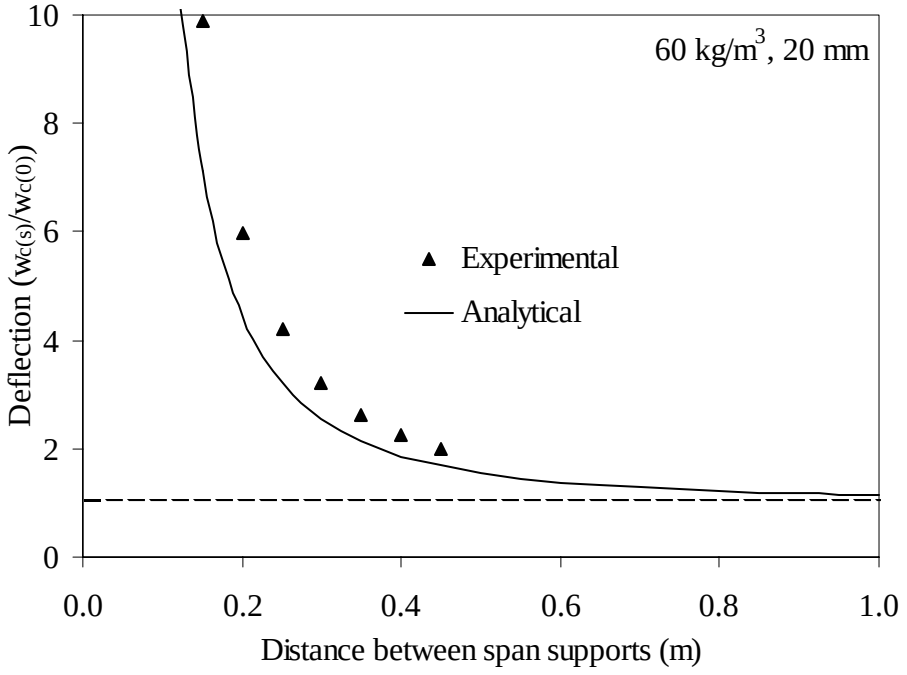


***Figure 5.20.*** *Experimental and analytical results for variation of deflection in three point bending as a function of span length for sandwich specimens with foam of 60 kg/m$^3$ density and 20 mm thickness.*

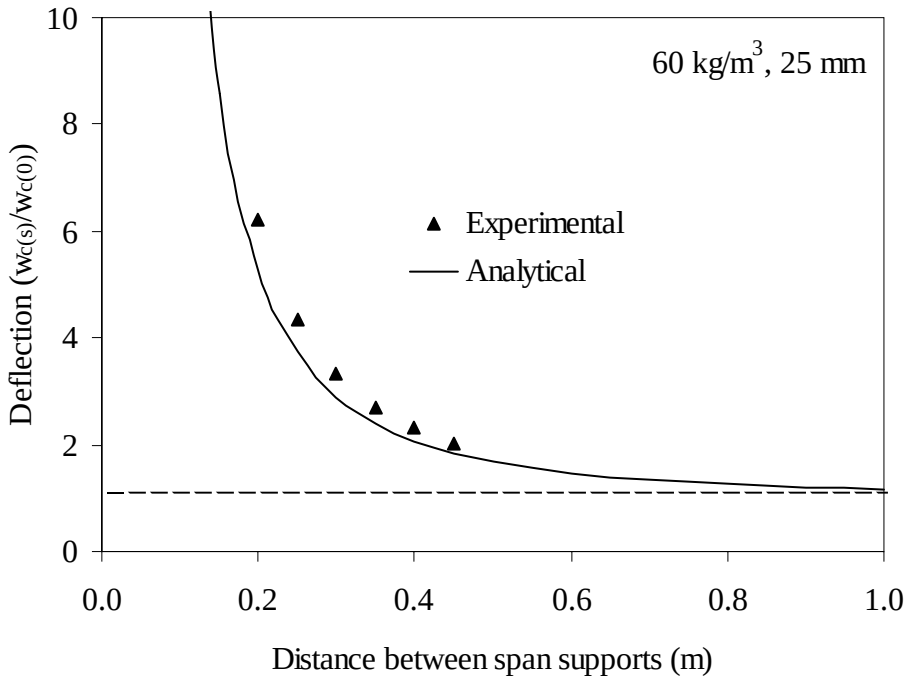


***Figure 5.21.*** *Experimental and analytical results for variation of deflection in three point bending as a function of span length for sandwich specimens with foam of 60 kg/m$^3$ density and 25 mm thickness.*

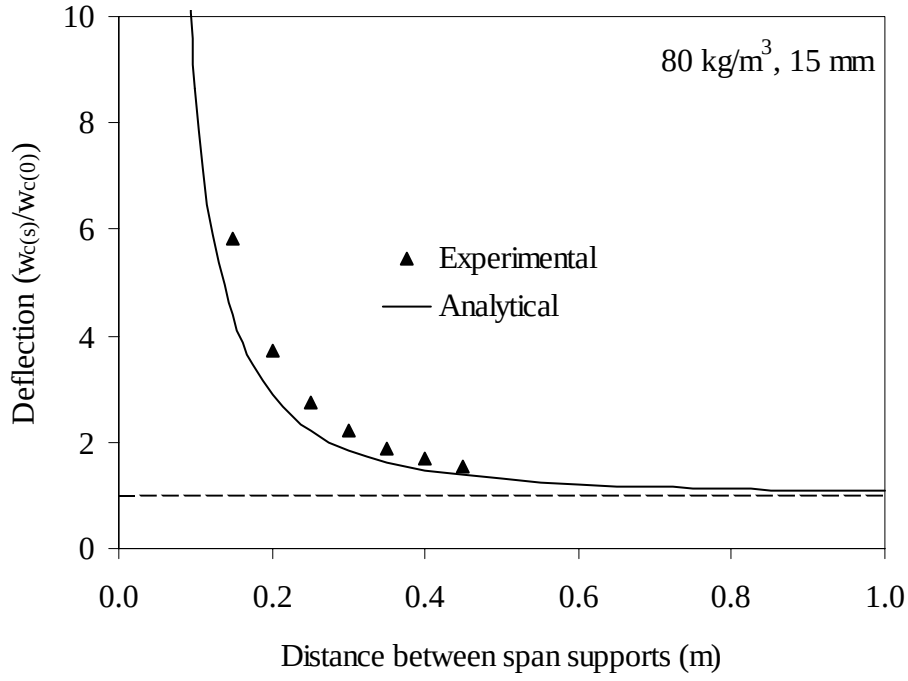


***Figure 5.22.*** *Experimental and analytical results for variation of deflection in three point bending as a function of span length for sandwich specimens with foam of 80 kg/m$^3$ density and 15 mm thickness.*

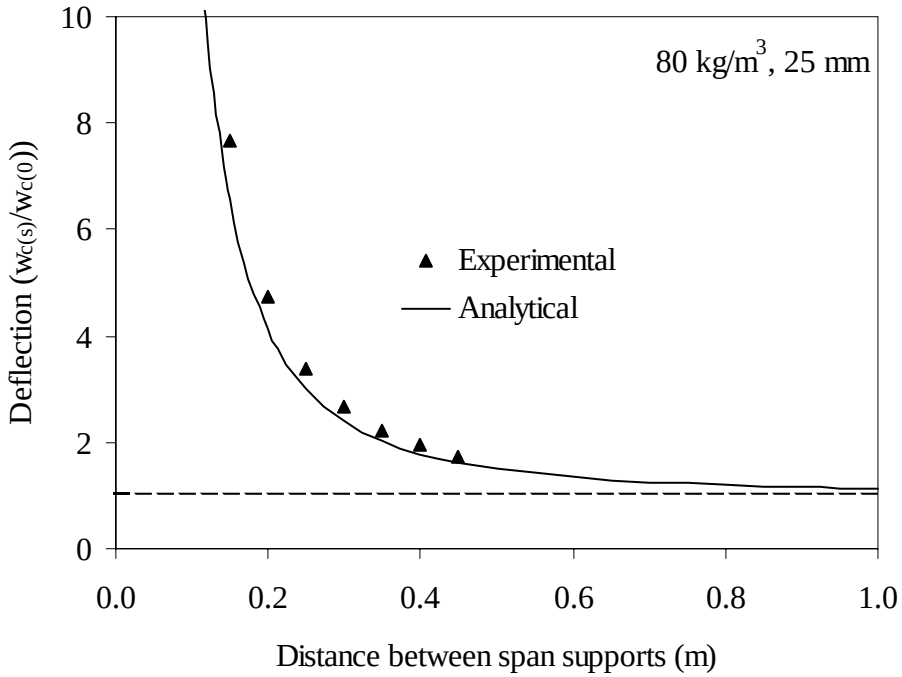


***Figure 5.23.*** *Experimental and analytical results for variation of deflection in three point bending as a function of span length for sandwich specimens with foam of 80 kg/m$^3$ density and 25 mm thickness.*

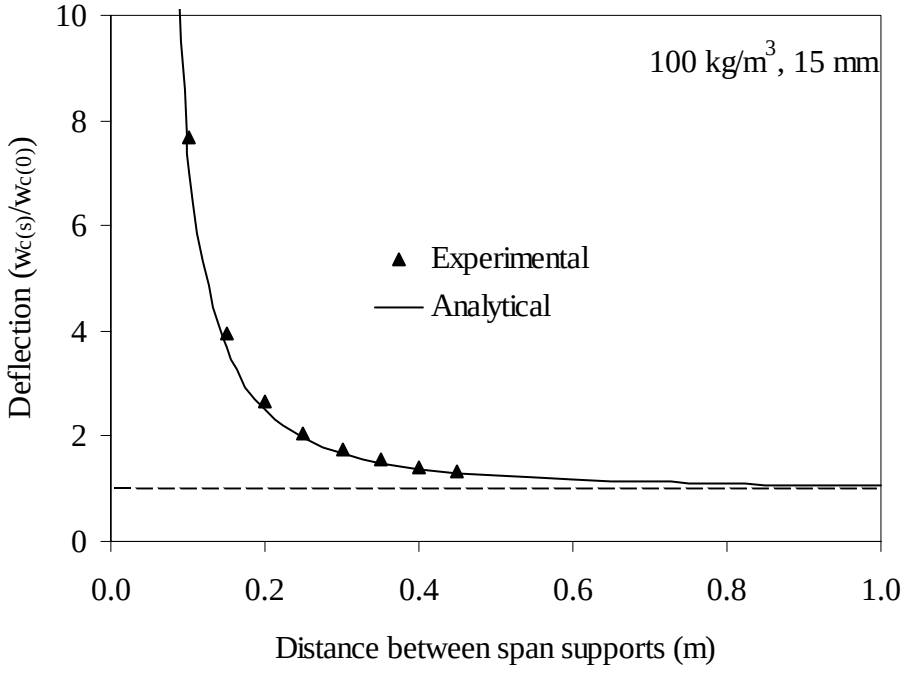


***Figure 5.24.*** *Experimental and analytical results for variation of deflection in three point bending as a function of span length for sandwich specimens with foam of 100 kg/m$^3$ density and 15 mm thickness.*

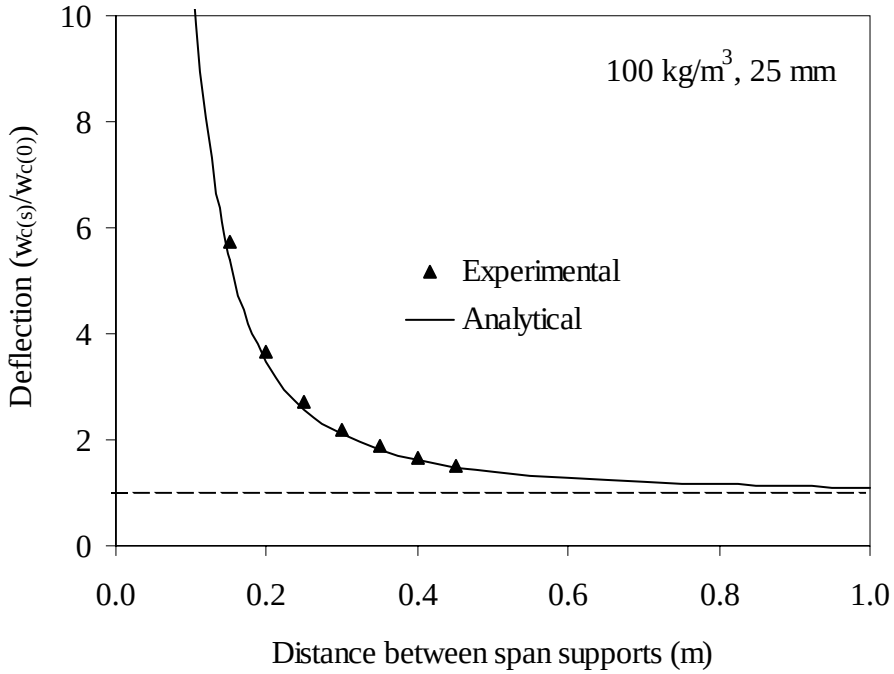


***Figure 5.25.*** *Experimental and analytical results for variation of deflection in three point bending as a function of span length for sandwich specimens with foam of 100 kg/m$^3$ density and 25 mm thickness.*

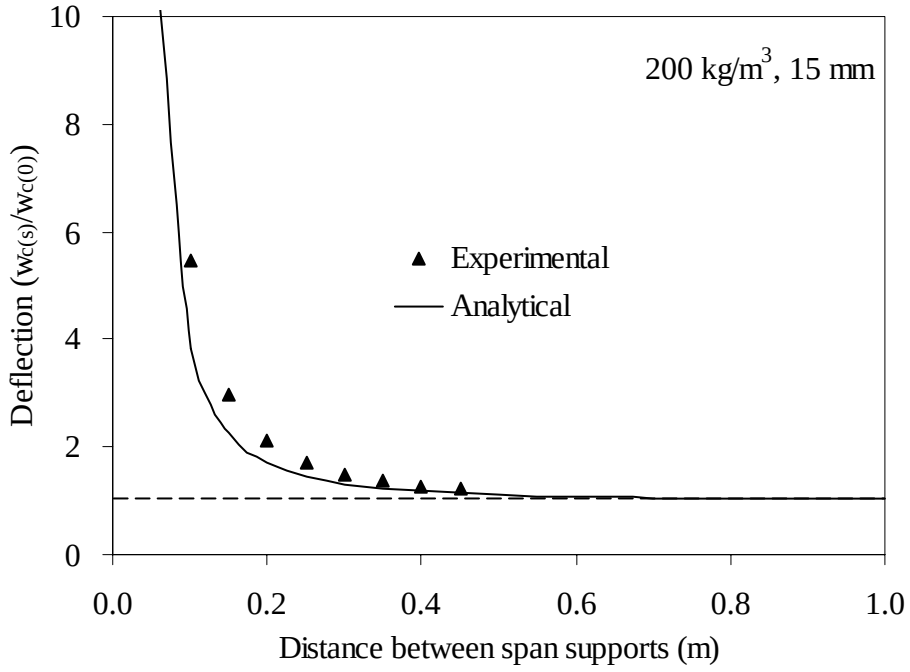


***Figure 5.26.*** *Experimental and analytical results for variation of deflection in three point bending as a function of span length for sandwich specimens with foam of 200 kg/m$^3$ density and 15 mm thickness.*

# Chapter 6
# Fatigue characterisation

## 6.1 Introduction

Repetitive stresses or deformations often cause damage or failure even if these are well below their allowable values for static strength. Fatigue failures occur in different forms. Mere fluctuations in externally applied stresses or strains result in mechanical fatigue. Cyclic loads acting in association with high temperatures cause creep-fatigue; when the temperature of the cyclically loaded component fluctuates, thermo-mechanical fatigue is induced. Recurring loads imposed in the presence of chemically aggressive or embrittling environment give rise to corrosion fatigue. The repeated application of loads in conjunction with rolling contact between materials produces rolling contact fatigue. In general, majority of failures in machinery and structural components can be attributed to one of the above processes. Such failures generally take place under the influence of cyclic loads whose peak values are considerably smaller than the safe loads estimated on the basis of static fracture analysis.

Generally, the fatigue of sandwich composites can be divided into three major groups.

1. The mechanisms of stress redistribution (changes in the state of stress);
2. The damage process (changes in the state of material);
3. Consequences (changes in stiffness, strength and life).

Fatigue damage in sandwich panels is the combination of damage in skins and the cores. Therefore, it is necessary to understand the mechanical behaviour of constituents of sandwich materials under fatigue. In the following section, a detailed study is presented about the constituents of sandwich composite materials under fatigue.

## 6.2 Mechanical behaviour of constituents of sandwich composite

Fatigue of the faces could be included in the design process since fatigue properties are fairly well known, and the loading situation is simple. The core, on the other hand, exhibits a more complex loading situation and fatigue data are rare. In polymer foam core sandwich structure, the core typically is the weakest part and it is expected that it may be the first to fail under cyclic loading. The fact that the cellular foam cores are viscoelastic makes the problem of fatigue even more complex. The mechanical properties of sandwich composites depend on the core and face materials as well as the thickness of core and faces.

There is a great need to improve our understanding of relationships between loads, material properties, damage, and long and short term performance of the constituents of sandwich composite materials behaviour. The level of understanding must advance so that the complex damage processes that occur in sandwich structures can accurately be monitored and predicted. This study shall focus on the fatigue performance of

constituents of sandwich composites that mainly include fatigue of skin and core individually and finally sandwich composite itself. The scope of this study is not to cover important macroscopic tests of sandwich structures, but to give insight into the underlying reasons for fatigue behaviour in sandwich and its constituents. We will therefore have a closer look at some useful tests methods to characterise the constituents of sandwich structure on specimen level in the following sections.

### 6.2.1 Fatigue characterisation of skins

Fatigue behaviour of laminates composite materials and structure is a quite complex phenomenon consisting of cyclic load or displacement events and processes. The event and processes, refereed as damage, combine in such a way as to alter the state of material and change the response of composite to the extent that it may eventually fail.

The purpose of this work is to give an experimental approach to study the fatigue behaviour of glass fibre epoxy cross-ply laminates in three point bending under cyclic fatigue. These experiments are jointly performed within the Composites and Mechanical Structural Group of Maine University as a part of common studies for the skin material [112].

#### *6.2.1.1 Fatigue tests*

Flexural fatigue tests are convenient to run because of their relatively low loads and simple fixtures. These are run in either simple bending or reverse bending. Fatigue tests were carried out on specimens identical to those used in static tests with a sinusoidal type of wave form at frequency of 10 Hz.

Tests were conducted under displacement control with laminate skins of glass fibres. Average displacement $d_{mean}$ is maintained constant and was equal to 45% of displacement at failure in static tests. Number of loading levels $r_d$ ($r_d = d_{max}/d_{rup}$; $d_{max}$ being the maximum displacement applied in fatigue) were chosen to plot the curves of stiffness loss and to draw the diagrams of fatigue life (Wöhler curves).

#### *6.2.1.2 Stiffness reduction*

Recording changes in stiffness of composite laminates under cyclic loading conditions is one of the most commonly used methods for study of the progression of damage during the fatigue of composites. During these tests, the evolution of the maximum load $F_{max}$ according to the number of cycles, for different levels of loading (*r)* was recorded. The maximum load $F_{max}$ is referred to $F_{0max}$, the maximum load in the first cycle.

Figure 6.1, shows the evolution of the load ($F_{max}/F_{0max}$) according to the number of cycles for displacement level of 0.60 ($r = F_{max}/F_{min}$). The results obtained for glass fibre laminates show that the loss of the load until the failure of the specimen takes place in three distinct stages. Stage one is characterised by an initial loss in stiffness caused by

matrix cracking and some early fibre fracture. Stage two is an intermediate stage representing a period of stable crack propagation in which stiffness reduction occurs as a result of formation of additional matrix cracking, crack coupling along ply interface, and initiation of internal delamination. The onset of stage three near to the end of life is characterised by a rapid decrease in stiffness as a result of failure of fibres, including delamination and coalescence of all damage mechanisms resulting in total failure of the laminate. The transition from stage one to stage two is indicated by the change in stiffness degradation (10 to 15%) due to damage development where as it corresponds to 80% of the fatigue life.

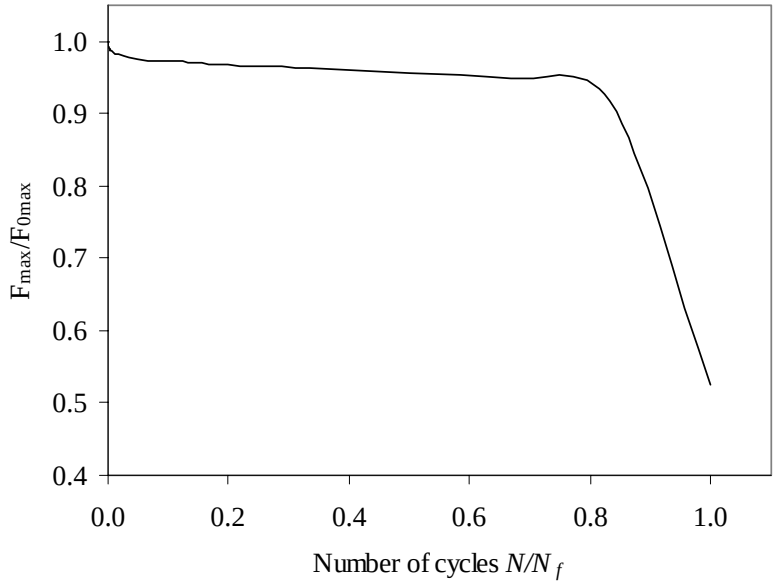


***Figure 6.1***. *Evolution of load versus number of cycles in three point bending.*

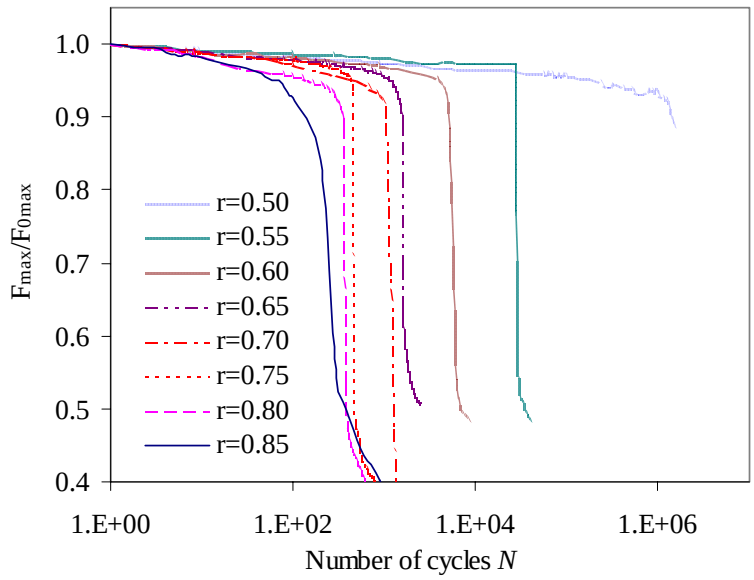


***Figure 6.2.*** *Evolution of the load versus number of cycles at different applied displacement levels.*

Figure 6.2 represents the evolution of the stiffness decrease ($F_{max}/F_{0max}$) according to the number of cycles for different applied displacement levels ($r$) using semi-logarithmic scale. From the figure it can be seen that the fatigue life increases with the decrease of applied displacement level ($r$). The brutal failure of laminate occurs after a weak reduction in stiffness for loading levels ($r$) of 0.55 to 0.85.

### *6.2.1.3 Fatigue life*

In order to predict fatigue life, it is necessary not only to establish the sequential development of damage mechanisms but also to quantify the growth rates of the mechanisms. The development of damage involves a sequence of mechanisms which may not be separable into distinct damage modes but rather into dominant damage modes. To determine performances of composite materials in fatigue, different criteria of damage assessment ($N_s$ , $N_3$ , $N_5$ , $N_{10}$ and $N_R$) are considered in the literature from the curves giving the evolution of the load according to the number of cycles. The most severe criterion is the one that characterise the material by the $N_s$ value that corresponds to the number of cycles at the end of the linear domain. The criteria $N_3$ , $N_5$ and $N_{10}$ correspond respectively to stiffness degradation of 3%, 5% and 10% of the load in relation to the initial load. The $N_R$ criterion corresponds to the number of cycles of the complete failure of the specimen when it is reached. We have chosen for our study the $N_{10}$ criterion which is commonly used in the literature [14,125].

Fatigue life can be given by *S-N* curves or Wöhler curves, giving the maximum applied displacement level according to the fatigue life at number of cycles $N_{10}$. Figure 6.3 represents Wöhler curve in displacement control. This curve gives the evolution of the loading level according to the number of cycles $N_{10}$, with an average displacement kept constant and equal to 45% of the failure displacement in static tests.

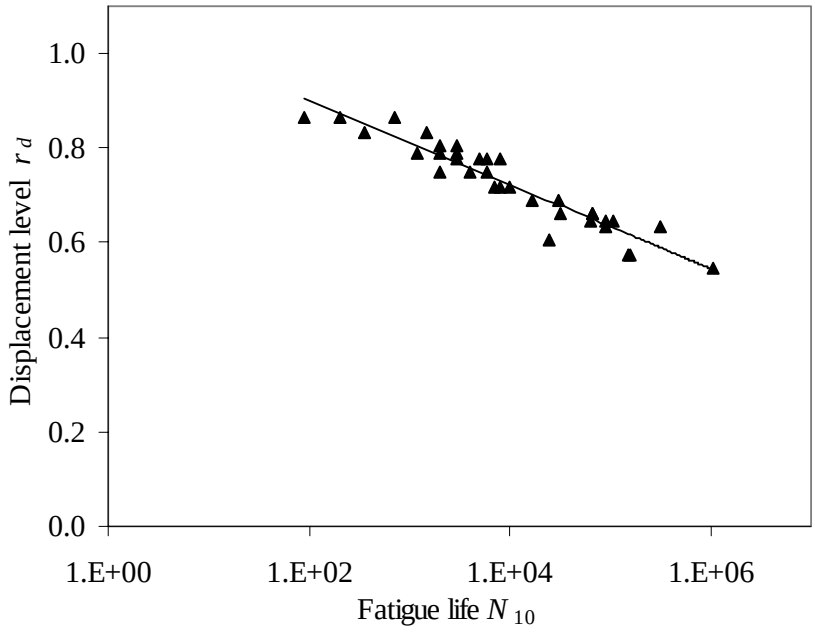


***Figure 6.3.*** *Wöhler curve for glass fibre laminates in three point bending.*

The fatigue life decreases with increasing the load displacement level. It is to be noted that the evolution of the loading level according to the fatigue life $N_{10}$ intersects the *y*-axis at about 1, which corresponds to a level of loading representing static failure.

#### *6.2.1.4 Failure topography*

An understanding of the failure modes and their dominance under service loading conditions is important in engineering design because for particular applications, they determine 'allowable design' for component. Static and cyclic loading, impact and environmental attack etc., all contribute to accumulation of damage in laminates.

The failure topography after cyclic fatigue is shown in figure 6.4. For cross ply laminates, crack propagation generally can progress with little hindrance in the direction parallel to the fibres, thus the transverse plies in cross ply laminates will fail under fatigue. Therefore, the dominant damage modes under fatigue are transverse cracks forming in the 90° plies and internal delamination at the 0/90° interface. The cracks induced in the 90° layer, destroy the load bearing 0° layers of glass fibre composites thus leading to total failure of the specimen. When the loading level is higher, several damages are initiated during the initial cycles. The fatigue in this case consists in propagating these damages quickly until the total failure. This failure is obtained within the first few hundred cycles. As for the small values of loading level *r,* there are some fibre failures on the compressed side of face, the transverse cracking in the 90° plies and the delamination between the tense layers but not complete failure.

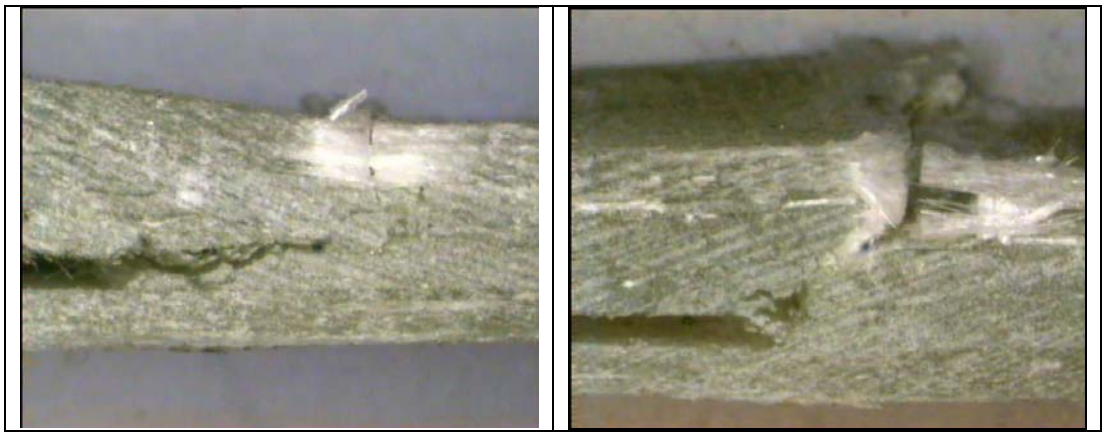

***Figure 6.4.*** *Fracture topography after the cyclic fatigue for glass fibre reinforced laminates.*

## 6.2.2 Fatigue characterisation of foams

#### *6.2.2.1 Introduction*

Rigid cellular foams are finding increased usage in structural applications as core material in sandwich structures configuration. Therefore, it is necessary to understand the behaviour of foams under different loading conditions during fatigue. Like in all

engineering materials, failure of the polymer foam often results as a consequence of accumulated irreversible damage or growth of a flaw to a critical dimension. In general, polymer foams are more sensitive to the testing environment than their metal or ceramic counterparts. The fatigue life of a polymeric component is controlled by several factors, which include the stress and strain amplitudes of the loading, the mean stress and the frequency of loading, temperature and loading process. These factors are of considerable interest and practicality for the safe design of polymeric sandwich structures. The aim of this work is to examine the mechanical behaviour and fatigue performance of a set of PVC foams, their microscopic failure mechanisms and to establish a relationship between viscoelastic properties of the foam under indentation, compression, flexural and shear testing during fatigue.

### 6.2.2.2 *Fatigue after indentation*

#### *6.2.2.2.1 Introduction*

It is well known that foams can fail in a number of different modes [117]. One mode of failure that has received little attention is indentation. Specifically, after indentation, how the mechanical properties of foam changes and affects the fatigue behaviour in various loading environments. Indentation of the core occurs at concentrated loads, such as fitting, corners or joints of a structure or component. As far as possible, a designer would avoid deliberate application of intense transverse loads to a foam but such loads can also arise accidentally, for example as a consequence of collisions or dropped objects, over tightening of screw in joining and therefore indentation also is then likely a failure mode. Sometime, this indentation remains unnoticed and can cause a severe problem in fatigue. For simplicity and to suppress and bypass the other failure modes, consideration was confined to the case in which the foam is supported on a solid rigid surface and subjected to fatigue after performing deliberate indentation as in our case using different mean displacement levels.

Viscoelastic behaviour of the polymeric foam plays an important role in absorbing and dissipating energy in a sandwich structures, especially during dynamic loading. Such dynamic loading could be in terms of cyclic or high strain rate loading during indentation.

#### *6.2.2.2.2 Fatigue tests*

Four values of applied mean displacement levels (0.16 to 0.66) were chosen in order to cover the significant active regions (damage development) of load-displacement curve as shown in figure 6.5, considering reduced indentation at a fixed displacement amplitude of 1.5 mm.

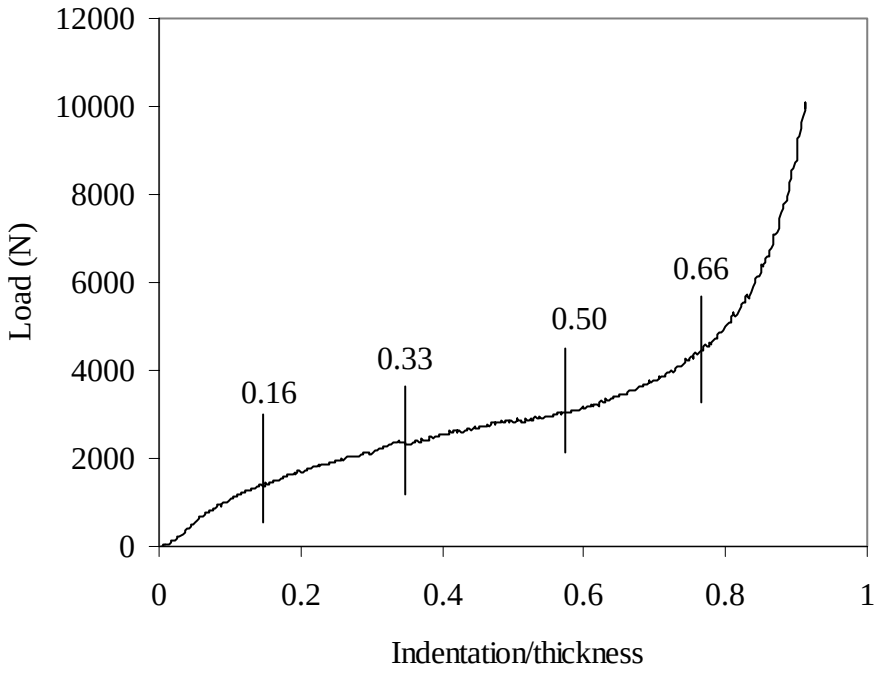


***Figure 6.5.*** *Choice of mean displacement level from static tests for designing fatigue indentation experiments.*

Fatigue indentation tests were performed on cross-linked PVC foams of 60, 80 and 200 kg/m$^3$ densities, using sinusoidal type of waveform at a loading of frequency of 5 Hz in displacement control. The lower side of the foam specimen is supported on a solid foundation that is mounted on the actuator of Instron Machine. A load cell of 100 kN capacity was used to test the core materials in fatigue and indentation. Dynamic fatigue indentation tests were performed using a cylindrical roller of diameter 35 mm. In fatigue indentation tests, the upper roller is pressed into the foam specimen at a steady rate and after reaching the prescribed mean displacement level, the fatigue test was started. Hysteresis curves, energy dissipation curves and stiffness versus number of cycles diagrams were generated, and the failure mechanisms were examined.

#### *6.2.2.2.3 Load displacement response (hysteresis curves)*

Figures 6.6 to 6.11, shows the experimental load displacement hysteresis curves for loading and unloading cycles at 1, 10, 100, 1000, 3000, 5000 and 10000 cycles for mean displacement levels of 0.16 and 0.66 for PVC foams of densities 60, 80 and 200 kg/m$^3$ respectively.

The foams exhibited considerable hysteresis, both in loading to maximum and in unloading to minimum. Each foam of different density shows different peak loads and hysteresis curves but the behaviour is almost similar for three foams. At small values of mean displacement level (0.16), the peak load and area in the hysteresis loops are small as compared to high value of mean displacement levels (0.66). Peak loads in the first cycle increased to almost double the value of peak load when applied displacement

level increases to 0.66 from 0.16 for foams of all the densities. It can be seen that hysteresis loops in the first cycle have large area in loading and unloading and high peak load for foams of all densities used in this study. With the increase in the number of cycles area under the hysteresis loops and peak load decreases due to damage development in foams. Small displacement levels resulted in small area under hysteresis loops, while high displacement levels resulted in large area in hysteresis loops.

After 1000 cycles, the hysteresis loops and peak load become stable for higher number of cycles for foams of three densities used in this study. Presumably due to fatigue, cell walls completely collapsed and no further decrease in peak load is possible at high number of cycles. This indicates that irreversible damage had taken place due to cycling, which is caused by the complete rupture of cell walls and fracture of cell edges that leads to the foam acting like a solid material.

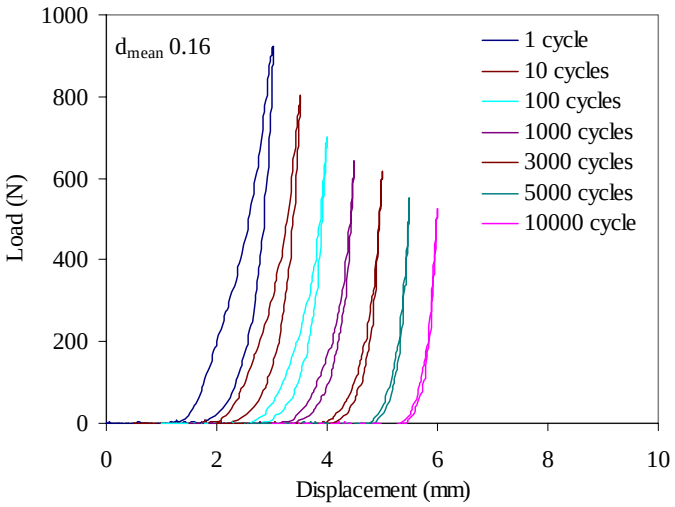


***Figure 6.6.*** *Hysteresis curves for foams of 60 kg/m$^3$ density for different number of cycles at mean displacement level of 0.16 in fatigue tests after indentation.*

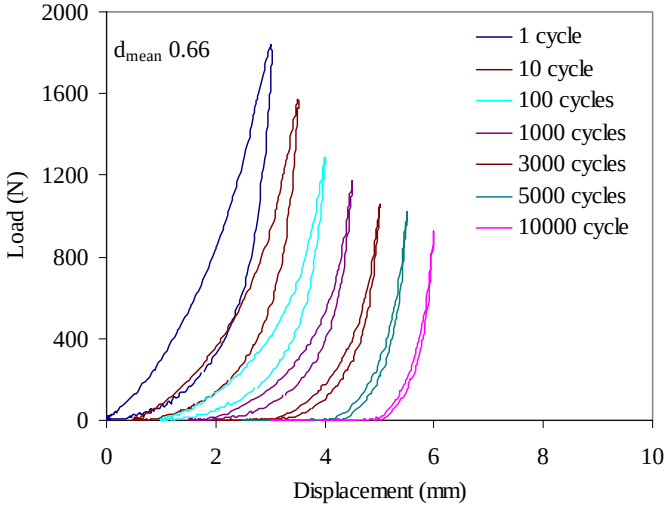


***Figure 6.7.*** *Hysteresis curves for foams of 60 kg/m$^3$ density for different number of cycles at mean displacement level of 0.66 in fatigue tests after indentation.*

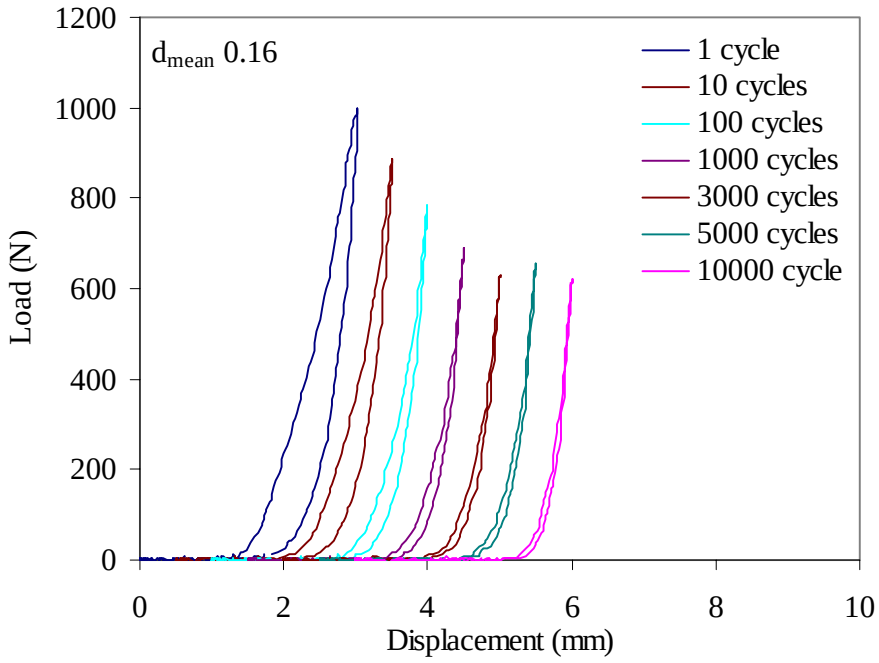


***Figure 6.8.*** *Hysteresis curves for foams of 80 kg/m$^3$ density for different number of cycles at mean displacement level of 0.16 in fatigue tests after indentation.*

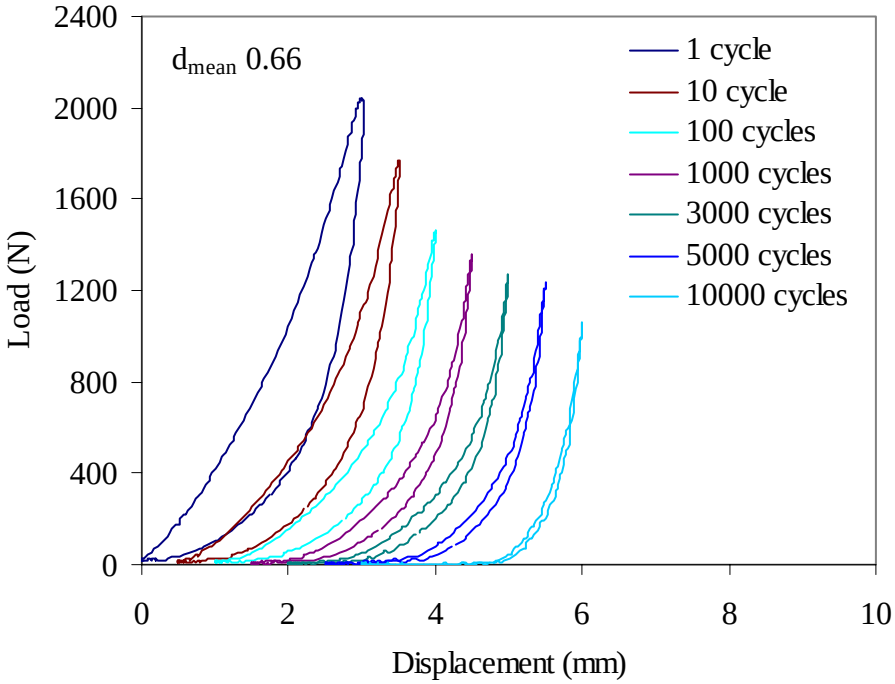


***Figure 6.9.*** *Hysteresis curves for foams of 80 kg/m$^3$ density for different number of cycles at mean displacement level of 0.66 mm in fatigue tests after indentation.*

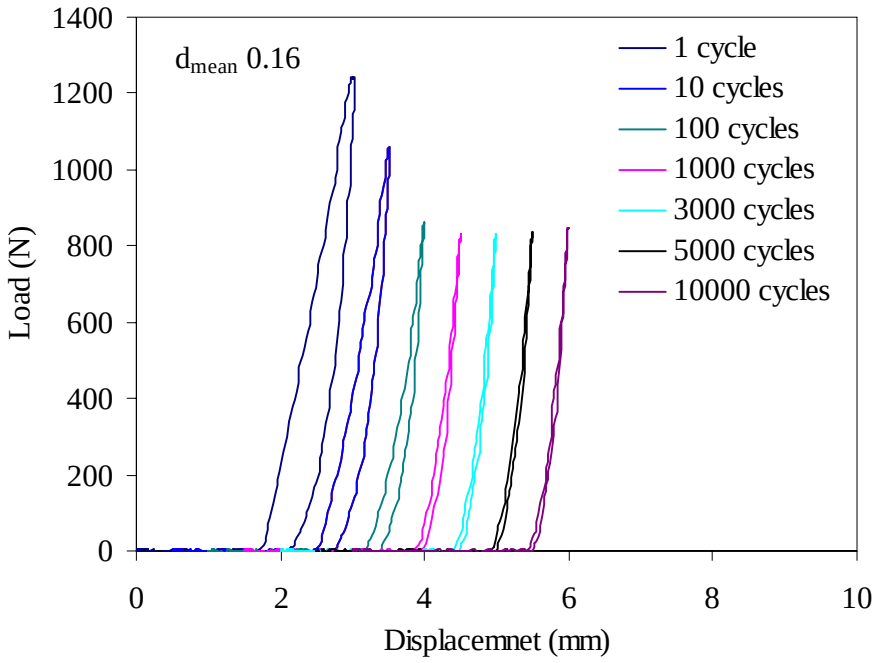


***Figure 6.10.*** *Hysteresis curves for foams of 200 kg/m$^3$ density for different number of cycles at mean displacement level of 0.16 in fatigue tests after indentation.*

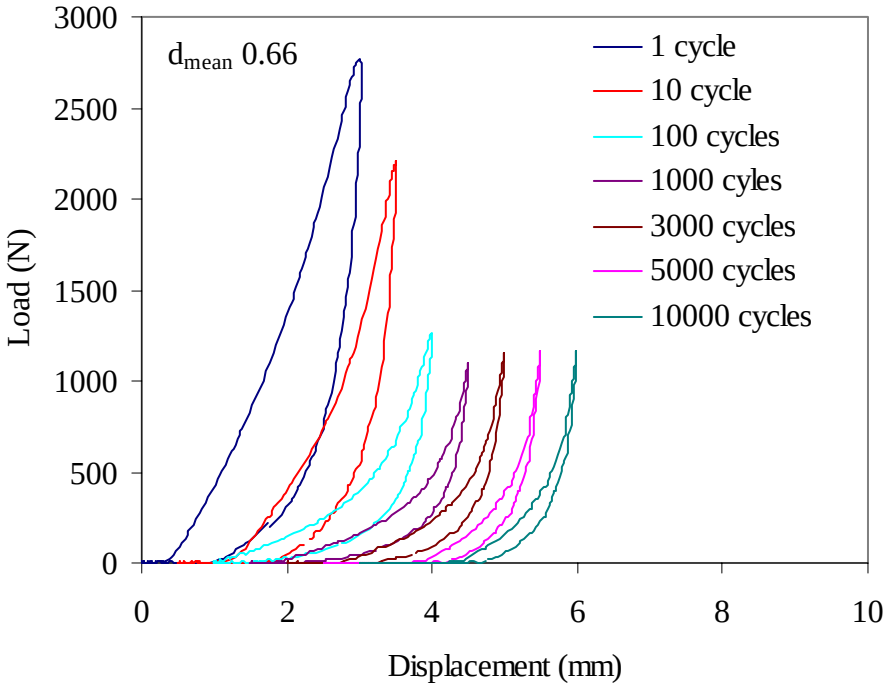


***Figure 6.11.*** *Hysteresis curves for foams of 200 kg/m$^3$ density at different number of cycles at mean displacement level of 0.66 in fatigue tests after indentation.*

#### *6.2.2.2.4 Energy dissipation*

A useful quantity for the estimation of fatigue behaviour of cellular foams is the dissipated energy. Cellular foams are excellent in absorbing energy, as this energy is dissipated within the foam when these materials undergo impact or indentation. In our studies, foam specimens are loaded in indentation and then subjected to cyclic fatigue. When the load is large enough to overcome yield stress of the foam material, plastic deformation and damage is induced, and a plot of load versus displacement has the form of the loop, due to hysteresis i.e. energy loss. The load-displacement behaviour observed depends upon deformation typically includes a significant strain energy contribution and the area enclosed by hysteresis loop corresponds to dissipated energy for each cycle. For any given cycle, the dissipated energy per unit volume is given by:

$$E_d = \int_{\varepsilon_{\min}}^{\varepsilon_{\max}} \sigma d\varepsilon \tag{6.1}$$

Figures 6.12 and 6.13 show, the energy dissipation versus number of cycles for different densities foams at mean displacement levels of 0.16 and 0.66. The low density foams (60-80 kg/m$^3$) are able to dissipate less energy compared to high density foams as can be seen from figure 6.12. High density foams dissipate more energy with the increase in number of cycles. The difference in dissipation energy is large within 1000 cycles and afterwards not much dissipation of energy is observed.

It is interesting to note that fatigue exhibits greater changes during the initial part of fatigue life due to energy dissipation in PVC foams. Air trapped in the foam cell plays an important role in dissipation of energy during fatigue. During loading and unloading foams, more energy dissipates in collapsing the cell walls, cell edge fracturing or foam softening. There is also rapid decrease in air contribution, which is explained by membrane rupture allowing air freer passage through the foam. This effect is dominant in initial cycles as in the subsequent cycling, this effect decreased more quickly. This phenomenon is characterised by large amount of energy dissipation during the initial number of cycles. It is observed that dissipated energy is almost proportional to applied displacement level. In the beginning, the value of dissipated energy is found 450 mJoule for foam of density 200 kg/m$^3$ at mean applied displacement level of 0.16. However, when the value of mean displacement level is increased to 0.66, the dissipation energy is also increased with same proportion i.e. 2000 mJoule. A relationship between the hysteresis energy loss and number of cycles has been established. It is assumed that damage in foams strongly depends on the mean displacement level as increasing the mean displacement levels increases the extent of initial damage. Similar, increase in dissipated energy for the specimens of the other two densities is observed that also increases at the same proportion rate with the increase in displacement levels.

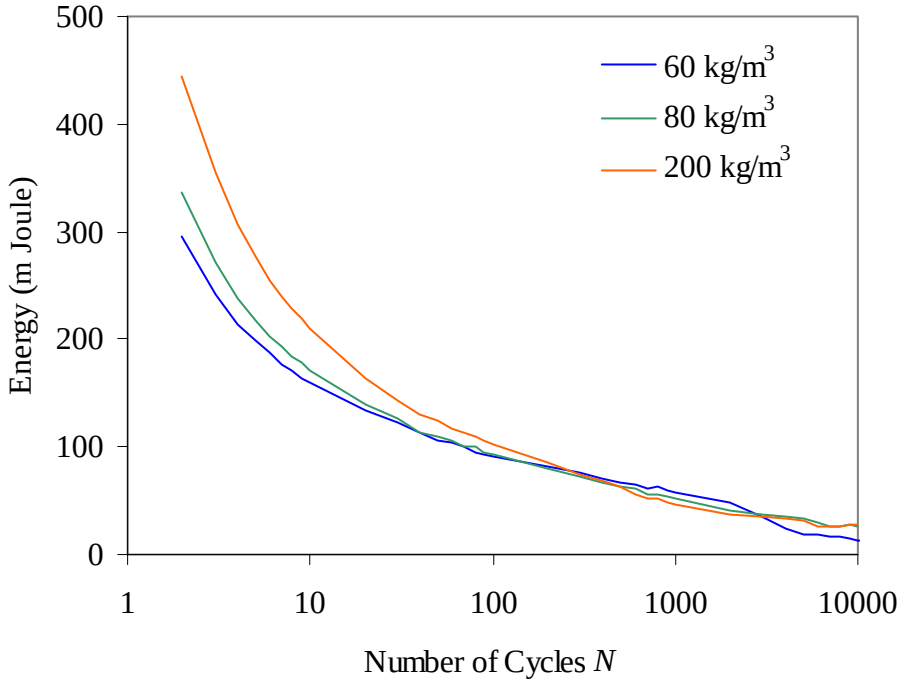


***Figure 6.12.*** *Evolution of energy dissipation with number of cycles for foams of three densities at low mean displacement levels of 0.16 in fatigue tests after indentation.*

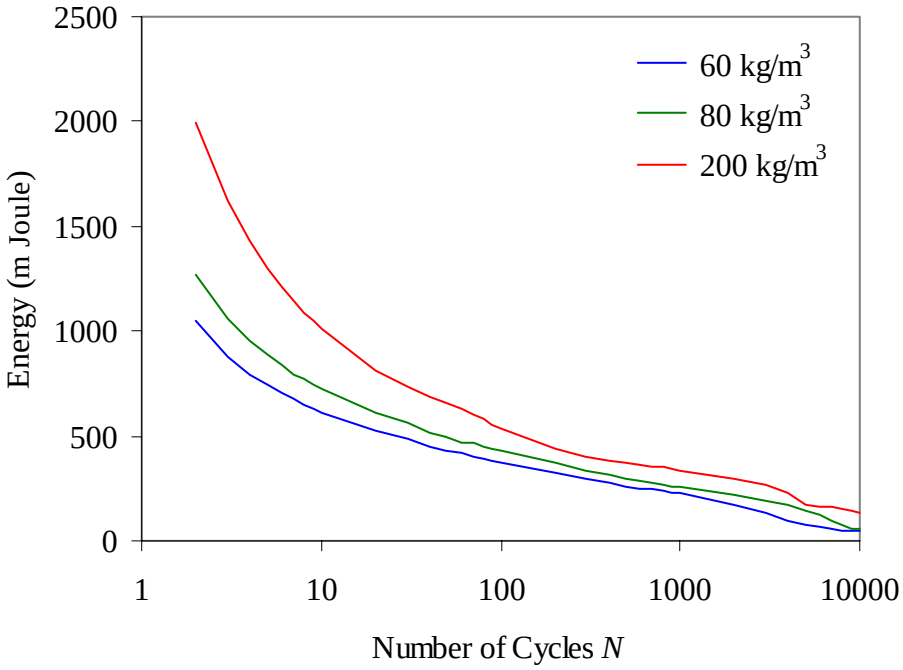


***Figure 6.13.*** *Evolution of energy dissipation with number of cycles for foams of three densities at high mean displacement levels of 0.66 in fatigue tests after indentation.*

### *6.2.2.2.5 Stiffness degradation*

The plots of stiffness versus number of cycles for foams of different densities are shown in figures 6.14 to 6.16. These curves were plotted for four mean displacement levels in the range (0.16 to 0.66) with same displacement amplitude of 1.5 mm for three different densities. It is observed from these figures that, with increasing the mean displacement levels, stiffness reduction increases. The rate of stiffness degradation depends on the displacement level and density. It can be seen that for small values of mean displacements levels, the stiffness reduction rate for three densities is almost same. While for higher densities and higher values of mean displacements, stiffness reduction rate become quite evident and showed a marked difference as represented in figure 6.16.

Figure 6.17 and 6.18 represents the comparison of three densities at two mean displacement levels (0.16 and 0.66). The stiffness degradation corresponds to two distinct stages. In the first stage, stiffness decreases rapidly within few hundred cycles that is about 40% for low displacement level (0.16) and 60% for high mean displacement level (0.66). In the second stage, stiffness started increasing with the number of cycles for high density foam (200 kg/m$^3$). This phenomenon is attributed to collapse of the cell walls of the foams which increases with the increase in number of cycles. Of course initial setting of mean displacement level caused initial damage in the foam resulting in partial collapse of cell walls, and these cell walls further deteriorated with the increase in the number of cycles. Stiffness reduction started rising again after certain number of cycles when cell walls totally collapsed and foam started behaving as a solid material.

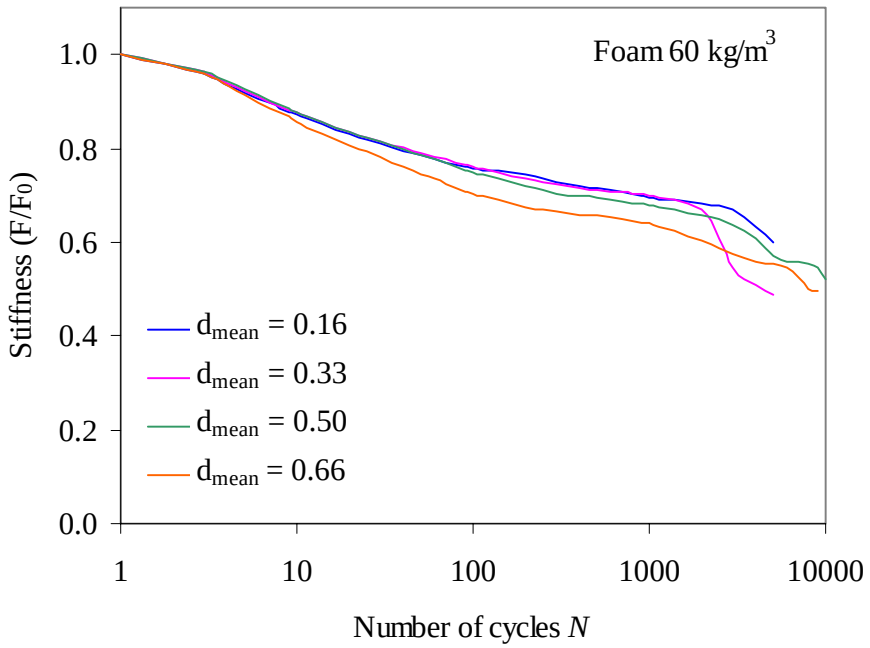


***Figure 6.14*** *Evolution of stiffness versus number of cycles for 60 kg/m$^3$ density foams at different mean displacement levels and constant amplitude of 1.5 mm during fatigue after indentation.*

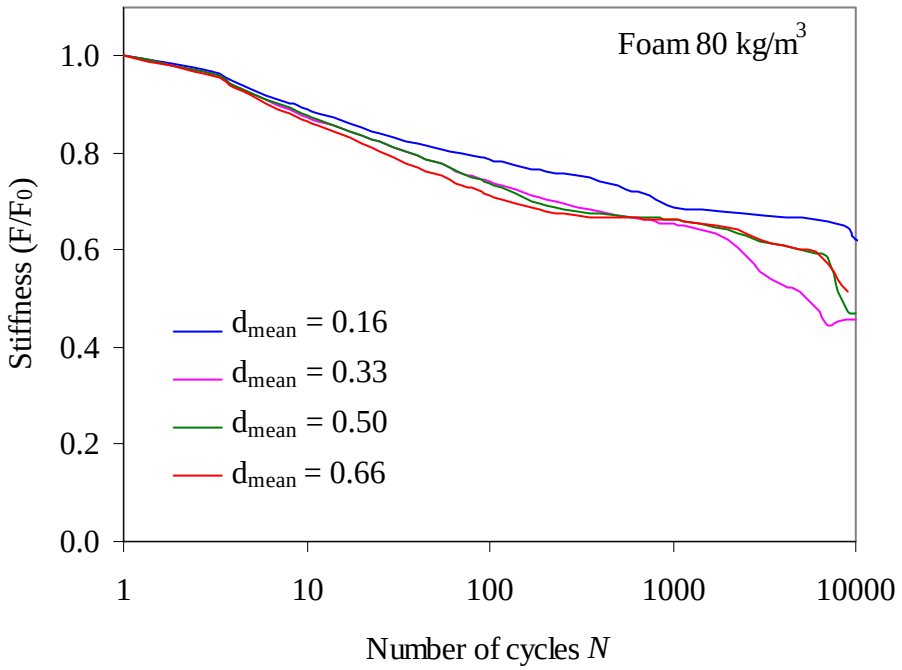


***Figure 6.15.*** *Evolution of stiffness versus number of cycles for 80 kg/m$^3$ density foams at different mean displacement levels and constant amplitude of 1.5 mm during fatigue after indentation.*

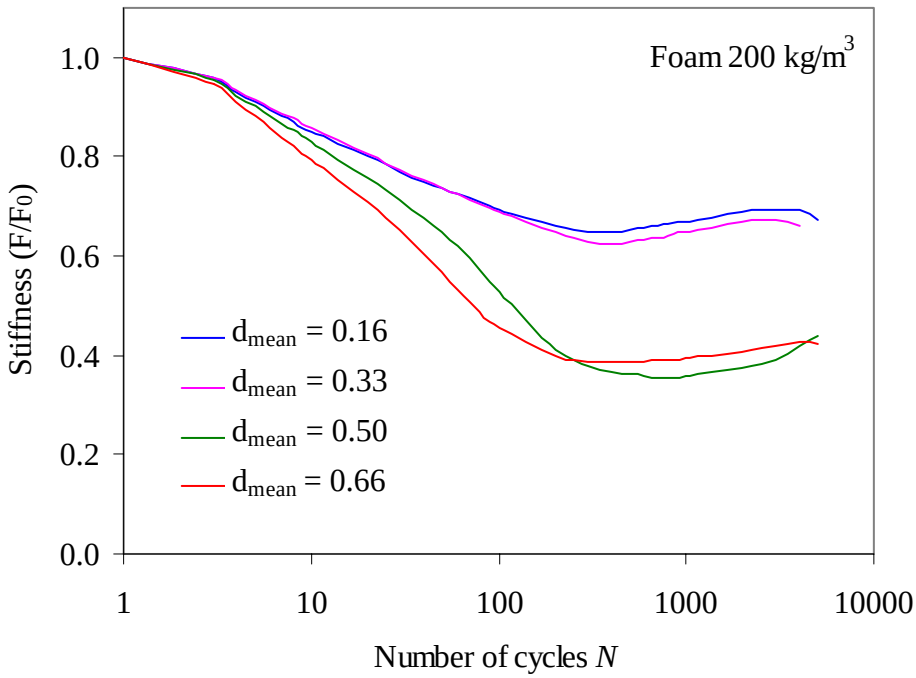


***Figure 6.16.*** *Evolution of stiffness versus number of cycles for 200 kg/m$^3$ density foams at mean average displacement levels and constant amplitude of 1.5 mm during fatigue after indentation.*

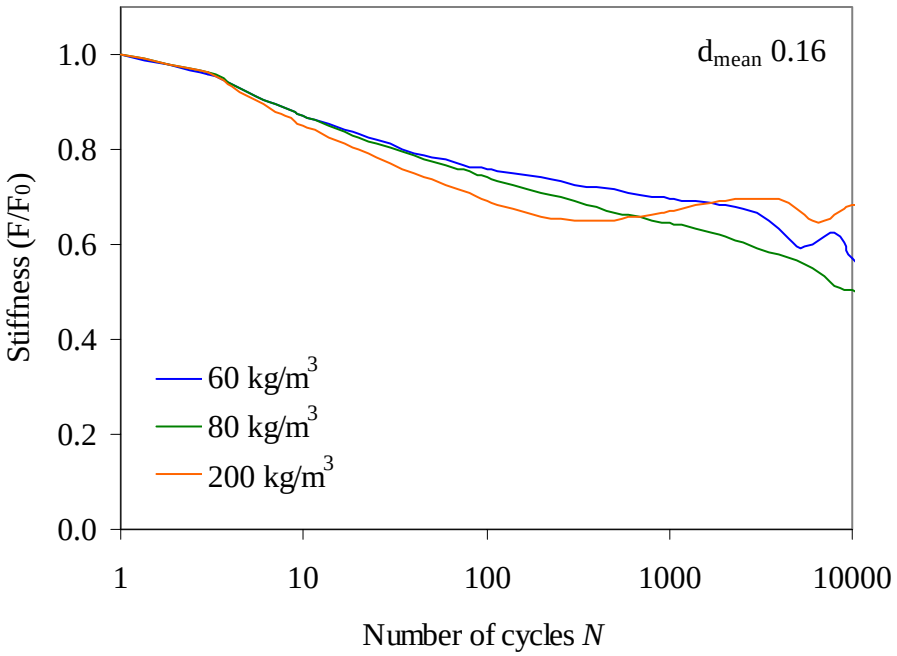


***Figure 6.17**. Evolution of stiffness versus number of cycles at mean displacement level of 0.16 for foams of different densities during fatigue after indentation.*

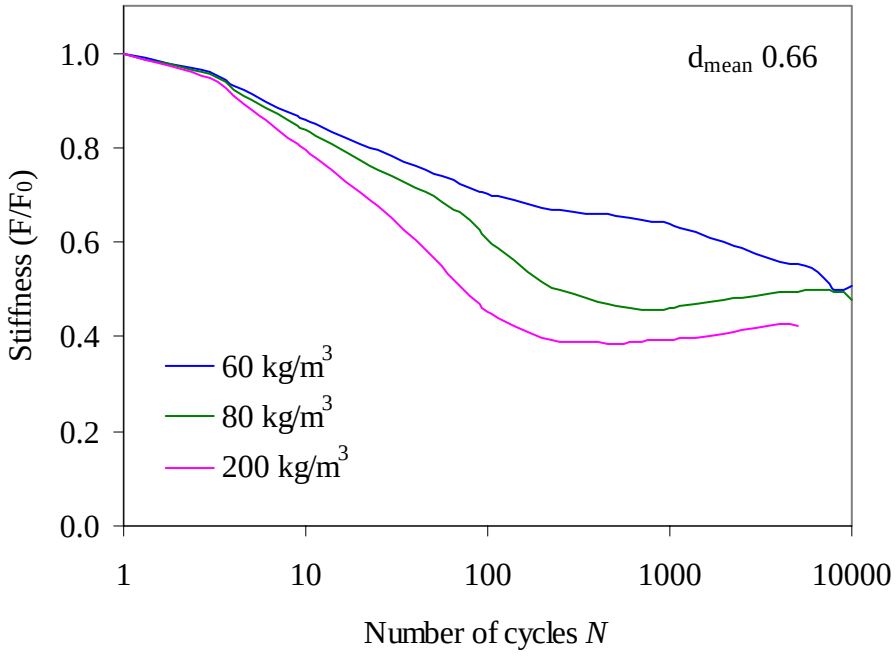


***Figure 6.18**. Evolution of stiffness versus number of cycles at mean displacement level of 0.66 for foams of different densities during fatigue after indentation.*

### *6.2.2.2 Flexural fatigue tests in foams*

The fatigue properties of flexible foams have long been a major source of controversy. Questions relating to the causes of fatigue, the relationship of fatigue to other physical properties, the ramifications of measuring errors, and the correct test methods have been debated for years with little quantitative results [122,123]. There is still no generally adopted procedure for the fatigue related failure mechanisms in foams. In this study attempts have been made to quantify certain aspects of fatigue in foams. In any sandwich structure, the core experiences a variety of stresses when the structure is loaded. Primarily these are seen as shear stresses through the thickness of the core, and complimentary shear stresses parallel to the plane of the skins, reaching a maximum at the centre of the core material. The core transmits the stresses into the skins via the core: skin adhesive bond without which the parts of the sandwich structure simply act independently and the stiffening effect of the sandwich is all but lost.

#### *6.2.2.2.1 Experimental procedures*

Static tests were first conducted to generate ultimate strength data, which was later used for determining the fatigue displacement levels. Details were given in the static test section 4.3.4. Flexural fatigue tests were performed at room temperature under displacement control at fixed displacement amplitude of 1.5 mm, on the foam specimens at different maximum applied displacement levels ($r$). The frequency of the tests was kept constant at 5 Hz. The dimensions of the specimens were $200\times50\times15mm^3$. The distance between the span supports was 150 mm and the diameter of the central roller was 20 mm.

#### *6.2.2.2.2 Results*

The load versus number of cycles curves provide much information about the sequence of events occurring during the loading. The main objectives within this investigation were to obtain basic knowledge on the flexural fatigue behaviour of PVC foams materials using constant amplitude loading. To investigate fatigue dependency of displacement amplitude and mean and maximum displacement, the testing was performed at different maximum applied displacement levels.

Figures 6.19 to 6.21 show the evolution of stiffness versus number of cycles for four foam densities. These results were obtained at three maximum applied displacement levels, $r$ = 0.25, 0.45 and 0.65. Tests were stopped when stiffness reduction of about 15% was achieved as there after several damage mechanisms were initiated and their descriptions become more difficult to explain. The rate of stiffness reduction is almost the same for four densities. It is assumed that at small values of $r$, there is no damage development in foams. While for higher value of $r$, stiffness degradation increases with increasing the density of foams, thus indicating initiation of damage. Stiffness reduction is high for high density foams. During the last stage of the curves the behaviour of foams differed depending on the value of $r$. With increasing the value of applied displacement level $r$ specimen failure and stiffness degradation is quite imminent as

seen in figure 6.21. It was observed from testing of foams that stiffness exhibits little changes before the failure. Failure is characterised as brittle in nature. No considerable changes were observed in stiffness before failure. Inspection of the curves reveal that less dense foams have relatively better stiffness than higher density foams. The final failure event was catastrophic due to sudden crack propagation which initiated at the tension side of the specimen, rapidly propagating along the compression side causing the specimen to break rapidly.

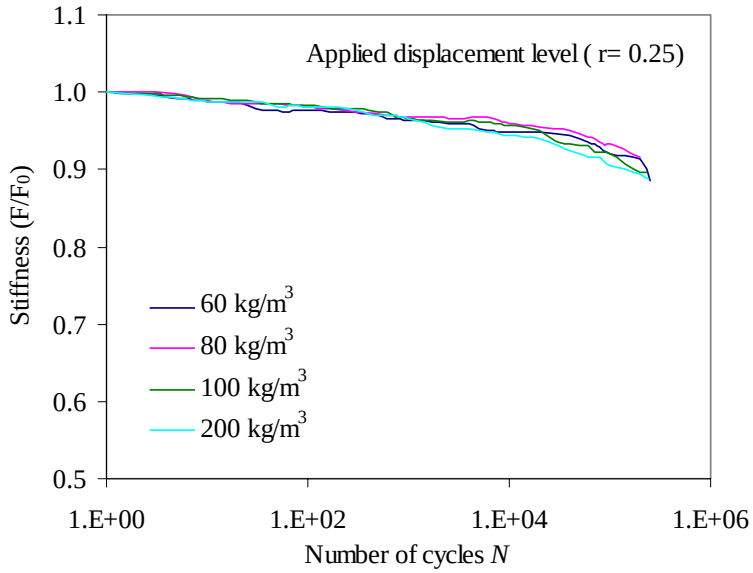


***Figure 6.19.*** *Evolution of stiffness with number of cycles for foams of four densities at maximum applied displacement level 0.25 under cyclic fatigue.*

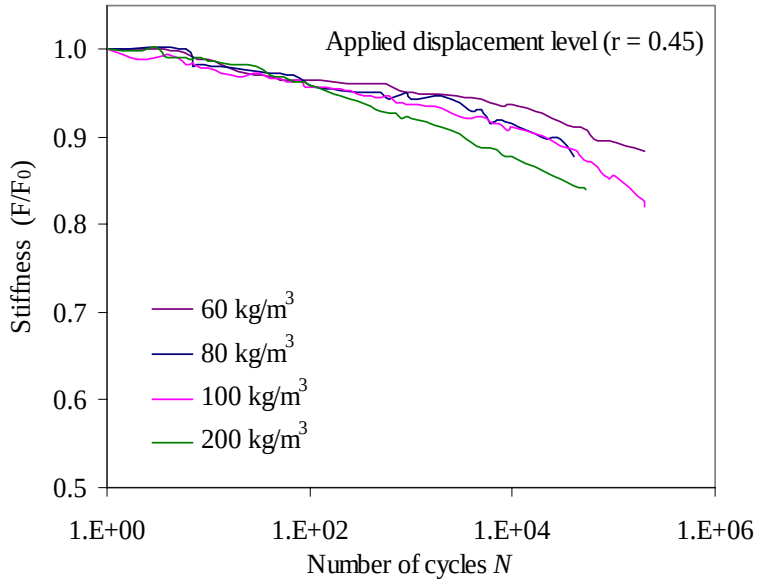


***Figure 6.20.*** *Evolution of stiffness with number of cycles for foams of four densities at maximum applied displacement level of 0.45 under cyclic fatigue.*

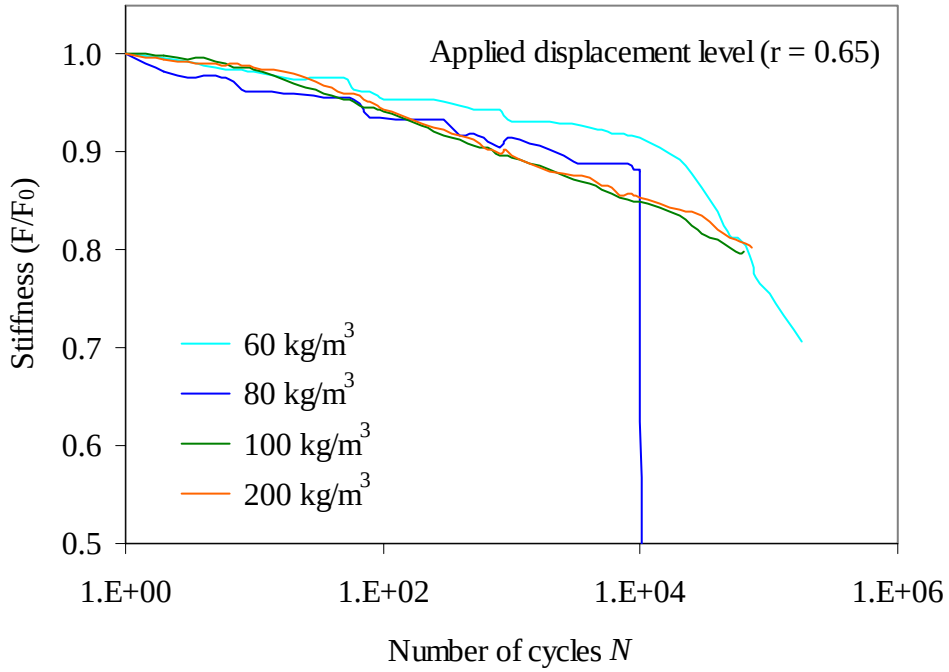


***Figure 6.21.*** *Evolution of stiffness with number of cycles for foams of four densities at maximum applied displacement level of 0.65 under cyclic fatigue.*

## 6.3 Fatigue characterisation of sandwich composites

### 6.3.1 Introduction

In many applications, sandwich structures are subjected to repetitive and variable loading conditions, therefore information about the effects of various loading parameters are particularly important. In the following section some of the important parameters are investigated.

### 6.3.2 Effect of frequency in fatigue

The effect of fatigue frequency on degradation of sandwich composites has been a source of controversy in the studies of composite materials. It is well known that the loading frequency affects the damage mechanism in composite materials and sandwich composites during fatigue tests. As for all composites containing polymer matrices, it is important that frequency should be low enough to avoid extensive heating that would affect the overall performance of the sandwich structures.

Under cyclic loading, and more particularly in viscoelastic materials, the increase in the frequency involves the increase in the rate of activation of the internal mechanisms of material and thus the increase in the internal temperature [8]. Several authors studied the effect of the frequency on the evolution of the damage mechanisms in composite

materials during fatigue tests [10-15]. Mandel et al. [5] reported that the increase in the frequency does not have a significant effect on the fatigue strength and the life span of composites material. While in another investigation on sandwich composites of PVC foams, Shenoi *et al.* [78] observed that the effect of rise in the temperature due to the increase in the frequency involves a reduction in certain mechanical properties such as stiffness and residual strength. In sandwich composites, core is the material which is highly sensitive to temperature. An increase in temperature due to frequency can affect the mechanical properties of sandwich composites.

In terms of structural integrity, the effect of loading frequency is particularly important to determine performance of sandwich composite structures. In the present study the effects of loading frequency were identified in sandwich composites.

#### *6.3.2.1 Testing procedure*

Experiments were performed to study the effects of frequency on the sandwich specimens. Sandwich specimens of foam 60 kg/m$^3$ and dimension 250×40×17 mm$^3$ were used in this study. The applied displacement is sinusoidal with various frequencies from 0.1 to 10 Hz. The applied mean displacement is equal to 20% of the failure displacement in static test. The amplitude is equal to 1 mm corresponding to 30% of the applied displacement level. These values are chosen so that the hysterisis of load displacement curve remains in the linear region. Duration of tests was the same for all specimens.

#### *6.3.2.2 Results*

Typical cyclic load-displacement curves which were obtained at the same loading conditions, for three values of frequencies corresponding to the low 0.1 Hz, intermediate 1 Hz and the high frequency of 10 Hz, are shown in figures 6.22 to 6.24 respectively. These curves were obtained from the envelopes of hysteresis at different cycles during a fatigue test.

It is observed from these figures that there is no significant difference or change in results for three frequencies used and load-displacement curves for the various frequencies are practically identical. Figure 6.25 shows the curves obtained from the envelopes of hysteresis at the last cycle for different loading frequencies. The values of dynamic stiffness were calculated using the average slope of any particular cycle from the hysteresis of the load-displacement curves at each frequency. Evolution of the dynamic stiffness for last cycle according to the frequency is shown in figure 6.26. Results show no significance changes in the stiffness with the increase in loading frequency in the 0.1 to 10 Hz range during cyclic fatigue. The stiffness changes in the sandwich specimens are found to be independent of the frequencies used in this study. Cornelia et al [14] also reported this kind of results in composite materials. Choice of frequency is important for fatigue experiments in order to optimise time and performance of the machine.

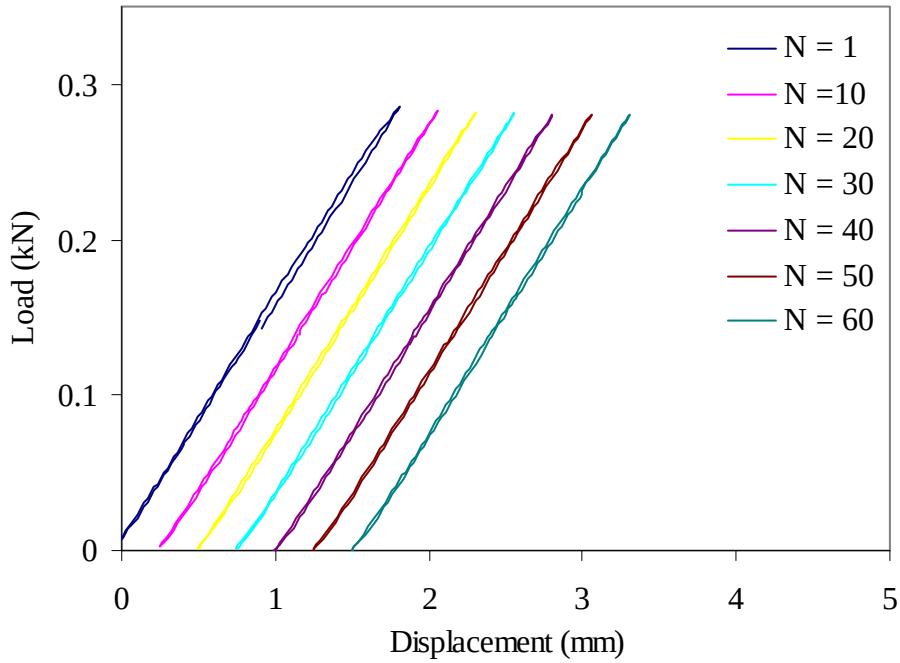


***Figure 6.22.*** *Load-displacement response of sandwich composites specimen under cyclic loading at low frequency 0.1 Hz.*

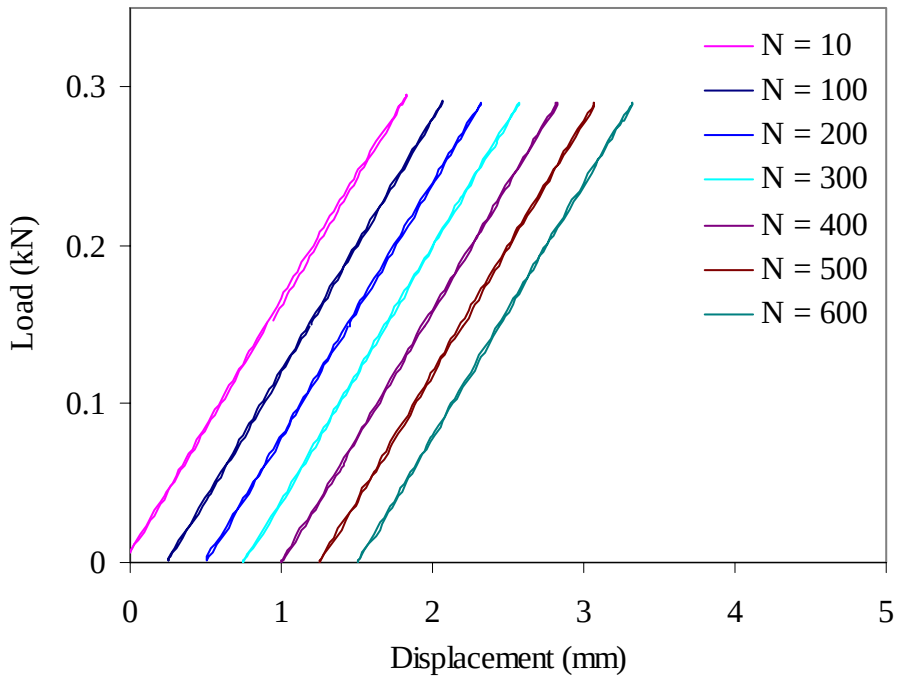


***Figure 6.23.*** *Load-displacement response of sandwich composites specimen under cyclic loading at medium frequency 1 Hz.*

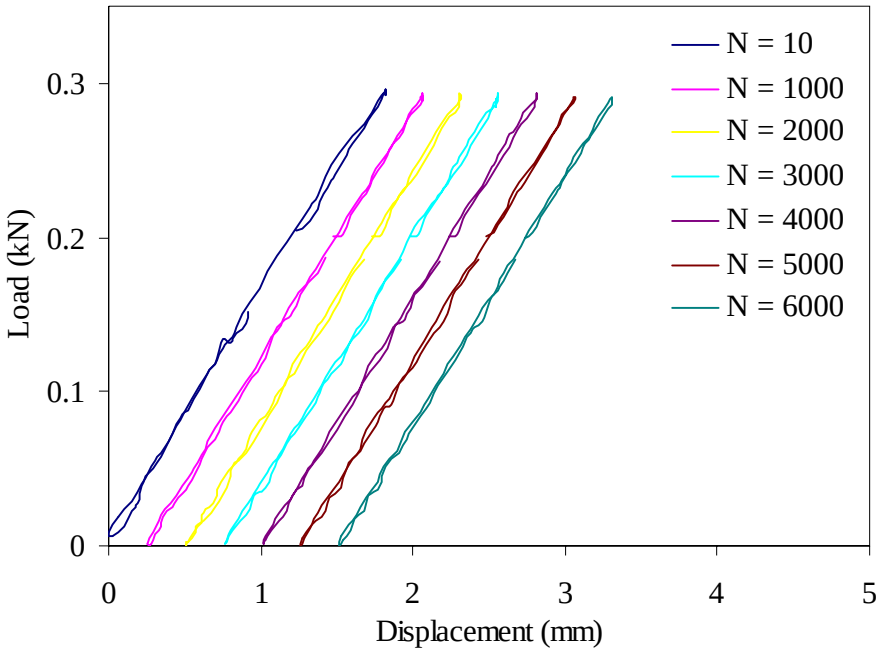


***Figure 6.24.*** *Load-displacement response of sandwich composites specimen under cyclic loading at high frequency 10 Hz.*

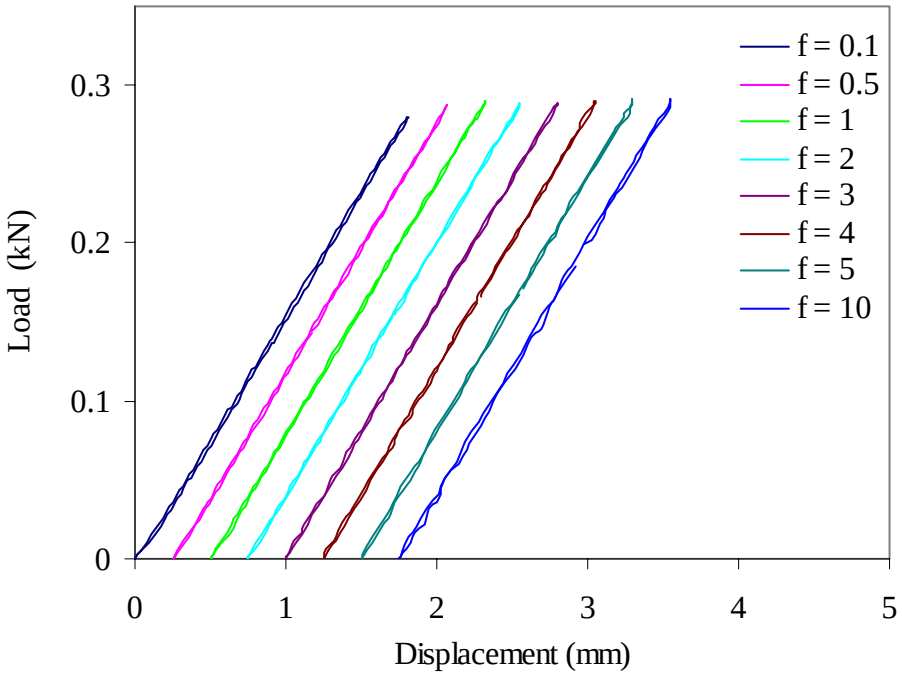


***Figure 6.25****. Load-displacement response of sandwich composites specimen at various loading frequencies in the last cycle.*

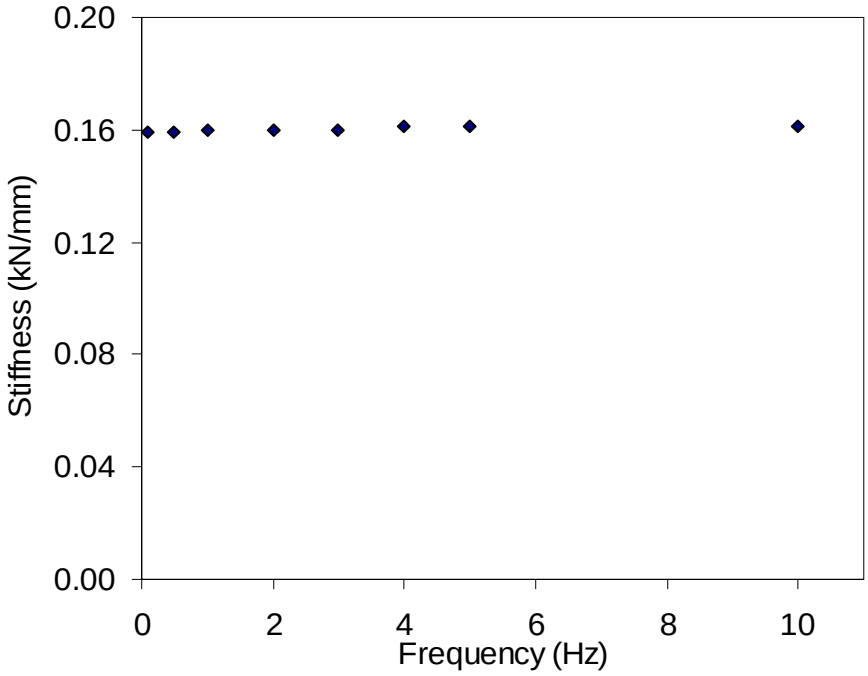


***Figure 6.26.*** *Effect of loading frequency on dynamic stiffness of sandwich specimens in the last cycle of the tests.*

### 6.3.3 Evaluation of static strength and stiffness after fatigue loading

#### *6.3.3.1 Experimental procedures*

In order to study the static strength of sandwich specimens after fatigue, a series of experiments was performed. The bending fatigue tests were performed under displacement control fatigue with two applied displacement levels (0.65, 0.95) at sinusoidal frequency of 10 Hz. Sandwich specimens of three foam densities (60, 80, 200 kg/m$^3$) having the same thickness were tested. These tests were carried out in fatigue to a given number of cycles and then static tests were performed at a constant speed of 5mm/min until failure without removing the specimen from the testing machine.

#### *6.3.3.2 Results*

Firstly, a number of experiments were performed at small value of applied displacement level of 0.65. Figures 6.27 to 6.29, show the load-displacement curves of the sandwich specimens of three different foam densities in static bending tests after cyclic fatigue at small applied displacement. Each curve representing static tests results after specimen fatigued to certain number of cycles that ranges from 10 cycles to $5\times10^5$. It is to be noted that there is no significant difference in static tests results of load-displacement curve even for a specimen fatigued to $5\times10^5$ cycles for sandwich specimens of three densities. Only one specimen of high density (200 kg/m$^3$) sandwich foam failed at $3\times10^5$ cycles without stiffness reduction. Residual static strength is

evaluated from the maximum load of the load-displacement curves for each number of cycles and is shown in figure 6.30 for sandwich specimens of three foam densities. Residual stiffness is obtained by the slope in linear part of load-displacement curves as shown in figure 6.31. From these graphs it is clear that changes in residual and stiffness remained almost same until 500,000 cycles. However, residual stiffness and strength is high for high density foam sandwich specimens.

Secondly, load-displacements curves were constructed for the experiments conducted at high value of applied displacement level (0.95) for sandwich specimen of 60 $kg/m^3$ foam density and are shown in figures 6.32. Considerable changes are observed in the load-displacement curves within first few hundreds cycles. This is an interesting result as it gives important evidence that stiffness loss during initial number of cycles is quite significant, particularly at high applied displacement level. The load displacement curves show initially a linear behaviour and then follow a non linear behaviour and finally a sudden drop in load is observed. The linear part, slope and maximum value of failure loads decreases with the increase in number of fatigue cycles.

Figures 6.33 and 6.34 show the evolution of the residual strength and residual stiffness according to the number of cycles after fatigue. There is a rapid decrease (50%) in residual strength and residual stiffness within first few hundred cycles. This is presumably due to development and initiation of various damage mechanisms (transverse matrix cracking and some fibre failure) that developed in face and core of sandwich specimen resulting in decrease in residual stiffness and static strength.

Static strength and residual strength are found to be highly dependent on the applied displacement levels. No considerable changes in stiffness and residual strength were observed for small values of applied displacement level but for high values of applied displacement level, it caused remarkable changes within few hundred cycles both in stiffness and strength. These results provide conclusive evidence that the decrease in residual strength and stiffness of sandwich structures is caused due to damage development in PVC foams and laminated skins during the bending fatigue tests.

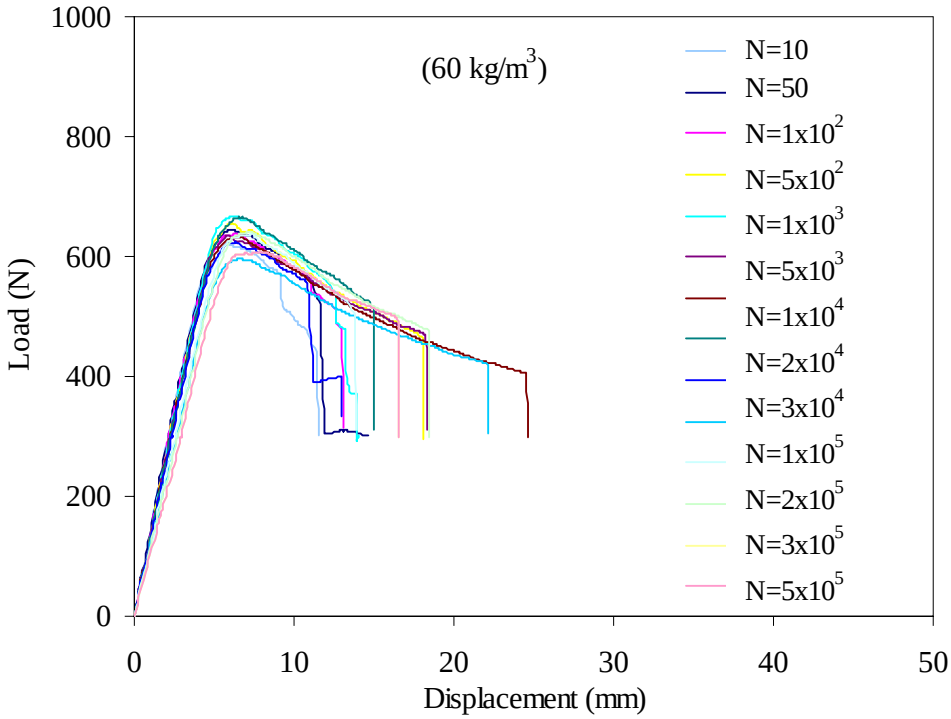


***Figure 6.27.*** *Load-displacement curves after fatigue with small value of applied displacement level (0.65) for sandwich specimens with foams of 60 kg/m$^3$ density.*

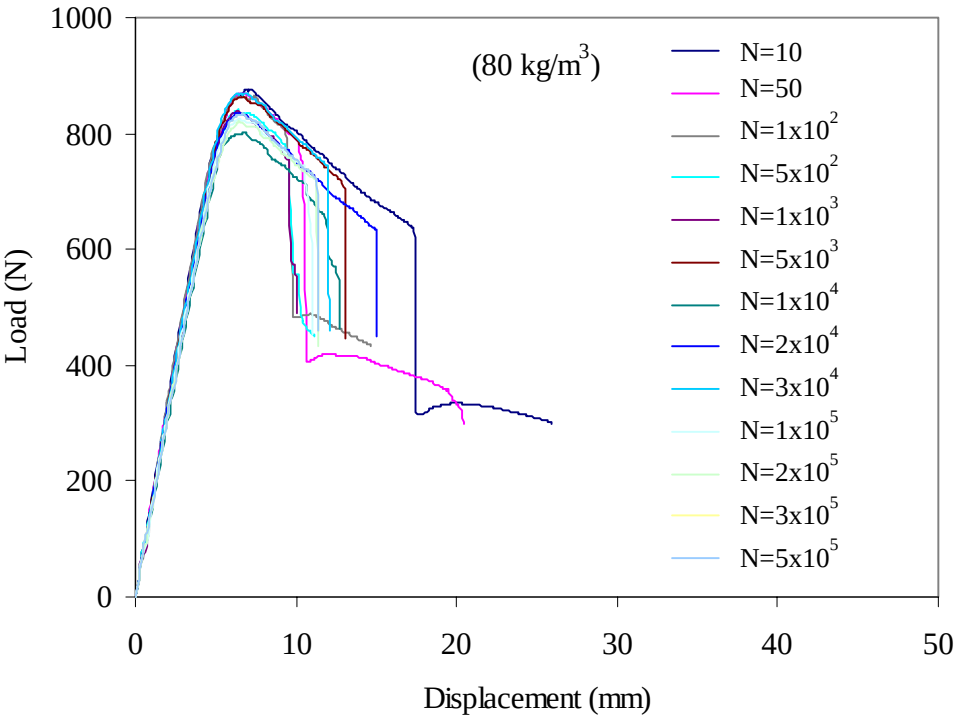


***Figure 6.28.*** *Load-displacement curves after fatigue with small value of applied displacement level (0.65) for sandwich specimens with foams of 80 kg/m$^3$ density.*

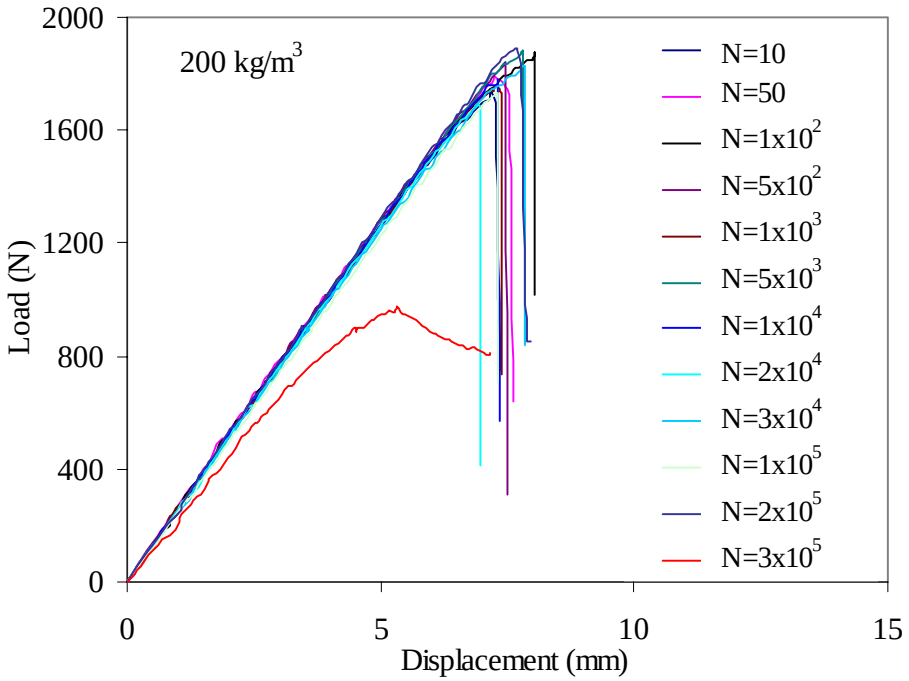


***Figure 6.29.*** *Load-displacement curves after fatigue with small value of applied displacement level (0.65) for sandwich specimens with foams of 200 kg/m$^3$ density.*

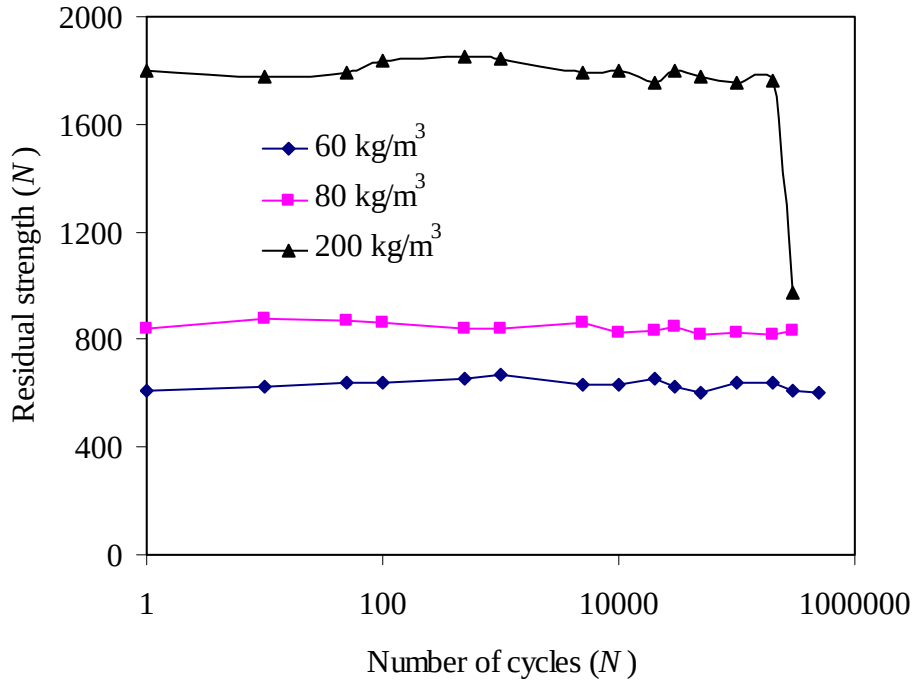


***Figure 6.30.*** *Evolution of residual strength after fatigue with small value of applied displacement level (0.65) for sandwich specimens with foams of 60, 80 and 200 kg/m$^3$ densities.*

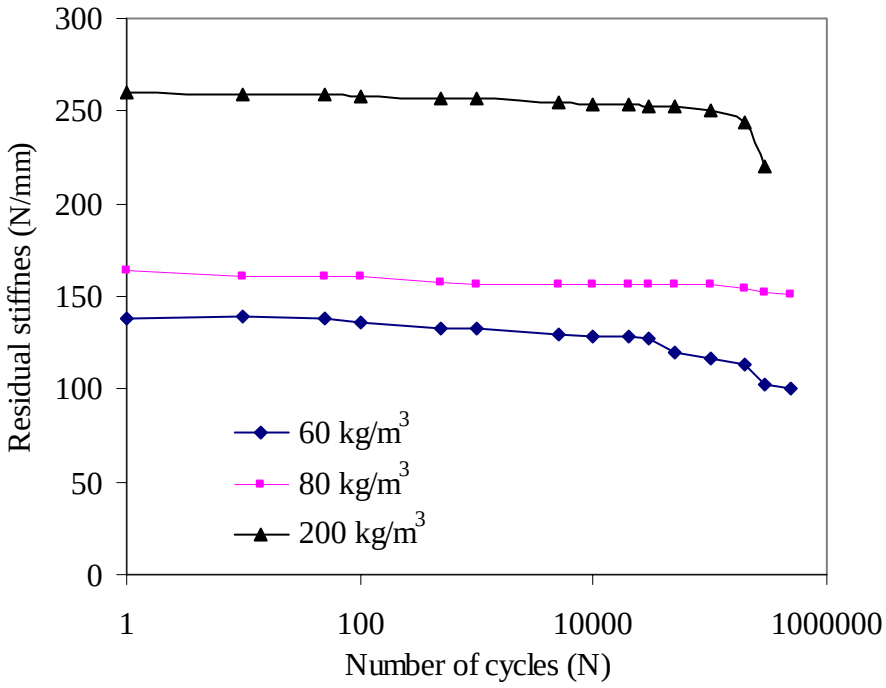


***Figure 6.31.*** *Evolution of residual stiffness after fatigue with small value of applied displacement level (0.65) for sandwich specimens with foams of 60, 80 and 200 kg/m$^3$ densities.*

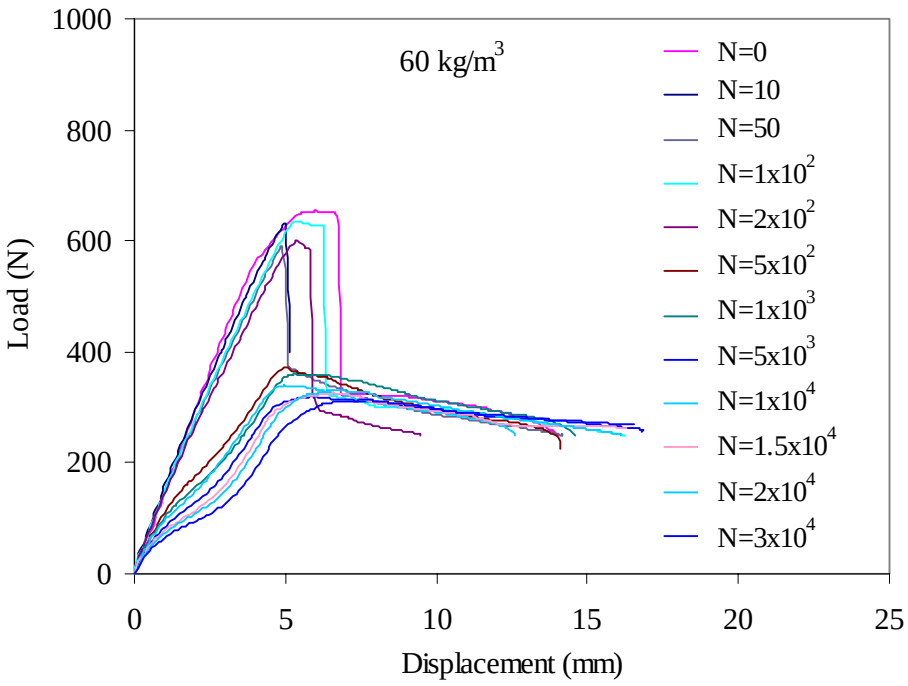


***Figure 6.32.*** *Load-displacement curves after fatigue with high value of applied displacement level (0.95) for sandwich specimens with foams of 60 kg/m$^3$ density.*

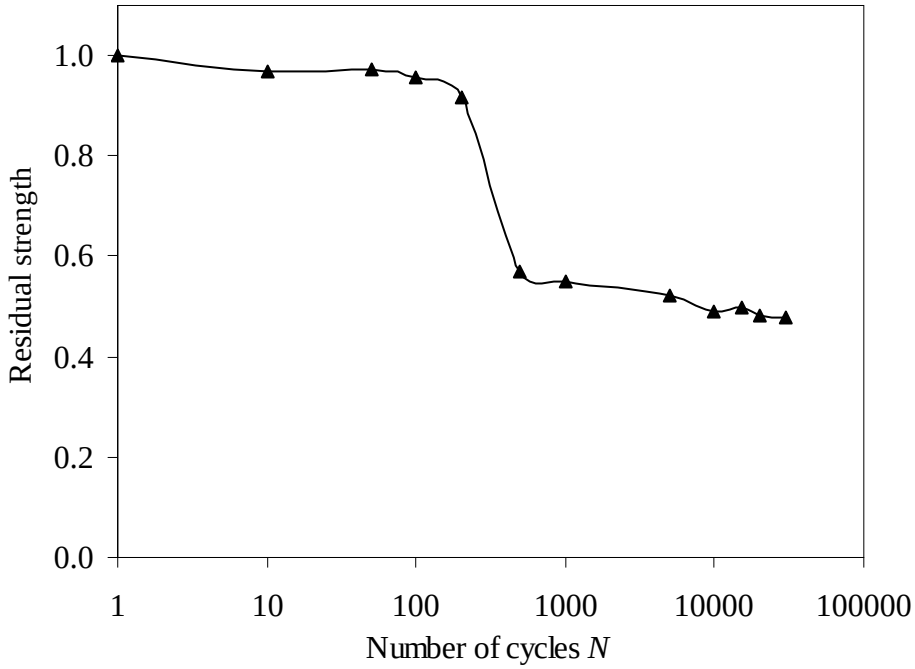


***Figure 6.33****. Evolution of the residual strength according to number of cycles after fatigue with high value of applied displacement level (0.95) for sandwich specimens with foam of 60 kg/m$^3$ density.*

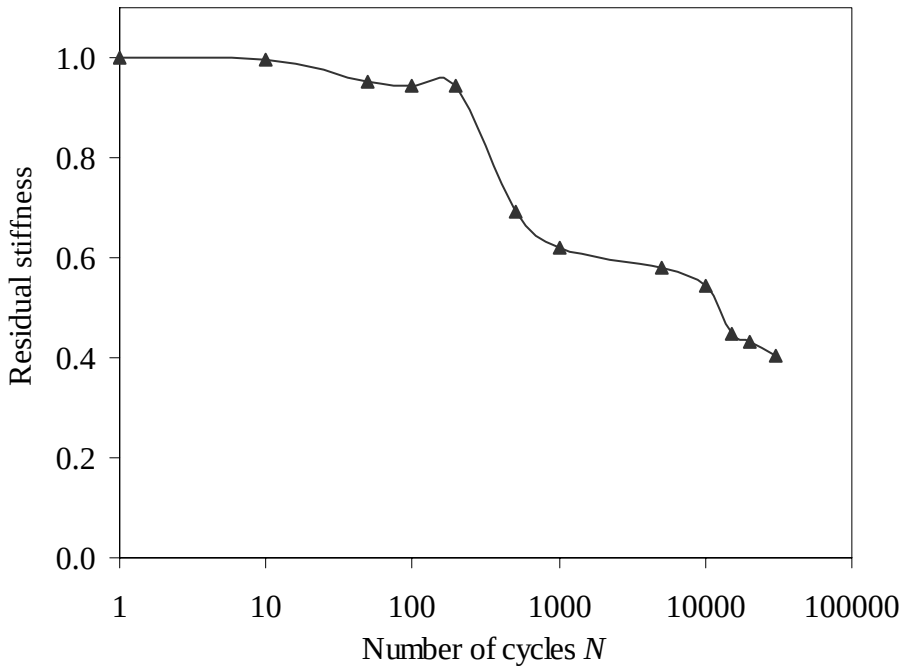


***Figure 6.34****. Evolution of the residual stiffness according to number of cycles after fatigue with high value of applied displacement level (0.95) for sandwich specimens with foam of 60 kg/m$^3$ density.*

### 6.3.4 Non cyclic fatigue

One important factor in the laminates and sandwich composites is their loss of stiffness over time due to many mechanisms, including non-cyclic fatigue. In many applications a structure will be subjected to a loading profile that is combination of cyclic and non-cyclic fatigue. Thus there is need to understand and quantify such kind of behaviour to ensure structural integrity. Due to the viscoelastic nature of polymeric materials, time dependence behaviour is quite important for the life of the structure and component. Components may also fail prematurely if they are subjected to significant loads over long period of time. Presently, relatively little is known about the behaviour of the sandwich materials in creep or relaxation during the three point bending. The study of the mechanical behaviour of the sandwich materials during the creep and relaxation in stress or strain is necessary. Then it is possible to highlight phenomena of damage with time and to envisage the catastrophic failure of the structure.

#### *6.3.4.1 Stress relaxation tests*

When a fixed amount of deformation is maintained for a long time such as tightening of screws, the resistance to load decrease with passage of time which results in stiffness reduction and therefore structure loses its ability to maintain that deformation properly. In order to understand this phenomenon, experiments were performed with sandwich specimens at different applied displacement levels. Figure 6.35, represents the evolution of the load with time for different values of displacement levels (0.50 to 0.98). Duration of tests was set at 2 hours as this time is sufficient to study the behaviour of these materials particularly the initial stages of damage and plastic deformation due to stress relaxation.

The evolution of stiffness during the stress relaxation tests in the foam core sandwich structures are categorised into two stages: First stage is referred to as initiation and development of damage in the skin due to development of cracks in matrix and fibre resulting in stiffness degradation. In the second stage of stress relaxation with the time, there is slow growth and progression of damage that initially developed in the skin, induce damages in the core resulting in further loss in stiffness.

#### *6.3.4.2 Creep tests*

Creep is the slow, progressive deformation of structure from prolonged exposure to stress. Sandwich specimens were subjected to a particular load and were kept there in an isothermal condition for certain period of time. The increase in displacement (deflection) with time was recorded at this stress (load) level.

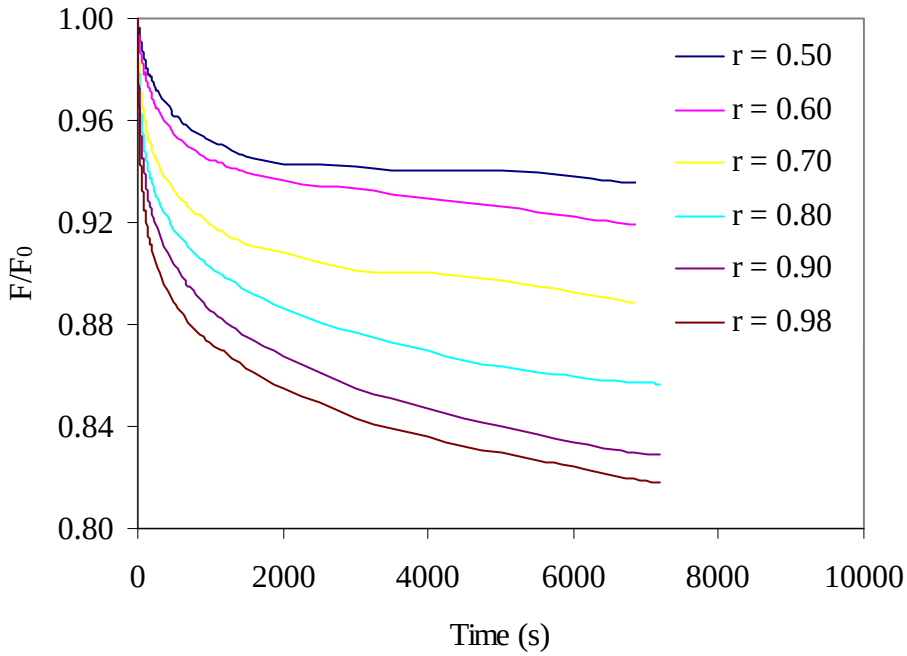


***Figure 6.35.*** *Evolution of the load with time for various displacements levels during relaxation tests.*

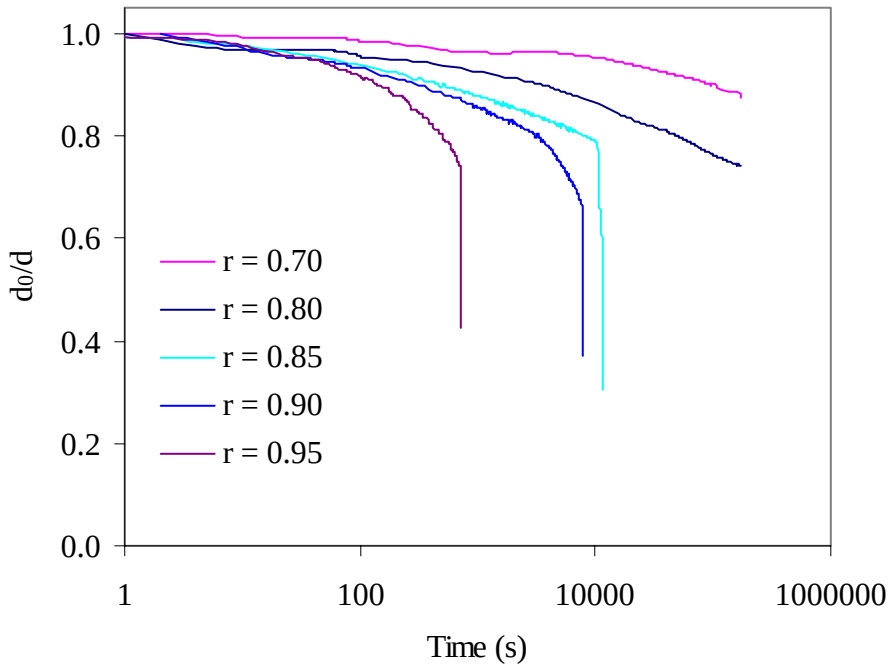


***Figure 6.36.*** *Evolution of displacement with time for various loads levels during creep tests.*

Figure 6.36, shows the evolution of displacement with time at various loading levels (0.70 to 0.95). The trend of these curves depends upon the loading levels. Two specimens, which were loaded with 70 % and 80% of the failure load did not break at the end of 48 hours. Specimen at 85% of failure displacement broke after 3 hours and 25 minutes. While other two specimens at 0.90 and 0.98 of applied displacement levels were broken after 2 hours and 20 minutes respectively. Figure 6.36, shows three regions for all curves:

- The first region is referred as a region of primary creep and has very short duration as compared to rest of creep curve, during which decrease in stiffness degradation is rapid.
- the second region corresponds to a gradual decrease in stiffness with time and it is slower than the first region.
- in the third region the stiffness degradation is very fast due to accumulation of all damage.

In sandwich composites, initially the creep response of the core can be treated as viscoelastic in nature, while skin is damaged due to matrix cracking and some fibre failures which resulted in a rapid decrease in stiffness. With further passage of time, interfacial debonding and initiation of core failure occurs and these mechanisms progress slowly, resulting in slow decrease in stiffness and finally all this damage combines leading to the failure of the sandwich specimens. It is observed that creep is also strongly dependent on applied load levels. For small values of load levels, it can be seen that stiffness degradation is small while for higher values of load levels, stiffness degradation is high. But in both cases, creep deformation process is dominant during the early stages of loading.

## 6.4. Mechanical behaviour of sandwich composite materials under cyclic fatigue

### 6.4.1 Introduction

The fatigue behaviour is of extreme importance for the life of a structure or component of materials used in any service conditions. Fatigue testing can be performed in tension, compression, bending or a combination of these loading modes. Fatigue characterisation can be performed by utilising different assessment methodologies. The evaluation of fatigue damage based on macroscopic analysis rather then microscopic analysis seemed more convenient. Stiffness monitoring is relatively easy method since it only requires continuous computer log of change in strain (displacement) from an linear voltage displacement transducer (LVDT) during fatigue tests. Stiffness exhibits greater changes during fatigue tests specifically at the early stage of fatigue life of specimen and can easily be monitored non-destructively without interrupting tests. The necessary experiments can be conducted within limited time of testing and *S-N* curves based on stiffness degradation can readily be produced for analysis purposes. Stiffness monitoring is useful for applications with design situations where failure criterion can be formulated as a decrease of young’s modulus, below a certain critical value

[125,126]. Our basic aim is to correlate the stiffness degradation with the damage accumulation in the sandwich material during the early stage of fatigue.

### 6.4.2 Load and displacement control fatigue

#### *6.4.2.1 Experiments and results*

Cyclic fatigue tests were performed to study the effect of cycling and the applied loading levels on the behaviour of the sandwich composites of 15 mm core thickness and core density of 60 kg/m$^3$. Fabrication, geometry and dimension of these sandwich specimens were already explained in the section 3.5.3. These tests were carried out under displacement and load control fatigue. Applied cyclic displacement or load levels were chosen from the results obtained from the static tests. The frequency of tests was set at 10 Hz with sinusoidal waveform.

For the fatigue tests with displacement control, the mean displacement $d_{mean}$ was kept constant at 50% of the ultimate static failure displacement $d_u$. The applied displacement ratio $R_d$ (ratio between the minimum and maximum applied displacement: $R_d = d_{min}/d_{max}$) was varied between 20% and 85% corresponding to displacement amplitude, which changes from 0.25 to 2.25 mm. During fatigue tests with displacement control, the decrease in the maximum load $F_{max}/F_{0max}$ was recorded according to the cycles number, where $F_{0max}$ is the value of the maximum load in the first cycle.

For the fatigue tests with load control, the applied load ratio $R_F$ (ratio between the minimum and maximum applied load: $R_F = F_{min}/F_{max}$) was kept constant at $R_F = 0$. The applied load level $r_F$ (ratio between the maximum applied load and the static ultimate load: $r_F = F_{max}/F_u$) was varied from 60% to 98%. During fatigue tests with load control, the increase in the maximum displacement $d_{max}$ was recorded and the ratio of $d_{0max}/d_{max}$ was plotted as a function of cycles number, where $d_{0max}$ is the value of maximum displacement at first cycle.

The experimental results for the stiffness ($F/F_0$ or $d_0/d$) changes versus number of cycles are shown in figures 6.37 and 6.38 for one particular load and displacement level. The number of cycles was normalised using the value of cycles to failure $N_f$.

In displacement control, there are three apparent regions for the degradation of stiffness as seen in figure 6.37. The onset of stiffness reduction identified as a starting point for damage initiation. There is rapid initial decrease in stiffness, in a time, short in comparison with the life of the specimen. The initial drop in stiffness during the first 10% of curve corresponds to the initiation of damage in the skin due to matrix cracking. After this a long region of gradual drop in the stiffness is observed which is attributed to the initiation and progression of damage in the skin and core due to interfacial debonding between skin and core just under the point of application load (central roller). Sudden drop of stiffness in third region is catastrophic in nature, as all the damage

mechanisms combine, leading to the complete stiffness reduction resulting in total failure of specimen.

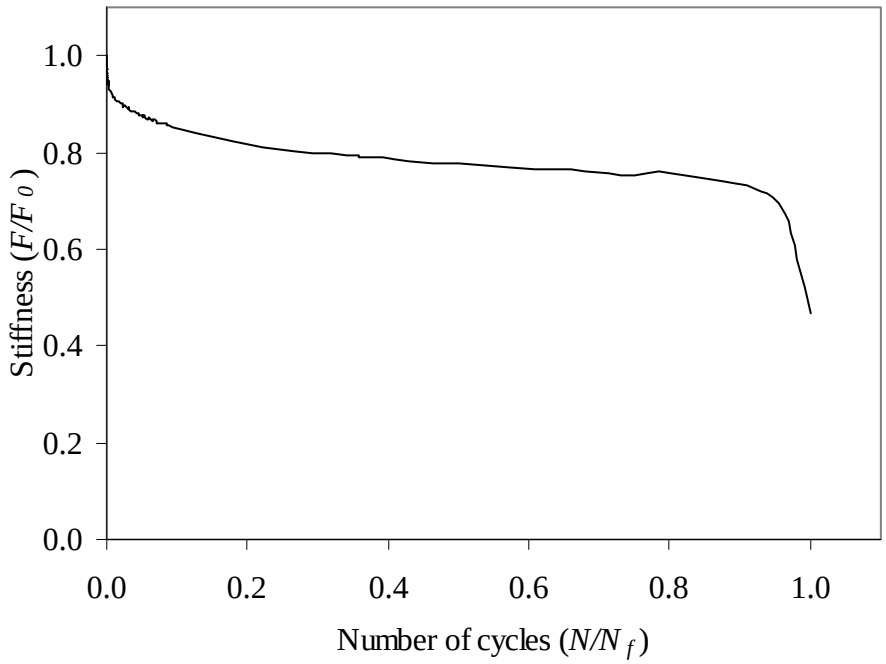


***Figure 6.37.*** *Mechanical behaviour of sandwich composite of glass fibre skin and PVC foam (60 kg/m$^3$ and core thickness 15 mm) under displacement control fatigue.*

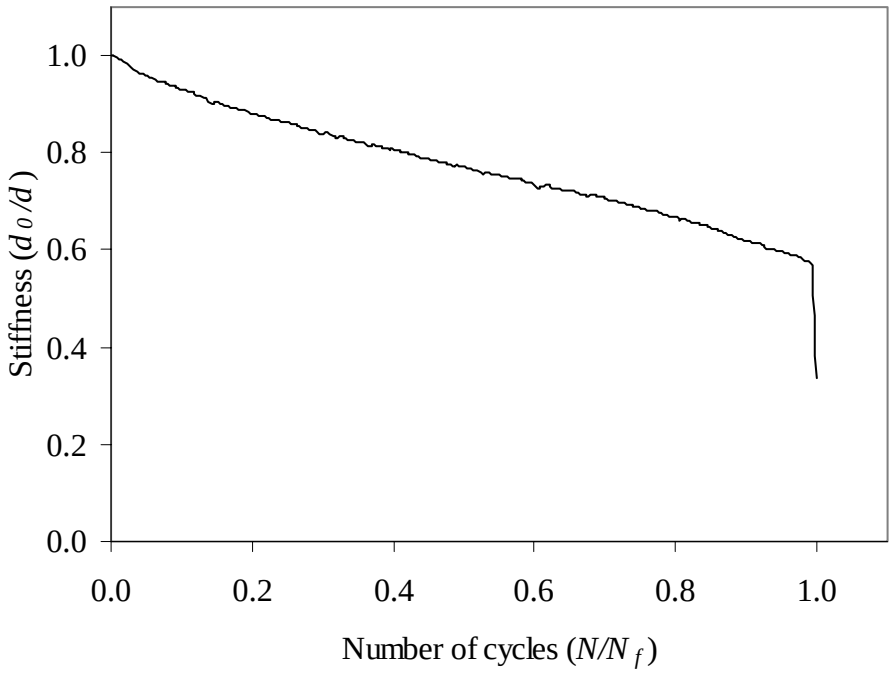


***Figure 6.38.*** *Mechanical behaviour of sandwich composite with glass fibre skin and PVC foam (60 kg/m$^3$ and 15 mm thickness) under load control fatigue.*

While in load control fatigue there are two apparent regions for degradation of stiffness as seen in figure 6.38. Initially stiffness decreases gradually which is due to the damage in the skin and debonding between core and skin and this damage continues to grow gradually, until near to the failure, when there is sudden drop in stiffness causing the specimens to complete failure.

Transition between stage I and stage II response, as indicated by change in stiffness data, occur within 10% to 15% of fatigue life. While the transition between stage II and stage III occurs between 95% to 98%. The relative time for the first region in displacement control experiments is much shorter, but stiffness drops considerably in this period indicating a rapid initiation and growth of damage in the skin due to transverse matrix cracking. The second region occupies a much greater proportion of the fatigue life, but decrease of stiffness is much lower representing a slow progression and accumulation of various damages. The third region is also of very short duration as stiffness dropped drastically due to rapid accumulation of all damages leading to final failure of the sandwich specimen.

#### *6.4.2.2 Effect of applied displacement level ( r )*

Applied stress level plays an important role in the fatigue life of the sandwich specimens. Small values of applied stress levels generate longer fatigue lives while high values produce short fatigue lives. Figures 6.39 and 6.40 show the combined graph of stiffness versus number of cycles at various applied loading levels for displacement and load control fatigue. Sandwich specimens of glass fibre skins and foam of 60 kg/m$^3$ density and 15 mm core thickness were tested at span length of 250 mm for displacement and load control experiments.

It is observed that with an increase in the applied displacement level ($r$), the fatigue life of specimen decreases considerably. It can be seen that when $r$ is 60% of the displacement at rupture, the fatigue life is about $10^6$ cycles and when the value of $r$ is 95%, the fatigue life is about in hundreds of cycles. When the applied displacement level is high, the behaviour is almost similar to that of static failure. It can be seen from figures 6.39 and 6.40, that for specimens tested at higher applied stress ratio ($r$), the transition occurred earlier than for those tested at lower applied loading levels. That transition is defined as the sequence of events (initiation, progression, accumulation of damage) that happened with the increase in number of cycles during fatigue tests.

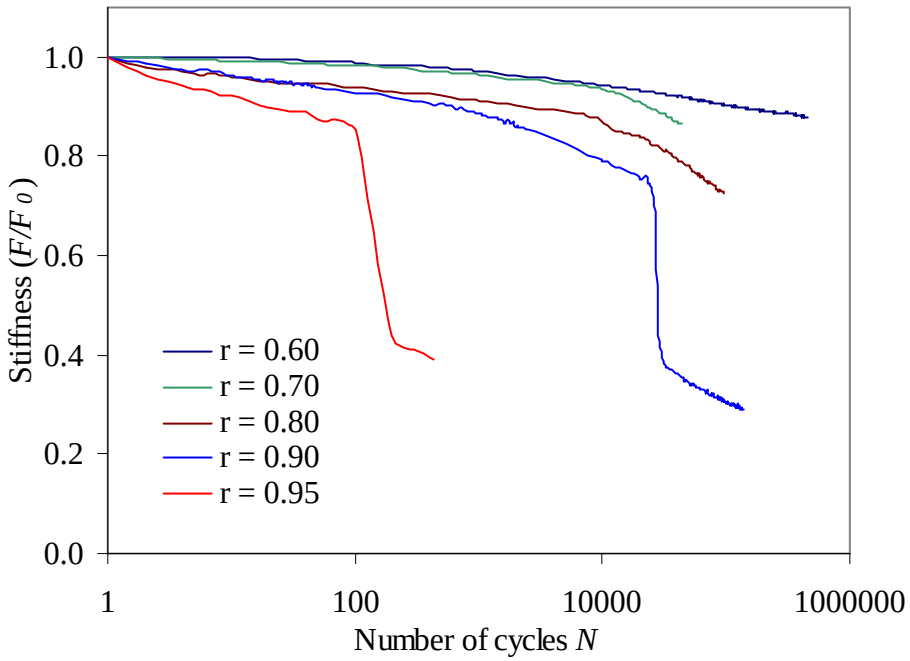


***Figure 6.39.*** *Evolution of stiffness with number of cycles at various applied displacement levels in displacement control fatigue for sandwich specimens with foam of 60 kg/m$^3$ density and thickness of 15 mm.*

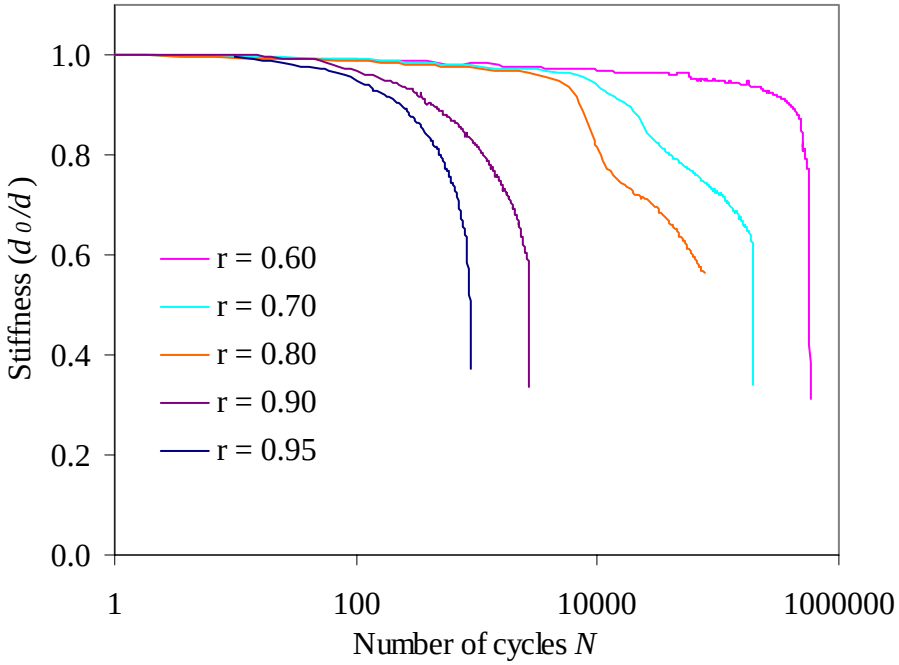


***Figure 6.40.*** *Evolution of stiffness with number of cycles at various applied load levels under load control fatigue for sandwich specimens with foam of 60 kg/m$^3$ density and thickness of 15 mm.*

### *6.4.2.3 Effect of displacement ratio (R)*

The stress ratio which is defined as the ratio of minimum stress divided by maximum stress has a great influence on the fatigue life of the sandwich composites. The variations of stiffness and fatigue life with stress ratio are due to changes in the rate of stress application. Experiments were conducted at four stress ratios ($R$ =0.1, 0.2, 0.5, 0.8) at same applied displacement level ($r$ = 0.90). Figure 6.41 shows the evolution of load versus number of cycles for different applied stress ratios. As can be seen in this figure that fatigue life increases with increasing the stress ratio. However, stiffness reduction decreases with increasing the stress ratio. It is to be noted that for lower stress ratio, the intensity of damage due to increase in stress amplitude is higher which causes earlier failure of sandwich specimens, but at higher stress ratio, although the extent of damage is there but the intensity is insufficient to cause sufficient damage. It has also been reported in the literature, that for given maximum stress, the fatigue life notably increases with increasing stress ratio [18]. Stiffness curves are fitted in equation [43].

$$Y = 1 - B\log N \tag{6.1}$$

Slope of equation B, which is defined as the rate of decay of stiffness permits to compare the rate of stiffness degradation for different stress ratios. It is observed that higher the $R$, higher the number of cycles to failures. It can be seen from the table 6.1 that value of slope $B$ decreases with increasing the stress ratio thus representing an increase in fatigue life.

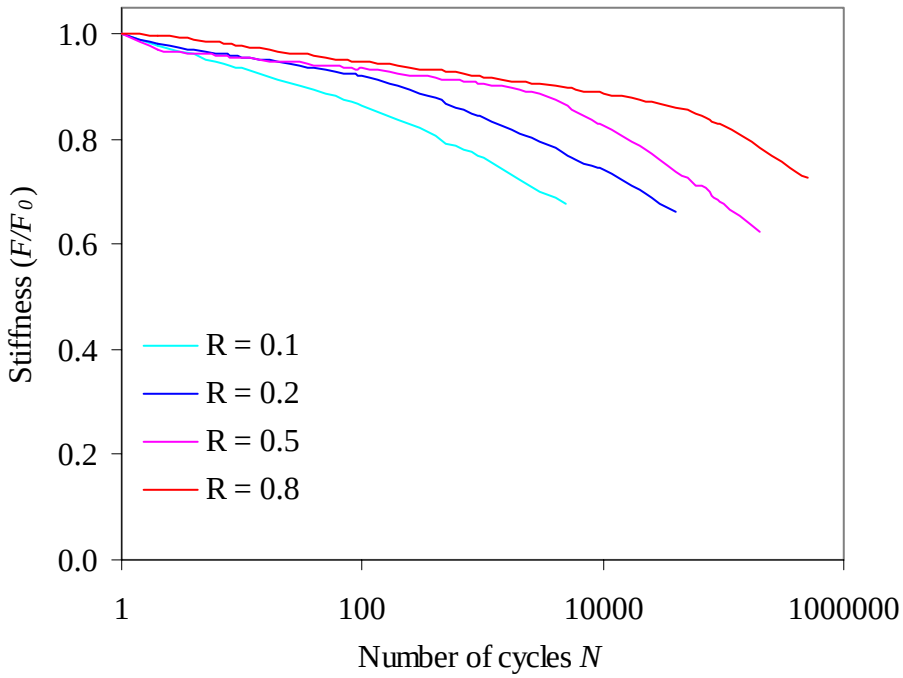


***Figure 6.41.*** *Evolution of stiffness versus number of cycles at different stress ratio for sandwich specimen of 60 kg/m$^3$ foam.*

***Table 6.1.*** *Parameters obtained from equation 6.1.*

| Stress Ratio ($R = d_{min}/d_{max}$) | Parameter B |
|---|---|
| 0.1 | 0.0373 |
| 0.2 | 0.0304 |
| 0.5 | 0.0254 |
| 0.8 | 0.0172 |

### *6.4.2.4 Constructions of Wöhler curves*

While traditions and history of fatigue of metallic materials originate from experiments by Wöhler (1860) who introduce the concept of stress-life *S-N* curve. This concept is extended to composites and further utilised for sandwich composite materials. Fatigue of sandwich structures and foam materials is still at the stage of evolution. A maturity of fatigue science mainly relies on solid basis of available fatigue data, which could be used for further developments of fatigue theories and models. Currently, there is an apparent lack of fatigue data on cellular foams materials and foam core sandwich structures.

If a test specimen of a material is subjected to a sufficiently severe cyclic stress, a fatigue crack or other damage will develop, leading to complete failure of the specimen. If the test is repeated at higher stress level, the number of cycles to failure will be smaller. The results of such tests from a number of different stress levels may be plotted to obtain stress-life curve, also called an *S-N* curve. Fatigue performance is often expressed in terms of the number of cycles to failure at a given maximum stress level. A complete description of fatigue performance requires the mean stress or fatigue stress ratio. *S-N* curves vary widely for different classes of materials, and they are affected by a variety of factors. Additional factors of importance include mean stress, geometry, chemical environments, temperature, cyclic frequency and residual stresses.

In this study, Wöhler curves (*S-N* curves) were constructed for sandwich composites of various core thickness and densities. These curves were constructed at 10% reduction in the initial stiffness representing as $N_{10}$.

### *6.4.2.5 Wöhler curves in load and displacement control fatigue*

Figures 6.42 and 6.43, represents the evolution of applied stress level with fatigue life at $N_{10}$ criterion in load and displacement control fatigue. It can be seen that with increasing the applied displacement or load levels, fatigue life decreased considerably. The fatigue life results clearly show the trend and relationship between stiffness reduction and fatigue life. Fatigue life of sandwich specimens can be predicted using these Wöhler curves. The variation of loading level $r$ with number of cycles can be described by the equation, both for displacement and load control by:

$$Y = A - B\log(N_{10}) \tag{6.2}$$

Where $Y$ is the applied stress level in load or displacement control and $N_{10}$ is the number of cycles at 10% reduction in the initial stiffness. The constants in the equation depend on the materials properties and on the parameters obtained from the static and fatigue tests. $A$ is the $y$-intercept of the straight line, physically representing the static strength of the material which is generally equal to unity and $B$ is absolute value of slope and refereed as a parameter which describe the degradation of stiffness with the increase in number of cycles. Equation (6.2) has been utilised by many researchers to describe the fatigue behaviour of composite materials [103,126]. This method was also utilised by Mandell to rank a variety of composite systems on the basis of their fatigue behaviour [127].

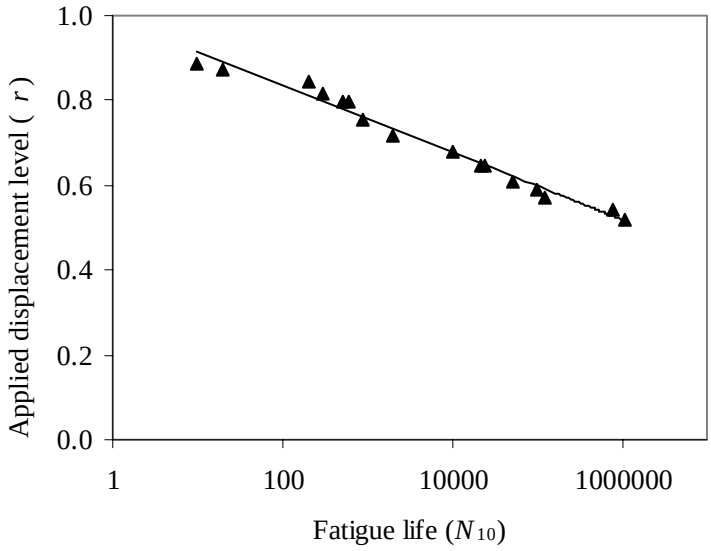


***Figure 6.42.*** *Wöhler curve for sandwich specimen under displacement control fatigue.*

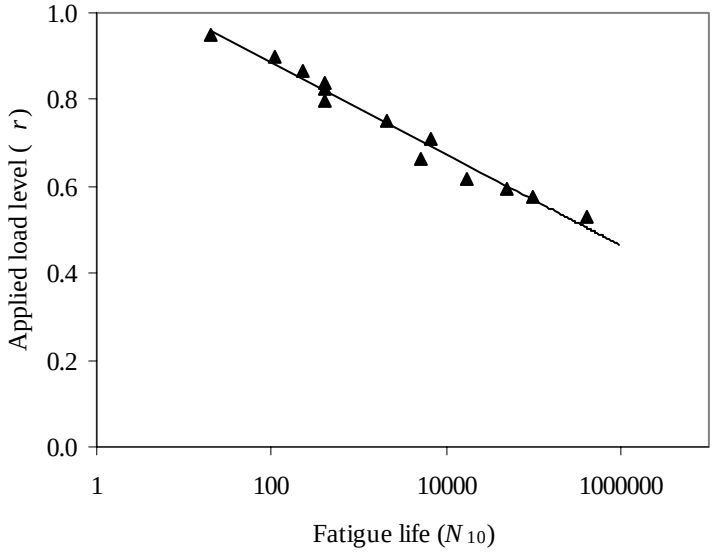


***Figure 7.43.*** *Wöhler curve for sandwich specimen under load control fatigue.*

### *6.4.2.6 Effect of the core density*

#### *6.4.2.6.1 Stiffness reduction*

Sandwich specimens of 60, 80, 100 and 200 kg/m$^3$ core densities of thicknesses 15 mm were used to study the effect of core density on the stiffness degradation of sandwich composites during fatigue. These tests were performed under displacement control fatigue. The ratio of span length between the outer supports to the specimen thickness (*l*/*h*) was kept constant equal to 16. Fatigue tests were carried out at constant mean displacement, which is 50% of static failure displacement for each sandwich specimens. Different applied maximum displacement ranges from 55% to 98% of displacement at rupture in static tests were used.

Figures 6.44 to 6.47 show the evolution of stiffness versus number of cycles at different applied displacement levels for sandwich specimens of different core densities. It has already been explained that with the increase in displacement levels, fatigue life decreases due to rapid growth of damage development. It is observed that for a small value of applied displacement level (0.60) there was no failure until $10^6$ cycles for all sandwich specimens. However, for high applied displacement levels (0.85-0.98) the failure is observed within $10^3$ cycles.

The comparison of stiffness reduction at one loading level of 0.80, for sandwich specimens having foams of four densities is shown in figure 6.48. It is clear from the this figure that stiffness reduction decreases with the increase in the foam density of the sandwich specimens. The stiffness reduction for sandwich of 200 kg/m$^3$ foam density is 10% until $10^6$ cycles. While for sandwich of 60 kg/m$^3$ foam density, stiffness reduction is 25% until $1\times10^5$ cycles. Stiffness reduction is attributed to the variation of the cell size of the foams. Low density foams offer less resistance to fatigue due to bigger cell size as this cell can easily be deformed resulting in stiffness reduction. On the other hand, high density foams are composed of small size cells which offer more resistance in fatigue as compared to big cells of the of low density PVC foams. The fatigue life of higher density core sandwich is found to be much higher than low density core sandwich specimens due to the size of cells of PVC foams.

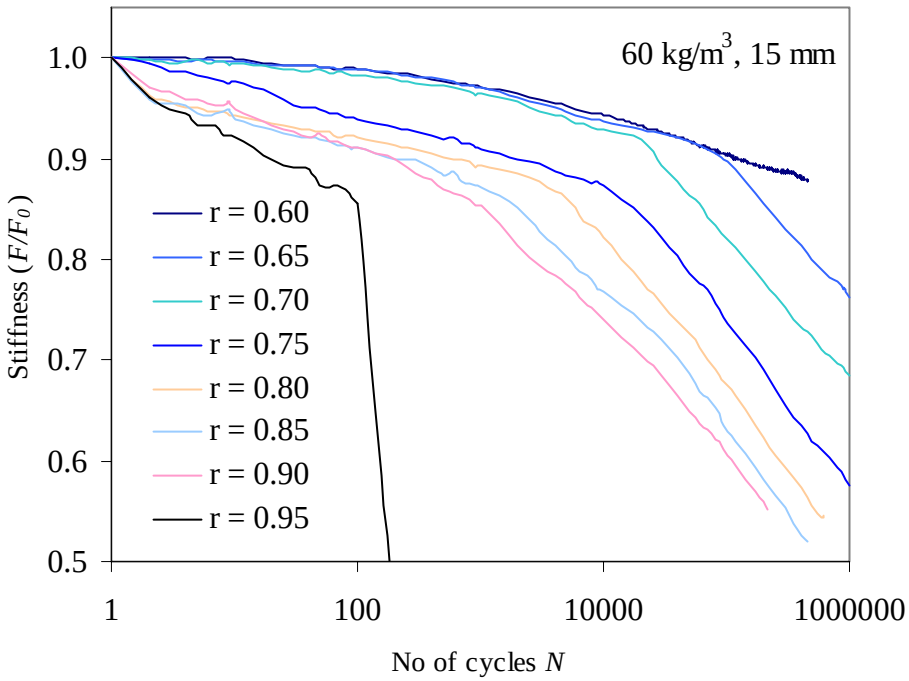


***Figure 6.44.*** *Evolution of stiffness with number of cycles at various applied displacement levels under displacement control fatigue for sandwich specimen having foam of 60 kg/m$^3$ and 15 mm thickness.*

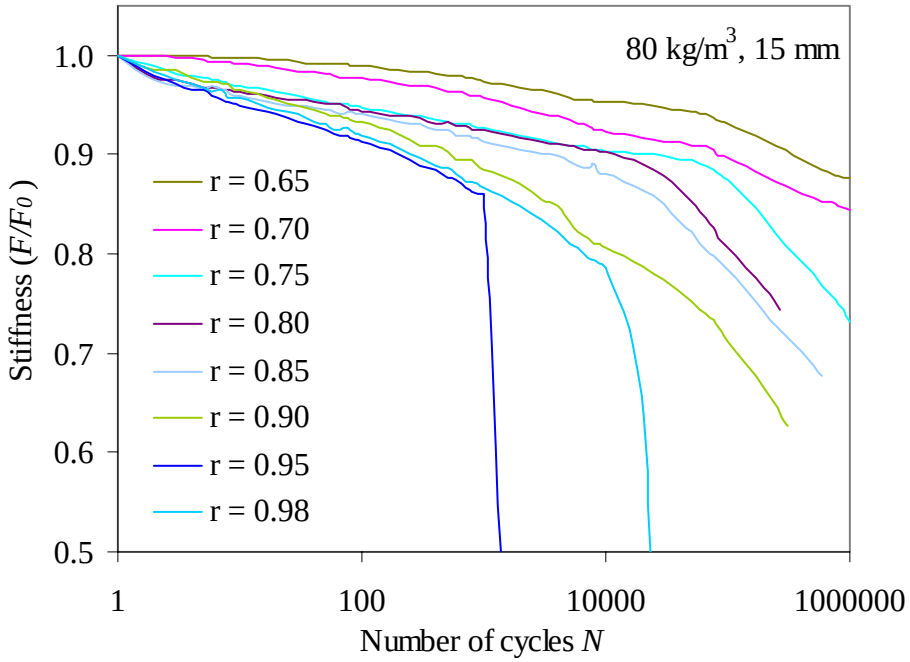


***Figure 6.45.*** *Evolution of stiffness with number of cycles at various applied displacement levels under displacement control fatigue for sandwich specimen having foam of 80 kg/m$^3$ and 15 mm thickness.*

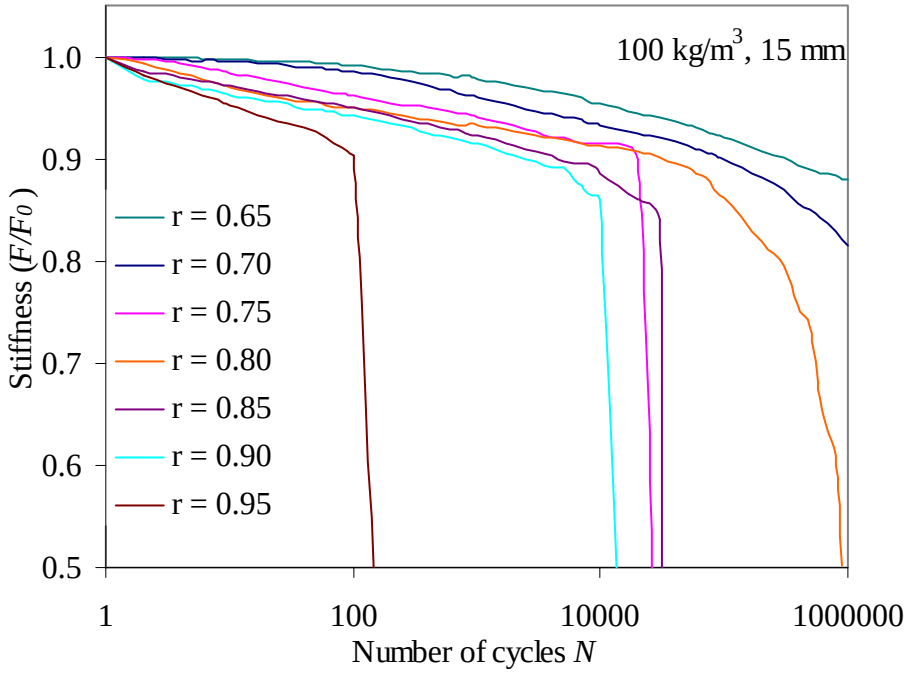


***Figure 6.46.*** *Evolution of stiffness with number of cycles at various applied displacement levels under displacement control fatigue for sandwich specimen having foam of 100 kg/m$^3$ and 15 mm thickness.*

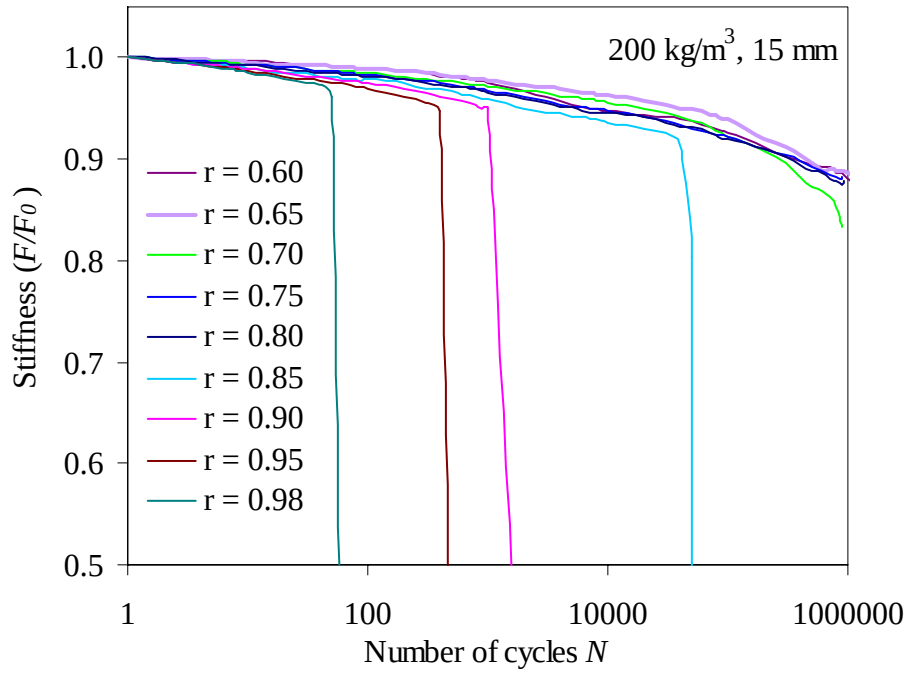


***Figure 6.47.*** *Evolution of stiffness with number of cycles at various applied displacement levels under displacement control fatigue for sandwich specimen having foam of 200 kg/m$^3$ and 15 mm thickness.*

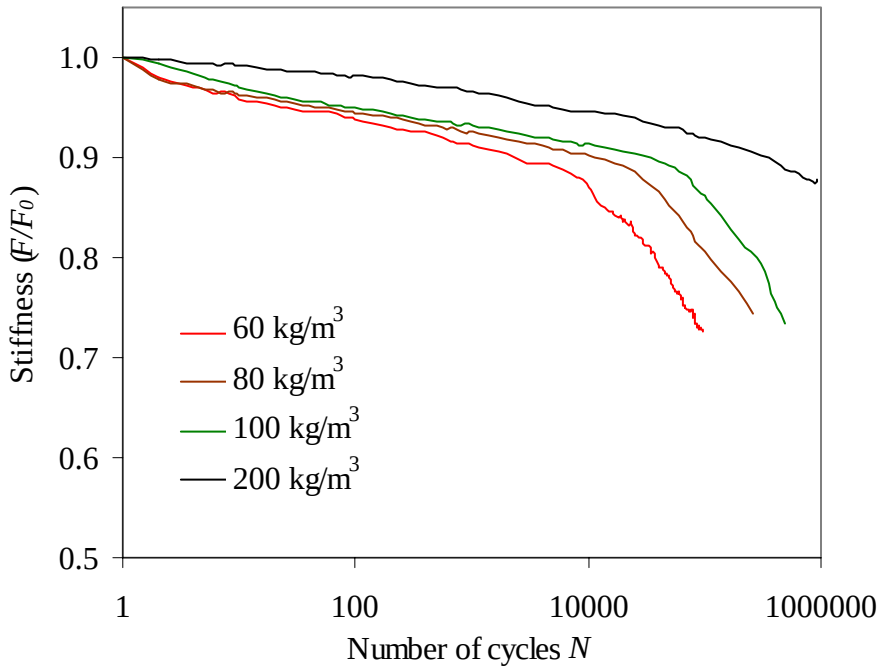


***Figure 6.48.*** *Comparison of evolution of stiffness versus number of cycles for sandwich specimens of four densities having the same thickness of 15 mm at one applied displacement level (0.80).*

### *6.4.2.6.2 Fatigue life*

In order to study the effect of core density of sandwich composites on fatigue life, Wöhler curves were constructed for specimens with PVC core of four different densities of thickness 15 mm. These curves are shown in figure 6.49, for maximum applied displacements ($d_{max}$) versus fatigue life ($N_{10}$). In fatigue situations the load cycles vary from low to high values continuously, and stress changes continuously during each cycle, thus causing increment of damage. An increase or change in applied displacement will cause more damage in each cycle. The damage also strongly depends on the density of the foam as is evident from the results. Fatigue life of sandwich specimens of higher density is longer then fatigue life of lower densities. Fatigue life increases with the increase in core density and decreases with the increase in maximum applied displacement levels. At one displacement level shown, it can be seen that fatigue life increases with increasing the core density.

The maximum applied displacements are normalised with displacement at failure in static tests. The curves for maximum applied displacement levels ($r$) versus fatigue life for four densities are shown in figure 6.50. It can be seen from these curves that at one displacement level the fatigue life of higher core density is more then fatigue life of lower density core sandwich specimens. High values of applied displacement level resulted in shorter fatigue lives and large values of ($r$) resulted in low fatigue life. These data points are fitted with equation 6.1, and values obtained for parameter $B$ permitted to compare the rate of stiffness degradation. The values of this parameters are given in the table 6.2. The rate of stiffness degradation represented by parameter $B$ increases

with increasing density. This parameter increases with increasing the core density thus can be used for fatigue life prediction.

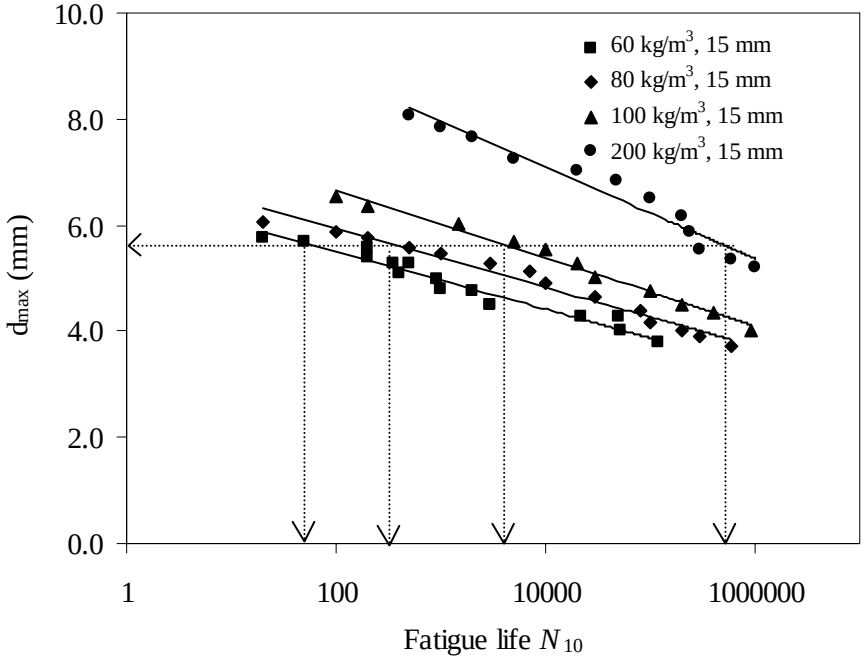


***Figure 6.49.*** *Evolution of maximum applied displacement with fatigue life for sandwich specimens of four densities having same thickness of 15 mm.*

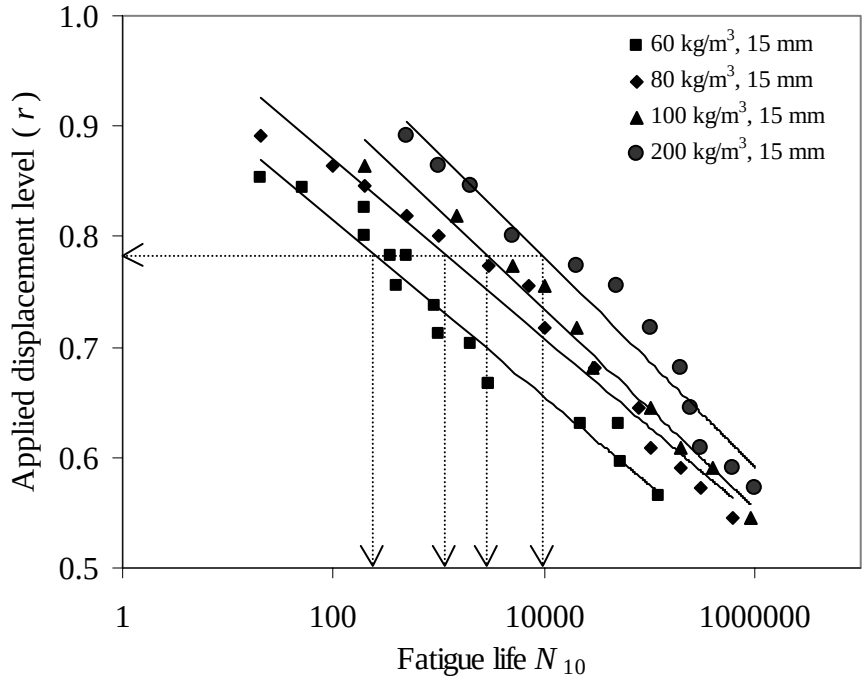


***Figure 6.50.*** *Wöhler curves for sandwich specimens of four core densities having same thickness of 15 mm.*

***Table 6.2.*** *Parameter obtained from equation (6.1).*

| Core density (kg/m$^3$)<br>Thickness (15 mm) | Parameter<br>*B* |
|---|---|
| 60 | 0.0380 |
| 80 | 0.0404 |
| 100 | 0.0432 |
| 200 | 0.0453 |

### *6.4.2.7 Effect of core thickness*

#### *6.4.2.7.1 Stiffness degradation*

Generally increasing the core thickness resulted in greater flexural failure stresses and strains. As with increasing the core thickness the bending moment and flexural rigidity increases rapidly. These properties are dependent on the quadratic moment of the cross-section of the specimen with respect to the mid plane, proportional to the cube of thickness. Figure 6.51 shows one particular case for the evolution of stiffness versus number of cycles for three different core thicknesses for sandwich specimens having foam of 60 kg/m$^3$ density at one displacement level of 0.70. The stiffness degradation started immediately after the first cycle and keeps on decreasing with the increase in the number of cycles. It is observed that with increasing the core thickness, the degradation of stiffness increases with the increase in number of cycles. Stiffness reduction is more in 25 mm thick sandwich specimen as compared to 20 and 15 mm thick sandwich core material as can be seen in figure 6.51. It was assumed that by increasing the core thickness, we actually increase the cross sectional area exposed to fatigue, thus more area is receiving damage due to fatigue, which results in the decrease in stiffness for larger core thickness sandwich specimens. Therefore, the greater the cross sectional area of the specimen, the more extensive will be damage due to fatigue. The same results were observed in sandwich specimens having core density 80 and 100 kg/m$^3$ and thickness of 15 and 25 mm (figure 6.52 and 6.53).

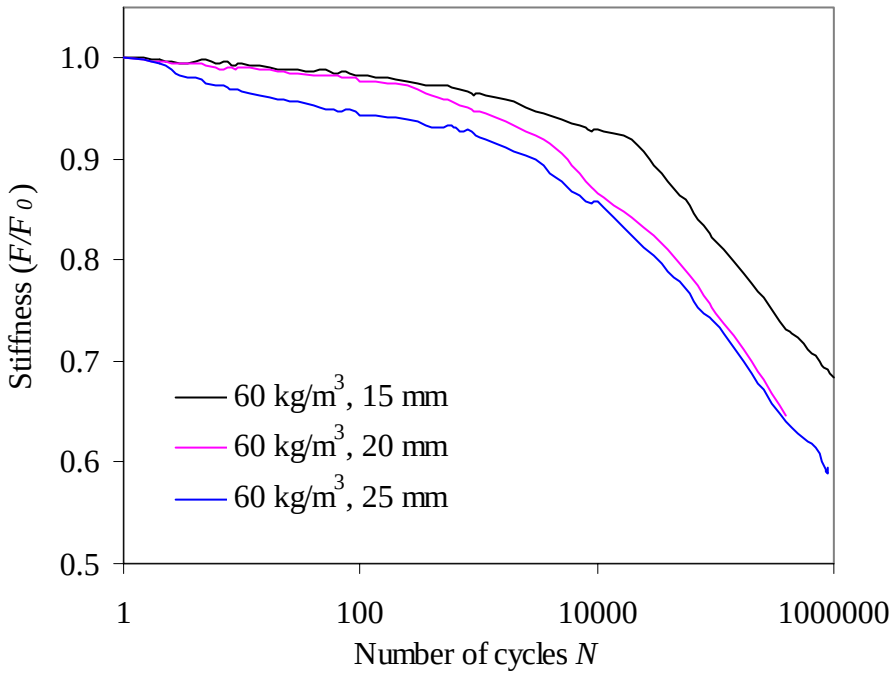


***Figure 6.51.*** *Comparison between the evolution of stiffness versus number of cycles for sandwich specimens of 60 kg/m$^3$ foam density for three different core thicknesses at a displacement level of 0.70.*

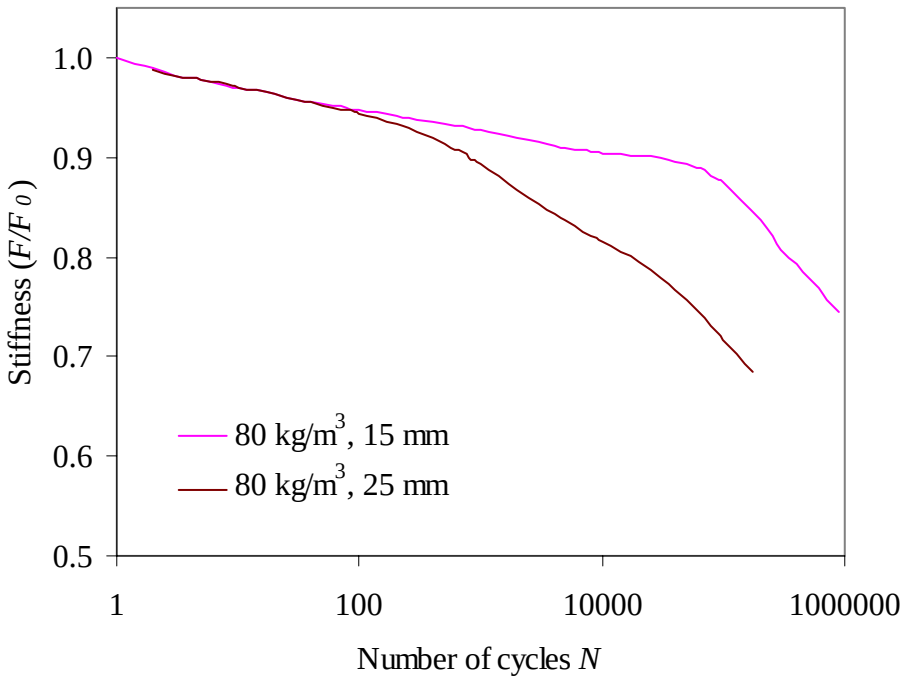


**Figure 6.52.** *Comparison between the evolution of stiffness versus number of cycles for sandwich specimens of 80 kg/m$^3$ foam density for two different core thicknesses at a displacement level of 0.70.*

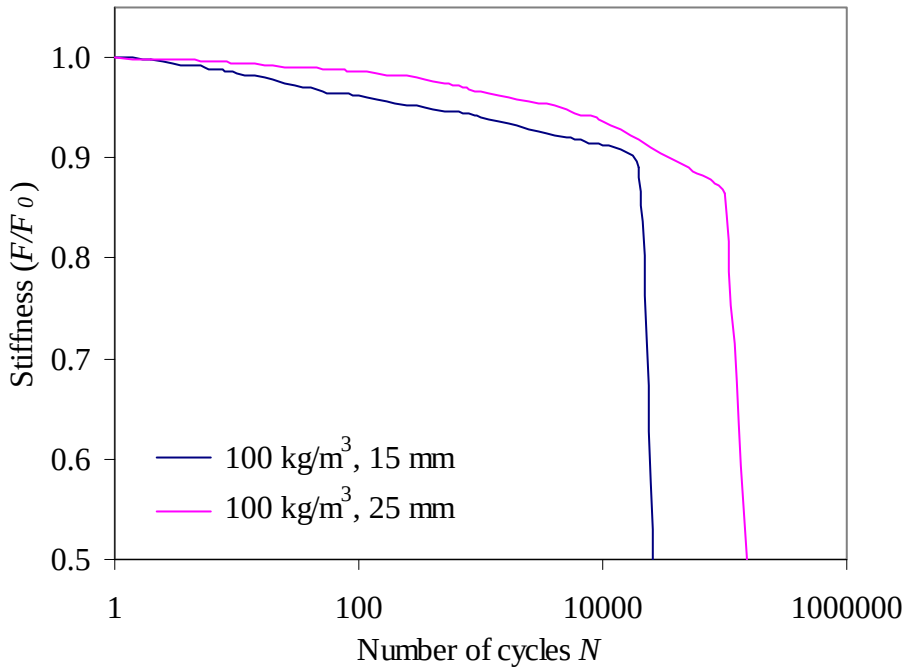


***Figure 6.53.*** *Comparison between the evolution of stiffness versus number of cycles for sandwich specimens of 100 kg/m$^3$ foam density for three different core thicknesses at a displacement level of 0.70.*

### *6.4.2.7.2 Fatigue life*

Figures 6.54 to 6.56 represent the maximum applied displacement versus fatigue life at $N_{10}$ criterion in displacement control fatigue. Wöhler curves were constructed form the experimental data obtained from stiffness based curves. These curves were plotted for maximum applied displacement versus number of cycles for various core thicknesses. Three thicknesses (15, 20 and 25 mm) were used for 60 kg/m$^3$ foam density sandwich specimen and two thicknesses (15, 20 mm) were utilised for 80 and 100 kg/m$^3$ foam density sandwich. Maximum displacement for each core thickness depends upon the displacement at rupture. Higher core thicknesses have generated high displacement at rupture. Definitely high maximum displacement corresponds to higher stress amplitude, which causes more damage in the sandwich specimens thus giving shorter fatigue lives. While at lower applied displacement, the stress amplitude is lower causing less damage resulting in longer fatigue lives. Experimental results of the higher core thickness are higher as compared to lower thickness sandwich specimens. It can be seen from the figure that at the same maximum displacement, the sandwich with thicker core (20 and 25 mm) has more fatigue life as compared to less thick core (15 mm). Obvious reason was that higher stress amplitudes cause more damage in thicker core as compared to lower thickness materials. The same trend was also observed in the case of sandwich specimens with higher densities and two thicknesses shown in figures 6.55 and 6.56. It can be seen from these results that when the maximum applied displacement is high, the fatigue life is small, while for small maximum displacement fatigue life is high.

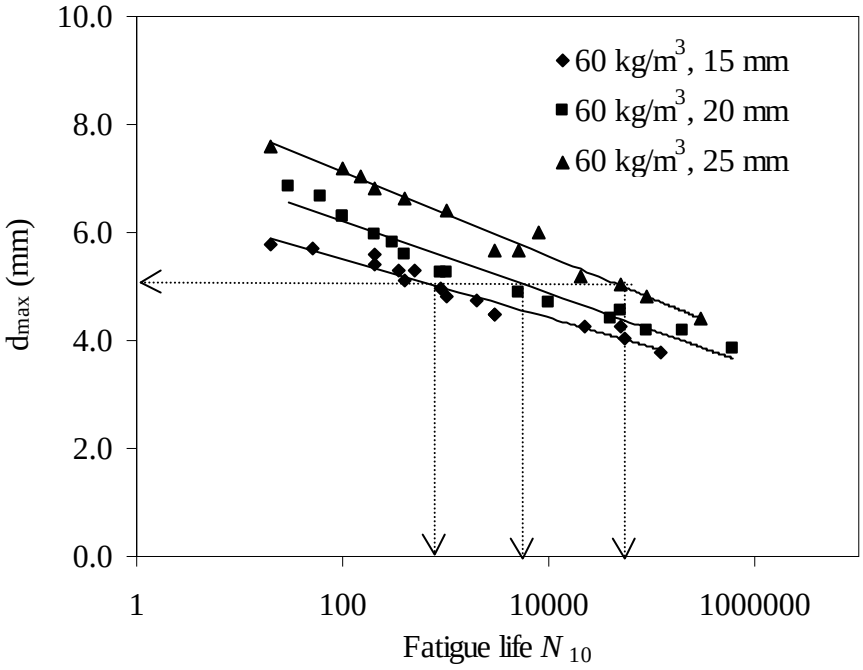


***Figure 6.54.*** *Evolution of maximum applied displacement with fatigue life for sandwich specimens of 60 kg/m$^3$ foam density of three core thicknesses.*

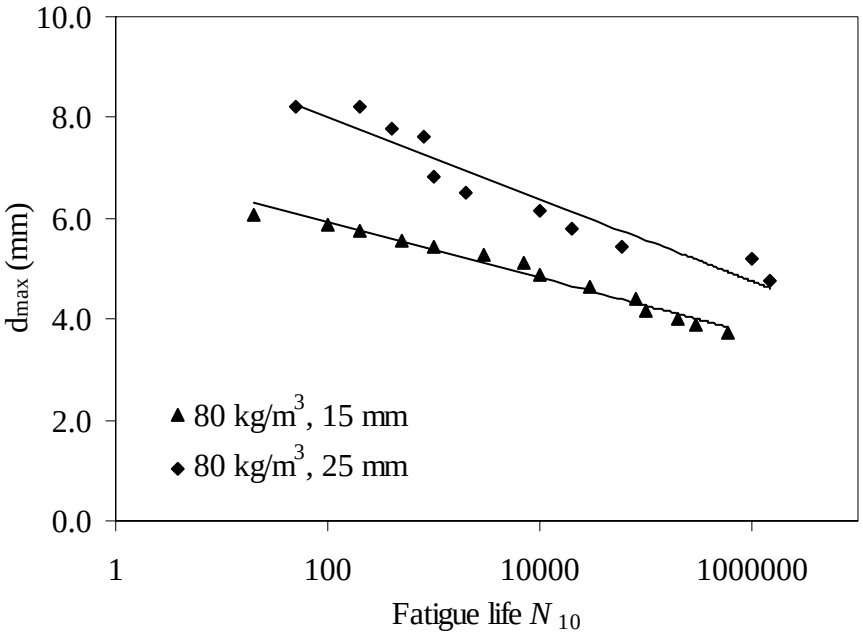


***Figure 6.55.*** *Evolution of maximum applied displacement with fatigue life for sandwich specimens of 80 kg/m$^3$ foam density of two core thicknesses.*

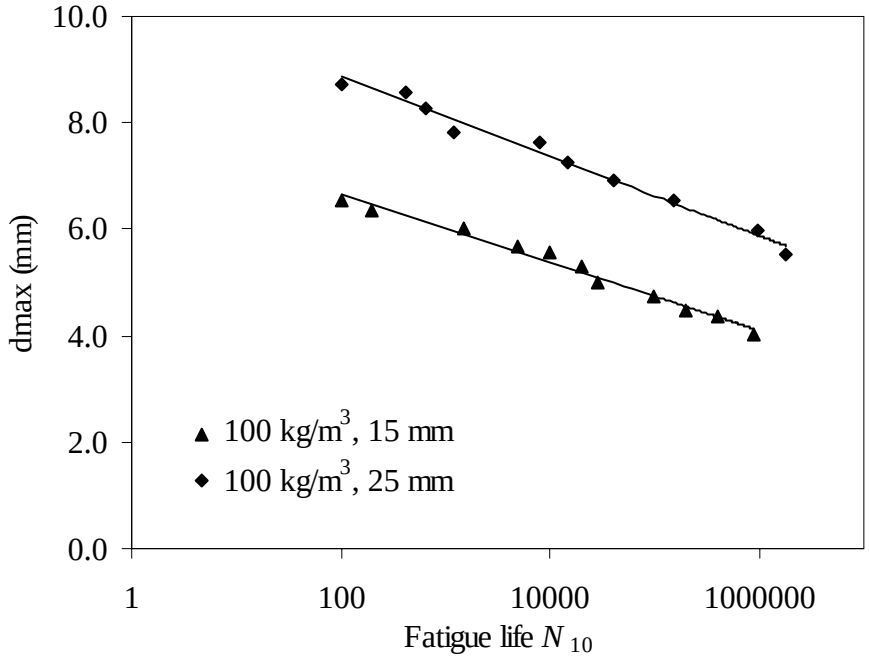


***Figure 6.56.*** *Evolution of maximum applied displacement with fatigue life for sandwich specimens of 100 kg/m$^3$ foam density of two core thicknesses.*

The maximum applied displacements are normalised with displacement at failure obtained in static tests. Wöhler curves were plotted as maximum applied displacement levels versus fatigue life for sandwich specimens of three core thicknesses of 60 kg/m$^3$ density and are shown in figure 6.57. For one maximum applied displacement level, it is observed that thicker core sandwich has a shorter fatigue life as compared to thinner core sandwich. The reasons are same as explained above that thicker materials suffer more damage in fatigue as compared to thinner materials. From these results it is clear that fatigue life increases with the decrease in core thickness for the same values of maximum applied displacement levels.

In the table 6.3, parameter *B* values obtained from the curves fitted with equation 6.1 for with sandwich specimens of three core thickness and four densities are presented. It can be seen that the parameter *B* increases with the increase in core thickness and densities of the core of the sandwich foams.

***Table 6.3.*** *The values of parameter obtained from the equation 6.2.*

| Density<br>Thickness | Parameter<br>B |
|---|---|
| 60 kg/m$^3$ (15mm) | 0.0380 |
| 60 kg/m$^3$ (20mm) | 0.0398 |
| 60 kg/m$^3$ (25mm) | 0.0407 |
| 80 kg/m$^3$ (15mm) | 0.0404 |
| 80 kg/m$^3$ (25mm) | 0.0410 |
| 100 kg/m$^3$ (15mm) | 0.0432 |
| 100 kg/m$^3$ (25mm) | 0.0452 |

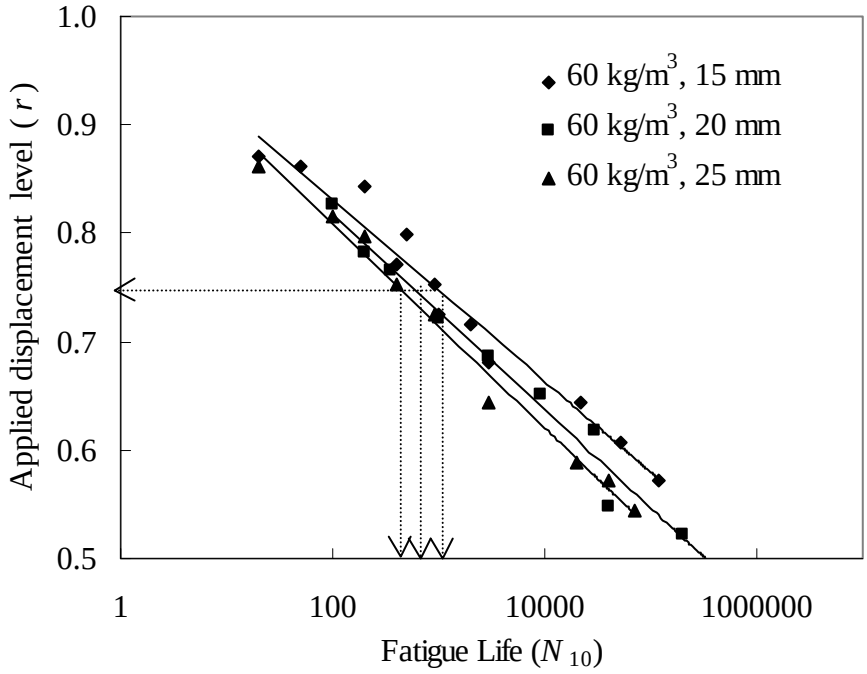


***Figure 6.57.*** *Wöhler curves for sandwich specimens of 60 kg/m$^3$ density having different core thickness.*

### 6.4.3 Fatigue scatter

As evident from the results, the nature of fatigue tests often produces considerable scatter of results. The observed scatter of results is especially true for foam core sandwich structures, which have in a sense, a physical arrangement of elements all having different mechanical properties, material variability and manufacturing inconsistency. In fatigue testing, the weakest link in such a structure will cause premature failure, which is often further exacerbated by imperfections in material quality and manufacturing defects. The results obtained from experiments certainly suggest that the presence of such factors had a varied degree of effect on specimen failure and scatter of results. By increasing the sample population the scatter and standard deviation can be reduced but the observed trend is not expected to change significantly over several orders of magnitude in cyclic life. The measured maximum percentage error in foam densities about the quoted manufactures nominal density (calculated by weighing the foams) was approximately ± 4%.

### 6.4.4 Evaluation of damage during fatigue

In sandwich composites materials, ductile and brittle fractures occur depending upon the type of material constituents and type of core materials. In the skin, the brittle face consists of either 0° or 90° plies on laminate level, or the fibres on the micro structural level. The ductile phase corresponds to the off axis plies where large shear deformation may take place. As cracks and other type of damage propagate during fatigue, they frequently cover both phases and it requires considerable experience to interpret

fractographic micrographs to figure out crack propagation. This problem is also discussed by Bascom and Gweon [129].

The most widely used post damage analysis is fractography, either in a scanning electron microscope (SEM) or by conventional optical microscopy. If the damage processes have mainly occurred only at ply level or at larger scales an optical microscope is likely to be sufficient, provided the depth of field is suitable at the given magnification. If the smaller details are sought, the electron microscope is the better option. The objective of fractrography in this framework is to trace back to the origin of structural failure, and identify the structural or material property that has initiated the accumulation of damage leading to catastrophic failure.

The interface of a sandwich is very complex with a composite face layer, its resin-rich outer surface bonded to the core, a core which has its surface cells filled with resin, and finally the core itself which is by no means homogeneous. The adhesive bond or rather the 'interface' connecting the face to the core has a very complicated structure. The face sheet is usually made of fibre composites and, especially in the case, if the laminate is hand laid-up, the core will have resin rich layers towards its surfaces. In this case, where foam core is used the outward cells are almost filled with resin. Hence, the core has an outer layer with different properties to the rest of the core. Underneath this surface is the virgin core material with its specific properties (not isotropic). The resin filled outer layer of the core often proves to be stronger than the core itself, and it is usually seen that the fracture occurs in the core, just underneath this interface.

Generally, failures can occur in the skins, the core or at the interface of the core and skin. Failures in the sandwich composites can be classified as [130]:

- Skin tensile or compression failure either in one ply of the skin laminate or through all plies,
- Interlaminar tearing of plies in the laminates,
- Debonding of the skin from the core,
- Core shear failure.

A sequence of typical failure mechanisms obtained from fatigue tests is shown in a series of six pictures. These pictures are taken at different number of cycles during two tests carried out at stress level of 0.70 and 0.95 and having density of 60 kg/m$^3$. It has been observed that the damage region tends to be much localised as being due to concentrated loading. In sandwich composite beam, most of the damage is taken by the skin (the first point of contact under central roller) causing fibre breakage and delamination in a small area around the damage site in vicinity of central roller.

In figure 6.58, picture (***a***) shows an initiation of damage in the skin and compression in the core at few hundreds of cycles. This picture is taken at $10^3$ cycles. With the increase in number of cycles ($10^4$ cycles) these damages (damaged cells) propagate and an initiation of interfacial debonding developed between skin and core as seen in picture

(***b***). The fractured cells were spread out and did not form a continuous crack or distinct crack tips. In the next stage, some of these cracks merged and formed a crack just below the layer of resin rich cells. The crack would then grow along the interface but still below the layer of resin rich cells. Quite an extensive predamaged area with many micro cracks was observed in the core structure and this was believed to be due to the large shear deformations and friction between the damaged and undamaged cells. These damage mechanisms continue to propagate along the interface, in the core material below the layer of resin-rich cells and adhered layer can be seen in picture (***c***) taken at $4\times10^5$ cycles. And with further increase in number of cycles resulting in the complete debonding between the top skin and the core as can be seen in picture (***d***) taken at 1 million cycles. It can be observed that when the interface becomes stronger, the failure is shifted to core, leaving some core material adhering to the face sheets. Under these conditions only the core and the bottom skin hold the applied load.

Another case at higher applied stress level of 0.95 is shown in pictures (***e***) and (***f***) which are taken close to the failure for two specimens. A crack is seen developed in the core at angle of 45° and propagated from top to the bottom of the skin. This is in agreement to another finding by Zenkert [74], who also observed this kind of crack in his work. It can be seen that these mechanisms which are initiated earlier lead to the propagation of shear crack in the core extending from top skin to the bottom skin resulting in the total failure of specimen. The type of damage mechanisms also depends upon the level of loading.

It was noticed that delamination crack was never at the core skin interface but 1-1.5 mm below the interface. After several examinations, it was revealed that resin penetrated/soaked into the core material by this depth. It was observed that the crack always initiated at the subsurface created by the resin impregnation, dry cells below the actual core-skin interface for high loading levels. This crack runs parallel to the beam axis from the point of initiation towards the end support. In the light of the information obtained on damage mechanisms, it can hardly be disputed that a single crack characterisation of damage would be far from reality.

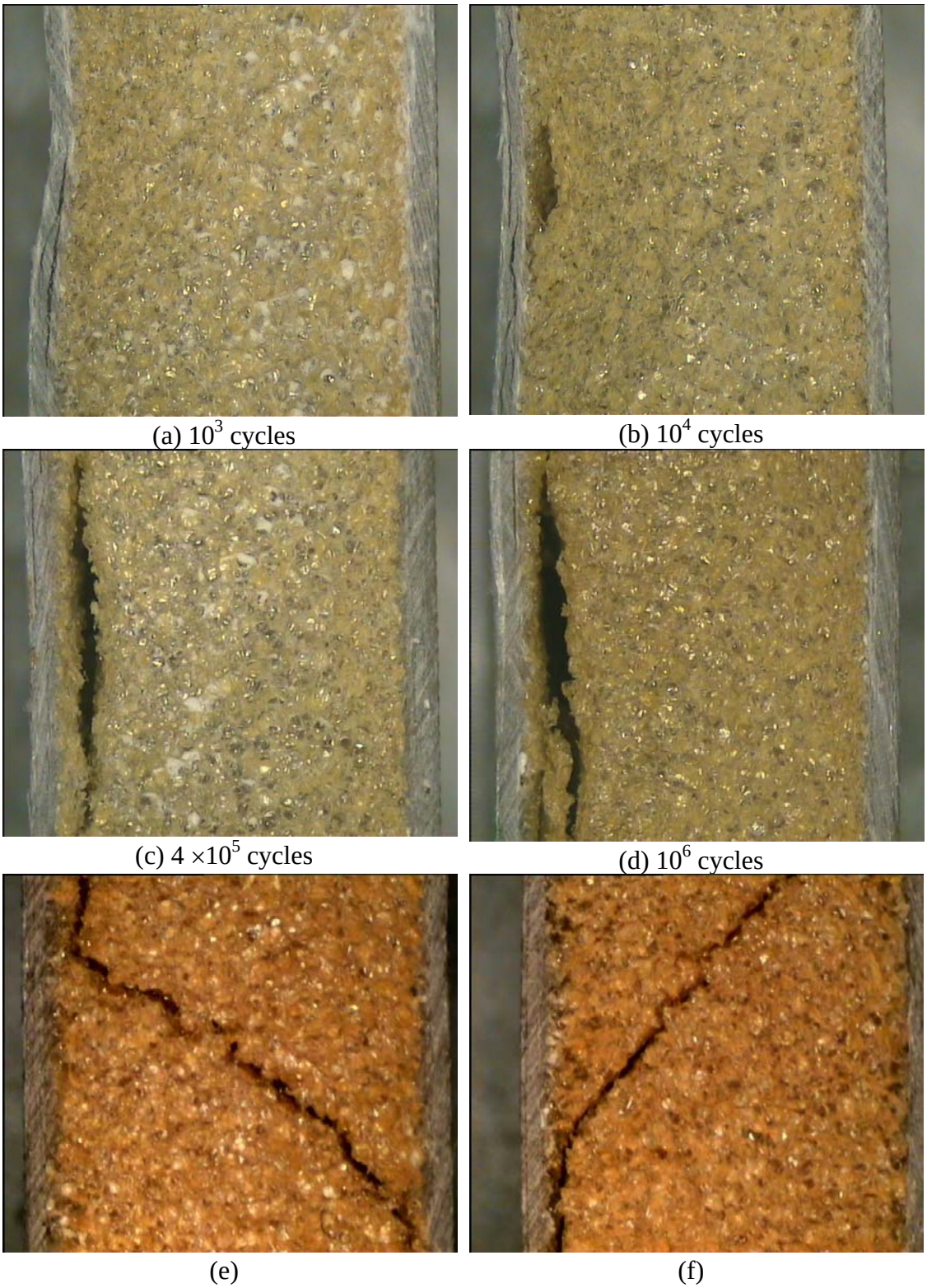


***Figure 6.58.*** *Propagation of damage with number of cycles during fatigue tests at moderate (r=0.70, a-d ) and high ( r=0.95, e-f ) applied displacement levels for sandwich specimens with foams of 60 kg/m$^3$ density.*

# Chapter 7
# Modelling the flexural behaviour of sandwich composite materials under cyclic fatigue

## 7.1 Introduction

Considering the complexity of failure mechanisms in sandwich composites under fatigue, the necessity for development of more simple models with fewer limitations is quite obvious. From a phenomenological view point, the fatigue damage in composites can be evaluated by measuring the damage in material properties, e.g. the stiffness or strength. Extensive research has been conducted to investigate the degradation of residual strength and stiffness. Since measurement of residual strength of composites involves the destruction of the test specimens, a fatigue damage model based on the residual strength may not be suitable for predicting and tracking the fatigue damage. On the other hand, measurements of residual stiffness can be made non-destructively and therefore can be related to damage development and fatigue life of the specimen. Hence, the stiffness degradation model may be more applicable to practical design of composite and sandwich composites structures. However, a comprehensive data base would be required in the fatigue analysis of sandwich composites, based on stiffness reduction, unless mathematical relationships can be developed to relate the residual stiffness to other readily material properties. If a such a relationship could be established, extrapolation of data at various stress levels would be established, thus reducing the amount of test data needed to characterise the materials behaviour.

The modelling of the fatigue behaviour of composite material during three point bending tests have been proposed by various authors [44,71,131]. These are based on the fatigue modulus reduction of laminate composites and of the sandwich composites. Hwang and Han [36] introduced the concept of fatigue modulus. They proposed a fatigue modules model based on the assumption that the fatigue modulus degradation follows a power function of fatigue cycles. Fatigue modulus occurs when the fatigue resultant strain reaches the ultimate strain. Whitworth [2,132] presented a phenomenological model for characterising the stiffness degradation and its possible relationship with residual strength. The fatigue modulus which is generally referred as stiffness can be defined as being the ratio between the applied stress and the strain at a given number of cycles [36,71]. This modulus is function of loading cycles $n$ and applied stress level $r$. The rate of decrease of fatigue modulus can also be related to an empirical power function of number of fatigue cycles [71].

Hwang and Han [104] have proposed four different damage functions based on fatigue modulus and material strains. These models were developed mainly for the purpose of predictions of multi-stress level fatigue life. Seven different *S-N* curve characterisation models have been applied to these functions, to produce 23 cumulative models. They have applied all these models to two stage loading for the low cycle fatigue of short glass and carbon fibre reinforced, thermoplastic. These models are given in table 7.1.

***Table 7.1.*** *Summary of existing damage models* [104]

| | **Damage Model Type** | | | |
|---|---|---|---|---|
| | **I** | **II** | **III** | **IV** |
| | $\frac{F_0 - F(n)}{F_0 - F_f}$ | $\frac{\varepsilon(n)}{\varepsilon_f}$ | $\frac{\varepsilon(n) - \varepsilon_0}{\varepsilon_f - \varepsilon_0}$ | $\frac{F_0^B - F^B(n)}{F_0^B - F_f}$ |
| 1 | $\frac{1}{p-q}\left[p - \left(p^B - \frac{n^C}{M}\right)^{\frac{1}{B}}\right]$ | $q\left[\frac{1}{p^B - \frac{n^C}{M}}\right]^{\frac{1}{B}}$ | $\frac{q}{p-q}\left[\frac{p}{p - \left(p^B - \frac{n^C}{M}\right)^{\frac{1}{B}}} - 1\right]$ | $\left(\frac{n}{N}\right)^C$ |
| 2 | $\left(\frac{n}{N}\right)^C$ | $\left(\frac{qM}{PM - n^C}\right)$ | $\frac{PM - N^C}{PM - n^C}\left(\frac{n}{N}\right)^C$ | — |
| 3 | $\frac{P}{p-q}\left[p - \left(p^B - \frac{n}{M}\right)^{\frac{1}{B}}\right]$ | $\frac{q}{p-q}\left[\frac{p}{p - \left(p^B - \frac{n^C}{M}\right)^{\frac{1}{B}}} - 1\right]$ | $\frac{q}{p-q}\left[\frac{p}{p - \left(p^B - \frac{n}{M}\right)^{\frac{1}{B}}} - 1\right]$ | $\left(\frac{n}{N}\right)$ |
| 4 | $\frac{1}{p-q}\left[p - \left(p^B - \frac{\ln n}{M}\right)^{\frac{1}{B}}\right]$ | $q\left[\frac{1}{p^B - \frac{\ln n}{M}}\right]^{\frac{1}{B}}$ | $\frac{q}{p-q}\left[\frac{p}{p - \left(p^B - \frac{\ln n}{M}\right)^{\frac{1}{B}}} - 1\right]$ | $\left(\frac{\ln n}{\ln N}\right)$ |
| 6 | $\left(\frac{1 - n^{-A}}{1 - N^{-A}}\right)$ | $\left(\frac{n}{N}\right)^C$ | $\left(\frac{1 - n^A}{1 - N^A}\right)$ | — |
| 7 | $\frac{p}{p-q}\left[1 - (1 + n^C)^{\frac{1}{B}}\right]$ | $\frac{q}{p}\left[\frac{1}{(1+n^C)}\right]^{\frac{1}{B}}$ | $\frac{p}{p-q}\left[\frac{q}{(1+n^C)^{\frac{1}{B}}} - 1\right]$ | $\left(\frac{n}{N}\right)^C$ |

Clark *et al*. [133] used the same approach as Hwang and Han [36] for the development of their model. But that model is suited to matrix dominated laminate behaviour where shear is a primary deformation mechanism. As the number of cycles increases at an applied shear stress, $\tau_a$ the resultant strain, $\gamma(n)$ at cycle $n$ becomes larger until it reaches the failure strain $\gamma_u$. The effective shear modulus is defined as $G_f$. It is assumed that the strain criterion holds where failure occurs when the cycle dependent fatigue strain is equal to static failure strain i.e. $\gamma(N_f) = \gamma_u$.

The fatigue modulus $G_f(n,r)$ at stress ratio $r$ and cycle number $n$ can be expressed by:

$$G_f(n,r) = \frac{\tau_a}{\gamma(n)} \tag{7.1}$$

The rate of decrease of fatigue modulus as proposed by Hawag and Han[36], can be related to an empirical power function of the form $An^C$. The theoretical decrease in modulus from an initial static value can be expressed as:

$$G_f(n) = G_0 - An^C \tag{7.2}$$

Where $A$ and $C$ are the material constants.

Clark *et al.* [133] modified this equation using the shear modulus concept and suggested that an exponential function can be effectively used instead of a power function. They developed analytical expression which can be written as:

$$\begin{aligned} G_f(n) &= G_0 && \text{for} \quad n \le n_{if} \\ G_f(n) &= G_0 - Ae^{(n-n_{if})C} && \text{for} \quad n \ge n_{if} \end{aligned} \tag{7.3}$$

where $n_{if}$ is the number of cycles to initiate damage.

A non linear *S-N* curve can be derived from the non-linear core modulus degradation equation. By assuming the failure strain criterion, the resultant cyclic shear strain at failure is equal to the ultimate static shear strain ($\gamma(N_f) = \gamma_u$.). The fatigue modulus at failure therefore become $G_f(N_f) = \tau_a/\gamma_u$. An applied stress ratio, $r$ can be derived as:

$$\frac{G_f(N_f)}{G_0} = \frac{\tau_a}{\gamma_u}\frac{\gamma_u}{\tau_u} = r \tag{7.4}$$

$$\frac{G_f(N_f)}{G_0} = 1 - \frac{1}{B}e^{(N_f - n_{if})C} \tag{7.5}$$

where $B = G_0/A$

$$r = 1 - \frac{1}{B}e^{(N_f - n_{if})C} \tag{7.6}$$

Where $r$ is equal to the ratio of applied stress to ultimate static stress ($r=\tau_a/\tau_u$). Equation (7.5) can be used to predict fatigue life for different levels of loading. At failure ($n=N_f$) and rearranging equation (7.6), the non-linear S-N equation becomes:

$$N_f = n_{if} + \frac{Ln[B(1-r)]}{C} \tag{7.7}$$

Equation (7.7) can be used to predict the number of cycles at failure for different applied stress levels thus defining the fitted curve to *S-N* data. The values of constants *A* and *C* can be determined from the equation (7.3).

One of the important issues which was not addressed clearly in the literature was about the type of loading as these authors didn't make any clear distinction between tests in stress control and in strain control. On the other hand, in our study, experimental results allowed us to note that the material behaviour during the fatigue test depends strongly on the control type. The stress evolution in strain control and the strain evolution in stress control are completely different .

We developed an analytical approach that allows to determine the fatigue life without doing a lot of experiments. Our approach is basically inspired by the models used by the authors [44,71,131,133], to develop our analytical equations. We propose to write the load or the displacement evolution according to the number of cycles during the fatigue test, using several empirical functions, such as logarithmic and exponential functions, whose coefficients depends on the material properties and loading conditions. These empirical functions are found to be best fit to our experimental results. The choice of functions will also depend on the type of loading. The simplicity of the proposed models is that it includes all type of damage involved in the stiffness reduction of the specimen. Any damage occurring during fatigue would be reflected in the degradation of stiffness and in turn, can be implicitly included in the model parameters.

## 7.2 Derivation of analytical models

### 7.2.1 Modelling for displacement control experiments

Fatigue tests were performed using displacement control with applied sinusoidal waveform of constant static mean displacement $d_{mean}$ and amplitude $d_{am}$. During the tests the decrease in load (stiffness) according to the number of cycles was recorded. Figure 7.1 represents a typical curve in sandwich composites, where the load reduction $F_{max}/F_{0max}$ is reported as function of number of cycles for a mean displacement $d_{mean}$ = 50%$d_u$, where $d_u$ is the value of the ultimate failure displacement in the static tests and for an amplitude $d_{am}$ = 1.75 mm

Results shown in figure 7.1, indicate that the load loss until the failure of the specimen proceeds in three distinctive stages: i) an initial stage characterised by a rapid load reduction; ii) an intermediate stage in which an additional load reduction occurred progressively, corresponding to the nearly total fatigue life of specimen; and iii) a final stage, in which a sharp load reduction is observed up to the specimen fracture. Load reduction is related to the decrease of the flexural fatigue modulus. The experimental

results showed that the load reduction can be expressed as a logarithmic function of number of fatigue cycle as:

$$\frac{F_{\max}}{F_{0\max}} = A_{0d} - A_d \ln(n) \tag{7.8}$$

Where $A_{0d}$ depends on the initial conditions and $A_d$ depends on the applied displacement levels and the material properties. This description can be applied to the first two stages of the curve shown in figure 7.1. Initially, in the first cycle, the maximum load is equal to maximum applied load $F_{0max}$. In these conditions the theoretical expression becomes:

$$\frac{F_{\max}}{F_{0\max}} = 1 - A_d \ln(n) \tag{7.9}$$

Examination of the evolution of parameter $A_d$ according to the displacement levels permitted us to assume that this parameter follows a power function and can be written as:

$$A_d = a_{0d} r^{a_d} \tag{7.10}$$

Where $a_{0d}$ and $a_d$ are the parameters which depends on the material properties and on the loading conditions.

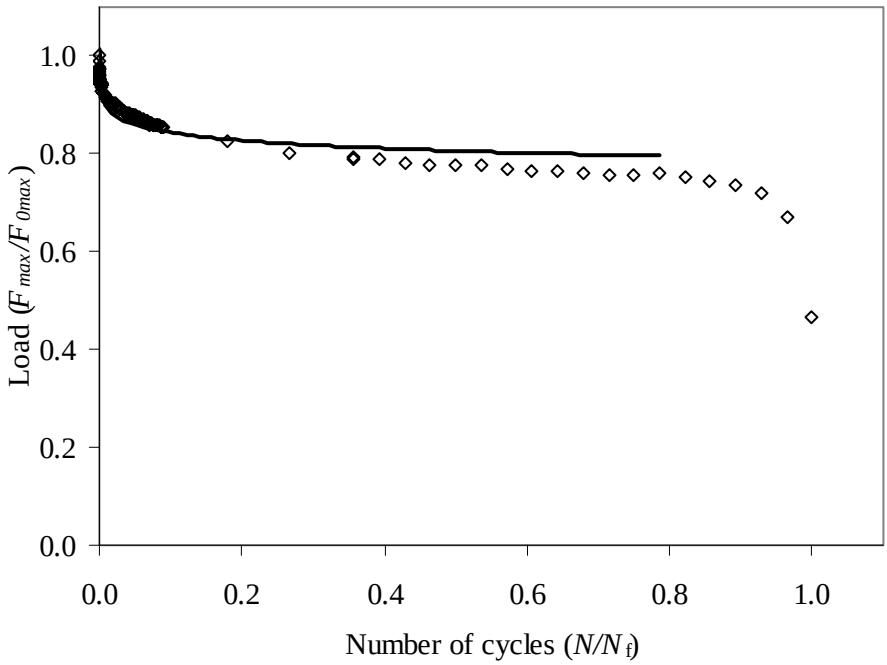


***Figure 7.1.** Evolution of load as function of number of cycles in sandwich composite with 60 kg/m$^3$ density foam under displacement control fatigue with logarithmic fit.*

Using equation (7.10) into equation (7.9), the load expression according to the number of cycles and the applied displacement level thus becomes:

$$\frac{F_{\max}}{F_{0\max}} = 1 - a_{0d} r^{a_d} \ln(n) \tag{7.11}$$

The coefficients $a_{0d}$ and $a_d$ can be determined experimentally.

### 7.2.2 Modelling for load control experiments

Fatigue tests were performed using load control. The applied waveform is sinusoidal with a constant static mean load $F_{mean}$ and amplitude $F_{am}$. During the tests, increase in displacement (stiffness) according to the number of cycles was recorded. The experimental results obtained in three point bending tests on sandwich composites specimens with load control are shown in figure 7.2. The applied load ratio $R_F$ was kept constant at zero and applied load level was 0.70. This results show that the transverse displacement ($d_0/d$) increases until the rupture of the specimen and proceeds in two stages: i) in a first stage an approximately progressive evolution of the displacement is observed corresponding to the nearly total loss of the fatigue life of specimen; and ii) a second stage which is very short with a rapid increase in the displacement resulting in total failure of specimen.

The displacement increase is related to the decrease of the fatigue flexural modulus (stiffness). The experimental results show that the transverse displacement increase can be expressed as an exponential function of number of cycles $n$ as:

$$\frac{d_{0\max}}{d_{\max}} = C_{0F} \exp(-C_F n) \tag{7.12}$$

Where, $C_{0F}$ depends on the initial conditions and $C_F$ depends on the applied load level and material properties. This description can be applied only to the first stage. In the first cycle, the maximum displacement is equal to $d_{0max}$ and equation (7.12) can be written as:

$$\frac{d_{0\max}}{d_{\max}} = \exp(-C_F n) \tag{7.13}$$

Furthermore, the experimental results show that parameter $C_F$ can be evaluated as a power law of the applied load level as:

$$C_F = c_{0F} r^{c_F} \tag{7.14}$$

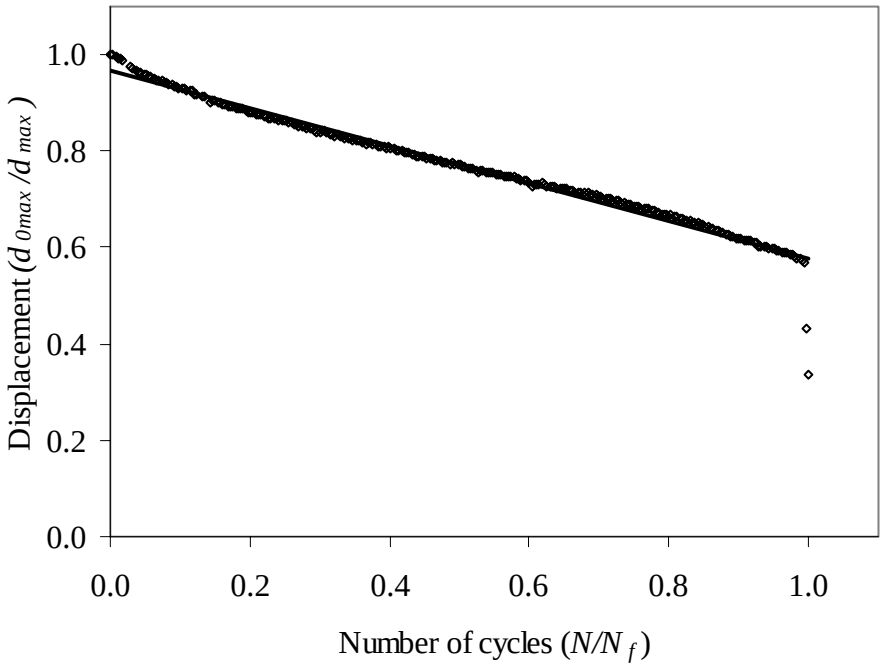


***Figure. 7.2.** Evolution of displacement as function of number of cycles in sandwich composite with 60 kg/m$^3$ density foam under load control fatigue with exponential fit.*

Where $c_{0F}$ and $c_F$ are parameters depending on material and loading conditions. Therefore, displacement increase can be written as:

$$\frac{d_{0\max}}{d_{\max}} = \exp(-c_{0F} r^{c_F} n) \tag{7.15}$$

The coefficients $c_{0F}$ and $c_F$ can be determined experimentally.

## 7.3 Derivation of model for fatigue life

### 7.3.1 Definition of the fatigue life criteria

The evaluation of the fatigue life is an important feature of fatigue behaviour of materials. In the case of the metallic materials subjected to stress control, the fatigue life is associated to the material failure. However, fatigue behaviour of composite material is quite different and sometimes it is not possible to obtain a complete failure during fatigue tests. Therefore it is necessary to define a critical number of cycles for describing the fatigue life of sandwich composite materials. To characterise materials performances in fatigue tests, different criteria's are presented in the literature from curves giving the evolution of the load or the displacement according to the time.

Several authors [71,133] used the failure strain criterion which considers that final failure of composite materials occurs when resultant strain reaches the ultimate static strain. While stiffness reduction is one of methods more commonly used to define the fatigue life. The stiffness reduction of composite laminates is a meaningful measure of

fatigue damage and it can be measured non-destructively. However, in order to predict fatigue life of sandwich composite on the basis of stiffness reduction, the stiffness at fatigue failure, referred to as failure stiffness, should be established. To predict fatigue life by stiffness degradation method, another failure condition is needed rather then total failure of the specimen such as predefined critical number of cycles representing certain damage state. Number of authors [124,134] considered that critical number of cycles were obtained when a given stiffness loss (predefined) was reached. Thus the critical cycle numbers can be associated to stiffness reduction. Fatigue life stays therefore on the conventional criteria for a percentage of given stiffness loss, generally $N_{10}$ criteria are reported in the literature [124,134]. In fact, initiation and development of damage is important as early as possible in fatigue life for some crucial structural components in order to avoid any catastrophic damage in the later stage. Most life prediction models are empirical and are based on macroscopic measurements, to which the parameters of model are fitted. There are many relations for predicting fatigue life such as power laws like Basquin's relations, straight line fits to *S*-Log *N* data, Coffin and Manson's relations etc.

### 7.3.2 Fatigue life prediction

In the case of fatigue tests with displacement control, the critical cycle number $N_{d\alpha}$ corresponding to a load reduction of $\alpha$% can be derived from equation (7.11) which leads to:

$$N_{d\alpha} = \exp\left(\frac{1-\beta}{a_{0d} r^{a_d}}\right) \tag{7.16}$$

$$\text{Where } \beta = 1 - \frac{\alpha}{100} \tag{7.17}$$

Similarly, in the case of fatigue test with load control, the critical cycle number $N_{F\alpha}$ corresponding to a displacement increase of $\alpha$% is deduced from equation (7.15):

$$N_{F\alpha} = -\frac{1}{c_{0F} r^{c_F}} \ln(\beta) \tag{7.18}$$

The use of expressions (7.16) and (7.18) is restricted to the cases where the load reduction or displacement increase of $\alpha$ % is reached. Moreover this concept cannot be applied for displacement level $r_d$ and load level $r_F$ near unity, where the specimen fracture occurs before significant reduction in load or increase in displacement.

## 7.4 Development of damage parameter equations

In order to ensure the structural integrity and reliability, a methodology for characterization of fatigue damage under service loading and relating it to material properties must be established. However, the fatigue damage of sandwich composites is a complex process that involves many different mechanisms and some of these mechanisms can occur simultaneously. Therefore, a material damage model including all the damages is difficult to establish. Consequently, macroscopic models which do not include microscopic information of damage states would be useful for practical design of sandwich composite structures. The fatigue life must be related to the damage state of the

material, if it is possible, to define a critical limit of damage state, for which the properties of the materials are not even damaging but can result in the further damage of material. It is necessary to find a parameter, which represents damage at a certain stage. In the course of this experimental programme, efforts were also diverted to the definition of meaningful fatigue parameter to be used eventually as overall damage measure. We introduce a notion of damage parameter, reflecting the damage state in the material during fatigue test. The measure of this parameter can be done regularly during the tests, without disrupting their progress, thus avoiding the effect of fatigue test interruptions.

The damage parameter during cyclic tests can be defined by a parameter $D$ which is equal to zero at $n$ equal to zero, corresponding to first cycle and equal to the unity when the criterion of failure ($N_c$) is reached.

$$\begin{aligned} D &= 0 \quad \text{if} \quad n = 0 \\ D &= 1 \quad \text{if} \quad n = N_c \end{aligned} \tag{7.19}$$

Different forms of the damage parameters $D$ were considered as a function of cycle number according to materials and loading conditions [36,71,133].

In the case of fatigue tests in displacement control, damage parameter $D$ can be evaluated accordingly [71,133] as:

$$D_d = \frac{F_{0\max} - F_{\max}}{F_{0\max} - F_{\alpha\max}} \tag{7.20}$$

Where $F_{\alpha\max}$ is the maximum applied load at the critical cycle number $N_{d\alpha}$ given by equation (7.16). Conditions defined in equation (7.19) can be verified by equation (7.20). Replacing equations (7.11) and (7.16) in equation (7.20) leads to following equation.

$$D_d = \frac{100}{\alpha}\left[ a_{0d} r^{a_d} \ln(n) \right] \tag{7.21}$$

For tests performed in the load control fatigue, where the displacement evolution is recorded according to the number of cycles, the damage parameter $D$ can be deduced by:

$$D_F = \frac{d_{\max} - d_{0\max}}{d_{\alpha\max} - d_{0\max}} \tag{7.22}$$

Introducing the maximum applied displacement $d_{\max}$ at $n$ number of cycles and the maximum applied displacement $d_{\alpha max}$ at the critical cycle number $N_{F\alpha}$, then using equation (7.15) and (7.18) in equation (7.22) results in the following general expression for fatigue damage:

$$D_F = \left( \frac{100}{\alpha} - 1 \right)\left[ \exp\left( c_{0F} r^{c_F} n \right) - 1 \right] \tag{7.23}$$

Thus, the concept of fatigue damage $D$ leads to another representation of fatigue degradation, initially expressed by equation (7.11) and (7.15). This concept is also useful to evaluate the cumulative damage and fatigue life in the case of multi-step loading.

## 7.5 Experimental characterisation

Initially number of static tests were performed to get the values for $F_{rup}$, $d_{rup}$ and stiffness for each sandwich composite specimen. Results from the static tests were used to design the fatigue experiments. Fatigue tests using of sinusoidal type of waveform were carried out at a constant frequency rate of 10 Hz for all the tests. Experimental conditions are described in section 6.4.2.1 of chapter 6.

## 7.6 Application of models

### 7.6.1 Load and the displacement evolution

Sandwich specimens of different foam densities were used in order to verify the validity of equations of the proposed model. According to the results considered in sub-sections 7.2, the load increase is described by equation (7.9) and the adjustment between the experimental results and equation (7.11) leads to the evaluation of the coefficient $A_d$ as a function of the applied displacement level $r_d$. The values of parameters $a_{0d}$ and $a_d$ for sandwich specimens of three densities are presented in table 7.1. These results were obtained using equation (7.10). These results are plotted for coefficients $A_d$ versus applied displacement level ($r_d$) in displacement control fatigue. A logarithmic function is found to be most appropriate curve fit in passing through the experimental points in fatigue tests with displacement control.

***Table 7.1.*** *Model parameters obtained from equation 7.10*

| Density of foam sandwich | Parameter $a_{0d}$ | Parameter $a_d$ |
|---|---|---|
| 60 kg/m$^3$ | 0.0193 | 2.013 |
| 80 kg/m$^3$ | 0.0192 | 2.553 |
| 100 kg/m$^3$ | 0.0156 | 2.843 |

While in load control fatigue, these results were plotted as coefficient $C_F$ versus applied load level ($r_F$) and a exponential function is found for describing well the experimental points. Experimental results obtained for sandwich specimens with foam of 60 kg/m$^3$ density, from the fatigue tests conducted under load control the displacement evolution is shown in figure 7.2. The displacement increase is described by equation (7.13) and adjustment between the experimental leads to the evaluation of the coefficient $C_F$ of equation (7.14) as a function of the applied displacement level $r_F$. Under load control fatigue, exponential function ($C_F$) described the experimental points very well. These results can be described by equation (7.14) with:

$$c_{0F} = 0.0005 \qquad c_F = 15.395$$

The values of two parameters allow us to characterise the fatigue behaviour of sandwich composites materials of various foam densities in terms of fatigue sensitivity. We noted that the evolutions of these parameters according to the loading level *r* are well described by the logarithmic and exponential functions since correlation coefficients are found to be close to 1.

### 7.6.2. Fatigue life predictions

Fatigue tests results are often expressed in terms of number of cycles until failure at a given maximum stress or strain level. The results of such tests are plotted as maximum fatigue stress or strain versus number of cycles to failure, often refereed to *S-N* curves or Wöhler curves. After all of the parameters were determined from static and fatigue tests, equations (7.16) and (7.18) were used to predict the fatigue life. Experimental and analytical model results were plotted in figures 7.3 to 7.5 under displacement control fatigue for sandwich specimens consisting of foam of 60, 80 and 100 kg/m$^3$ densities with the $N_{10}$ criterion corresponding to 10% reduction in initial stiffness. Figure 7.6 shows the analytical and experimental results for sandwich specimen of 60 kg/m$^3$ density foam in load control fatigue.

Analytical model results also described very well with the evolution of experimental points and this was true for sandwich specimens consisting of three foam densities. It is observed from the figures 7.3 and 7.6 that for low number of cycles, the load level is near to unity which shows, that: when the applied load is near to the static failure, the failure is imminent in the initial number of cycles. While for the low loading levels, the failure is expected for the very high numbers of cycles.

Generally, the experimental results, giving the applied stress level *r* as a function of the lifetime *N*, are fitted by a linear relation of the form:

$$r = d - k \log N \, . \tag{7.23}$$

This relation is used by number of researchers to describe the fatigue phenomena. But this linear relation does not verify the experimental observation that no fracture is obtained for very low values of the applied stress level. However, analytical expressions (7.16) and (7.18) developed in this study, verify this property. Which shows decrease of the slope of the *S-N* curves for low values of the applied displacement levels (figures 7.3 to 7.6). A reasonable agreement between experimental and analytical results are found for all the sandwich specimens of various foam densities.

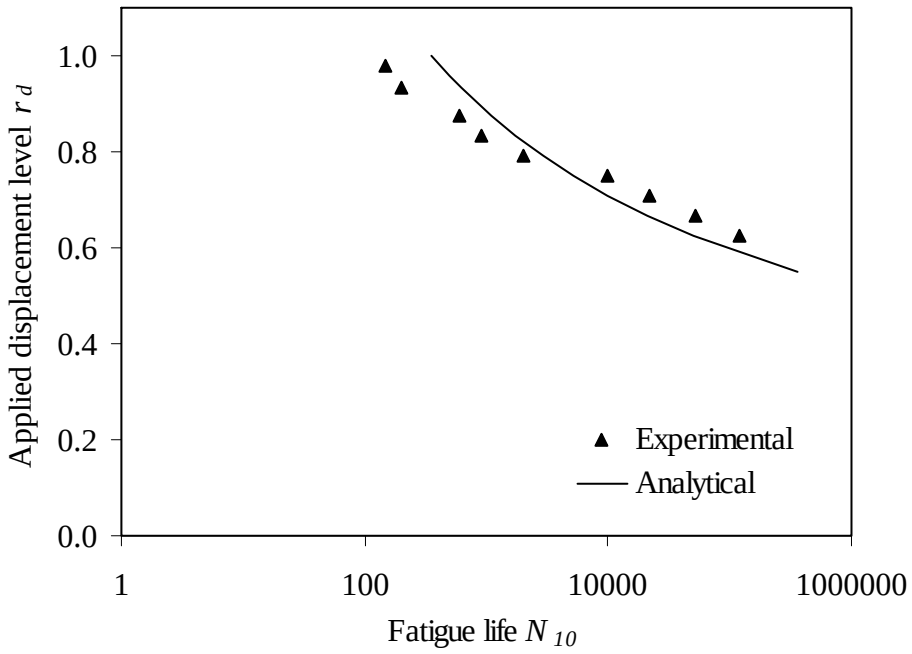


***Figure 7.3.*** *Wöhler curve of the sandwich composites (foam of 60 kg/m$^3$ density) in displacement control fatigue.*

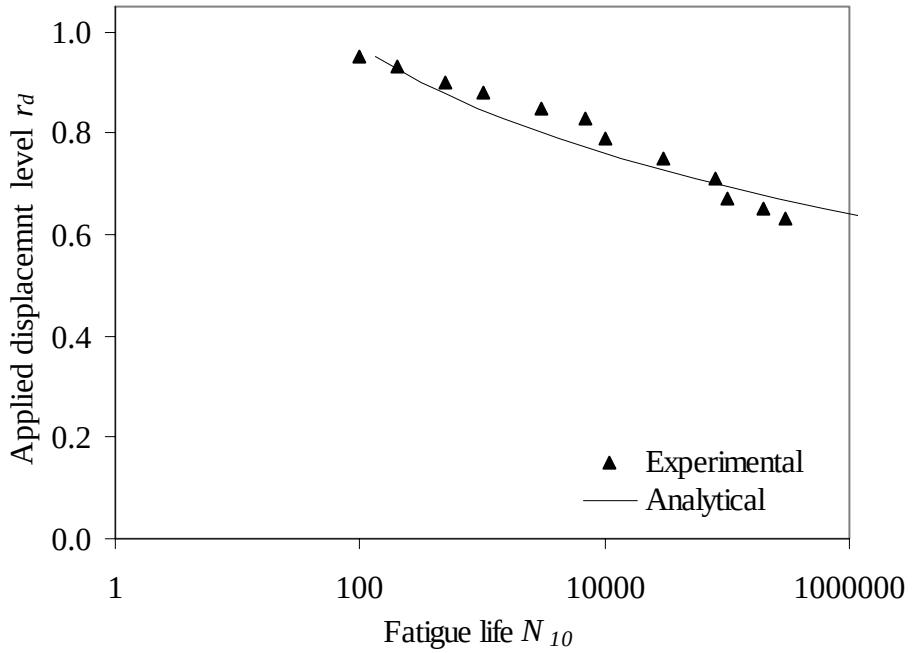


***Figure 7.4.*** *Wöhler curve of the sandwich composites (foam of 80 kg/m$^3$ density) in displacement control fatigue.*

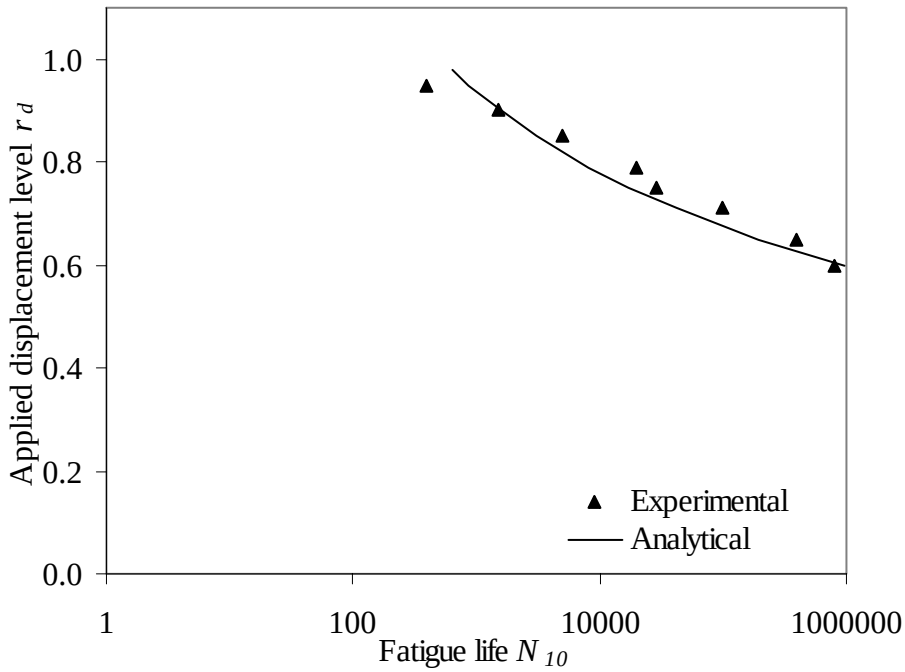


***Figure 7.5.** Wöhler curve of the sandwich composites (foam of 100 kg/m$^3$ density) in displacement control fatigue.*

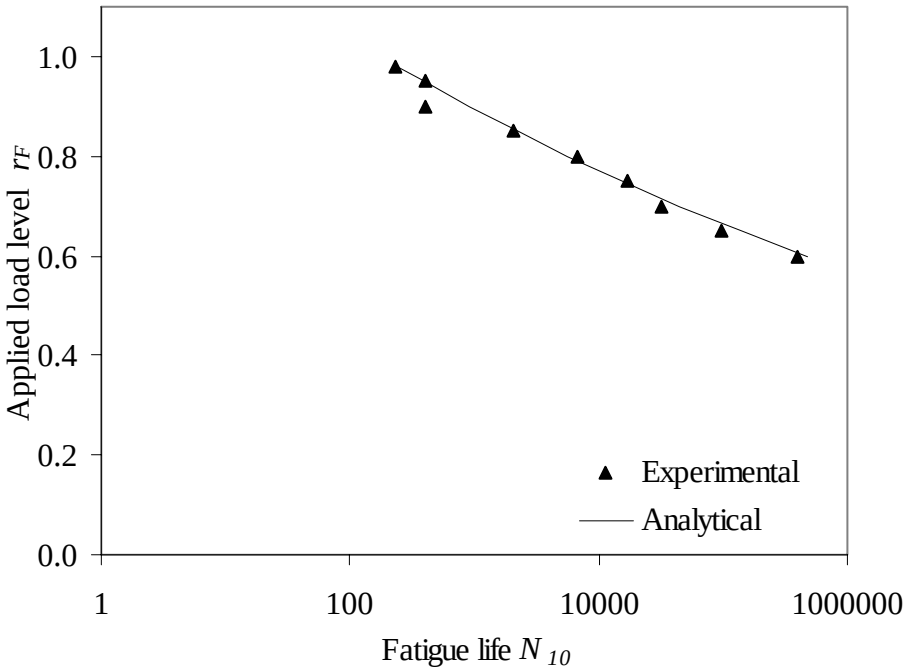


***Figure 7.6**. Wöhler curve of the sandwich composites (foam of 60 kg/m$^3$ density) in load control fatigue.*

### 7.6.3 Damage prediction

The fatigue behaviour of the sandwich composites under cyclic fatigue mainly depends on the progressive developments of damage mechanisms such as matrix cracking, delamination, fibre breakage in the skins and interfacial debonding between core and skin, shear cracks in the core. In sandwich composites damage starts very early and extent of the damage zone grows steadily, while damage type in these zones can change (from skin to core). In our work we combine all damage mechanisms in a global damage parameter $D$, that strongly depends on core characteristics, applied loading level $r$ and type of loading. Values of damage parameter $D_d$ is calculated from the equation (7.21) for the displacement control fatigue. While in load control fatigue, values of damage parameters $D_F$ is obtained from equation (7.23).

Experimental and analytical results were shown in series of figures 7.7 to 7.15 in the case of displacement control fatigue. These graphs were plotted for three applied loading levels of 0.65, 0.80 and 0.95. These values of applied loading levels were chosen to observe the effect of loading level on the damage parameter evolution. In addition, sandwich specimens of three foam densities were used for experimental and analytical results.

It can be observed from the figures 7.7 to 7.15 that evolution of damage follows two apparent stages with the increase in number of cycles. Initially there is very rapid growth of damage within few number of cycles. This rapid growth is attributed to initiation of damage in skins, specifically the transverse matrix cracking in skin. Afterwards, there is gradual increase in damage with the increase in the number of cycles. The second stage is assumed to be initiation and slow progression of damage in the skin and core.

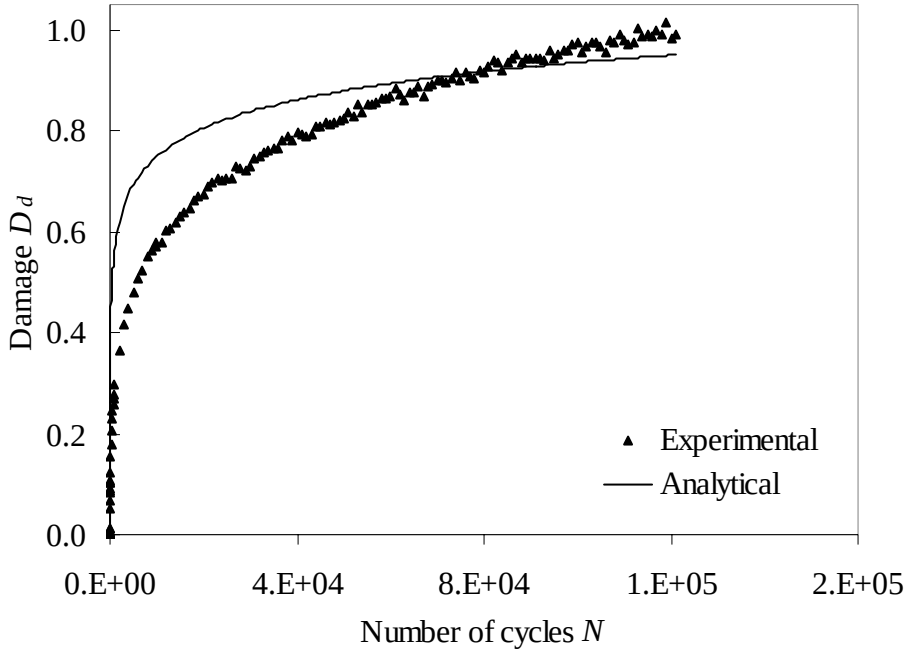


***Figure 7.7.*** *Evolution of the damage in the sandwich composites of foam density 60 kg/m$^3$, according to number of cycles in displacement control, experimental and analytical results for loading levels of $r_d$ = 0.65.*

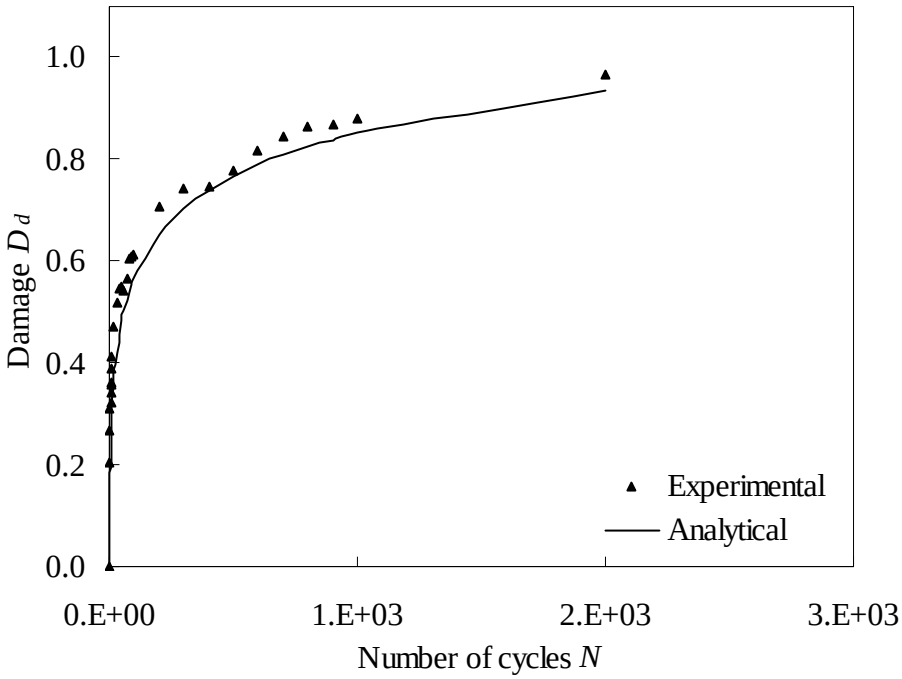


***Figure 7.8.** Evolution of the damage in the sandwich composites of foam density 60 kg/m$^3$ according to number of cycles in displacement control fatigue, experimental and analytical results for displacement level of $r_d$ = 0.80.*

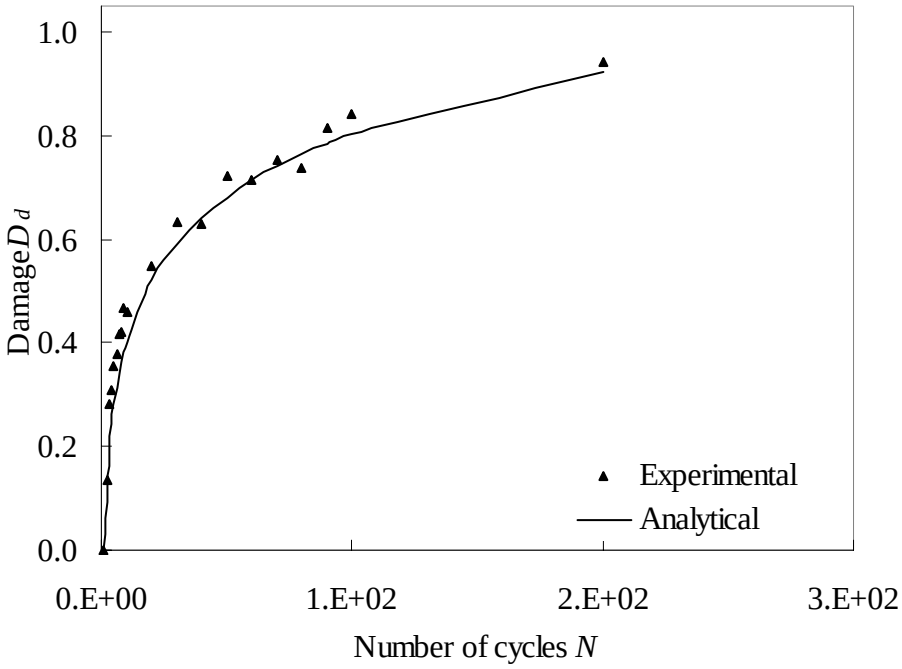


***Figure 7.9.** Evolution of the damage in the sandwich composites of foam density 60 kg/m$^3$ according to number of cycles in displacement control, experimental and analytical results for displacement level of $r_d$ = 0.95.*

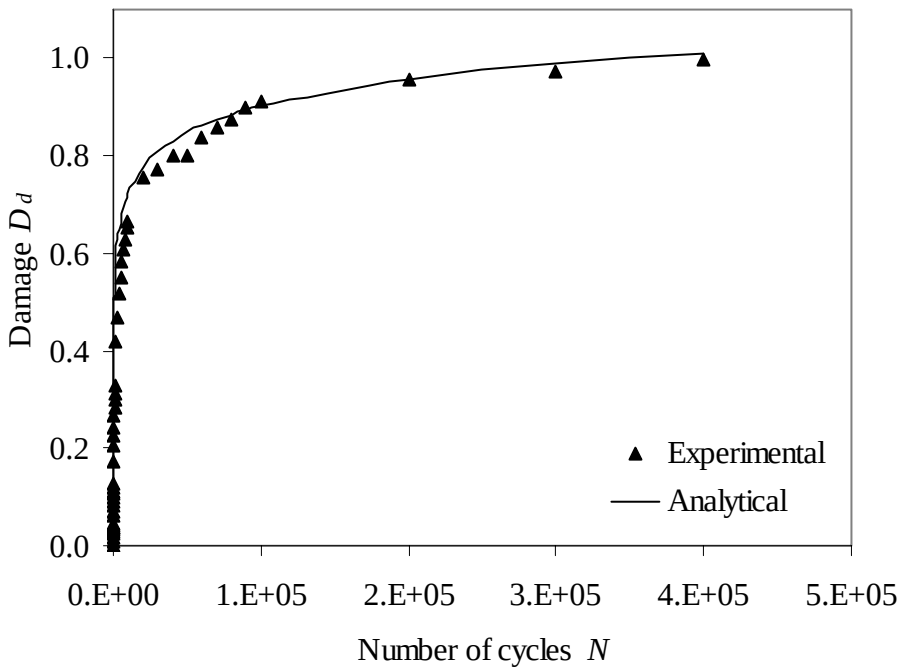


***Figure 7.10.*** *Evolution of the damage in the sandwich composites of density 80 kg/m$^3$ according to number of cycles in displacement control, experimental and analytical results for displacement level of $r_d$ = 0.65.*

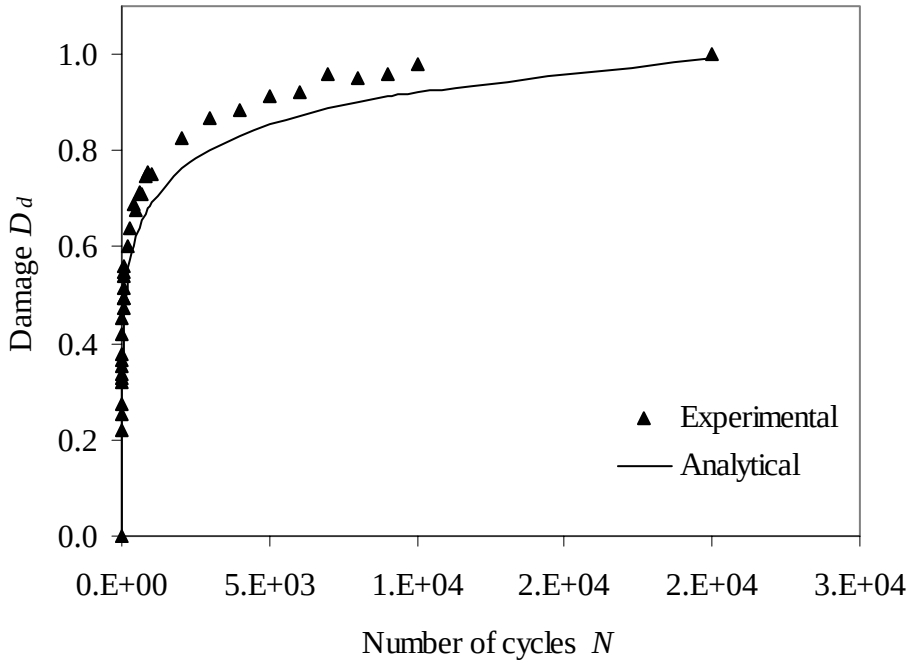


***Figure 7.11.*** *Evolution of the damage in the sandwich composites of density 80 kg/m$^3$ according to number of cycles in displacement control, experimental and analytical results for displacement level of $r_d$ = 0.80.*

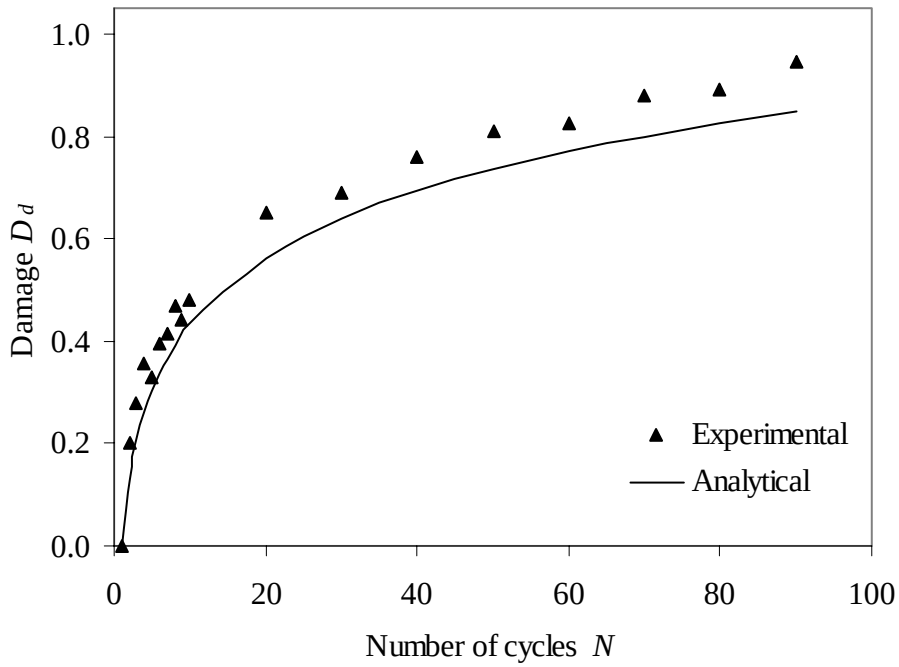


***Figure 7.12.** Evolution of the damage in the sandwich composites of foam density 80 kg/m$^3$ according to number of cycles in displacement control, experimental and analytical results for displacement level of $r_d = 0.95$.*

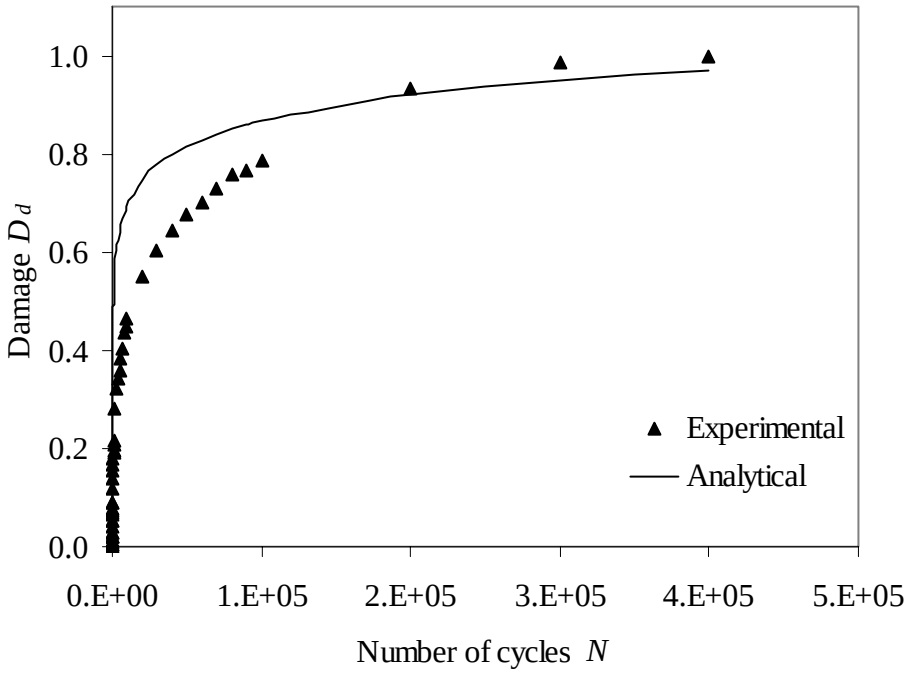


***Figure 7.13.** Evolution of the damage in the sandwich composites of foam density 100 kg/m$^3$ according to number of cycles in displacement control, experimental and analytical results for displacement level of $r_d = 0.65$.*

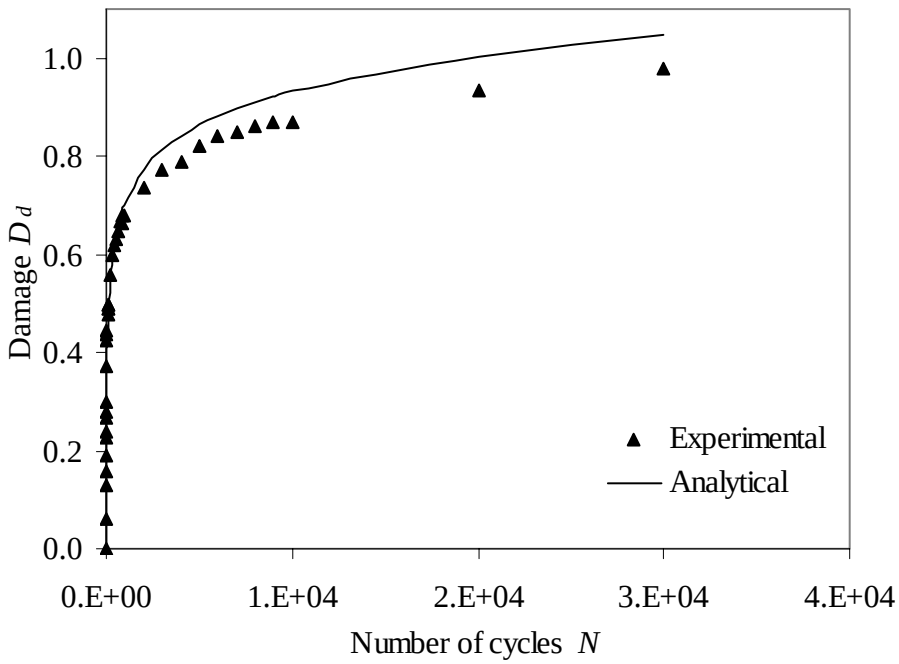


***Figure 7.14.*** *Evolution of the damage in the sandwich composites of foam density 100 kg/m$^3$ according to number of cycles in displacement control, experimental and analytical results for displacement level of $r_d = 0.80$.*

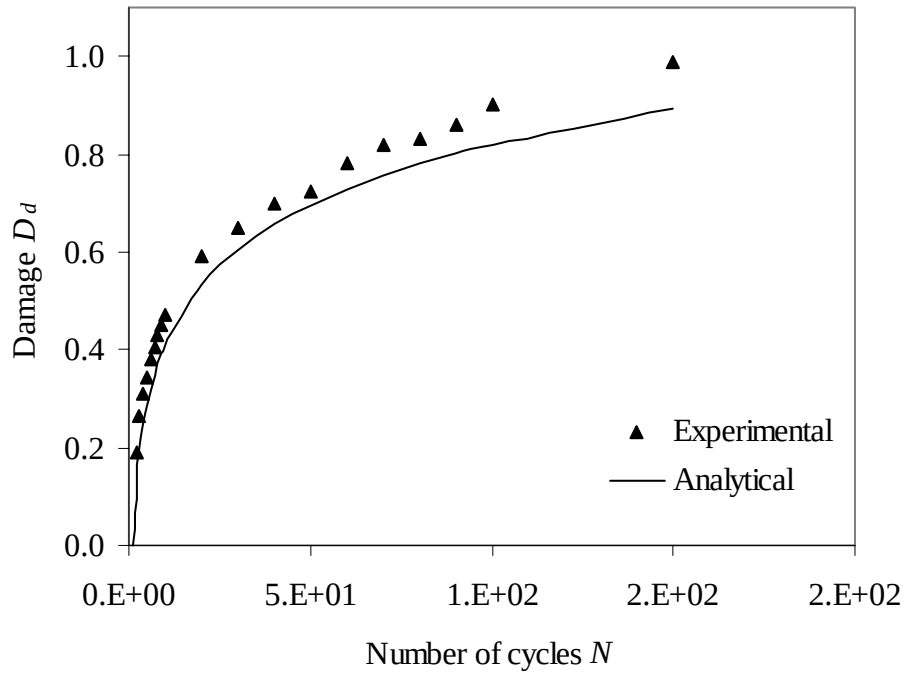


***Figure 7.15.*** *Evolution of the damage in the sandwich composites of foam density 100 kg/m$^3$ according to number of cycles in displacement control, experimental and analytical results for displacement level of $r_d = 0.95$.*

From these results, it is observed that for low values of applied displacement levels, analytical results are found higher then experimental results for initial number of cycles. However, for higher values of applied displacement levels, there is good agreement between experimental and analytical results. A similar trend is observed for the sandwich specimens of other densities. We noted that growth of damage is very fast in the first cycles. These numbers of cycles are considered very important as it gives rises a certain values for the initiation and progression of damage in a specific number of cycles. A good agreement between the analytical model and experimental results can be observed for three applied displacement levels and for the sandwich specimens of three foam densities.

Evolution of the damage parameter *D* according to number of cycles in load control fatigue is shown in figures 7.16 to 7.18 for sandwich specimens of 60 kg/m$^3$ density. These graphs are plotted for three values of applied loading levels 0.60, 0.80 and 0.95 respectively. Figures 7.16 to 7.18 show a progressive development of damage until failure. In spite of scatter in experimental data points, model values pass through these experimental points. In load control fatigue, analytical and experimental values were also found to be in reasonably good agreement with each other.

The type of loading plays an important role as it controls the type of damage modes in sandwich composites. This phenomena is clearly observed in the experiments performed under both type of loading controls, in this study. In displacement control experiments, rapid early initiation and development of damage is attributed to the fixation of initial mean displacement level, which in this study is 50% of the ultimate failure displacement. This level was sufficient to cause initial damage in the sandwich specimen without being subjected to fatigue. When this slightly damage specimen is subjected to fatigue, there is a rapid increase in damage developments that were observed at the early stage of fatigue and can be seen in figures 7.7 to 7.15 for three types of applied displacement levels.

While in load control experiments, there is no such initial loading and we observe a continuous development of damages which increases with the increase in number of cycles. The stiffness damage relationships provide an important link between the micromechanics and overall mechanical response of sandwich structure. The relationships are amenable to special case of damages due to phenomenological nature of fatigue. In sandwich composites damage starts very early and extent of the damage zone grow steadily under fatigue, while damage type in these zones can change from one state to another that is from skin to core which also depends upon the type of loading control.

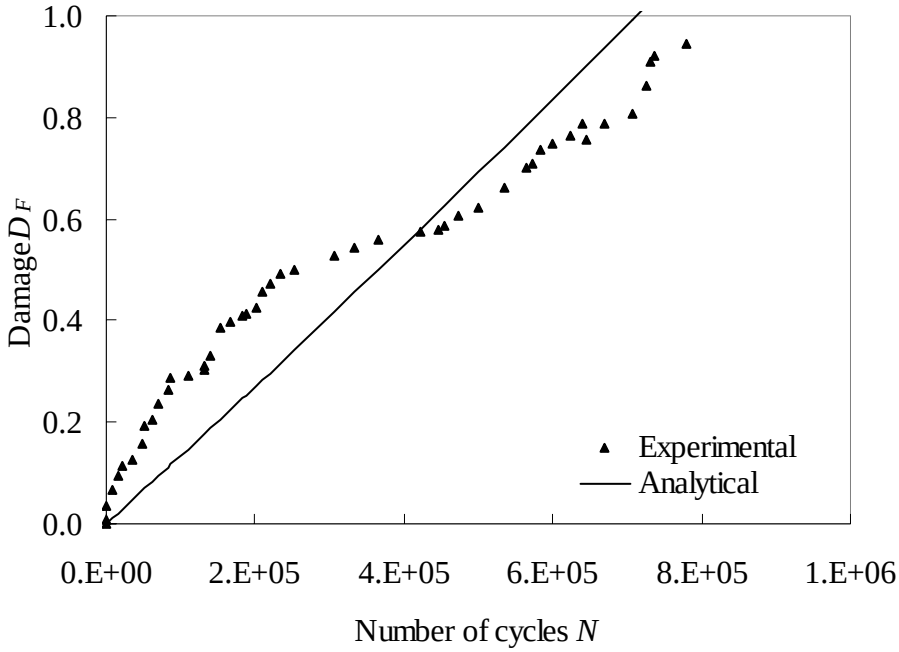


***Figure 7.16.*** *Evolution of the damage in the sandwich composites according to the number of cycles in load control, experimental and analytical results for load level $r_F$ = 0.60.*

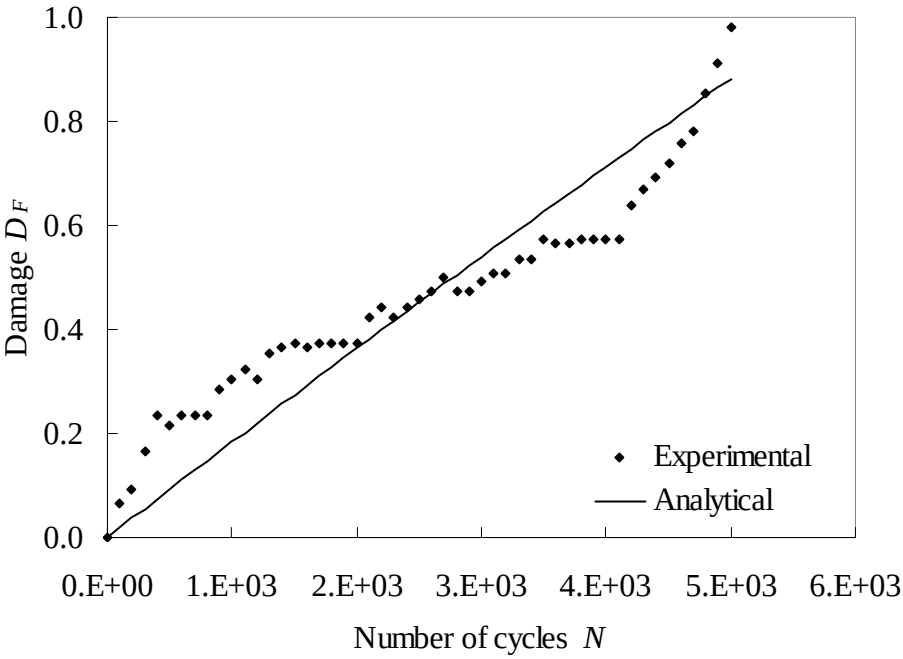


***Figure 7.17.*** *Evolution of the damage in the sandwich composites according to the number of cycles in load control, experimental and analytical results for load level of $r_F$ = 0.80.*

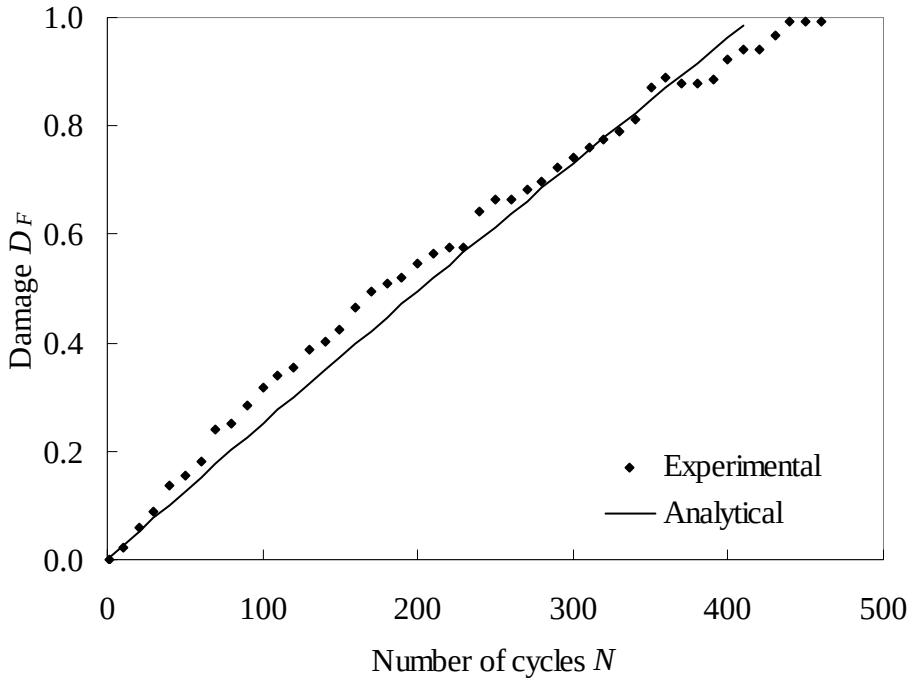


***Figure 7.18.** Evolution of the damage in the sandwich composites according to the number of cycles in load control, experimental and analytical results for load level of $r_F$ = 0.95.*

# Chapter 8
# Conclusions

The research work presented in this thesis has involved an extensive investigation of the mechanical behaviour of sandwich composite and its constituent elements under static and cyclic fatigue. The main thrust to the work has been led by the literature survey presented in chapter two, which has highlighted many areas where the knowledge is limited or controversial. The outcome of this work is the development of experimental and analytical procedures for fatigue life predictions and damage development of sandwich composite materials.

Initially, detailed experimentally studies were focussed on characterising the static behaviour of the constituents of sandwich composites and then on the overall behaviour on sandwich composites. Foams play an important role in the performance of sandwich composites in different loading environments. Detailed experimental characterisations of foams in static tests during compression, indentation, shear and in flexural testing were conducted with respect to their densities. An interesting database was generated for fatigue testing in the later stage.

Later, studies were concentrated on characterising the response of sandwich specimens when subjected to three point bending in static tests. In order to consider the various conditions such as pure bending and transverse shear, experimental investigation has been done with sandwich specimens of various core thickness and different density foams at various span lengths in three point bending. These results were analysed, bending and shear coefficients were calculated at different span lengths. Sandwich beam theory was used to calculate the bending and shear coefficients of sandwich specimens, when subjected to three point bending. A reasonable agreement between the theory and experimental results was observed for determining the bending and shear stiffness coefficients. Deflections of the beams were correlated with theoretical results for sandwich specimens of various core thickness and densities. Bending and shear modulus increase with increasing core density. However, bending modulus decreases with increasing core thickness. Span length plays an important role for bending and shear stiffness of the sandwich beam. Large span lengths are greatly influenced by pure bending while small span lengths are responsible for shear phenomena in the sandwich beam under three point bending. Therefore, there must always be a compromise in choosing these coefficients for better performance of sandwich structures in static flexural testing.

Results from on-line photography revealed different failure mechanisms during static tests. Low density foam sandwich specimens failed by buckling of the skin. While high density foam sandwich specimens failed by interfacial debonding and skin failure.

Static tests results were used as a baseline for the fatigue testing strategy for skins, foams and sandwich specimens. An understanding of physical phenomena relating to

fatigue behaviour of skins, cores and sandwich structure with respect to the core thicknesses and densities has been achieved.

The effects of experimental variables, on the fatigue behaviour of sandwich composites were also studied. Fatigue design data generally include the effects of various combinations of the test parameters, i.e. frequency of applied load, stress ratio, stress level, thickness of the core, density of the core materials and failure criteria in fatigue testing etc. Therefore, any combination of these experimental parameters greatly influences the performance of the sandwich structure during fatigue. Experimental results of these investigations have highlighted the influence of these parameters on the performance of sandwich composites.

Monitoring of stiffness variation during fatigue tests showed that stiffness is a good measure for the 'health' of the specimen. All the sandwich specimens and their constituents elements showed significant stiffness degradation during the early part of fatigue life and then a gradual decrease until a rapid drop in stiffness due to failure. This parameter is related to be global state of the structure or component during fatigue.

A distinctive difference in the behaviour of sandwich specimens is observed when studying static strength after fatigue. If the maximum applied displacement level is low, it is conceivable that the material is responding in a linear elastic manner to applied loading and the damage state is not increasing. However, higher displacement levels are of major concern, as the damage process grows rapidly leading to a considerable reduction in stiffness degradation and the damage process is irreversible. Specimens were fatigue loaded at maximum applied displacement level of 65% of ultimate failure displacement, no considerable changes were observed in residual stiffness and strength even after 50000 cycles. But when the applied displacement level is increased to 95% of ultimate failure displacement, stiffness and residual strength decreased considerably. It is therefore concluded that a decrease in strength degradation is caused by stiffness degradation due to damage development in sandwich specimens during fatigue, which also strongly depends on the applied displacement level.

Density variation in the foams within sandwich composite materials was found to be a key parameter to consider in controlling the fatigue failures. Fatigue life can be improved by increasing the density of foams in sandwich composites materials, while increasing the thickness of the foams within sandwich composites increases the static strength. Choice of the thickness of core and density therefore depends upon the type of loading of sandwich structure.

The fatigue failure of the sandwich composites is characterised by three stages corresponding to crack initiation, progressive damage developments and finally the failure. Each stage corresponds to different failure mechanisms which is reflected in the form of stiffness changes and that also depends on the type of loading, the maximum applied displacement levels, applied displacement ratio, core thickness, core density of sandwich specimens, etc. It has also been identified that there are considerable

differences in the behaviour of sandwich composites under displacement and load control fatigue.

From the damage propagation sequence it was observed that interfacial debonding between top skin and core is one of the major causes in decreasing the specimens stiffness during fatigue particularly at low displacement levels. Initiation of interfacial debonding keeps on increasing with number of cycles until a stage reached where there is complete debonding between the top skin and core resulting in total loss of stiffness. But even at this stage, structure holds the load as bottom skin is still intact with the core.

The other failure modes of the sandwich specimens were the rupture of the top skin and interfacial debonding followed by shear crack development in the core, in the case when applied loading displacement level is high. Fracture features of the specimens observed visually and with an optical microscope after tests are discussed and related to characteristics of load versus number of cycles.

A stiffness reduction approach was adopted which was further based on the interpolation by the empirical functions of our test results, whose coefficients depends on the material properties and loading conditions. This approach enabled the fatigue life of the sandwich composite materials to be predicted while avoiding the large number of experiments that would normally be required. Wöhler curves were utilised in order to obtain a comparison between experimental results and analytical results. In addition, a simple approach based on the analogy between the mechanical behaviour and the fatigue damage evolution of sandwich composites during fatigue was employed. Damage accumulation models were proposed to check the experimentally observed stiffness degradation. The models developed were applied to analyses the fatigue life and damage of sandwich composites under fatigue. The beauty and simplicity of proposed model is that it includes all type of damage involved in the stiffness reduction of the specimen. There is no need to consider a particular damage mechanism. Any damage occurring during fatigue would be reflected in the degradation of the stiffness and, in turn, can be implicitly included in the model parameters. Only a limited number of parameters are needed and they are determined easily from the experiments. The magnitude of the testing programme and amount of test data could be reduced by implementing this modelling scheme. A distinctive difference is observed in the evolution of damage in displacement and load control fatigue. A good agreement was found between the experimental and analytical results.

It is the author’s hope that present work would provide a good experimental database for a step towards understanding the complex nature of damage development in sandwich composites under static and cyclic fatigue.

# References


1. Sendeckyj, J. P., (1990)., "Life prediction for resins-matrix composite materials", In: Reifsnider KL (ed), Fatigue of Composite Materials, Composite Material Series 4, Elsevier, pp. 431-483.
2. Whitworth, H., A., (1987)., "Modelling stiffness reduction of graphite/epoxy composite laminates", Journal of Composite Materials, Vol. 21, pp. 362-372.
3. Trantina, G. and Nimmer, R., (1993)., "Structural analysis of thermoplastic components", Technical Standards Services Ltd, UK.
4. Hohne, L. and Christine, U., (1994)., "Modelling of time strength behaviour of soda-lime silica glass in moist environments", Glass Technology 67, No. 8, pp. 87-95.
5. Mandell, J. F. and Meier, U., (1983)., "Effect of stress ratio, frequency, and loading time on tensile fatigue of glass reinforced epoxy", Long term behaviour of composites, ASTM STP 813, pp. 55-77.
6. Rotem, A., (1993)., "Load frequency effect on the fatigue strength of isotropic laminates", Composites Science and Technology, Vol. 46, pp. 1129-138.
7. Demers, C., (1997)., "E-glass fibre-reinforcement polymeric composites, tension-tension axial fatigue life diagrams", The National Seminar on Advanced Composite Material Bridges May 5-7, FHWA Sponsor.
8. Sims G. D. and Gladman, D. G., (1978)., "Effect of test conditions on the fatigue strength of a glass-fabric laminate: Part A-Frequency," Plast. Rubb. Mater. Appl. pp. 41-48.
9. McBagonluri, F. and Lesko, J. J., May (1997)., "The effect of frequency of fatigue cycling and applied stress level on temperature change in a glass/vinyl ester composite coupon", Progress Report to the National Institute for Standards and Technology, Gaithersburg, MD.
10. Ellyin, F., Kujawski. D. and Chiu., A. S., (1993)., "Cyclic behaviour of fibre glass-epoxy composite laminates", 9th International Conference on Composite Materials(ICCM/9), Composite Behaviour, Vol. 5, pp 700-706.
11. Saff, C. R., (1983)., "Effect of loading frequency and lay up on fatigue life of composites", Long Term Behaviour of Composites, ASTM 813, pp. 77-91.
12. Curtis, P. T., (1989)., "The behaviour of fibrous composite materials", Journal of Strain analysis, Vol. 24, No. 24, pp. 237-257.
13. Ellyin, F., and Kujawski, D., (1995)., "Tensile and fatigue behaviour of glass fibre/epoxy laminates", Construction and Building Materials, Vol. 9, pp. 425-430.
14. Cornelia, E. D., 1 July (1998)., "Tension tension axial fatigue of E-glass fiber-reinforced polymeric composites: fatigue life diagram", Construction and Building Materials, Vol. 12, (5), pp. 303-310.
15. Olsson, K. A., and Lönnö A., (1992)., "Sandwich construction-recent research and development: GRP sandwich technology for high speed vessels", Sandwich

Construction 2, Proceeding of 2nd International Conference on Sandwich Construction, Editors: Weissman-Burman, K. A. Olsson, Engineering Materials Advisory services.

16. Challis, K. E., (1986) , "Thermal stability of structural PVC foams", Cellular Polymers, Vol. 5, pp. 103-121.
17. El Kadi, H. and Ellyin, F., (1994)., "Effect of stress ratio on the fatigue of unidirectional glass fibre/epoxy composite lamina", Composites, Vol. 25, No. 10, pp. 917-924.
18. Amore D. A., Caprino, P., Zhou, J. and Nicolais, J., (1996)., "Effect of stress ratio on the flexural fatigue behaviour of continuous strand mat reinforced plastics", Composite Materials,Vol. 5 (1), pp. 1-8.
19. Burman, M. and Zenkert, D., (1996)., "On crack initiation and growth in cellular foams subjected to fatigue shear loading", Fatigue 96, Proceeding of the Sixth International Fatigue Congress, 6-10 May, Berlin, Germany, Pergamon Press, Vol. 3, pp. 1549-1554.
20. Berthelot, J. M., (2003)., "Transverse cracking and delamination in cross-ply glass-fibre and carbon-fibre reinforced plastic laminates: Static and fatigue loading", Applied Mechanical Review, Vol. 56, No. 1, pp. 111-147.
21. Sullivan, J. B., Cassin, G., T. and Rosen, W. B., (1990)., "Micromechanical analysis of unidirectional composites with fibre geometries and fibre/matrix interface conditions", Proceeding of American Society for composites, East Lasting, Michigan, USA, 12-14 June 1990, pp. 144-153.
22. Averill, C. R., and Carman, P. G., (1991)., "Analytical modelling of micromechanical stress variations in continuos fibre reinforced composites", Local Mechanics Concepts for Composite Materials System, Blacksburg, Virginia, USA, 28-31 October 1991, pp. 27-61.
23. Jones, C. R., (1990)., "Micromechanics and properties of fibre composites", Composite Materials in Aircraft Structures, pp. 69-92.
24. Sorensen, F. B., Talreja, R., and Sorensen, T. O., (1992)., "Micromechanical analysis of damage mechanisms in ceramic-matrix composites during mechanical and thermal cycling", Composites (31 March-2 April 1992), pp. 129-140.
25. King, R. T., Blackketter, E. D., Walrah, E. D. and Adams, F. D., (1992)., "Micromechanics prediction of shear strength of carbon fibre/epoxy matrix composites: the influence of the matrix and the interface strength", Journal of Composite Materials, Vol. 26, pp. 558-573.
26. Aboudi, J., (1988)., "Micromechanical analysis of the strength of unidirectional fibre composites", Composite Science Technology, Vol. 33, pp. 79-76.
27. Aboudi, J., (1987)., "Closed form constitutive equations for metal matrix composites", International Journal of Engineering Science, Vol. 25, pp. 1229-1240.
28. Aboudi, J., (1987)., "Stiffness reduction of cracked bodies", Engineering Fracture Mechanics, Vol. 26, pp. 637-650.
29. Dvorak, J. G., and Bahei-El-Din, A. Y., (1982)., "Plasticity analysis of fibrous composites", Journal of Applied Mechanics, Vol. 49, pp. 327-335.

30. Dvorak, J. G., and Rao, M., S. M., (1976)., "Axisymmetric plasticity theory of fibrous composites", International Journal of Engineering Science, Vol. 14, pp. 361-373.

31. Kwon, W. Y., (1992)., "Thermo-elastviscoplastic finite element plate bending analysis of composites", Engineering Computations, Vol. 9, pp. 595-607.

32. Kwon, W. Y. and Berner, M., J., (1995)., "Micromechanics model for damage and failure analysis of laminated fibrous composites", Engineering Fracture Mechanics, Vol. 52, No. 2, pp. 231-242.

33. Berthelot, J.,M., EL Mahi, A., Leblond, P; and Le Core, J. F., (1998)., "Development of transverse cracking in cross-ply laminates during tensile and fatigue loading", Progress in Rubber and Plastic Technology, Vol. 14, pp. 50-74.

34. Berthelot, J. M. and le Core, J. F., (1999)., "Modelling the transverse cracking in cross-ply laminates", Composites, Vol. 30B, pp. 569-577.

35. Huston, J. R., (1994)., "Fatigue life prediction in composites", International Journal of Pressure Vessel and Piping, Vol. 59, pp. 131-140.

36. Hwang, W. and Han, K. S., (1986)., "Cumulative damage models and multi-stress fatigue life predictions", Journal of Composite Materials, Vol. 20, pp. 125-133.

37. Broutman, L. J. and Sahu, S., (1972)., "Composite Materials, Testing and Design ($2^{nd}$ Conference)", ASTM STP 497, American Society for Testing and Materials, Philadelphia, pp. 170-188.

38. Reifsnider, K. L. and Gao, Z., (1991)., "A micromechanics model for composites under fatigue loading", International Journal of Fatigue, Vol. 17 (2), pp. 179-156.

39. Subramaniam, S., Reifsnider, K. L. and Stinchcomb, W. W., (1995)., "A cumulative damage model to predict fatigue life of composite laminates including the effect of a fibre-matrix interphase", International Journal of Fatigue, Vol. 13 (2), pp. 343-351.

40. Rotem, A., (1986)., "Fatigue and residual strength of composite laminates", Engineering Fracture Mechanics, Vol. 25, No.5-6, pp. 819-827.

41. Schaff, J. R. and Davidson, B. D., (1997a)., "Life prediction methodology for composite structures. Part I- Constant amplitude and two stress level fatigue", Journal of Composite Materials, Vol. 31, No. 2, pp. 128-1571

42. Schaff, J. R. and Davidson, B. D., (1997b)., "Life prediction methodology for composite structures. Part II- Spectrum fatigue", Journal of Composite Materials, Vol. 31, No. 2, pp. 158-181

43. Caprino, G. and D'Amore, A., (1998)., "Flexural fatigue behaviour of random continuous fibre reinforced thermoplastic composites", Composite Science and Technology, Vol. 58, pp. 957-965.

44. Caprino, G. and Giolelo, G., (1999)., "Fatigue life of glass fabric/epoxy composites", Composites, Part A: Applied Science and Manufacturing", Vol. 30, pp. 299-304.

45. Hahn, H. T. and Kim, R. Y., (1976)., "Fatigue behaviour of composites laminates", Journal of Composite Materials, Vol. 10, pp. 156-180.

46. Shokrieh, M. M., and Lessard, B. L., (1997)., "Multiaxial fatigue behaviour of unidirectional plies based on uniaxial fatigue experiments: I. Modelling", International Journal of Fatigue, Vol. 19, No. 3, pp. 2107-207.

47. Haplin, J. C., Jerina, K., L. and Johnson, T. A., (1973)., "Analysis of the test methods for high modulus fibres and composites", ASTM STP 521, American Society for Testing and Materials, Philadelphia, pp. 5-64.

48. Hahn, H. T. and Kim, R. Y., (1975)., "Proof testing of composites materials", Journal of Composite Materials, Vol. 9, pp. 299-311.

49. Yang, J. N. and Liu, M. D., April (1977)., "Residual strength degradation model and theory of periodic proof tests for graphite/epoxy laminates", Journal of Composite Materials, Vol. 11, pp. 176-202.

50. Chou, P. C. and Croman, R. J., (1978)., "Residual strength in fatigue based on the strength-life equal rank assumption", Journal of Composite Materials, Vol. 12, pp. 177-194.

51. Chou, P. C. and Croman, R. J., (1979)., "Composite Materials, Testing and Design ($5^{th}$ Conference)", ASTM STP 674 (Ed. S. W. Tsai), American Society for Testing and Materials, Philadelphia, pp. 431-454.

52. Sendeckyj, G. P., (1981)., "Test methods and design allowable for fibrous composites", ASTM STP 734 (Ed. C. C. Chamis), American Society for Testing and Materials, Philadelphia, pp. 245-260.

53. Daniel, I. M. and Charewicz, A., (1986)., "Fatigue damage mechanisms and residual properties of graphite/epoxy laminates", Engineering Fracture Mechanics, Vol. 25, pp. 793-808.

54. Reifsnider, K. L. and Stinchcomb, W. W., (1986), "Composite Materials: Fatigue and Fracture", ASTM STP 907 (Ed. H. T. Hahn), American Society for Testing and Materials, Philadelphia, pp. 298-313.

55. Reifsnider, K. L., (1986)., "The critical element model: a modelling philosophy", Engineering Fracture Mechanics, Vol. 25, pp. 739-749.

56. Reifsnider, K. L., (1991)., "Fatigue of Composites Materials", (Ed. K. L. Reifsnider), Elsevier, Amsterdam, pp. 11-77.

57. Reifsnider, K. L., (1982)., "Composite Materials, Testing and Design ($10^{th}$ volume)", ASTM STP 1120 (Ed. G. C. Crimes), American Society for Testing and Materials, Philadelphia, pp. 205-223.

58. Adam, T., Dickson, R. F., Fernando, G., Haris, B. and Reiter, H., (1986)., "The fatigue behaviour of kevlar/carbon hybrid composites", IMechE Conference Publications (Institute of Mechanical Engineers), Vol. 2. pp. 329-335.

59. Fong, J. T., (1982)., "Damage in composites materials", ASTM STP 775 (Ed. K. L. Reifsnider), American Society for Testing and Materials, Philadelphia, pp. 243-266.

60. Poursartip, A., Ashby, F. M. and Beaumont, R., W. P., (1986)., "The fatigue damage mechanics of carbon fibre composites laminate:- Development of model", Composite Science and Technology, Vol. 25, pp. 193-218.

61. Yang, J. N., Jones, S. H., Yang, S. H. and Meskinki, A., (1990)., "A stiffness degradation model for graphite/ epoxy laminates", Journal of Composite Materials, Vol. 24, pp. 753-769.

62. Wu, Wen-Fang, Lee, J. J., Choi, T. S., (1996)., "A study of fatigue damage and fatigue life of composite laminates", Journal of Composite Materials, Vol. 30, No. 1, pp. 123-137.

63. Yang, J. N., Lee, L. J. and Sheu, D. Y., (1992)., "Modulus reduction and fatigue damage of matrix dominated composite laminates", Composite Structures, Vol. 21, pp. 91-100.

64. Lee, J. L., Fu, E. K. and Yang, N. J., (1996)., "Prediction of fatigue damage and life for composite laminates under service loading spectra", Composites Science and Technology, Vol. 56, pp. 635-648.

65. Whitworth, H. A., 1998 "A stiffness degradation model for composite laminates under fatigue loading", Composite Structures, Vol. 40, No. 2, pp. 261-264.

66. Yao, X. W. and Himmel, N., (2000)., "A new cumulative fatigue damage model for fibre-reinforced plastics", Composites Science and Technology, Vol. 60, pp. 59-64.

67. Hashin, Z. and A. Rotem., (1973)., "A fatigue criterion for fibre reinforced materials," Journal of Composite Materials., Vol. 7, pp. 448-464.

68. Hashin, Z., (1985)., "Cumulative damage theory for composite materials: residual life and residual strength methods", Composite Science and Technology, Vol. 23, pp. 1-19.

69. Yao, X. W. and Himmel, N., (2000)., "A new cumulative fatigue damage model for fibre reinforced plastics", Composite Science and Technology, Vol. 60, pp. 59-64.

70. Kam, Y. T., Tsai, Y. S. and Chu, H. K., (1997)., "Fatigue reliability analysis of composite laminates under spectrum stress", International Journal of Solids Structures, Vol. 34, pp. 1441-1461.

71. Hwang W., Lee C. S. Park H. C. and Han K. S., (1995)., "Single and multi-stress level fatigue life prediction of glass/epoxy composites", Journal of Advanced Materials, pp. 3-9.

72. Whitworth, H. A., (1990)., "Cumulative damage in composites", Journal of Engineering Materials and Technology, Vol. 112, pp. 358-361.

73. Zenkert D., (1997)., Handbook of Sandwich Construction, EMAS Publishing, West Midlands, UK.

74. Zenkert, D. and Vikstrom, M., (1992)., "Shear cracks in foam core sandwich panels: Non-destructive testing and damage assessment", journal of Composites Technology & Research, Vol. 14, No. 2, pp. 95-103.

75. Zenkert, D., (1990)., "Strength of sandwich beam with mid plane debondings in core", Composite Structures, Vol. 15, pp. 279-299.

76. Olsson, K. A. and Lonno, A., (1989)., "Test procedures for foam core materials", In: K. A. Olsson and R. P. Reichard, Eds., Proceeding of the First International Conference on Sandwich Constructions, EMAS Ltd, UK, pp. 293-318.

77. Nordstranda, T. M. and Carlssonb L. A., (1997)., "Evaluation of transverse shear stiffness of structural core sandwich plates" Composite Structures, Vol. 16, No.6, pp. 649-662.

78. Daniel, M. I. and Jandro, L. A., (2000)., "Fabrication, testing and analysis of composite sandwich beams", Composite Science and Technology, Vol. 60, pp. 2455-2463.

79. Shenoi, R. A., Aksu., A. and Allen H. G., (1993)., "Flexural fatigue characteristic of FRP sandwich beam", Fatigue Fracture and Engineering Material, Vol. 16, No. 6, pp. 649-662.

80. Shenoi, R. A., Clark, S. D., and Allen, H. G., (1995)., "Fatigue behaviour of polymer composite sandwich beams", Journal of Composite Materials, Vol. 29(18), pp. 2423-2445.

81. Burman, M. and Zenkert, D., (1997)., "Fatigue of foam core sandwich beams-1: undamaged specimens", International Journal of Fatigue, Vol. 19(7), pp. 551-561.

82. Burman, M. and Zenkert, D., (1997)., "Fatigue of foam core sandwich beams-2: effect of initial damage", International Journal of Fatigue, Vol. 19(7), pp. 551-561.

83. Dransfeld, C., Loiselet, K., Hofmann, D., Stadelmann, R. and Berger, L., (2000)., Proceedings of the Fifth International Conference on Sandwich Construction, 5-7 September 2000, Zurich, Switzerland, Sandwich Construction 5, pp. 553-564.

84. Papanicolaou, C. G. and Bakos, D., (1996)., "Interlaminar fracture behaviour of sandwich structures", Composites Part A, Vol. 27A, pp. 165-173.

85. Kim, J. and Swanson, R. S., (2001)., "Design of sandwich structures for concentrated loading", Composite Structures", Vol. 52, pp. 365-373.

86. Caprino, G., Teti, R. and Messa, M., (1995)., "Long term behaviour of PVC foam cores for sandwich construction", Proceedings of the third International Conference on Sandwich Construction, September, Southampton, UK, Sandwich Construction 3.

87. Caprino, G. and Langella, A., (2000)., "Study of a three point bending specimen for shear characterisation of sandwich cores", Journal of Composite Materials, Vol. 34, pp. 791-814.

88. Judawisastra, H., Ivens, J, and Verpoest, I., (1999)., "Determination of core shear properties of three dimensional woven sandwich composites", Plastic, Rubber and Composites, Mechanical Sandwich Structures, Vol. 28, No. 9, pp. 452-457.

89. Allen H J., Analysis and design of structural sandwich panels, London: Pergamon Press, 1969.

90. Thomsen, O. T., (1993)., "Analysis of local bending effects in sandwich plates with orthotropic face layers subjected to local loads", Composite Structures, Vol. 25, pp. 511-520.

91. Thomsen, O. T., (1995)., "Theoretical and experimental investigation of local bending effects in sandwich plates", Composite Structures, Vol. 30., pp. 85-101.

92. Frostig, Y and Baruch, M., (1990)., "Bending of sandwich beams with transversely flexible core", AIAA Journal, Vol. 28(11), pp. 523–531.

93. Frostig, Y., Baruch M., Vilnai O. and Sheinman , I., (1991)., "Bending of non-symmetric sandwich beams with flexible core: bending behavior", Journal of ASCE, EM Division, Vol. 117(9), pp. 1931–1952.

94. Johnson, L., L., Contact Mechanics, Cambridge University Press, 1985.

95. Frostig, Y., (1992)., "Behaviour of delaminated sandwich beams with transversely flexible core-high order theory"., Composite Structures, Vol. 20, pp. 1–16.

96. Frostig, Y., Baruch, M., Vilnai, O. and Sheinman, I., (1992)., "A high order theory for the bending of sandwich beams with a flexible core", Journal of Engineering Mechanics, Vol. 118(5), pp. 1026–1043.

97. Frostig, Y., Baruch, M. (1993)., "High order buckling analysis of sandwich beams with a flexible core". Journal of Engineering Mechanics, Vol. 119(3), pp. 476–495.

98. Frostig, Y. (1993)., "On stress concentration in the bending of sandwich beams with a transversely flexible core", Composite Structures, Vol. 24, pp. 161–169.

99. Frostig, Y., (1993)., "Bending of sandwich beams with transversely flexible core and transverse diaphragms", Journal of Engineering Mechanics, 119 (5), pp. 955–972.

100. Frostig, Y and Shenar, I, (1995)., "High order bending of sandwich beam with transversely flexible core and unsymmetrical laminated composite skins", Composite Engineering, Vol. 5(4), pp. 405–414.

101. Thomsen, O. T. and Frostig, Y., (1997)., "Localised bending effects in sandwich panels: photoelastic investigation versus high-order theory sandwich theory results", Composite structures, Vol. 37(1), pp. 97-108.

102. Frostig, Y. and Baruch, M., (1996)., "Localized load effects in the high-order bending of sandwich panels with transversely flexible core", Journal of Engineering Mechanics, Vol. 122(11), pp.1069-1076.

103. Hwang W. and Han S. K., (1986)., "Fatigue of composite materials- Damage model and life prediction", Journal of Composite Materials, Vol. 20, pp. 154-165.

104. Hwang W. and Han S. K., (1989)., "Fatigue modulus concept and life prediction" Composite Materials: Fatigue and Fracture, Second Volume, ASTM STP 1012, Paul A. Lagace, Ed., American Society for Testing and Materials, Philadelphia, pp. 87-102.

105. Read, L. C. J. P. and Shenoi, A. R., (1995)., "A review of fatigue damage modelling in the context of marine FRP laminates", Marine Structures, Vol. 8, pp. 257-278.

106. Zhang, S. Y. and Zhao, B., (1989)., "Creep behaviour of woven roving GRP in three point bending", Proceeding of the seventh ICCM, pp. 21-26.

107. Zhang, S. Y. and Zhao, B., (1990)., "Creep behaviour of laminated GRP in three point bending", Composite Structures, Vol. 13, pp. 217-234.

108. Ericksen, R. H., (1976)., "Room temperature creep of kevlar 49/epoxy composites", Composites, Vol. 7, pp. 189-194.

109. Sun, T. C., and Chin, S. E. (1981)., "Fatigue retardation due to creep in a fibrous composites", ASTM STP 723, pp. 233-242.

110. Crowther, M. F., and Phillips, G. M., (1989)., "Creep-fatigue interaction in glass/polyester composites", Composite Science and Technology, vol. 36, pp. 191-210.

111. Browman, J. and Baker, M., B., (1986)., "A methodology for describing creep-fatigue interactions in thermoplastic components", Polymer Engineering and Science, Vol. 26, No. 22, pp. 1582-1590.

112. Bezazi A., R., El Mahi A., Berthelot J. -M. and Bezazi B., (2002)., "Influence of reinforcement in cross-ply laminates in flexural testing", New Trends in Fatigue and Fracture – Metz 8-9 April 2002.

113. Berthelot, J., M., Leblond, P., EL Mahi, A. and Le Core, J. F., (1996)., "Transverse cracking of cross ply laminates", Composites, 27A, pp. 989-1001.

114. Berthelot, J., M.,.EL Mahi, A., Leblond, P and Le Core, J., F., (1998)., "Development of transverse cracking in cross-ply laminates during tensile and fatigue loading", Progress in Rubber and Plastic Technology, Vol. 14, pp. 50-74.

115. Uemura, M., and Iwai, I., (1990)., "Flexural testing and evaluation methods of advanced composites materials", Seminaire Franco-japonais sur les materiaux composites, Paris le Bourget.

116. Benienda, W., K., Robert, G. D., and Papadopoulos, D. S., (1992)., "Effect of contact stress in four point bending of graphite/epoxy and graphite/PMR-15", Composite beams SAMPE., USA, Vol. 23, No. 3, pp. 20-28.

117. Gibson, L.J. and Ashby, M.F., (1997)., Cellular Solids: Structure and Properties, Second Edition, Cambridge University Press, Cambridge, U.K.

118. Berthelot, J.,M. and Lolive, E., (2002)., "Non linear behaviour of foam cores and sandwich materials, Part I: Materials and Modelling", Journal of Sandwich Structures and Material, Vol. 4 pp. 219-247.

119. Lolive, E. and Berthelot, J. M., (2002)., "Non linear behaviour of foam cores and sandwich materials, Part 2: Indentation and three point bending", Journal of Sandwich Structures and Material, Vol. 4 pp. 297-351.

120. Berthelot, J., M., (1999)., Composite Materials. Mechanical Behaviour and Structural Analysis. New York: Sprinnger, U. S. A.

121. Kherbouche, A., (1994)., "Contibution au predimensionnement des structures composites sandwiches", PhD thesis, Université du Maine, Le Mans, France.

122. Zenket, D., (1995)., An Introduction to Sandwich construction, EMAS Ltd, Solihull, UK.

123. Walter, S., (1996)., "A history of fatigue", Engineering Fracture Mechanics, Vol. 54(2), pp. 263-300.

124. Ferreira, J.A.M., Costa J. D. M., Reis P.N.B., and Richardson M.O.W., (1999)., "Analysis of fatigue and damage in glass-fibre reinforced polypropylene composite materials", Composites Sciences and Technology; Vol. 59, pp. 1461-1467.

125. Brondsted, P., Andersen, S. I. and Lilholt, H., (1996)., "Fatigue performance of glass/polyester laminates and the monitoring of material degradation", Mechanics of Composite Materials, Vol. 31 (1), pp. 21-29.

126. Philippidis, T. P. and Vassilopoulos, A. P., (1999)., "Fatigue of composites laminates under off-axis loading", International Journal of Fatigue, Vol. 21(3), pp 253-262,

127. Mandell J. D., (1990)., "Fatigue behaviour of short fibre composites materials", Fatigue of Composite Materials, Vol. 4, Reifnsnider Ed, Elsevier, Amsterdam,.

128. Mandell, J. F., (1982)., Fatigue behaviour of fibre resin composites, developments in reinforced plastics, App. Sci. Pub., edit Pinchard P.G., London-New York.

129. Bascom, W. D. and Gweon, S. Y., (1989)., "Fractography and failure mechanisms of carbon fibre reinforced composites materials", In Fractography and Failure Mechanisms of Polymer and composites, Roulin-Moloney, A. C., Ed, Elsevier, London UK, pp. 351-385.

130. Agrwal, B. D. and Broutman. L. J., (1980)., Analysis and Performance of Fibre Composites, Wiley InterScience, New York.

131. D'amore A., Caprino G., Stupak R., Zhou J., and Nicolais L., (1996)., "Effect of stress ratio on the flexural fatigue behaviour of continuous stand mat reinforced plastics", Science and Engineering of Composites Materials, Vol. 5(1), pp. 1-8.

132. Whitworth H. A., (1998)., "A stiffness degradation model for composite laminates under fatigue loading", Composite Structures, Vol. 40, No.2, pp 95-101.

133. Clark S. D., Shenoi R. A., Allen H. G., (1999)., "Modelling the fatigue behaviour of sandwich beams under monotonic, 2 step and block loading regimes", Composites Science and Technology, Vol. 59, pp. 471-486.

134. Salvia M. L. F., Fournier P. P., Vincent, L., (1997)., "Flexural fatigue behaviour of UDGFRP experimental approach", International Journal of Fatigue, Vol. 19, No. 3, pp. 253-262.

135. SICOMIN, Manufacturer PVC Foams, Epoxy Resins, Glass Fibres Rn 567, Quartre Moutte, 1330220 Château-les Martigues, France.

# Appendix A
# Theory of sandwich plates

A sandwich consists of three main parts: face (or skins), core and bonding material. Generally, the skins are laminates of thickness $h_1$ (the lower skin) and thickness $h_2$ (upper skin) and thickness of the core is $h_c$.

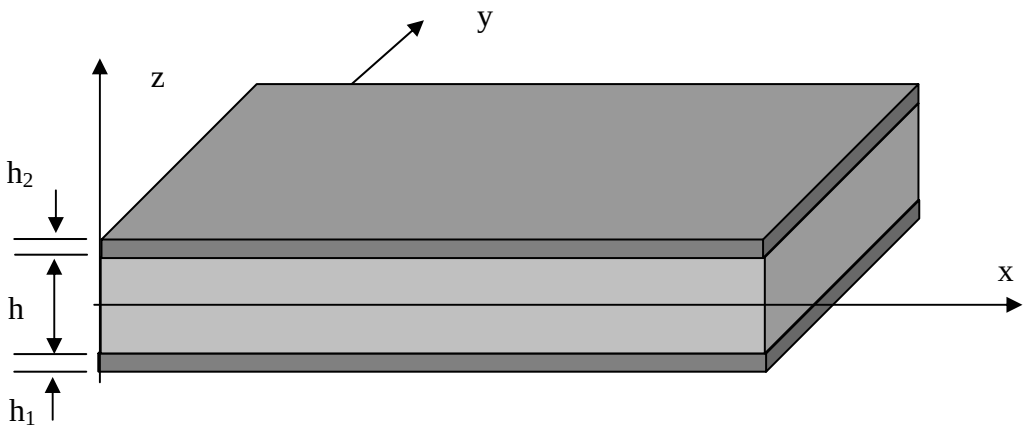


**Figure 5.1**. Symmetrical sandwich beam

## A.1 Assumptions for sandwich theory

A standard x-, y-, z- coordinate system as shown in figure 5.1 is used to derive the equations. The origin of coordinate system lies in the middle plane (for sandwich in the geometrical symmetry plane of the core). The following basic assumptions are made:

1. The thickness of the core is much greater than that of skins, $h_c >> h_1, h_2$.
2. The in plane displacements $u_c$ and $v_c$ of the core are linear functions of the z-coordinate.
3. The in-plane displacement u and v are uniform through the thickness of the skins.
4. The transverse displacement w is independent of the *z*-coordinate: the deformation $\varepsilon_{zz}$ is neglected.
5. The core transmits only the transverse shear stresses, $\sigma_{xz}$, $\sigma_{yz}$: the stresses $\sigma_{xx}$, $\sigma_{yy}$: $\sigma_{xy}$, are neglected:
6. The transverse shear stress $\sigma_{xz}$, $\sigma_{yz}$ are neglected within the skins.
7. Shear stresses are constant through the skins.
8. The core is considered isotropic.

Finally, the theory treats the elasticity problems of small deflections.

## A.2 Displacement Field

Assumption 2 implies a first order model for core displacement:

$$\begin{aligned} u_c(x,y,z) &= u_0(x,y) + z\varphi_x(x,y), \\ v_c(x,y,z) &= v_0(x,y) + z\varphi_y(x,y), \end{aligned} \tag{A.1}$$

with

$$\begin{aligned} u_0(x,y) &= u_c(x,y,0), \\ v_0(x,y) &= v_c(x,y,0), \end{aligned} \tag{A.2}$$

The continuity of the displacement at the core skin interface, associated with assumption 3, leads to following expressions for the displacements within the skins:

- lower skin:

$$\begin{aligned} u_1(x,y,z) &= u_0(x,y) - \frac{h_c}{2}\varphi_x(x,y), \\ v_1(x,y,z) &= v_0(x,y) - \frac{h_c}{2}\varphi_y(x,y), \end{aligned} \tag{A.3}$$

- upper skin:

$$\begin{aligned} u_2(x,y,z) &= u_0(x,y) + \frac{h_c}{2}\varphi_x(x,y), \\ v_2(x,y,z) &= v_0(x,y) + \frac{h_c}{2}\varphi_y(x,y). \end{aligned} \tag{A.4}$$

Assumption 4 is written:

$$w(x,y,z) = w_0(x,y) \tag{A.5}$$

The theory of sandwich plates is based upon the determination of five functions of displacement and rotation, $u_0$, $v_0$, $w_0$, $\varphi_x$ and $\varphi_y$, analogues to those introduced in the theory of laminate that take into account transverse shear.

### A.3 Strain field

The strain field in the skins is deduced from the displacement fields given in equation (A.3) and (A.4). It is written:

$$\begin{bmatrix} \varepsilon_{xx}^i \\ \varepsilon_{yy}^i \\ \gamma_{xy}^i \end{bmatrix} = \begin{bmatrix} \varepsilon_{xx}^0 \\ \varepsilon_{yy}^0 \\ \gamma_{xy}^0 \end{bmatrix} + (-1)^i \frac{h_a}{2} \begin{bmatrix} \kappa_x \\ \kappa_y \\ \kappa_{xy} \end{bmatrix}, \quad i = 1,2 \tag{A.6}$$

with notations:

$$\begin{aligned} \varepsilon_{xx}^0 &= \frac{\partial u_0}{\partial x}, \quad \varepsilon_{yy}^0 = \frac{\partial v_0}{\partial y}, \quad \gamma_{xy}^0 = \frac{\partial u_0}{\partial y} + \frac{\partial v_0}{\partial x} \\ \kappa_x &= \frac{\partial \varphi_x}{\partial x}, \quad \kappa_y = \frac{\partial \varphi_y}{\partial y}, \quad \kappa_{xy} = \frac{\partial \varphi_x}{\partial y} + \frac{\partial \varphi_y}{\partial x} \end{aligned} \tag{A.7}$$

The transverse shear strains in skin are neglected.

The strain field in the core is deduced from the displacement field equation A.1. It is written as:

$$\begin{aligned}
\varepsilon_{xx}^{c} &= \frac{\partial u_c}{\partial x} = \frac{\partial u_0}{\partial x} + z\frac{\partial \varphi_x}{\partial x} \\
\varepsilon_{yy}^{c} &= \frac{\partial v_c}{\partial y} = \frac{\partial v_0}{\partial y} + z\frac{\partial \varphi_y}{\partial y} \\
\varepsilon_{zz}^{c} &= \frac{\partial w_0}{\partial z} = 0 \\
\gamma_{xy}^{c} &= \frac{\partial u_c}{\partial y} + \frac{\partial v_c}{\partial x} = \frac{\partial u_0}{\partial y} + \frac{\partial v_0}{\partial x} + z\left(\frac{\partial \varphi_x}{\partial y} + \frac{\partial \varphi_y}{\partial x}\right) \\
\gamma_{yz}^{c} &= \frac{\partial w}{\partial y} + \frac{\partial v_c}{\partial z} = \frac{\partial w_0}{\partial y} + \varphi_y \\
\gamma_{xz}^{c} &= \frac{\partial w}{\partial x} + \frac{\partial u_c}{\partial z} = \frac{\partial w_0}{\partial x} + \varphi_x
\end{aligned} \tag{A.8}$$

The strain field has the same form as the strain fields introduced in the theory of laminates with transverse shear. It is the superposition of two strain fields.

- The mid plane and flexural strain field:

$$\begin{bmatrix} \varepsilon_{xx}^{c} \\ \varepsilon_{yy}^{c} \\ \gamma_{xy}^{c} \end{bmatrix} = \begin{bmatrix} \varepsilon_{xx}^{0} \\ \varepsilon_{yy}^{0} \\ \gamma_{xy}^{0} \end{bmatrix} + z\begin{bmatrix} \kappa_x \\ \kappa_y \\ \kappa_{xy} \end{bmatrix}, \tag{A.9}$$

- the transverse shear strain field:

$$\begin{bmatrix} \gamma_{yz}^{c} \\ \gamma_{xz}^{c} \end{bmatrix} = \begin{bmatrix} \dfrac{\partial w_0}{\partial y} + \varphi_y \\ \dfrac{\partial w_0}{\partial x} + \varphi_x \end{bmatrix} \tag{A.10}$$

## A.4 Stress field

The stresses in the $k_{th}$ layer may be expressed by a general equation:

$$\begin{bmatrix} \sigma_{xx} \\ \sigma_{yy} \\ \sigma_{xy} \\ \cdots \\ \sigma_{yz} \\ \sigma_{xz} \end{bmatrix} = \begin{bmatrix} Q'_{11} & Q'_{12} & Q'_{16} & \vdots & 0 & 0 \\ Q'_{12} & Q'_{22} & Q'_{26} & \vdots & 0 & 0 \\ Q'_{16} & Q'_{26} & Q'_{66} & \vdots & 0 & 0 \\ \cdots & \cdots & \cdots & \cdots & \cdots & \cdots \\ 0 & 0 & 0 & \vdots & C'_{44} & C'_{45} \\ 0 & 0 & 0 & \vdots & C'_{45} & C'_{55} \end{bmatrix}_k \begin{bmatrix} \varepsilon^i_{xx} \\ \varepsilon^i_{yy} \\ \gamma^i_{xy} \\ \cdots \\ \gamma^i_{yz} \\ \gamma^i_{xz} \end{bmatrix} \tag{A.11}$$

The stiffness $Q'_{ij}$ and $C'_{ij}$ of the *k*th layer are referred to the laminate's reference directions. There expressions are given in equation A.18.

The stress field in the core is deduced from assumption 5:

$$\sigma^a_{xx} = \sigma^a_{yy} = \sigma^a_{xy} = \sigma^a_{zz} = 0 \tag{A.12}$$

The core transmits only shear stresses:

$$\begin{bmatrix} \sigma^c_{yz} \\ \sigma^c_{xz} \end{bmatrix} = \begin{bmatrix} C'_{44} & C'_{45} \\ C'_{54} & C'_{55} \end{bmatrix} \begin{bmatrix} \gamma^c_{yz} \\ \gamma^c_{xz} \end{bmatrix} \tag{A.13}$$

Where the coefficients $C'^c_{ij}$ are expressed as functions of coefficients $C^c_{ij}$ refereed to the core principal directions as follow

$$\begin{aligned} C'^c_{44} &= C_{44}\cos^2\theta + C_{55}\sin^2\theta \\ C'^c_{45} &= (C_{55} - C_{44})\sin\theta\cos\theta \\ C'^c_{55} &= C_{44}\sin^2\theta + C_{55}\cos^2\theta \end{aligned} \tag{A.14}$$

Where $\theta$ is the angle that the core principal directions make with reference directions of the sandwich plate.

The coefficients of $C^c_{ij}$ in principal directions are themselves written as functions of shear stiffness of the core, measured in principal directions, as follow:

$$C^c_{44} = G^a_{23} \qquad C^c_{55} = G^a_{13} \tag{A.15}$$

Assumption 6 implies that the transverse shear stresses are zero in all the *kth* layers of the lower and upper skins:

$$\sigma^k_{xz} = \sigma^k_{yz} = 0 \tag{A.16}$$

The stresses in the skins are deduced from strains by the relation using above equation:

$$\begin{bmatrix}\sigma_{xx}^{k}\\ \sigma_{yy}^{k}\\ \sigma_{xy}^{k}\end{bmatrix}=\begin{bmatrix}Q_{11}^{'} & Q_{12}^{'} & Q_{16}^{'}\\ Q_{12}^{'} & Q_{22}^{'} & Q_{26}^{'}\\ Q_{16}^{'} & Q_{26}^{'} & Q_{66}^{'}\end{bmatrix}_{k}\begin{bmatrix}\varepsilon_{xx}^{i}\\ \varepsilon_{yy}^{i}\\ \gamma_{xy}^{i}\end{bmatrix},\quad i=1,2 \tag{A.17}$$

The reduced stiffness $Q_{ij}^{'}$ of the $k_{\text{th}}$ layers are refereed to stiffness of the skin of the sandwich for the $k_{\text{th}}$ layer of lower ( $i$ = 1) or upper skin ($i$ = 2). Their expressions are given below:

$$\begin{aligned}
Q_{11}^{'} &= Q_{11}\cos^4\theta + Q_{22}\sin^4\theta + 2(Q_{12}+2Q_{66})\sin^2\theta\cos^2\theta\\
Q_{12}^{'} &= (Q_{11}+Q_{22}+4Q_{66})\sin^2\theta\cos^2\theta + Q_{12}(\cos^4\theta+\sin^4\theta)\\
Q_{16}^{'} &= (Q_{11}-Q_{12}-2Q_{66})\sin\theta\cos^3\theta + (Q_{12}-Q_{22}+2Q_{66})\sin^3\theta\cos\theta\\
Q_{22}^{'} &= Q_{11}\sin^4\theta + 2(Q_{12}+2Q_{66})\sin^2\theta\cos^2\theta + Q_{22}\cos^4\theta\\
Q_{26}^{'} &= (Q_{11}-Q_{12}-2Q_{66})\sin^3\theta\cos\theta + (Q_{12}-Q_{22}+2Q_{66})\sin\theta\cos^3\theta\\
Q_{66}^{'} &= (Q_{11}+Q_{22}-2(Q_{12}+Q_{66})\sin^2\theta\cos^2\theta + Q_{66}(\sin^4\theta+\cos^4\theta)\\
C_{44}^{'} &= C_{44}\cos^2\theta + C_{55}\sin^2\theta\\
C_{45}^{'} &= (C_{55}-C_{44})\sin\theta\cos\theta\\
C_{55}^{'} &= C_{44}\sin^2\theta + C_{55}\cos^2\theta
\end{aligned} \tag{A.18}$$

The reduced stiffness constants in the material directions can be expressed as functions of the engineering moduli and is given in the following equation.

$$\begin{aligned}
&Q_{11}=\frac{E_L}{1-\dfrac{E_T}{E_L}\nu_{LT}^2},\ Q_{22}=\frac{E_T}{E_L}Q_{11},\ Q_{12}=\nu_{LT}Q_{22}\\
&Q_{66}=G_{LT},\quad C_{44}=G_{TT'},\quad C_{55}=G_{LT'}
\end{aligned} \tag{A.19}$$

## A.5 Governing equations of sandwich plates

The constitutive equations of sandwich plates express the resultants and moments:

- The in-plane resultants:

$$\begin{bmatrix}N_x\\ N_y\\ N_{xy}\end{bmatrix}=\int_{-(h_a/2+h_1)}^{-h_a/2}\begin{bmatrix}\sigma_{xx}\\ \sigma_{yy}\\ \sigma_{xy}\end{bmatrix}dz+\int_{h_a/2}^{h_a/2+h_2}\begin{bmatrix}\sigma_{xx}\\ \sigma_{yy}\\ \sigma_{xy}\end{bmatrix}dz \tag{A.20}$$

- The bending and twisting moments:

$$\begin{bmatrix} M_x \\ M_y \\ M_{xy} \end{bmatrix} = \int_{-(h_a/2+h_1)}^{-h_a/2} \begin{bmatrix} \sigma_{xx} \\ \sigma_{yy} \\ \sigma_{xy} \end{bmatrix} z dz + \int_{h_a/2}^{h_a/2+h_2} \begin{bmatrix} \sigma_{xx} \\ \sigma_{yy} \\ \sigma_{xy} \end{bmatrix} z dz \tag{A.21}$$

- The shear resultants:

$$\begin{bmatrix} Q_x \\ Q_y \end{bmatrix} = \int_{h_a/2}^{-h_a/2} \begin{bmatrix} \sigma_{xz} \\ \sigma_{yz} \end{bmatrix} dz \tag{A.22}$$

The equations of the plates are obtained from the equations of deformable solids by integrating through the thickness of the plates. By adopting the scheme of displacement in first order of the system, the rotational inertia terms can be neglected and in the absence of body forces and shear stresses on the faces, the equations of plates simply as:

$$\begin{aligned} &\frac{\partial N_x}{\partial x} + \frac{\partial N_{xy}}{\partial y} = \rho_s \frac{\partial^2 u_0}{\partial t^2} \\ &\frac{\partial N_y}{\partial y} + \frac{\partial N_{xy}}{\partial x} = \rho_s \frac{\partial^2 v_0}{\partial t^2} \\ &\frac{\partial Q_x}{\partial y} + \frac{\partial Q_y}{\partial y} + q = \rho_s \frac{\partial^2 w_0}{\partial t^2} \\ &\frac{\partial M_x}{\partial x} + \frac{\partial M_{xy}}{\partial y} - Q_x = 0 \\ &\frac{\partial M_x}{\partial y} + \frac{\partial M_{xy}}{\partial x} - Q_y = 0 \end{aligned} \tag{A.23}$$

Where $\rho_s$ is the weight per unit area of the laminate at a point.

The five expressions, which are regrouped in the fundamental equations of plates, are related to each other in shear and twisting flexural moment. They are well applicable to laminates as well as to sandwich composites.

By substituting the expression (5.14)-(5.17) of stresses into the preceding expressions for resultants and moments, following constitutive equation is obtained:

$$\begin{bmatrix} N_x \\ N_y \\ N_{xy} \\ M_x \\ M_y \\ M_{xy} \\ Q_y \\ Q_x \end{bmatrix} = \begin{bmatrix} A_{11} & A_{12} & A_{16} & B_{11} & B_{12} & B_{16} & 0 & 0 \\ A_{12} & A_{22} & A_{26} & B_{12} & B_{22} & B_{26} & 0 & 0 \\ A_{16} & A_{26} & A_{66} & B_{16} & B_{26} & B_{66} & 0 & 0 \\ C_{11} & C_{12} & C_{16} & D_{11} & D_{12} & D_{16} & 0 & 0 \\ C_{12} & C_{22} & C_{26} & D_{12} & D_{22} & D_{26} & 0 & 0 \\ C_{16} & C_{26} & C_{66} & D_{16} & D_{26} & D_{66} & 0 & 0 \\ 0 & 0 & 0 & 0 & 0 & 0 & F_{44} & F_{45} \\ 0 & 0 & 0 & 0 & 0 & 0 & F_{45} & F_{55} \end{bmatrix} \begin{bmatrix} \varepsilon_{xx}^0 \\ \varepsilon_{yy}^0 \\ \gamma_{xy}^0 \\ k_x \\ k_y \\ k_{xy} \\ \gamma_{yz}^a \\ \gamma_{xz}^a \end{bmatrix} \tag{A.24}$$

with

$$\begin{aligned} A_{ij} &= A_{ij}^1 + A_{ij}^2, \\ B_{ij} &= \frac{h}{2}(A_{ij}^2 + A_{ij}^1), \\ C_{ij} &= C_{ij}^1 + C_{ij}^2, \\ D_{ij} &= \frac{h}{2}(C_{ij}^2 + C_{ij}^1), \end{aligned} \tag{A.25}$$

and

$$A_{ij}^1 = \int_{-h(h_c/2+h_1)}^{-h_c/2} (Q_{ij}^{'})_k dz = \sum_{k=1}^{n_1} \int_{h_{k-1}}^{h_k} (Q_{ij}^{'})_k dz = \sum_{k=1}^{n_1} (Q_{ij}^{'})_k e_k, \tag{A.26}$$

$$C_{ij}^1 = \int_{-(h_c/2+h_1)}^{-h_c/2} z(Q_{ij}^{'})_k dz = \sum_{k=1}^{n_1} \int_{h_{k-1}}^{h_k} z(Q_{ij}^{'})_k dz = \sum_{k=1}^{n_1} (Q_{ij}^{'})_k e_k z_k, \tag{A.27}$$

$$A_{ij}^2 = \int_{h_c/2}^{h_c/2+h_2} (Q_{ij}^{'})_k dz = \sum_{k=1}^{n_2} \int_{h_{k-1}}^{h_k} (Q_{ij}^{'})_k dz = \sum_{k=1}^{n_2} (Q_{ij}^{'})_k e_k, \tag{A.28}$$

$$C_{ij}^2 = \int_{h_c/2}^{h_c/2+h_2} z(Q_{ij}^{'})_k dz = \sum_{k=1}^{n_2} \int_{h_{k-1}}^{h_k} z(Q_{ij}^{'})_k dz = \sum_{k=1}^{n_2} (Q_{ij}^{'})_k e_k z_k, \tag{A.29}$$

$$F_{ij} = h_c C_{ij}^{'a}, \tag{A.30}$$

Where $n_1$ and $n_2$ are the numbers of layers respectively in the lower and upper skins and $C_{ij}^{'a}$ are the transverse shear constants of the core.

The constitutive equation has a similar form to the equation obtained from the theory of laminates with transverse shear. It differs by the term $C_{ij}$, which induce an asymmetry in the stiffness matrix.

In the case of symmetric sandwich plates, the lower and upper skins are identical, hence:

$$A_{ij}^1 = A_{ij}^2, \qquad C_{ij}^1 = -C_{ij}^2 \tag{A.31}$$

and from this it results that:

$$A_{ij} = 2A_{ij}^2, \qquad D_{ij} = -hC_{ij}^2 \tag{A.32}$$

$$B_{ij} = 0, \qquad C_{ij} = 0 \tag{A.33}$$

the equation then simplifies and new equation can be written as:

$$\begin{bmatrix} N_x \\ N_y \\ N_{xy} \\ M_x \\ M_y \\ M_{xy} \\ Q_y \\ Q_x \end{bmatrix} = \begin{bmatrix} A_{11} & A_{12} & A_{16} & 0 & 0 & 0 & 0 & 0 \\ A_{12} & A_{22} & A_{26} & 0 & 0 & 0 & 0 & 0 \\ A_{16} & A_{26} & A_{66} & 0 & 0 & 0 & 0 & 0 \\ 0 & 0 & 0 & D_{11} & D_{12} & D_{16} & 0 & 0 \\ 0 & 0 & 0 & D_{12} & D_{22} & D_{26} & 0 & 0 \\ 0 & 0 & 0 & D_{16} & D_{26} & D_{66} & 0 & 0 \\ 0 & 0 & 0 & 0 & 0 & 0 & F_{44} & F_{45} \\ 0 & 0 & 0 & 0 & 0 & 0 & F_{45} & F_{55} \end{bmatrix} \begin{bmatrix} \varepsilon_{xx}^0 \\ \varepsilon_{yy}^0 \\ \gamma_{xy}^0 \\ k_x \\ k_y \\ k_{xy} \\ \gamma_{yz}^a \\ \gamma_{xz}^a \end{bmatrix} \tag{A.34}$$

In the case of symmetric sandwich plates, there is no coupling between stretching and bending. The constitutive equation then takes a form identical to constitutive equation of symmetric laminates with transverse shear.

## A.6 Fundamental equations

The governing equations of sandwich plates are obtained by introducing the constitutive equations (A.4) into the governing equation (A.3) of the plates. On neglecting the terms of rotational inertia, these relations can be written as:

$$A_{11}\frac{\partial^2 u_0}{\partial x^2}+2A_{16}\frac{\partial^2 u_0}{\partial x\partial y}+A_{66}\frac{\partial^2 u_0}{\partial y^2}+A_{16}\frac{\partial^2 v_0}{\partial x^2}+(A_{12}+A_{66})\frac{\partial^2 v_0}{\partial x\partial y}+A_{26}\frac{\partial^2 v_0}{\partial y^2}+B_{11}\frac{\partial^2 \varphi_x}{\partial x^2}$$
$$+2B_{16}\frac{\partial^2 \varphi_x}{\partial x\partial y}+B_{66}\frac{\partial^2 \varphi_x}{\partial y^2}+B_{16}\frac{\partial^2 \varphi_y}{\partial x^2}+(B_{12}+B_{66})\frac{\partial^2 \varphi_y}{\partial x\partial y}+B_{26}\frac{\partial^2 \varphi_y}{\partial y^2}=\rho_s\frac{\partial^2 u_0}{\partial t^2} \tag{A.35}$$

$$A_{16}\frac{\partial^2 u_0}{\partial x^2}+(A_{12}+A_{66})\frac{\partial^2 u_0}{\partial x\partial y}+A_{26}\frac{\partial^2 u_0}{\partial y^2}+A_{66}\frac{\partial^2 v_0}{\partial x^2}+2A_{26}\frac{\partial^2 v_0}{\partial x\partial y}+A_{22}\frac{\partial^2 v_0}{\partial y^2}+B_{16}\frac{\partial^2 \varphi_x}{\partial x^2}$$
$$+(B_{12}+B_{66})\frac{\partial^2 \varphi_x}{\partial x\partial y}+B_{26}\frac{\partial^2 \varphi_x}{\partial y^2}+B_{66}\frac{\partial^2 \varphi_y}{\partial x^2}+2B_{26}\frac{\partial^2 \varphi_y}{\partial x\partial y}+B_{22}\frac{\partial^2 \varphi_y}{\partial y^2}=\rho_s\frac{\partial^2 v_0}{\partial t^2} \tag{A.36}$$

$$F_{55}\left(\frac{\partial \varphi_x}{\partial x}+\frac{\partial^2 w_0}{\partial x^2}\right)+F_{45}\left(\frac{\partial \varphi_x}{\partial y}+\frac{\partial \varphi_y}{\partial x}+2\frac{\partial^2 w_0}{\partial x\partial y}\right)+F_{44}\left(\frac{\partial \varphi_y}{\partial y}+\frac{\partial^2 w_0}{\partial y^2}\right)+q=\rho_s\frac{\partial^2 w_0}{\partial t^2} \tag{A.37}$$

$$C_{11}\frac{\partial^2 u_0}{\partial x^2}+2C_{16}\frac{\partial^2 u_0}{\partial x\partial y}+C_{66}\frac{\partial^2 u_0}{\partial y^2}+C_{16}\frac{\partial^2 v_0}{\partial x^2}+(C_{12}+C_{66})\frac{\partial^2 v_0}{\partial x\partial y}+C_{26}\frac{\partial^2 v_0}{\partial y^2}+D_{11}\frac{\partial^2 \varphi_x}{\partial x^2}$$
$$+2D_{16}\frac{\partial^2 \varphi_x}{\partial x\partial y}+D_{66}\frac{\partial^2 \varphi_x}{\partial y^2}+D_{16}\frac{\partial^2 \varphi_y}{\partial x^2}+(D_{12}+D_{66})\frac{\partial^2 \varphi_y}{\partial x\partial y}+D_{26}\frac{\partial^2 \varphi_y}{\partial y^2}-F_{55}(\varphi_x+\frac{\partial w_0}{\partial x}) \tag{A.38}$$
$$-F_{45}(\varphi_y+\frac{\partial w_0}{\partial y})=0$$

$$C_{16}\frac{\partial^2 u_0}{\partial x^2}+(C_{12}+C_{66})\frac{\partial^2 u_0}{\partial x\partial y}+C_{26}\frac{\partial^2 u_0}{\partial y^2}+C_{66}\frac{\partial^2 v_0}{\partial x^2}+2C_{26}\frac{\partial^2 v_0}{\partial x\partial y}+C_{22}\frac{\partial^2 v_0}{\partial y^2}+D_{16}\frac{\partial^2 \varphi_x}{\partial x^2}$$
$$+(D_{12}+D_{66})\frac{\partial^2 \varphi_x}{\partial x\partial y}+D_{26}\frac{\partial^2 \varphi_x}{\partial y^2}+D_{66}\frac{\partial^2 \varphi_y}{\partial x^2}+2D_{26}\frac{\partial^2 \varphi_x}{\partial x\partial y}+D_{22}\frac{\partial^2 \varphi_y}{\partial y^2}-F_{45}(\varphi_x+\frac{\partial w_0}{\partial x}) \tag{A.39}$$
$$-F_{44}(\varphi_y+\frac{\partial w_0}{\partial y})=0$$

The surface mass of the sandwich plate, is expressed in the following manner:

$$\rho_s = \int_{-h/2}^{h/2} \rho dz \tag{A.40}$$

Equations (A.35-A.39) allows us, in principal, to determine the five functions with the boundary conditions and permit us to determine the solutions of all the mechanic problems associated with sandwich structures.

In the case of symmetric sandwich materials and with static loadings, these relations can be further simplified as

$$A_{11}\frac{\partial^2 u_0}{\partial x^2} + A_{66}\frac{\partial^2 u_0}{\partial y^2} + (A_{12} + A_{66})\frac{\partial^2 v_0}{\partial x \partial y} = 0 \tag{A.41}$$

$$(A_{12} + A_{66})\frac{\partial^2 u_0}{\partial x \partial y} + A_{66}\frac{\partial^2 v_0}{\partial x^2} + A_{22}\frac{\partial^2 v_0}{\partial y^2} = 0 \tag{A.42}$$

$$F_{55}\left(\frac{\partial^2 w_0}{\partial x^2} + \frac{\partial \varphi_x}{\partial x}\right) + F_{44}\left(\frac{\partial^2 w_0}{\partial y^2} + \frac{\partial \varphi_y}{\partial y}\right) + q = 0 \tag{A.43}$$

$$D_{11}\frac{\partial^2 \varphi_x}{\partial x^2} + +D_{66}\frac{\partial^2 \varphi_x}{\partial y^2} + (D_{12} + D_{66})\frac{\partial^2 \varphi_x}{\partial x \partial y} - F_{55}(\varphi_x + \frac{\partial w_0}{\partial x}) = 0 \tag{A.44}$$

$$(D_{12} + D_{66})\frac{\partial^2 \varphi_x}{\partial x \partial y} + D_{22}\frac{\partial^2 \varphi_y}{\partial y^2} - F_{44}(\varphi_y + \frac{\partial w_0}{\partial y}) = 0 \tag{A.45}$$

Above equations are used determine the permissible strain fields in symmetric sandwich associated with the boundary conditions.

# Résumé

L'objectif de ce travail est de mettre en évidence un comportement général vis à vis de la fatigue des composites sandwichs en flexion. Il consiste à réunir un ensemble de données sur le comportement et les modes d'endommagement au cours de la fatigue en flexion trois-points des sandwichs. Les matériaux étudiés sont fabriqués au laboratoire par moulage sous vide sous forme de plaque. Ils sont constitués de peaux en stratifiés époxyde-fibres de verre du type $[0/90]_s$ et d'une âme en mousse PVC de différentes densités et différentes épaisseurs. Ce type de matériau sandwich, qui associe de bonnes propriétés mécaniques à un coût relativement faible, est particulièrement adapté aux applications industrielles de grande diffusion.

Une étude détaillée est menée pour caractériser le comportement mécanique des constituants du sandwich en statique et en fatigue. La peau est sollicitée en flexion, alors que l'âme est sollicitée en compression, en cisaillement, en flexion trois-points et en poinçonnement.

La théorie des plaques sandwiches dans le cas de la flexion trois-points est utilisée pour caractériser la performance des sandwichs en fonction de la densité et de l'épaisseur de l'âme. Plusieurs distances entre appuis sont considérées. Les résultats obtenus par cette analyse sont comparés à ceux expérimentaux obtenus à partir des essais statiques. Un bon accord a été trouvé entre les résultats expérimentaux et analytiques.

Des essais de fatigue cyclique sont conduits en contrôle force et en contrôle déplacement sur des éprouvettes sandwiches. L'analyse des faciès de rupture en fatigue a montré que la rupture de l'éprouvette sandwiche est gouvernée par la croissance au cours du cyclage de la décohésion de la peau et de l'âme, amorcée au voisinage de l'appui central et se propageant entre l'âme et la peau entraînant la rupture totale du sandwich. Ensuite, la durée de vie des matériaux sandwichs en fonction des conditions de chargement est déterminée en utilisant le critère $N_{10}$, correspondant à une réduction de la rigidité de 10% par rapport à sa valeur initiale. Les durées de vie sont caractérisées par les courbes de Wöhler et ont permis de mettre en évidence l'influence de l'épaisseur et de la densité de l'âme du sandwich sur la tenue en fatigue des matériaux.

Les résultats déduits des essais de fatigue ont permis également de développer une description du comportement en fatigue des matériaux sandwichs en flexion 3-points. Cette description est abordée en utilisant la réduction de la rigidité en fonction du nombre de cycles. Ensuite, une approche fondée sur l'analogie entre le comportement et l'évolution de l'endommagement par fatigue des sandwichs est utilisée pour définir le paramètre d'endommagement. Le modèle développé est appliqué à cette approche pour analyser l'endommagement de différents sandwichs au cours du cyclage. La confrontation des résultats analytiques et expérimentaux sont pour la plupart en bonne concordance. Le modèle analytique bien qu'il soit basé sur une approche simple, a conduit à une évaluation correcte de la durée de vie et du développement de l'endommagement des matériaux.



**Mots clés:**

Composites sandwichs, mousse PVC, stratifiés, flexion de poutres, fatigue, comportement mécanique, endommagement, modèle analytique, durée de vie, Wöhler courbes